Towards defining the cellular and molecular function of the broad-spectrum antiviral IFITM proteins

Stuart Malcolm Weston

Supervisor: Professor Mark Marsh

Medical Research Council

Laboratory for Molecular Cell Biology

University College London

November 2016

A thesis presented for the degree of

Doctor of Philosophy

Abstract

The InterFeron Inducible TransMembrane proteins (IFITMs) are broad-spectrum antiviral factors. *In vitro*, these proteins inhibit cellular entry of many enveloped viruses. In vivo, mice lacking expression of all Ifitm genes, or Ifitm3 alone, have been shown to have increased pathogenesis from influenza A, respiratory syncytial, West Nile and chikungunya virus infections. While much is known about the breadth of antiviral action of the IFITM proteins, and more is being learnt about function *in vivo*, there is currently a poor understanding of aspects of their cell biology and their precise mechanism(s) of antiviral action. The work presented here aims to further understanding of both of these aspects of IFITM biology.

Using morphological and biochemical techniques, I first proposed a novel topology model for the IFITMs, in which the N-terminal domain resides in the cytoplasm, while the C-terminal domain resides in the extracellular/lumenal space. Building on this knowledge, an analysis of the cellular distribution was performed to better understand how the IFITMs interact with the viruses they inhibit. The alphavirus, Semliki Forest virus (SFV) was, for the first time, established as a model system to investigate the antiviral functions of the IFITMs. In these studies I established that IFITM3 blocks viral entry following endocytosis and exposure of virus to low pH and before virus release to the cytoplasm. Finally, the properties of IFITM restriction of SFV were compared to those associated with other viruses that enter cells by similar mechanisms. These experiments showed that related viruses exhibit distinct patterns of IFITM restriction suggesting these different viruses may target distinct membrane sub-domains for fusion.

Overall, the work presented here extends our understanding of IFITM membrane topology and cellular distribution, defines IFITM-mediated inhibition of alphavirus infection and raises questions about the mechanisms of inhibition for different IFITM proteins.

Declaration

I, Stuart Weston, confirm that the work presented in this thesis is my own. Where information has been derived from other sources, I confirm that this has been indicated in the thesis.

Acknowledgements

I would like to start by thanking Mark for his guidance through my PhD and always very much providing motivation to improve my work. I leave the lab being far better equipped than when I joined. I must also extend a huge degree of thanks to all the members of the Marsh lab who I've had the chance to work with. I must particularly acknowledge Steffy, Scott and Michela. Steffy for always being willing and able to do the experiments I didn't fancy. Scott who taught me how to perform all the experiments I did fancy. And Michela for doing those Cat 3 ones that I wasn't allowed. As well as all being fantastic people to work with and bounce ideas off.

Huge thanks must also go to everyone who has helped with proofing this thesis. Understanding the pains of thesis writing, Siân, Scott, Michela and Nikki have all given really useful comments. Conversely, my two flatmates, Marcus and Rich, for entertainment and numerous distractions while I should have been writing.

My next port of call is to thank people involved with experiments presented here. I must thank members of Paul's lab for cells, constructs and general all-round help, Sarah, Rachael and Carmen (and Paul himself for bringing this project to Mark). Thanks must also go to LMCB people, Ian for EM and Christin for Opera imaging and analysis. The LMCB has also been a wonderful place in which to work, and a key to keeping me going when times were tough. Members of the LMCB tea team, excellent football team and all other friends I've made here.

That just leaves me to thank, tea and coffee for getting me through my days. Alcohol, the cause of, and solution to all of life's problems. And finally my parents for all their love and support, and anyone else I haven't remembered to include.

Contents

List of Figures

List of Tables

List of Abbreviations

AmphoB	Amphotericin B
ANDV	Andes virus
AP	Adaptor protein (eg. AP-2 or AP-3)
Baf A	Bafilomycin A1
BDBV	Bundibugyo virus
CCV	Clathrin coated vesicle
CCR5	C-C motif chemokine receptor 5
CD	Cluster of differentiation (eg. CD4, CD63, CD225 etc)
CIL	Conserved intracellular loop
CME	Clathrin-mediated endocytosis
CPZ	Chlorpromazine
CTD	C-terminal domain
CXCR4	C-X-C motif chemokine receptor 4
DENV	Dengue virus
DiD	1,1'-dioctadecyl-3,3,3',3'-tetramethyline-dodicarbocyanine perchlorate
EBOV	Ebola virus
EEA1	Early endosomal antigen 1
EEV	Extracellular enveloped virion
EM	Electron microscopy
ER	Endoplasmic reticulum

ESCRT	Endosomal sorting complexes required for transport
FCS	Foetal calf serum
FMDV	Foot and mouth disease virus
GFP	Green fluorescent protein
HA	Hemagglutinin
HCV	Hepatitis C virus
HIV	Human immunodeficiency virus
HSV	Herpes simplex virus 1
HT	Homotrimer
HTNV	Hantaan virus
IAV	Influenza A virus
IFITM	Interferon inducible transmembrane protein (Ifitm refers to murine IFITM proteins)
IFN	Interferon
ILV	Intralumenal vesicle
ISG	Interferon stimulated gene
JSRV	Jaagsiekte sheep retrovirus
kDa	Kilodalton
LACV	La Crosse virus
LAMP1	Lysosomal associated membrane protein 1
LBV	Lagos bat virus
LCMV	Lymphocytic choriomeningitis virus
LLOV	Lloviu virus
LSB	Laemmli sample buffer

MARV	Marburg virus
MERS-CoV	Middle East respiratory syndrome coronavirus
MFI	Mean fluorescence intensity
MOI	Multiplicity of infection
MOKV	Mokola virus
MLV	Murine leukaemia virus
MV	Mature virion
MVB	Multi-vesicular body
MW	Molecular weight
NTD	N-terminal domain
NP	Nuclear protein
OMSK	Omsk virus
pfu	Plaque forming unit
PIP	Phosphatidylinositol phosphate (eg. PI(3)P)
ProtK	Proteinase K
PTM	Post-translational modification
PVDF	Polyvinylidene fluoride
RABV	Rabies virus
RESTV	Reston virus
RSV	Respiratory syncitial virus
RV	Reovirus
RVFV	Rift Valley fever virus
SARS-CoV	Severe acute respiratory syndrome coronavirus
SBTI	Soy bean trypsin inhibitor
SFV	Semliki Forest virus

SINV	Sindbis virus
SIV	Simian immunodeficiency virus
SUDV	Sudan virus
TAFV	Tai Forest virus
TfR	Transferrin receptor
Tx100	Triton-X100
VACV	Vaccinia virus
VSV	Vesicular stomatitis virus
WCBV	West Caucasian bat virus
WNV	West Nile Virus
YFV	Yellow fever virus
ZIKV	Zika virus

Chapter 1

Introduction

Viral infections are a severe global health burden. However, viruses themselves are molecularly inert and only generate pathological consequences by co-opting cellular machinery to replicate and spread between infected and uninfected cells. The negative consequences of viral replication have driven the evolution of protective antiviral mechanisms within host cells and organisms. In multicellular organisms, the major countermeasure to viral infection is the immune system. In humans, this system can be broadly divided into two connected arms, the innate and adaptive immune responses. The innate immune response is triggered by the cellular detection of pathogens and acts rapidly and non-specifically to impair replication and spread. The adaptive immune response is triggered by the innate response and is therefore more slow acting, but plays vital roles in clearance of infection to further limit the severity of disease and provides immunological memory. The interferon (IFN) response is the major innate antiviral immune response initiated in humans. Upon detection of viral infection, cells can produce IFN as a danger signal to alert surrounding cells, and produce a broad 'antiviral state,' associated with the IFN-induced expression of hundreds of IFN stimulated genes (ISGs).

It is nearly 60 years since IFN was first identified by virtue of its ability to interfere with influenza virus replication [1]. However, the full array of cellular genes induced by IFN, and their roles in establishing an antiviral state remains largely unknown. Until recently, only a handful of ISGs had been characterised and the encoded proteins generally have very broad activity, such as 2'5'-oligoadenylate synthase/ribonuclease L and protein kinase R (see [2] for review). However, in recent years many studies have used unbiased screening

approaches to better investigate broad sets of ISGs, often finding genes with virus specific functions (see [3–6] for some examples). Similar approaches have been used to identify host factors that can modulate viral infection, which have also identified ISGs. One such screen by Brass *et al.* used genome-wide siRNA-mediated knockdown of host factors to identify genes that modulate influenza A virus (IAV) infection [7]. Amongst other proteins, this screen identified interferon inducible transmembrane protein 3 (IFITM3). In the human genome, *IFITM3* is one of a group of five *IFITM* genes, although only *IFITM1*, *2* and *3* are induced by IFN. Knockdown of IFITM3 was found to enhance IAV infection, conversely overexpression of IFITM1, 2 or 3 inhibited replication. Not only were the IFITM proteins antiviral against IAV, they also inhibited replication of multiple flaviviruses, suggesting they have broad-spectrum antiviral activity [7].

Since the initial identification of IFITM-mediated antiviral activity these proteins have been extensively studied. Through multiple studies, the antiviral activity has been extended to numerous viruses; currently representatives of over 10 viral families have been found to be inhibited by one or more IFITM proteins (see [8–11] for various reviews and Tables 1.1 and 1.2). Shortly after the discovery of their antiviral activity, the IFITM proteins were shown to restrict IAV infection by inhibiting delivery of incoming viral nucleic acid to the nucleus, suggesting that IFITM expression affected virus entry [12]. IAV has since become the most highly characterised virus for IFITM-mediated inhibition of entry, which is suggested to occur at the point of fusion between viral and cellular membranes [13, 14]. However the precise molecular mechanism(s) underlying IFITM-mediated restriction remain unknown. Furthermore, since few of the viruses shown to be inhibited by IFITM proteins have been analysed in great detail, whether these proteins inhibit entry of all viruses in the same way, or have different modes of action, is also unknown. Moreover, many aspects of IFITM cell biology still lack proper definition.

The work presented in this thesis was designed to develop a better understanding of both the cell biology and antiviral functions of the IFITM proteins. Work was performed to define the membrane topology [15] and cellular distribution of the IFITM proteins. Representatives of the previously untested alphavirus family were assessed for IFITM-mediated antiviral activity, with the focus being on the well characterised Semliki Forest virus (SFV). Finding that the alphaviruses are indeed inhibited by IFITM proteins, and

thoroughly characterising this inhibition [16] provides a powerful tool for further defining IFITM antiviral function. Building on the work with alphaviruses, further viral families were tested. Flaviviruses were found to have different sensitivity towards IFITM isoforms than alphaviruses while the poxvirus, vaccinia virus (VACV), was found to be insensitive to all IFITM proteins. These differences in sensitivity suggest IFITM-mediated inhibition may vary between viruses. Understanding these differences will also move towards a better understanding of IFITM antiviral function.

In order to contextualise the work presented throughout this thesis, certain concepts will be introduced in this chapter. Because the IFITM proteins inhibit viral entry, there is a summary of the mechanisms used by enveloped viruses to enter cells, with a focus on alphavirus entry and membrane fusion. The alphaviruses are the main system used in this work to study IFITM-mediated inhibition of viral infection, so these viruses will also be introduced. Finally, the IFITM proteins will be discussed to give appropriate background to the questions addressed in this thesis.

1.1 Enveloped virus cell entry

To allow for viral replication, genetic material must be transferred from infected to uninfected cells. The lipid bilayers of cells, and enveloped viruses, are physical barriers to this transit that must be overcome. Viruses therefore occupy an interesting ecological niche, requiring stability within an extracellular environment, to protect the genome between cells (or host organism), but also liability to penetrate cellular membranes, disassemble and deliver their genetic payload. Viruses are therefore produced as metastable particles; stable within an extracellular environment, but able to rapidly disassemble upon receiving appropriate triggers from a potential host cell.

The first interaction viruses have with new host cells is at the plasma membrane. Many of these interactions are non-specific, often through glycoprotein or glycolipid structures, referred to as attachment factors. One such factor is heparan sulfate that is used by multiple viruses (e.g. herpes simplex virus-1 [17], dengue virus [18], Sindbis virus [19], and various others [20]). Binding to attachment factors promotes interaction with receptor molecules to promote entry (see [21–23] for reviews). Receptors are essential for viral

replication, while attachment factors facilitate infection. These interactions are often dictated by the envelope glycoproteins that protrude on the surface of enveloped viruses.

Upon virus binding to receptors at the cell surface, one of two fates can ensue. Either the virus can directly penetrate the plasma membrane, or can be internalised via one or more of several endocytic mechanisms of the cell. As discussed previously, viruses are produced as metastable particles, requiring triggers to transition into a state capable of delivering genetic material into a cell. For viruses that can penetrate the plasma membrane, this trigger is the binding of cell surface receptor(s). One classical example of this is HIV-1, where binding to CD4, followed by binding to co-receptors (either C-C motif chemokine receptor 5 [CCR5] or C-X-C motif chemokine receptor 4 [CXCR4]) promotes conformational changes to the envelope glycoprotein to fuse the viral envelope with the plasma membrane (reviewed in [24]). While some viruses can fuse at the cell surface, the vast majority of studied viruses are taken into cells by endocytosis [22]. The changing environment within the endosomal system provides the trigger(s) for fusion: generally these are low pH, protease activation of viral proteins and/or further receptor binding.

1.1.1 Endocytosis

Many animal viruses subvert endocytic mechanisms of cells [22]. One of the most highly characterised endocytic pathways, and one used by alphaviruses, is clathrin-mediated endocytosis (CME), where clathrin acts as a coat protein for the formation of transport vesicles [25]. When cell surface receptors are destined for CME, there are various stages to the formation of a clathrin coated vesicle (CCV). Initially a membrane pit needs to form through invagination of the plasma membrane. Clathrin is unable to bind directly to lipids or cargo proteins, and therefore relies on adaptor proteins such as AP-2. It had been thought that binding of AP-2 to the plasma membrane through interaction with cargo proteins [26], and the lipid phosphatidylinositol-4,5-bisphosphate ($PI(4,5)P_2$; [27]), resulted in the initial curvature to form a pit. However, it has since been suggested that curvature may initially be induced by binding of Fer/Cip4 homology domain-only proteins (FCHO), epidermal growth factor substrate 15 (Eps15) and intersectins [28]. Once AP-2 has localised to the plasma membrane, it can recruit clathrin from the cytosol to form polygonal networks of clathrin triskelia [29]. The forming clathrin coated pit ulti-

mately needs to pinch off from the plasma membrane and release into the cytosol, which is achieved by the GTPase action of dynamin [30]. Once the vesicle has been released, the clathrin coat must be disassembled by the actions of the ATPase heat shock cognate protein 70 (Hsc70; [31]), allowing the vesicle to fuse with the endosomal system.

Various other endocytic mechanisms have evolved [32], but a full discussion of most of these is outside the scope of this work (see Fig. 1.1 for a summary diagram). CME has been highlighted because alphaviruses subvert this system for uptake from the plasma membrane and delivery to the endosomal system (discussed further below). However, it is also pertinent to briefly discuss macropinocytic uptake as this is used by VACV and possibly yellow fever virus 17D strain (YFV), both of which are investigated here for sensitivity to IFITM proteins. Macropinocytosis is a form of large-scale uptake that involves actin based protrusions from the plasma membrane that fuse with themselves, or back with the plasma membrane. The closure of these protrusions by membrane fusion forms an encased volume of extracellular fluid which can enter into the endosomal system. These protrusions from the surface of cells gives a characteristic plasma membrane ruffling. Thus in contrast to CME, where a pit invaginates towards the cytosol, in macropinocytic uptake, membrane extends away from the cell to internalise extracellular fluid and molecules. Along with the dependence on regulators of actin polymerisation such as p21 protein-activated kinase 1 (PAK1) and Ras-related C3 botulinum toxin substrate 1 (Rac1), macropinocytosis is also dependent on PI(3)-kinase, Na^+/H^+ exchangers and various other cellular factors (see [22, 32] for reviews).

The endosomal system is a highly regulated, directional pathway for protein sorting. Upon arrival at early endosomes, cargoes have one of three fates: recycling to the plasma membrane, retrograde transport to the trans-Golgi network, or transport to later endocytic compartments including the lysosomes. For the purposes of this introduction the maturation of early endosomes into late endosomes and cargo degradation in lysosomes will be discussed. The other fates will not be discussed because enveloped viruses generally do not use the recycling or retrograde pathways for entry into cells.

Early endosomes are produced by the fusion of multiple incoming transport vesicles, and are the initial sites of sorting to determine the fate of incoming cargo. The organelles acquire a defined lipid and protein composition [34]. One of the master regulators of early

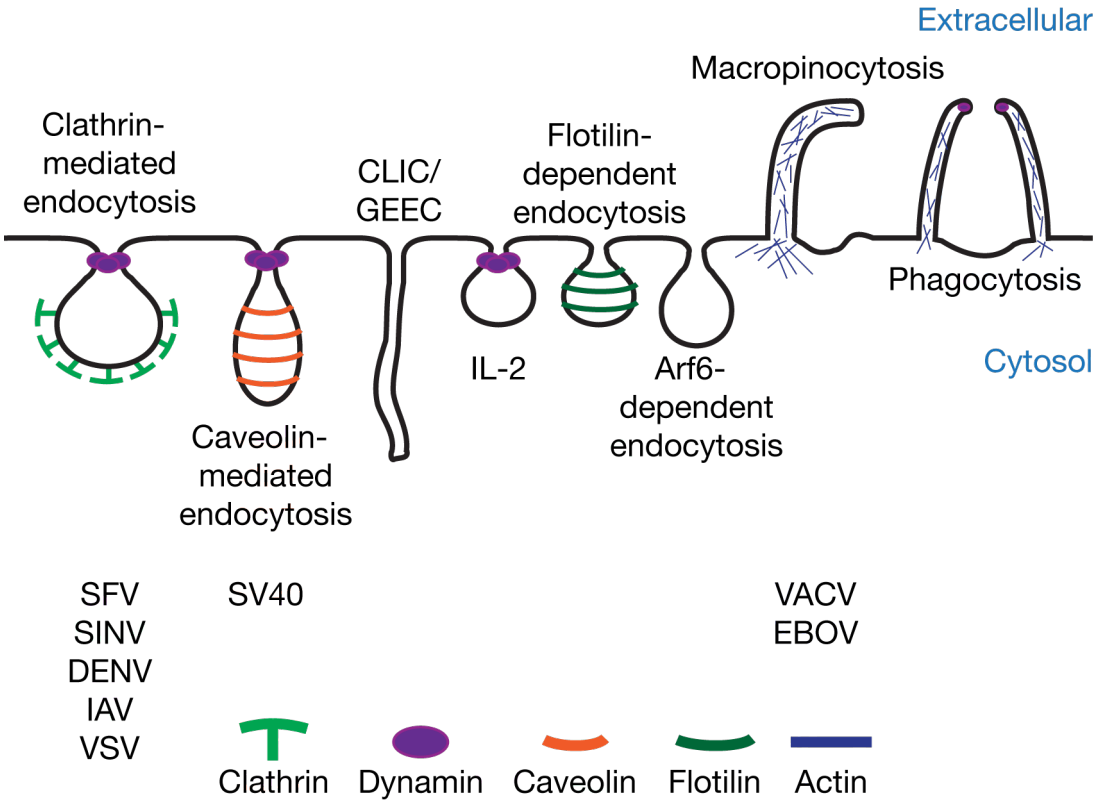

Figure 1.1: **Summary of endocytic internalisation mechanisms.** Various mechanisms have evolved to allow for internalisation of substrates from the cell surface or the extracellular space of mammalian cells. Key features of the internalisation mechanisms are summarised here, such as the dependence on coat proteins (e.g. clathrin or caveolin), dynamin-dependence or a need for actin-based protrusions from the cell surface. The CLIC/GEEC pathway is characterised by clathrin-independent carriers (CLICs) that form at the plasma membrane and later mature into early endocytic compartments referred to as glycosylphosphotidylinositol-anchored protein enriched compartments (GEECs). The pathway labelled as IL-2 (interleukin-2) is a clathrin-independent, dynamin-dependent internalisation pathway that has been best characterised for the internalisation of IL-2. Viruses are capable of subverting these internalisation mechanisms as part of their entry pathway, with most viruses using the clathrin-mediated endocytic pathway, some examples are provided. Larger viruses such as vaccinia virus and Ebola virus rely on on uptake through macropinocytosis. Details adapted from [21, 22, 32, 33].

endosomal identity is the small GTPase Rab5, which localises to the plasma membrane and early endosomal membranes [35], and is activated by Rabex-5 [36]. Once associated with membranes in the active GTP bound form, Rab5 recruits various effectors that define organelle identity and perform the sorting functions of early endosomes (reviewed in [34, 37, 38]). One such group of proteins are PI3-kinases that generate PI(3)P on the cytoplasmic surface of early endosomes [39]. PI(3)P can subsequently regulate recruitment of additional proteins to endosomes such as early endosomal antigen 1 (EEA1), through the FYVE domain (Fab1, YOTB, Vac1, EEA1) [40]. The vacuolar ATPase (vATPase) is also recruited to early endosomes, which functions to pump H^+ ions into the lumen of the organelle, and cause gradual acidification. The lumen of early endosomes ranges from pH 6.8 - 6.1 [34], and this acidification is often necessary for ligand release from receptors as part of the sorting process of early endosomes. Lowered pH is also required for the degradative pathway because hydrolyases in lysosomes have optimal activity in acidic conditions. The gradual reduction of lumenal pH also plays roles in maturation of early endosomes into late endosomes, and has been subverted by numerous viruses to promote their entry into cells, as discussed in more detail below.

Concomitantly with the lowering of endosomal pH, various other switches occur as early endosomes mature to late endosomes. Rab5 and a variety of effectors again helps dictate these changes, and there is a switch from Rab5 to Rab7, which functions to define late endosome identity [41, 42]. Initially, Rab7 is recruited to Rab5 containing endosomes, and this in turn suppresses the action of Rab5. These Rab5/Rab7 hybrid endosomes generate Rab7 positive sub-domains which have then been observed to break away from Rab5 sub-domains in a fission event, producing Rab7 marked late endosomes [42]. Similarly, a PI switch occurs, with PIKfyve being recruited to membranes rich in PI(3)P (early endosomes), which promotes the formation of $PI(3,5)P_2$ on the surface of late endosomes (reviewed [34]). Late endosomes continue to mature, and the lumenal pH becomes more acidic, ranging from pH 6.0 to 4.9 [34].

In conjunction with the various protein and lipid changes as endosomes mature, there are also membrane remodelling events. Membrane proteins destined for degradation are tagged with ubiquitin by cytosolic enzymes. This post-translational modification (PTM) promotes the recruitment of the endosomal sorting complexes required for transport (ES-

CRT) to form intralumenal vesicles (ILVs; reviewed [43]). ESCRT promotes inward budding and scission from the limiting membrane of late endosomes to produce multivesicular bodies (MVBs). These late endosomes/MVBs will eventually fuse with lysosomes, exposing the ILVs to the hydrolytic interior of lysosomal compartments, which can have a pH as low as 4.5 [34, 43]. This endocytic pathway, and various proteins and lipids associated with it has been summarised in Fig. 1.2.

Virus entry through the endocytic system

A large number of enveloped viruses have adapted to subvert endocytic uptake and trafficking to mediate their entry into cells. By entering into the endocytic system, virus particles can be transported through the cytosol towards the nucleus, which may be advantageous to viruses that replicate in the nucleus. This transport may also allow for bypass of physical barriers to infection such as the actin cortex and may act as an immune avoidance strategy since fusion with internal membranes will not leave any viral membrane proteins exposed on the cell surface. This route of entry also provides many different triggers to regulate membrane fusion and penetration to the cytosol, allowing precise timing of cell entry and potentially escape from premature activation within extracellular spaces. As will be discussed in more detail below, SFV only requires the trigger of low pH, with a threshold at pH $\leq$ 6.2 [45–48]. Thus, CME of SFV particles and delivery to early endosomal compartments is sufficient to provide a trigger for entry. Other viruses, such as IAVs, have lower pH threshold (pH 5.2 - 4.9), requiring trafficking to late endosomal compartments [49–51].

Low pH alone is not always sufficient to promote membrane fusion. Dengue virus (DENV) appears to have a two stage activation process where low pH acts as an initial trigger in early endosomes and anionic lipids in late endosomes act as the secondary trigger to enable cellular entry [52]. Severe acute respiratory syndrome coronavirus (SARS-CoV) requires proteolytic activation of envelope glycoproteins by cathepsins, which are optimal at acidic pH. It appears that SARS-CoV only require access to low pH compartments for optimal function of the proteases, rather than for low pH-induced conformational changes to the viral envelope glycoproteins [53]. Ebola virus (EBOV) has a similar dependency on cathepsins to activate the envelope glycoproteins, and like SARS-CoV, only requires access

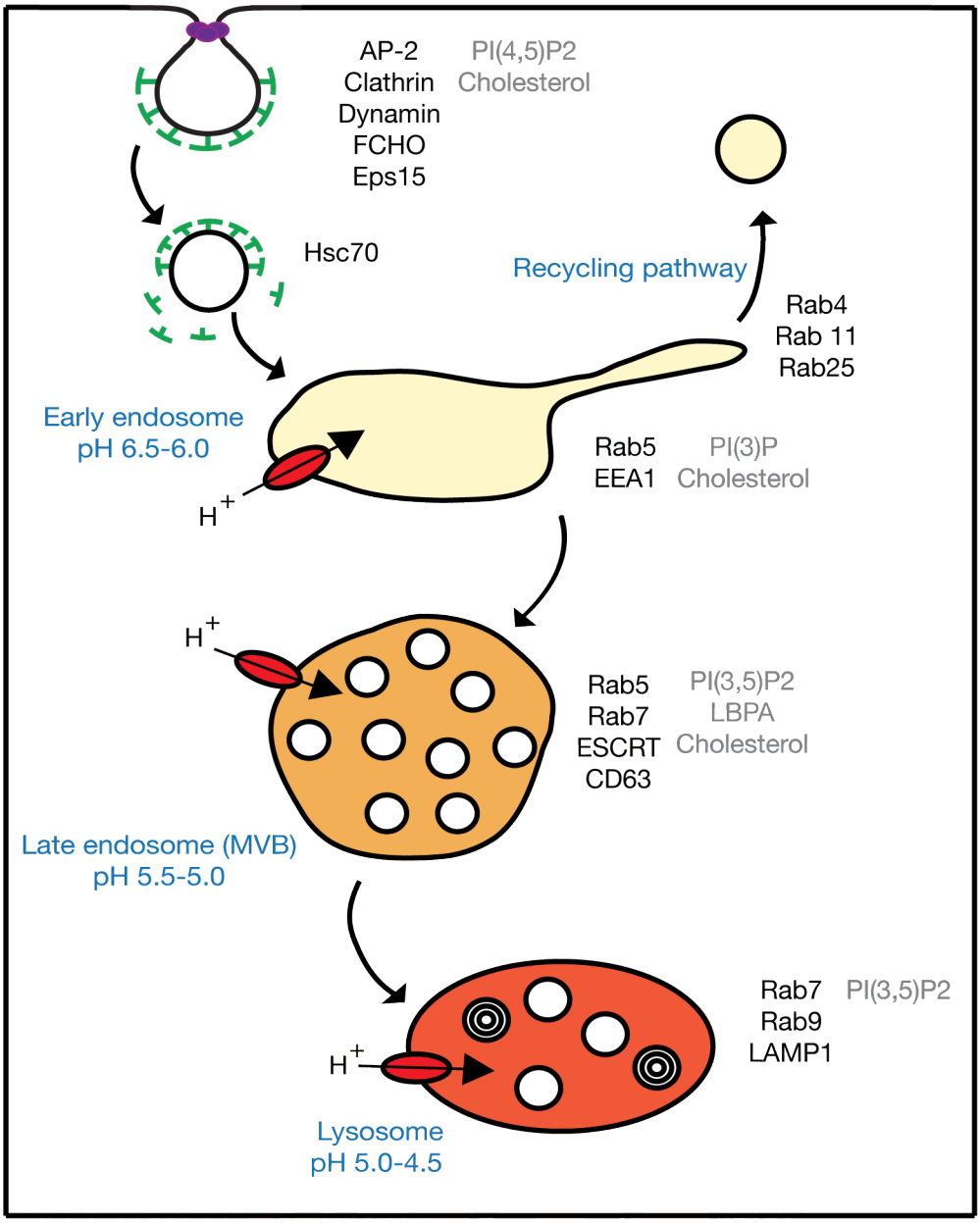

Figure 1.2: **Summary of the endosomal maturation pathway.** Clathrin-mediated endocytic uptake from the cell surface delivers cargo into the endosomal system. The organelles of this system can be broadly divided into early, recycling and multivesicular endosomes, along with lysosomes. Various different cellular proteins and lipids define these different organelles and regulate their function, with examples of these given. See Section 1.1.1 for further discussion of endosomal maturation. Details adapted from [22, 34, 38, 44].

to low pH compartments for optimal function of these proteases [54]. However, EBOV appears to have an interesting requirement for multiple intracellular receptors to facilitate entry along with proteolytic processing. Both of the late endosomally localised Niemann-Pick C1 [55] and two pore calcium channel [56] proteins are required for EBOV entry into cells. Lassa fever virus (LASV) has a similar requirement for delivery into late endosomal compartments to engage an intracellular receptor molecule. LASV initially binds to the cell surface through interactions with α-dystroglycan [57], and is internalised through a macropinocytic mechanism [58]. Upon transit through the endosomal system, low pH induces conformational changes to the LASV envelope glycoprotein allowing interaction with LAMP1 [59], and subsequent membrane penetration. There are a variety of triggers used by viruses to promote their cellular entry.

1.1.2 Virus-cell membrane fusion

Regardless of the various triggers required by enveloped viruses, and the different routes that are used to receive these, cytosolic entry is achieved by fusion of viral and cellular membranes. Viral envelope glycoproteins mediate not only cell attachment but also the membrane fusion reaction which results in coalescence of viral and cellular membranes to produce a fusion pore, which allows delivery of viral genetic material into the cytosol. The envelope glycoproteins responsible for merging lipid membranes are termed fusion proteins and come in a variety of structures. Some viruses have only a single envelope glycoprotein which is responsible for regulating cell attachment and membrane fusion (e.g. vesicular stomatitis virus G protein [VSV-G]), while other viruses have a single glycoprotein which is proteolytically cleaved to allow receptor engagement and membrane fusion (e.g. HIV-1 and IAV). Some viruses produce two glycoproteins which play different roles in the entry pathway (e.g. alphavirus E1 [membrane fusion] and E2 [cell attachment] and paramyxovirus H, HN or G [attachment] and F [membrane fusion] [60]). There can also be even greater complexity; herpes simplex virus-1 (HSV-1) has five glycoproteins with various roles (gB, gC, gD, gH and gL) although one of these (gC) is non-essential for infection [61]. Poxviruses have even more complexity, encoding eleven different proteins which form the entry-fusion complex, along with four proteins which mediate cell attachment [62]. Viral fusion proteins interact with the target membrane through a short hydrophobic

sequence of amino acids, referred to as the fusion peptide [63]. Overall, fusion proteins can be divided into three sub-categories, type I, II and III (see [24, 64] for more detailed reviews).

Type I fusion proteins

Type I fusion proteins are characterised by their production as trimeric inactive precursors that are proteolytically activated. The type I fusion proteins are predominantly composed of α helices. The hemagglutinin (HA) protein of IAV is a highly characterised example. HA is initially produced as a fusion inactive precursor, HA0, which is assembled into a metastable trimeric complex in the endoplasmic reticulum (ER) of infected cells. Upon exit from the ER into the secretory pathway, HA0 is cleaved by cellular proteases [65], forming a disulphide linked C-terminal membrane anchor, HA2, and an N-terminal HA1, which remain associated in a trimeric complex within membranes [66, 67]. Low pH causes the HA1 heads of the trimer to dissociated and move apart to expose the fusion peptide of HA2, which can insert into target membrane to drive fusion. These low pH-induced conformational changes are irreversible. Additional examples of type I fusion proteins include the HIV-1 Env protein, which is initially synthesised as a gp160 protein which is proteolytically cleaved into gp120 and gp41 (analogous to HA1 and HA2, respectively) and and the F protein of paramyxoviruses.

Type II fusion proteins

In contrast to type I fusion proteins, type II fusion proteins are produced as part of a complex containing an N-terminal chaperone protein. The type II fusion proteins are predominantly composed of β strands. A pertinent example of a type II fusion protein is E1 of SFV. When initially synthesised in an infected cell, the E1 protein forms a heterodimer with p62. Interaction of p62 with E1 produces a fusion incompetent complex [68] that is protected from premature activation in low pH compartments of the secretory system. En route to the cell surface, p62 is proteolytically processed to E2 and E3, which remain associated with E1 [69]. E2 is a transmembrane protein, while E3 is a small peptide on the periphery of the complex. E3 remains associated with E1/E2 on SFV particles, but dissociates from Sindbis virus (SINV), and is unnecessary for fusion [70]. Upon receiving

a low pH trigger, E2 dissociates from the complex [71, 72], allowing E1 to undergo conformational changes, insert into target membrane and become homotrimeric, to ultimately promote fusion [72–74]. (See Section 1.2 for further discussion). As with type I fusion machinery, the low-pH induced conformational changes are irreversible. Flaviviruses also have type II fusion machinery.

Type III fusion proteins

Type III fusion proteins do not undergo proteolytic activation during their synthesis, nor are they produced with a chaperone protein, separating them from both type I and type II fusion proteins. There are other structural differences between type III and the other two classes, but they are arranged as a trimer on the surface of cellular and viral membranes. The type III fusion peptide faces the virus membrane, rather than being buried in the envelope glycoprotein, as for type I. Upon receiving appropriate triggers, conformational changes occur to extend and rotate the fusion protein, allowing interaction with target membrane. Example for the type III fusion proteins are the G protein VSV [75] and the gB protein of HSV-1 [76]. The low pH-induced changes to VSV-G are reversible, in contrast to type I and II fusion machineries.

Membrane fusion

Given the various different structures of viral fusion proteins, the sequence of events underlying membrane fusion are believed to be remarkably similar (see Fig. 1.3 for a schematic of type II fusion protein mediated fusion). Upon receiving the appropriate trigger (low pH for alphaviruses) to initiate membrane fusion, individual viral envelope glycoprotein complexes undergo large conformational changes to extend and interact with the target membrane, through the fusion peptide (Fig. 1.3 C). Either before, or after the initial insertion, fusion proteins trimerise and form an intermediate, pre-hairpin structure between the two membranes (Fig. 1.3 D). This intermediate subsequently folds back on itself to a more energetically favourable conformation to produce a hairpin structure, that pulls the two membranes into close apposition. The energy released by the unfolding and re-folding of the fusion proteins is enough to overcome the thermodynamic barrier of membrane fusion, and produces a hemifusion intermediate (Fig. 1.3 E). At the stage of hemifusion,

lipid mixing between outer leaflets has occurred, but the contents of the two systems are still separated by the inner leaflets of each bilayer [77]. After hemifusion, a fusion pore can start to open. The opening of such a pore can be transient, or more long lived [77]. However, once the pore has enlarged and become established, it is irreversibly open and the viral genomic material can escape into the cytosol to initiate infection (see [24, 64, 78–80] for various reviews. More specific examples for SFV are provided in Section 1.2).

Virus entry summary

Without the ability to enter cells, viruses would be unable to replicate. The lipid bilayer of cells imposes a physical barrier to this process, but viruses have evolved to subvert the normal functioning of cells to overcome this. For enveloped viruses, the process of membrane fusion allows penetration of lipid bilayers, and delivery of viral genetic material into a cell. The membrane fusion reaction is regulated by viral fusion proteins, and initiated after receiving appropriate triggers from the cellular environment. For some viruses this trigger can be the binding of cell surface receptor proteins. However, the vast majority of enveloped viruses have adapted to subvert the endocytic mechanisms of the cell, allowing them to use the changing environment of the endocytic system to regulate their penetration to the cytosol and provide other advantages as discussed previously. Regardless of the required trigger, upon activation, the viral envelope glycoproteins undergo large conformational changes to insert into a target membrane, while remaining anchored in the viral membrane. Subsequently, the re-folding of these proteins brings the two membranes into close apposition to allow them to fuse, via a hemifusion intermediate, and produce a pore through which viral genetic material can escape. The routes of virus entry into cells by CME and pH-induced membrane fusion have been introduced as these are the most pertinent to the main virus system used in the work presented in this thesis, SFV.

1.2 Semliki Forest virus

The main virus used throughout the work on IFITM-mediated inhibition of viral infection presented in this thesis is the alphavirus SFV, of the *Togaviridae* family. SFV was first isolated in the Semliki forest of Uganda in 1944 [81]. SFV, and other alphaviruses are small

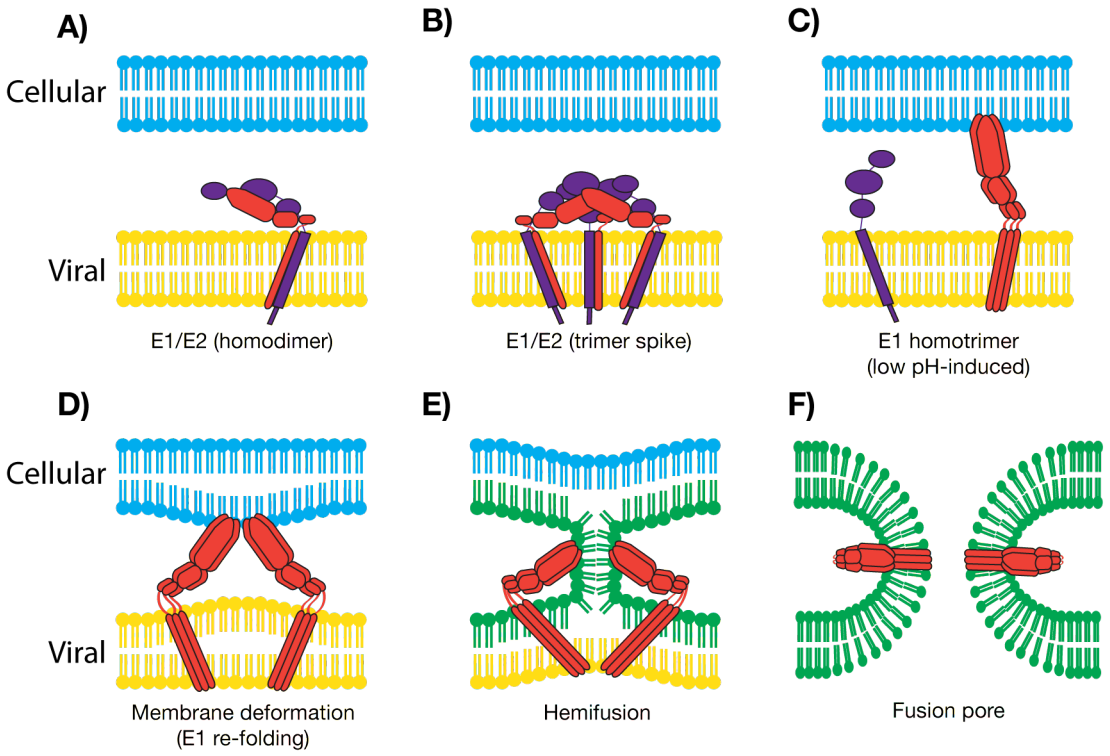

Figure 1.3: **A schematic of membrane fusion mediated by type II fusion proteins.** A) For clarity, the representation of an individual E1/E2 heterodimer on the surface of a viral particle (E1 in red and E2 in purple). B) E1/E2 heterodimers are found as a trimeric complex on the surface of a virus particle. C) Upon receiving appropriate triggers (in the case of SFV, low pH), the E1/E2 complex dissociates allowing the E1 protein to undergo a large conformational change to extend and interact with target membrane through the fusion peptide. D) As part of the conformational changes E1 forms homotrimeric complexes. These complexes begin to fold back on themselves, pulling the two membranes into close apposition. E) A hemifusion intermediate is formed through the mixing of lipids of the outer viral and cellular membrane leaflets. The re-folding of the fusion protein provides the energy to overcome the thermodynamic barrier of membrane fusion. F) Small, transient fusion pores can form following hemifusion and can eventually resolve into a full fusion pore by the coalescence of the inner viral and cellular membrane leaflets. Content mixing can then occur between the two systems, allowing deposition of viral genetic material into the cytosol. Image adapted from [64].

(∼70 nm diameter), icosahedral viruses with RNA genomes of ∼12 kb [82, 83]. These viruses are encased in a host derived lipid bilayer, with the E1/E2 envelope glycoproteins protruding on the surface. The icosahedral symmetry and ordered arrangement of the virus gives rise to 80 copies of E1/E2 heterodimers that exist as trimers on the surface of SFV and other alphaviruses [82–84]. Beneath the lipid bilayer, connected to the E2 protein, is the viral capsid (240 copies), in which a single strand of positive sense RNA is found (the nucleocapsid).

SFV was the first virus shown to use CME for internalisation from the cell surface and delivery into the endosomal system for infection [45, 85], following attachment to cells through the E2 protein [86, 87]. The importance of CME for SFV infection has been shown through various approaches such as inhibition of CME with monoclonal antibodies [88] or dominant negative mutants of regulators of CME [89, 90]. While well established as being internalised by CME, no cell surface receptor has been conclusively defined for SFV. Major histo-compatilibity complex (MHC) antigens were suggested as a surface receptor [91], but the virus has also been found to replicate in cells that lack MHC expression [92]. SFV can infect a very broad range of host cells, and therefore likely has promiscuous receptor usage, or targets highly conserved molecules [83].

Following CME from the cell surface, SFV is delivered into endosomes and uses the low pH of these compartments as a trigger for penetration into the cytosol [45, 93–96]. Low pH has been suggested as the only necessary trigger for SFV membrane penetration because the virus can fuse with protein-free liposomes following low pH treatment [47]. SFV also needs no other endosomal-specific triggers as low pH treatment of cell surface bound virus can allow cytosolic penetration [47], at least in some cell types [97].

As discussed in Section 1.1.2, SFV produces type II fusion machinery made of the E1 and E2 envelope glycoproteins. Following delivery into endosomes of sufficiently low lumenal pH to activate the fusion machinery (pH $\leq$ 6.2; [45–48]) the E2 protein dissociates from the E1 protein [71, 72], allowing for extension of the E1 fusion peptide and insertion to target membranes [98]. Once inserted into the target membrane, E1 protein forms homotrimeric complexes which become insensitive to digestion with trypsin [96, 98]. The interaction of E1 with a target membrane depends on the presence of cholesterol and sphingomyelin [99, 100]. As in other fusion mechanisms, E1 then folds back on itself into

a post-fusion helical bundle [98]. Lipid mixing between viral and endosomal membranes can be detected by spread of lipid dyes such as pyrene [101]. Hemifusion intermediates produced by E1-induced fusion have also been detected in cell-cell fusion assays [102]. It therefore appears that as described previously, membrane fusion induced by SFV E1 proceeds through hemifusion intermediates before a full fusion pore allows for cytosolic access. Experimental evidence suggests the nucleocapsid is released into the cytosol and then uncoats through interaction with ribosomes [103]. Once uncoated, the positive sense RNA genome can itself interact with ribosomes and start the replication cycle to produce progeny virions (see Fig. 1.4 for subsequent detail to the SFV life cycle).

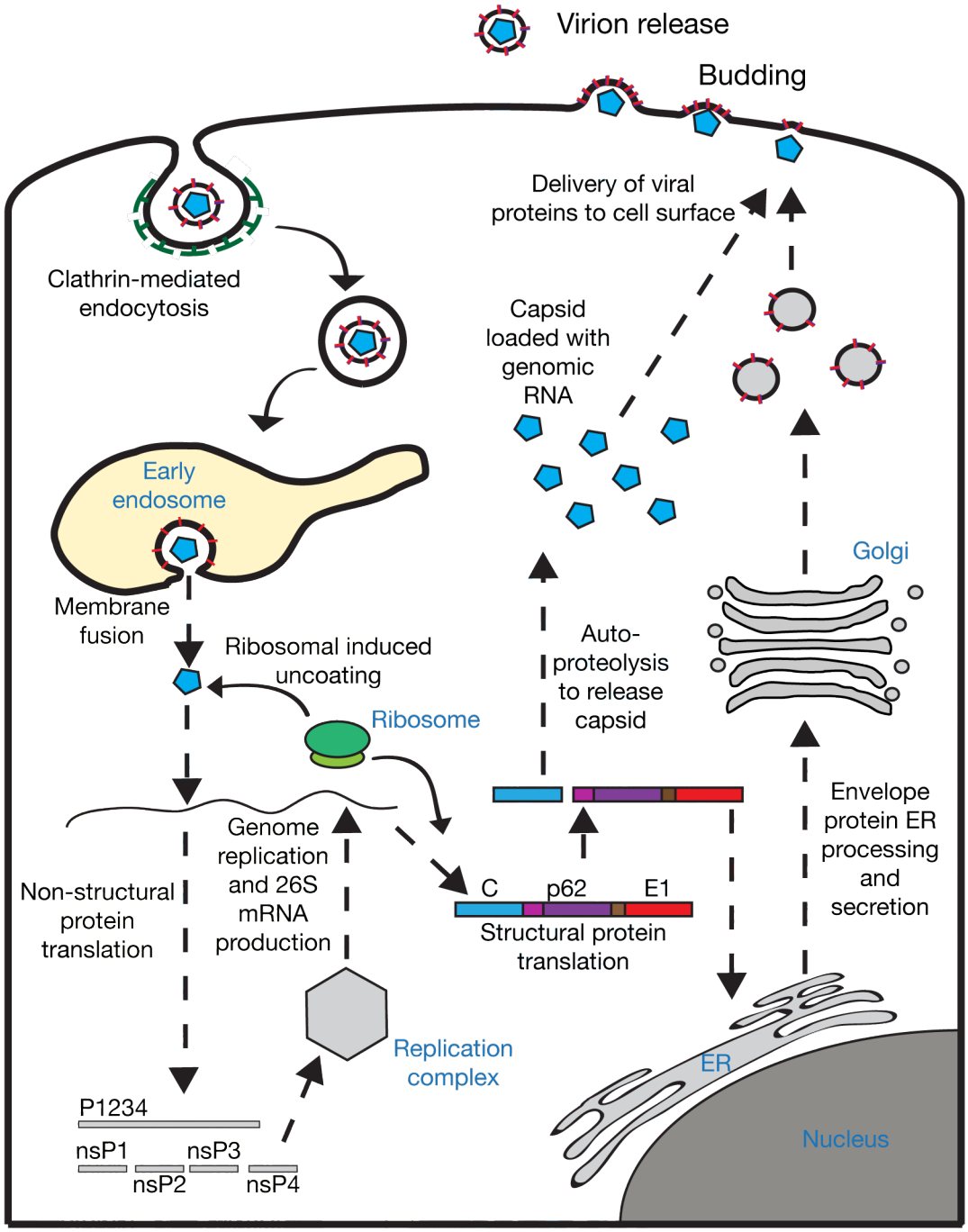
Virion release
Budding
Delivery of viral proteins to cell surface
Clathrin-mediated endocytosis
Capsid loaded with genomic RNA
Early endosome
Golgi
Membrane fusion
Ribosomal induced uncoating
Ribosome
Auto-proteolysis to release capsid
Envelope protein ER processing and secretion
Genome replication and 26S mRNA production
Non-structural protein translation
C
p62
E1
Structural protein translation
Replication complex
ER
P1234
nsP1
nsP3
nsP2
nsP4
Nucleus

Figure 1.4: **SFV viral life cycle.** A schematic representation of the SFV viral life cycle. Following attachment to cells, SFV is internalised by clathrin-mediated endocytosis (clathrin coat proteins displayed in dark green). Clathrin-coated vesicles uncoat after releasing from the plasma membrane, and are delivered into the endosomal system. SFV particles will then be subject to the changing environment within the lumen of endosomes. Fusion between viral and cellular membrane is stimulated at pH $\leq$ 6.2, promoting release of the viral nucleocapsid into the cytosol. The nucleocapsid is uncoated through an interaction with ribosomes (displayed in light green), releasing the positive sense RNA genome. Translation can be initiated from this genomic RNA to produce the viral non-structural proteins (nsPs). These nsPs then regulate the replication of the genome and production of a sub-genomic 26S mRNA, from which the structural proteins are produced (also see Fig. 1.5). The structural proteins are initially translated as a large polyprotein which is co-translationally cleaved by the autoproteolytic activity of the capsid (C) protein. The release of capsid exposes a signal peptide sequence that directs insertion of the envelope proteins into the endoplasmic reticulum (ER) membrane. The envelope proteins are processed in the ER to form heterodimeric complexes of p62/E1. These heterodimeric complexes are trafficked from the ER to the Golgi apparatus and continue through the secretory pathway to be delivered to the plasma membrane. Through the secretory pathway p62 is proteolytically cleaved to produce E2 and E3 which both remain associated with E1. The capsid is loaded with genomic RNA and similarly delivered to the plasma membrane where it can associated with envelope protein complexes. These interactions promote the outward budding of the plasma membrane until virons are released into the extracellular space to spread to new target cells. Image adapted from [83].

The SFV structural proteins are produced as a single polypeptide from a subgenomic RNA (Fig. 1.5). This polyprotein contains the capsid and envelope proteins, along with a small protein called 6K (whose function is poorly defined). The capsid protein has autocatalytic activity to allow release of this protein from the polypeptide during translation. The released capsid can then associate with genomic RNA in the cytosol to produce viral nucleocapsids. Cleavage of capsid exposes a signal peptide sequence at the N-terminal end of the envelope proteins, which dictates co-translational insertion to the ER membrane [104, 105]. The E1 and p62 proteins are processed in the ER along with 6K. E1 and p62 form heterodimeric complexes in the ER. This processes is dependent upon the E3 protein segment of p62 as replacement of this amino acid sequence results in loss of heterodimeric complexes [106]. The envelope proteins are subsequently delivered through the secretory system to the plasma membrane. During this transit the p62 protein is cleaved to E2 and E3 by cellular furin [69, 107]. Again, E3 is necessary through this transport step to provide protection from premature activation of the fusion machinery in the low pH compartments of the secretory pathway [108]. Once delivered to the plasma membrane, E2 proteins form a direct interactions with the nucleocapsid. This interaction promotes

the formation of virions, and there appears to be a requirement of cholesterol for viral budding from the cell surface ([109–111], also see [82, 83, 112] for reviews and Fig. 1.4).

A wealth of experimental information has been generated describing the mechanisms used by SFV to enter into cells. This alphavirus therefore provides a powerful tool with which to study IFITM proteins, cellular antiviral factors capable of blocking virus entry. SFV also has advantages in the ease with which it can be produced to high titres and its safety to work with. Additionally, much work defining IFITM antiviral activity has been performed with IAV (see Section 1.3.2), which enters cells by fusion with late endosomes, while SFV enters cells by penetration of early endosomes. Using SFV as a new model system therefore allows for the development of understanding of any similarities and differences between inhibition of different viruses, especially with regards to the different sites of entry into cells.

1.3 IFITM proteins

The human IFITM proteins were first identified over 30 years ago by virtue of their induction by interferon treatment [113]. The proteins were originally denoted 9-27 (IFITM1, also referred to as Leu13 antigen), 1-8D (IFITM2) and 1-8U (IFITM3). Early work on IFITM1 suggested potential roles in both B and T cells [114–119], while murine Ifitms were suggested to have developmental functions [120–123]. The importance of IFITM1 function in adaptive immune cells remains unclear, and the role of Ifitm proteins in murine development has been questioned by the fact that *Ifitm* knockout mice show no developmental defects [124].

While characterised as ISGs, the first suggestion of an IFITM protein having antiviral activity was not made until 1996 when IFITM1 was found to inhibit replication of VSV (but not IAV), albeit less potently than another ISG, MxA [125]. However, it was not until 2009 that the IFITM proteins started to be studied intensively because of their antiviral function [7]. Brass *et al.* designed a genome-wide siRNA screen to detect cellular factors involved in the replication of IAV in the U2OS cell line [7]. Amongst many other hits, the knockdown of IFITM3 was found to enhance IAV infection of U2OS cell. Further investigation validated this result in various other cell lines [7]. Moreover, it was

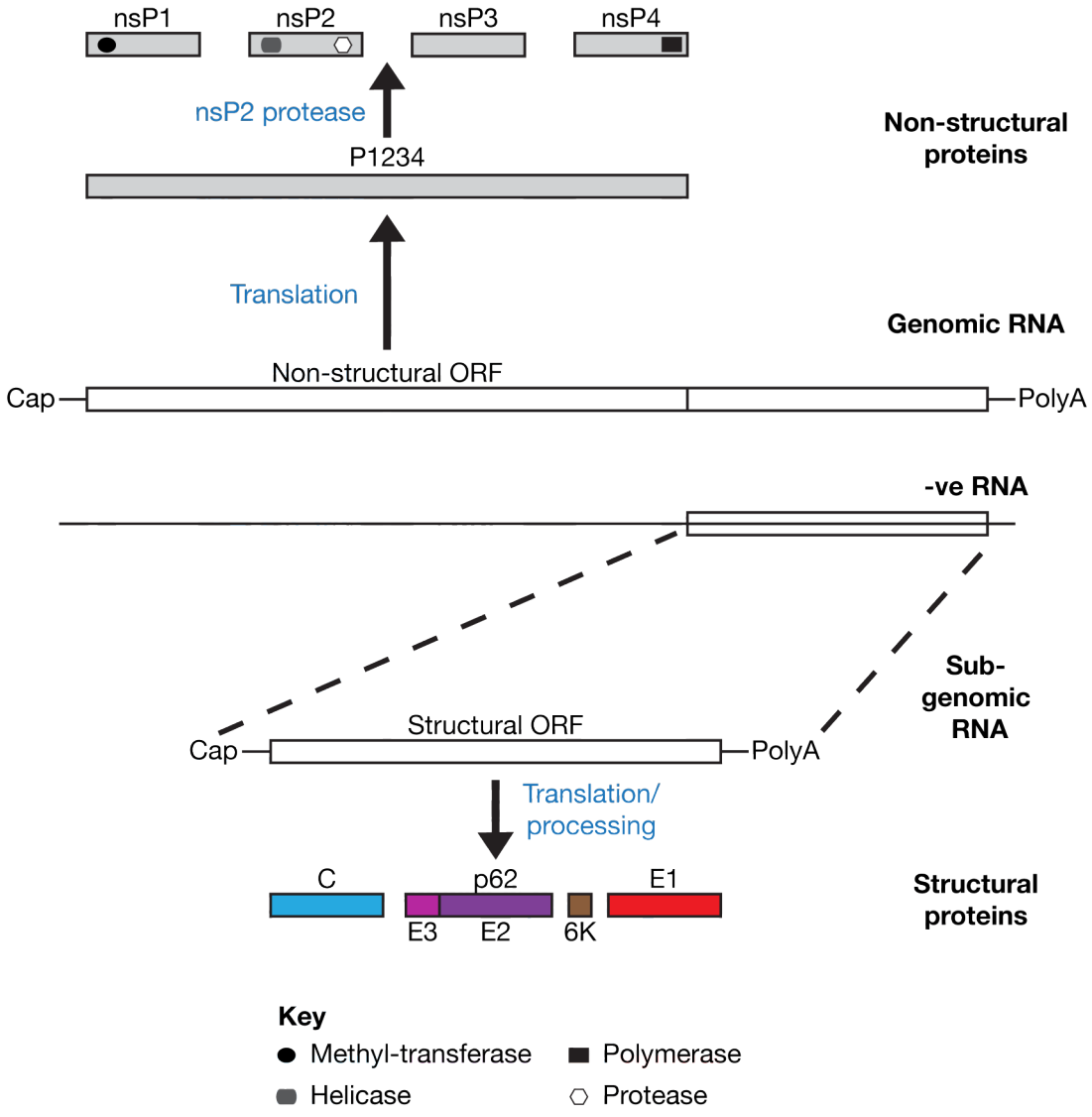

Figure 1.5: **SFV genomic structure and protein production.** A schematic representation of the SFV genomic structure and how the various structural and non-structural proteins are produced. The genomic RNA has an 5' 7-methylguanosine cap (Cap) and a 3' polyadenylated tail (PolyA). Upon release into the cytosol, the positive sense genomic RNA associates with ribosomes and the P1234 polyprotein is translated. The P1234 polyprotein is cleaved into the non-structural proteins (nsP) by the proteolytic activity of the nsP2 unit. The non-structural proteins form the RNA dependent RNA polymerase that produces negative (-ve) sense RNA from the template genomic RNA. From this -ve sense RNA the subgenomic 26S mRNA encoding the structural proteins is produced. These proteins are initially translated as a polyprotien. Capsid (C) has autoproteolytic activity and can cleave the growing polypeptide chain. This cleavage releases capsid and exposes a signal peptide sequence at the N-terminal end of the envelope proteins that allows co-translational insertion to the ER membrane. Signalses cleave after p62 and again after the small peptide 6K, releasing E1. The p62 protein is later cleaved in the secretory pathway to produce E2 and E3 which associated with E1 to form the viral envelope glycoprotein complex. Image adapted from [82, 83]. Also see Fig. 1.4.

also demonstrated that overexpression of IFITM3, as well as IFITM1 and IFITM2, could suppress replication of IAV *in vitro*. During this initial characterisation, the IFITM proteins were suggested to impact viral entry by virtue of their ability to inhibit infection of HA-pseudotyped retroviral particles. This antiviral function was not specific to IAV as various members of the flavivirus family were also shown to be inhibited. However, no antiviral activity was detected against the retrovirus murine leukaemia virus (MLV) nor arenaviruses [7]. Since the work of Brass *et al.* many different viruses or pseudotyped particles have been found to be inhibited by IFITM proteins (see Tables 1.1 and 1.2 and Section 1.3.2), but how the IFITM proteins inhibit such a broad array of viruses is not understood.

1.3.1 IFITM evolution

It has been suggested that the *IFITM* genes arose through gene duplication events early in vertebrate evolution [126]. This early evolution in the vertebrate lineage is supported by identification of an *IFITM*-like gene in lampreys [126]. The human genome contains three IFN-inducible *IFITM* genes, however in addition to *IFITM1*, *2* and *3* (IFN-induced) there are two additional *IFITM* genes, *IFITM5* and *IFITM10*. *IFITM1, 2, 3* and *5* are found clustered within a 26 kb region of chromosome 11, while *IFITM10* is located 1.4 Mb away [126–128]. IFITM5 is expressed primarily in osteoblasts and has roles in bone mineralisation [129]. Little is known about the function of *IFITM10* which, like *IFITM5*, lacks a functional IFN-responsive sequence element. It is unknown whether IFITM5 or IFITM10 have antiviral function. The murine genome encodes two further *Ifitm* genes (*Ifitm4 and Ifitm6*), but most research has focused on the murine orthologues of *IFITM1, 2* and *3*. Various other mammalian species have been found to have *IFITM* genes and antiviral function has been demonstrated for some of these [126–128, 130–133]. IFITMs have also been identified and shown to have antiviral activity in some birds [134, 135].

The IFITMs are part of a larger protein family known as the dispanins which is found in both eukaryotes and prokaryotes [127]. Interestingly, *Mycobacterium* IFITM-related proteins have been proposed to have antiviral activity when expressed in human cells [136]. This dispanin family is defined by the presence of a highly conserved CD225 domain, which in the IFITMs occupies the central portion of the proteins (Fig. 1.6). In terms of

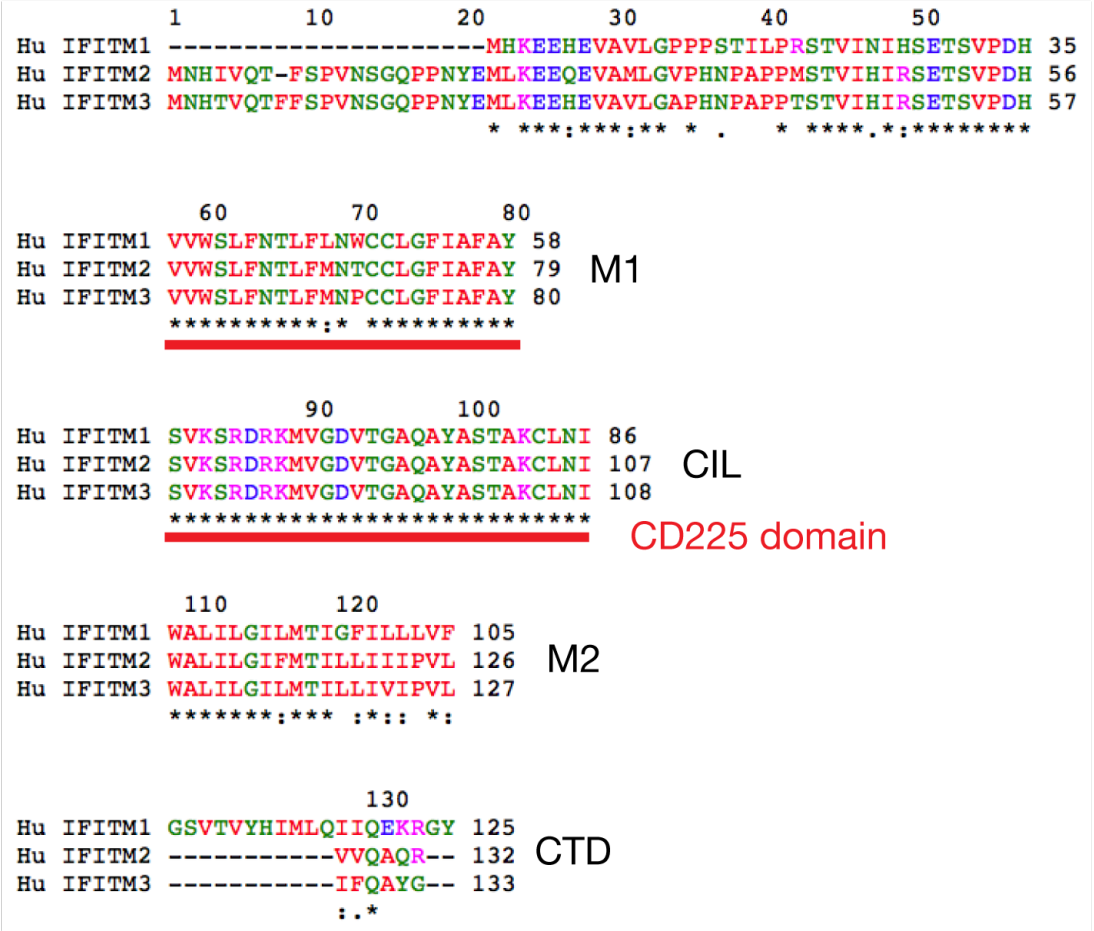

Figure 1.6: **Sequence alignment of human IFITM1, 2 and 3.** The amino acid sequences of IFITM1, IFITM2 and IFITM3 were aligned using the ClustalOmega tool (EMBL-EBI; `http://www.ebi.ac.uk/Tools/msa/clustalo/`). * denotes identical amino acids, : and . represent similarities between amino acids. The sequences have been divided into the domains of the IFITM proteins; NTD (N-terminal domain), M1 (membrane domain 1), CIL (conserved intracellular loop), M2 (membrane domain 2), CTD (C-terminal domain). See Fig. 1.8 for diagrams of the topological structures that have been proposed for IFITM proteins. The position of the highly conserved CD225 domain is denoted.

their amino acid sequences, IFITM2 and IFITM3 are very similar, with ∼91% sequence identity. Comparatively, IFITM1 shares ∼81% and ∼84% identity with IFITM2 and 3, respectively. Since the CD225 domain is so highly conserved, the variations between the IFITM amino acid sequences reside in the N- and C-terminal domains (NTD and CTD). IFITM1 has a 21 amino acid truncation compared to IFITM3 (20 amino acid compared to IFITM2) at the NTD, while the CTD of IFITM1 is longer than those of IFITM2 and IFITM3 (see Section 1.3.3 for a discussion of the implications of these differences and Fig. 1.6 for sequence alignments).

1.3.2 IFITM antiviral activity

In vitro

It has become well established that the IFITM proteins can act as broad-spectrum antiviral factors in cell culture. Overexpression, knockdown and genetic knockout have all been used to investigate antiviral activity against both full viruses and viral particles pseudotyped with various envelope glycoproteins. A summary of published literature on IFITM-sensitive viruses is provided in Tables 1.1 and 1.2. Since infection by pseudotyped virus particles can be inhibited by IFITM proteins this gave the first indications that these proteins could inhibit viral entry. However, there remains a lack of detailed understanding regarding the mechanism(s) of antiviral activity. It is also unclear why some viruses are insensitive to IFITM-mediated inhibition (Table 1.3), and what dictates the sensitivity of different viruses to different IFITMs.

Family	Viruses	System	Restriction	References	Notes
Alphavirus	SINV	L	M3 > M2	[16]	No IFITM1 restriction
	SFV	L	M3 > M2	[16]	No IFITM1 restriction
Bunyavirus	ANDV	L	M1 = M2 = M3	[137]	
	HTNV	L	M1 = M2 = M3	[137]	
	LACV	L	M1 = M2 = M3	[137]	
	RVFV	L	M2 = M3	[137]	No IFITM1 restriction
Coronavirus	229E	P	M1 > M3 > M2	[138]	
	MERS	P	M2	[138]	M1 and M3 not statistically significant
	NL63	P	M3 > M1	[138]	M2 not statistically significant
	SARS	P	M1, M2 and M3	[138–141]	Variability between studies (M2 maybe highest)
Filovirus	BDBV	L/P	M1 = M2 = M3	[142]	
	EBOV	L/P	M1, M2 and M3	[139, 142, 143]	Variability between studies
	LLOV	L/P	M2 = M3	[142]	No M1 inhibition
	MARV	L/P	M1, M2 and M3	[139, 142]	Variability between studies
	RESTV	L/P	M2 > M3 > M1	[142]	
	SUDV	L/P	M2 = M3 > M1	[142]	
	TAFV	L/P	M2 > M3 > M1	[142]	
Flavivirus	DENV	L	M1 = M3 > M2	[144]	
	HCV	L/P	M1 > M2 = M3	[145, 146]	
	OMSK	P	M3 > M1 > M2	[7]	
	WNV	P	M3 > M1 > M2	[7, 147]	[147] no M1 inhibition
	YFV	P	M3 > M1 > M2	[7]	
	ZIKV	L	M3 > M1 = Y20A	[148]	M2 not tested

Table 1.1: Summary of IFITM restricted viruses (part 1). A summary of published literature on IFITM restriction of different viruses (M1, M2 and M3 represent IFITM1, 2 and 3, respectively). Citations refer to work in cell culture using over expression systems only (human and murine IFITMs included). The viruses have been categorised based on viral family. The systems used have been denoted, L; 'live' full virus, and P; pseudotyped virus. Attempts have been made to generalise the sensitivity of each virus to different IFITMs, if no consensus could be determined a note has been made to explain the reason. See List of Abbreviations for full virus names.

Family	Viruses	System	Restriction	References	Notes
Paramyxovirus	RSV	L	M1 = M3 > M2	[149]	
Picornavirus	FMDV	L	M3*	[149]	*Only swine M3 tested
Orthomyxovirus	IAV	L/P	M3 > M2 > M1	[7, 12–14, 132–135, 138–140, 142–144, 150–160]	
Reovirus	RV	L	M3	[161]	M1 and M2 not tested
Retrovirus	JSRV	P	M1 > M2 = M3	[13]	
	HIV-1	L	M1, M2 and M3	[133, 162–169]	Variability on strain
	HIV-2	L	M2 > M3 > M1	[168]	
	SIV	L	M1, M2 and M3	[168]	Variability on strain
Rhabdovirus	LBV	P	M3 > M2	[132, 134]	M1 not tested
	MOKV	P	M3	[132]	M1 and M2 not tested
	RABV	P	M3 > M2	[132, 134]	M1 not tested
	VSV	L/P	M3 > M1 > M2	[7, 12–14, 138, 142, 143, 146, 152, 153, 156, 157, 163, 170]	Rarely tested in detail
	WCBV	P	M3	[132]	M1 and M2 not tested

Table 1.2: Summary of IFITM restricted viruses (part 2). A summary of published literature on IFITM restriction of different viruses (M1, M2 and M3 represent IFITM1, 2 and 3, respectively). Citations refer to work in cell culture using over expression systems only (human and murine IFITMs included). The viruses have been categorised based on viral family. The systems used have been denoted, L; 'live' full virus, and P; pseudotyped virus. Attempts have been made to generalise the sensitivity of each virus to different IFITMs, if no consensus could be determined a note has been made to explain the reason. See List of Abbreviations for full virus names.

Family	Viruses	System	References	Notes
Adenovirus	AdV5	P	[141]	
Arenavirus	MACV	P	[7, 138, 139, 142, 144, 152]	
	JUNV	L	[137]	
	LASV	P	[7, 14, 138, 140, 142, 152]	
	LCMV	P	[7, 153]	
Bunyavirus	CCHFV	L	[137]	
Coronavirus	OC43	L/P	[140]	M2 and M3 enhance, M1 no impact
Herpesvirus	HCMV	P	[141, 171]	
Papilomavirus	HPV16	L/P	[141]	M1 and M3 enhance, M2 no impact
Paramyxovirus	SeV	L	[155]	
Reovirus	Reovirus ISVPs*	L	[161]	
Retrovirus	MLV	L/P	[7, 138, 139, 142, 143, 146, 152, 153]	

Table 1.3: Summary of viruses not restricted by IFITM proteins. A summary of published literature on viruses shown to not be restricted by IFITM proteins. Citations refer to work in cell culture using over expression systems only (human and murine IFITMs included). The viruses have been categorised based on viral family. The systems used have been denoted, L; 'live' full virus, and P; pseudotyped virus. A small subset of viruses have been shown to have infection enhenced in IFITM expressing cells and details of this have been included as 'notes.' See List of Abbreviations for full virus names. * Reovirus ISVPs (infectious subvirion particles) do not require endosomal proteases for cellular entry. ISVP entry is therefore pH-independent, in contrast to reovirus entry.

Inhibition of pseudotyped virus particles strongly suggested IFITM proteins interfere with viral entry. However, the work of Feeley *et al.* first started to develop a detailed understanding of where in the IAV entry pathway IFITM proteins are targeting [12]. This work made use of an IAV engineered to produce green fluorescent protein tagged nuclear protein (GFP-NP) and demonstrated that IAV particles were able to bind to IFITM3 expressing cells and be internalised, but that the GFP-NP did not reach the nucleus. Instead, the GFP signal appeared to accumulate in endosomal compartments, suggesting that IFITM3 expression was blocking release of IAV genetic material into the cytosol. This was further confirmed by the use of β-lactamase assays which showed that IFITM3 expression could block deposition of viral contents into the cytosol, suggesting IFITM3 may inhibit viral-cell membrane fusion [12].

As discussed previously, viral-cell membrane fusion is achieved through a complex series of events, from initial interaction of fusion proteins with target membrane, through a hemifusion intermediate, and culminating in a fusion pore. It has been suggested that IFITM expression can inhibit viral penetration into the cytosol, by blocking the establishment of hemifusion [13]. This proposal was made based on assays using cell-cell fusion, where donor cells expressing the envelope glycoproteins of a virus are loaded with aqueous dye and then mixed with target cells lacking viral protein. In the work of Li *et al.* [13], cells expressing representatives of each class of fusion protein were used (IAV and JSRV [type I], SFV [type II] and VSV [type III]). Upon providing appropriate triggers (e.g. low pH), the envelope glycoprotein can be activated to promote fusion of target and donor cells (fusion from within), allowing the spread of aqueous dye into the target cells. Li *et al.* made use of a cold arrested state in which low pH treatment at 4℃ can induce hemifusion, but not full fusion [13]. The subsequent raising of temperature to 37℃, or treating with chlorpromazine (CPZ) allows for the formation of a fusion pore, through which dye can spread. Working with the envelope glycoproteins of the Jaagsiekte sheep retrovirus (JSRV) and IAV, they found that in control cells, following the generation of a cold arrested state, subsequent treatments could allow for dye spread. However, when target cells were expressing IFITMs, CPZ treatment resulted in comparatively reduced dye transfer. Raising the temperature to 37℃ gave a greater degree of dye spread than CPZ treatment, but this was still lower than the dye transfer seen with target cells lacking

IFITM expression. Additionally, it was shown that treating cells with oleic acid could rescue the IFITM-mediated inhibition of cell-cell fusion. Hemifusion is promoted by negative curvature of lipid membranes, and oleic acid induces greater negative curvature, suggesting that by promoting hemifusion, IFITM-mediated inhibition can be overcome. This inhibition of the establishment of hemifusion intermediates suggests that the IFITM proteins alter the properties of the membrane they reside in; indeed, it was suggested that the presence of IFITM proteins in cell membranes reduces their fluidity by Li *et al.* [13], and others [156], suggesting a higher energy barrier to the establishment of hemifusion intermediates.

The work of Li *et al.* focused on cell-cell fusion [156]. There are differences between the fusion of two plasma membranes and the fusion of viral and endosomal membrane. Firstly, the level of membrane curvature could be higher when a virus and endosome fuse than when cells fuse. Secondly, the lipid compositions of the plasma membrane and endosomes is different [34, 172]. If IFITM proteins modulate membrane properties, the composition may be an important consideration. Taking a different approach to study how IFITM proteins block viral entry, Desai *et al.* used DiD-labelled virus [14], a well established system for studying membrane fusion. DiD is a lipophilic dye whose fluorescence self-quenches at high concentration, for instance when loaded into the envelope of a viral particle (IAV in the work of Desai *et al.*). At lower concentrations, the self-quenching is removed and DiD fluorescence intensity increases; for instance when the dye disperses into endosomal membranes following viral-induced fusion. The initial stages of lipid mixing are all that are required to dequench DiD and lead to an increase in fluorescence intensity. In order to then determine whether content transfer has occurred (i.e. determine if hemifusion has been resolved to a pore), viruses can also be loaded with content markers which will be deposited into the cytosol. Using this system, Desai *et al.* [14] demonstrated that DiD-labelled IAV particles dequench in the presence of IFITM3 but that the addition of oleic acid had no impact (in contrast to results seen by Li *et al.* [13]). While IAV particles could establish hemifusion in the presence of IFITM3, using HA pseudotyped retrovirus particles, labelled with DiD and carrying fluorescent cargo, it was observed that there was no content mixing after hemifusion. The work of Desai *et al.* [14] therefore suggested that IFITM3 was blocking the establishment of fusion pores, after the formation of hemifusion

intermediates, in contrast to the model proposed by Li *et al.* [13]. The differences seen may be down to the different systems of cell-cell fusion and virus-cell fusion that were used.

Whether or not hemifusion can be established when IFITM proteins are present remains unclear, as does the mechanism(s) underlying any inhibition, and whether there is any involvement of reduced fluidity of cellular membranes [13, 156]. It also remains unknown wether all IFITM proteins operate through the same mechanism for all viruses that are restricted. It has been suggested that IFITM proteins can directly interact with vesicle-membrane-protein-associated protein A (VAPA) [152]. VAPA is an ER localised protein involved in regulating cellular cholesterol levels. It was proposed that IFITM interaction with VAPA out-competes binding of oxysterol-binding protein and results in an accumulation of cholesterol in endosomal membranes. This cholesterol accumulation was proposed to be responsible for IFITM-mediated inhibition of viral entry. How the ER localised VAPA and IFITM proteins, which localise to endosomes and the plasma membrane (discussed in more detail in Section 1.3.3), interact in cells is unclear. The results of Amini-Bavil-Olyaee *et al.* [152] have also been challenged by other studies suggesting that cholesterol accumulation does not play a role in IFITM-mediated inhibition [14, 156]. However, cholesterol may still play roles in IFITM function, as the cholesterol binding drug amphotericin B (AmphoB), and derivatives, have been shown to negate IFITM3-mediated inhibition of IAV [156] and simian immunodeficiency virus (African green monkey [SIVagm] strain; [168]). However, AmphoB treatment had no impact on EBOV infection [142].

While most viruses have been proposed to be inhibited by IFITM proteins during entry into new host cells, there are exceptions to this model. It has been suggested that IFITM proteins can incorporate into budding HIV particles and reduce their infectivity in subsequent cells [133, 166, 167]. In one of these studies, it was demonstrated in cell-cell spread assays that when IFITM3 was expressed in target cells, there was only modest inhibition of HIV-1 infection [166]. However, the expression of IFITM3 in donor cells reduced infection of target cells, with the argument made that was as a result of reduced infectivity of the released virus [166]. IFITM3 was found to be the most potent for inhibiting infection in new target cells following incorporation into HIV-1 particles, which is interesting given that HIV-1 generally buds from the plasma membrane but IFITM3 is

generally localised to intracellular compartments [166, 167]. It has also been suggested that IFITM protein expression in HIV-1 infected cells can alter the trafficking and processing of Env [173], although this has been challeneged by a subsequent study [133].

The importance of IFITM incorporation into HIV-1 virions has been challenged by a recent study, in which it was suggested that IFITM proteins can inhibit infection of HIV-1 irrespective of incorporated IFITM protein [169]. Interestingly, this study found that different strains of HIV-1 had differential sensitivity to IFITM proteins based on the co-receptor usage; CXCR4 tropic lab-adapted viruses were found to be more sensitive to the endosomal IFITM2 and IFITM3 (discussed in Section 1.3.3), while CCR5 tropic viruses were found to be more sensitive to the plasma membrane localised IFITM1 (discussed in Section 1.3.3; [169]). These differences in sensitivity to IFITM inhibition perhaps explain some of the discrepancies between the various studies of HIV-1. These data also suggest that the route of entry into the cell may alter the sensitivity to IFITM proteins, with it being tempting to speculate that CXCR4 tropic viruses may fuse at endosomal membrane sites, while CCR5 tropic viruses may fuse at the plasma membrane. In agreement with this idea, mutation of IFITM2 or IFITM3 to cause accumulation of protein at the plasma membrane (again see Section 1.3.3) altered the inhibition of the different HIV-1 strains [169]. Finally, it was also demonstrated that HIV-1 transmitter founder viruses are refractory to IFITM-mediated inhibition, but viruses collected from patients 6 months later were sensitive, most likely as a result of mutations to Env which were associated with evasion from neutralising antibodies [169]. The impact IFITM proteins have on HIV-1 infection therefore appear to be highly complex and potentially multifaceted.

In summary, while much has been learnt about the breadth of IFITM-mediated antiviral activity in cell culture, there is currently a lack of understanding of the mechanism(s) underlying this function. Most data point towards inhibition occurring at the stage of entry, although there have been suggestions of an alternative function of IFITMs incorporating into nascent virions. IAV has been the most intensively studied virus for IFITM-mediated inhibition, but there is debate over whether IFITMs inhibit fusion before, or after the establishment of a hemifusion intermediate. There is a suggestion that cholesterol may have some function in IFITM-mediated inhibition, though it remains unclear what this is. Furthermore, whether all viruses are inhibited by the mechanisms described

for IAV and whether all three human IFITM proteins inhibit through this mechanism, or not, remains to be established, as do the reasons for certain viruses being refractory to the antiviral function of IFITM proteins.

In vivo

Compared to the study of IFITM proteins in cell culture systems, there is relatively little data on the impact they have *in vivo*. The first studies to show *in vivo* relevance of IFITM proteins used mice genetically deleted for the whole *Ifitm* locus (*Ifitm -/-* or *Ifitm3* alone (*Ifitm3 -/-*). Both sets of mice were developmentally unaltered, but upon challenge with IAV rapidly developed fulminant viral pneumonia and had to be euthanised as a result of excessive weight loss [174, 175]. In contrast, after a brief loss of body weight, wild type littermates recovered from the infection. *Ifitm3 -/-* mice showed similar severity of disease as *Ifitm -/-* mice suggested that Ifitm3 may be the key protein for controlling IAV infection in mice. Additionally, it has been demonstrated that both wild type and *Ifitm3 -/-* mice had increased pathogenesis from IAV infection when treated with a derivative of AmphoB, validating the *in vitro* data [156].

A role for Ifitm3 in the murine adaptive immune response has also been suggested. Wakim *et al.* demonstrated that after challenge with influenza, there was a prolonged expression of Ifitm3 in lung resident memory CD8+ T cells [176]. This prolonged expression did not appear to be dependent on continued IFN production, but was associated with hypomethylation of the *Ifitm3* promoter in the IAV-specific memory T cells. The suggestion was made that these Ifitm3 expressing CD8+ T cells were more resistant to subsequent influenza challenge, potentially enhancing their efficacy in the memory response to viral infection [176]. Whether similar epigenetic changes occur in humans following influenza infection remains to be determined.

In addition to displaying enhanced pathogenesis in mice, the work of Everitt *et al.* [174] also identified a potential genetic association between severe influenza infection and a single nucleotide polymorphism (SNP - rs12252) in human *IFITM3*. The SNP codes for a minor C allele which generally occurs at low frequency compared to the major T allele, except in a Han Chinese population where the C allele has much higher frequency [177]. In patients hospitalised by seasonal or pandemic influenza infection, there was a

~19 fold enrichment in the presence of the CC allele [174]. It was also found that 69% of Chinese patients with severe pandemic IAV infection were CC positive, compared to only 25% who had mild symptoms [177]. This minor allele was suggested to alter a splice site in the *IFITM3* gene which could result in a 21 amino acid truncation at the NTD of IFITM3 [174]. However, this truncated protein was not detected in lymphoblastoid cell lines expressing the CC variant, although a lower level of IFITM3 protein expression was detected, as compared to the TT variant [174]. The exact consequence of the CC allele remains unclear. The findings of Everitt *et al.* that rs12252-C associates with severe influenza has been challenged [178], although other studies and a meta-analysis of data have supported the initial work [177, 179, 180]. It has also been suggested that rs12252-C is associated with more rapid progression to AIDS following HIV-1 infection [181]. To date, no other viruses or IFITM SNPs have been associated with increased severity of disease in humans.

Along with the above mentioned work analysing IAV infection of *Ifitm3 -/-* mice, various other pathogens have been tested [182]. This work suggested that the *Ifitm3 -/-* mice had no altered sensitivity to bacterial (*Salmonella typhimurium, Citrobacter rodentium, Mycobacterium tuberculosis*) nor protozoan (*Plasmodium berghei*) infections. However, when challenged with respiratory syncitial virus (RSV), the mice showed more severe disease, implicating Ifitm3 in the control of RSV infection. Subsequent work further demonstrated that IFITM proteins could inhibit RSV *in vitro* [149].

Most recently, two papers from the Diamond and Farzan labs have shown that Ifitm proteins are involved with control of West Nile virus and alphavirus infections (CHIKV and VEEV) in mice [183, 184]. Both studies suggest that *Ifitm3* is the major component of controlling the early phases of infection. In the absence of Ifitm3, there were higher viral titres at early time points following infection, enhanced inflammatory responses and increased dissemination of virus [183, 184]. *Ifitm3 -/-* mice were found to have greater morbidity and mortality to both VEEV and WNV [183, 184].

To date, five different viruses (from four families) have been shown to have enhanced pathogenesis in *Ifitm3 -/-* mice, and a genetic link has been suggested between a SNP in the *IFITM3* gene with more severe IAV infection and more rapid progression to AIDS from HIV-1 infection in humans. It therefore appears likely that at least IFITM3 has roles in

control of viral infection *in vivo*. What roles IFITM1 and IFITM2 may be playing remains unknown. In parallel with developing a more detailed understanding of the antiviral function of the IFITM proteins in cell culture, future work directed at testing further pathogens in mice and a better analysis of the potential genetic link between IFITM SNPs and severe disease in humans are necessary to fully define the importance of these proteins.

1.3.3 IFITM cell biology

Along with the knowledge that has been generated regarding the antiviral function of the IFN-induced IFITM proteins, there has also been study of their cell biology. Precisely connecting knowledge of the cell biology and regulation of IFITM proteins with their antiviral function remains an on-going challenge.

Cellular localisation

The IFITM proteins inhibit viral entry into cells, therefore understanding their cellular localisation is integral for understanding how they can impinge on the various viruses they inhibit. Various different studies have made attempts to define the localisation of the IFITM proteins. Much of this work has relied on immunofluorescence microscopy and co-staining epitope-tagged forms of IFITM proteins with various markers of cellular structures. A general consensus has emerged that the IFITM proteins are predominantly endosomal, displaying varying degrees of co-localisation with many different endosomal markers [12, 134, 139, 143, 146, 152, 154, 159, 160, 162, 163]. This is particularly true for IFITM3, though IFITM2 has been less intensely studied. However, IFITM3 has also been suggested to be localised to the ER [7, 150, 151], though the functional significance of this is unclear.

Part of the work presented in this thesis was aimed at addressing the localisation of the proteins. In A549 cells, IFITM1 is localised at the plasma membrane [15], while IFITM2 and IFITM3 are dispersed through the endosomal system, but IFITM3 has greater localisation to early endosomes, while IFITM2 has greater localisation to late endosomes [16]. IFITM1 has also been suggested to be localised within the endosomal system by others [159, 185]. Part of these discrepancies may come down to cell type variation or

sample preparation. Based on the data within this thesis (and as in [15, 16]) a model can be suggested whereby the three IFITM proteins occupy the major portals of entry for many different viruses, be it the plasma membrane, or endo/lysosomal membranes (see Fig. 1.7 and [10]). It is tempting to speculate that differences in localisation may impact on the antiviral properties of each of the IFITM proteins. This will be discussed throughout work presented here.

It is clear in A549 cells at least, that IFITM1 is primarily localised to the plasma membrane, while IFITM2 and IFITM3 are primarily found within internal membrane compartments. The major determinant for this difference in localisation appears to be in the NTD. As discussed previously, IFITM1 has a 20 and 21 amino acid truncation compared to IFITM2 and IFITM3, respectively. Within this additional stretch of amino acids found on IFITM2 and IFITM3, there is a Yxxϕ motif that acts as a sorting signal for CME (where Y represents tyrosine, x represents any amino acid and ϕ represents a hydrophobic residue; 19-YEML-22 and 20-YEML-23, for IFITM2 and IFITM3, respectively. See Fig. 1.6). Yxxϕ motifs have been characterised through their ability to interact with the clathrin adaptor AP-2 (Section 1.1.1), and therefore direct CME of proteins presenting such a motif [186]. Indeed, deletion of the first 21 amino acids, or mutation of the Y residue alone, results in accumulation of IFITM3 at the plasma membrane [163]. These mutant forms of IFITM3 were found to have reduced antiviral activity against IAV and HIV-1 [163, 174]; this is interesting considering the apparent link between rs12252-C, which may truncate IFITM3 by 21 amino acids, and the increased severity of IAV and HIV-1 infection seen in humans [174, 177, 179–181]. However, the loss of antiviral function against IAV *in vitro* has been challenged [187]. That the Yxxϕ motif is indeed functioning as a membrane trafficking signal was demonstrated by work showing that IFITM3 directly interacts with AP-2, and mutation of this motif abolishes the interaction [143].

In addition to the work on sorting motifs in IFITM NTDs, it has been suggested that there is a di-basic sorting motif (122-KRGY-125) in the IFITM1 CTD that can regulate ubiquitination of IFITM1 and interaction with AP-3 [159]. It was proposed that mutation of these resides could disrupt IFITM1 localisation and could alter IFITM1-mediated antiviral activity against JSRV [159]. It has also been suggested that alterations to the IFITM1 CTD can change cellular distribution and antiviral activity against HIV-

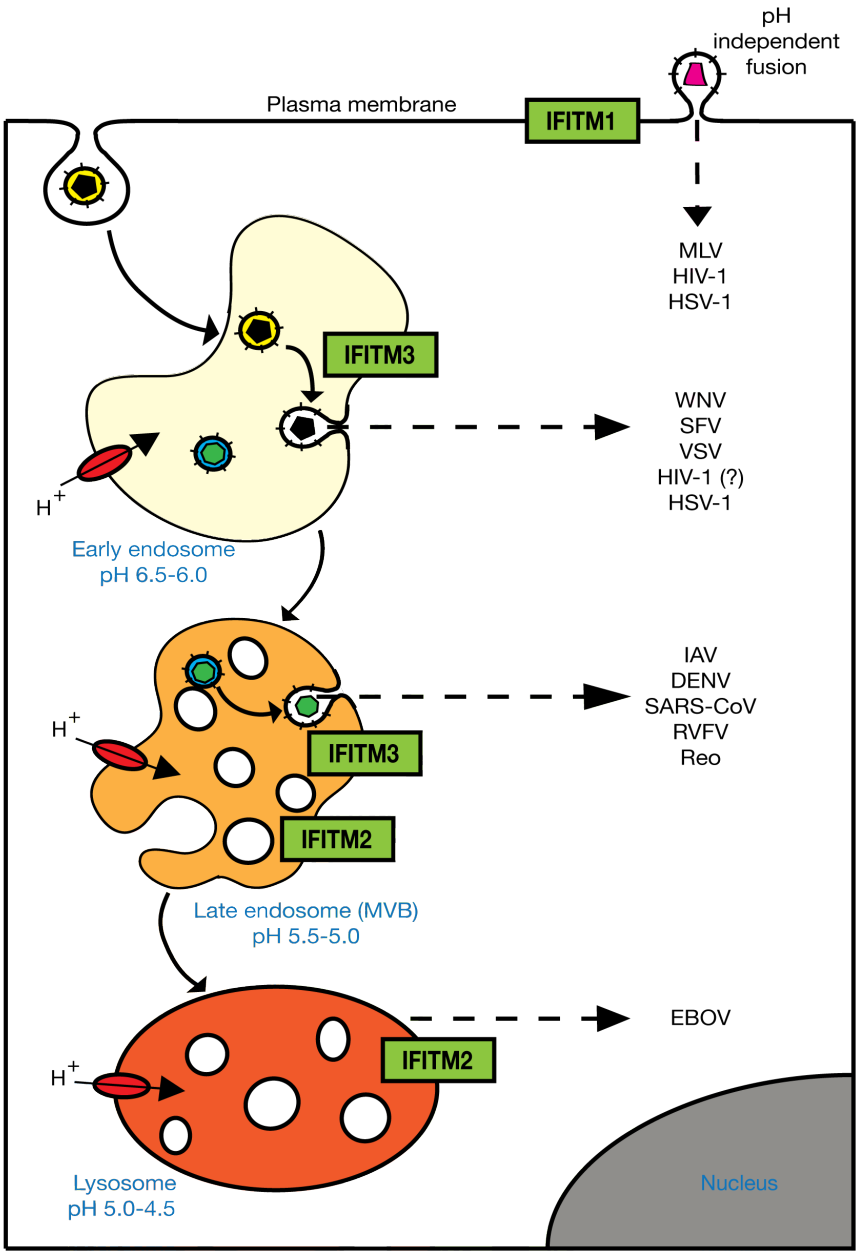

Figure 1.7: **IFITM cellular distribution and select viral entry sites.** When expressed individually in A549 cells, the IFITM proteins are found to occupy various cellular membrane compartments. As displayed in Chapter 3 and [15, 16], IFITM1 is predominantly localised at the plasma membrane, while IFITM2 and IFITM3 are dispersed through the endosomal system. IFITM3 appears to have greater localisation to early endosomal compartments than IFITM2, while IFITM2 appears to have greater localisation to late endosomal compartments than IFITM3. Many different viruses (some examples provided here) penetrate into the cytosol through the different membrane compartments the IFITM proteins are found to be predominantly located in. It could therefore be hypothesised that the localisation of the IFITM protein may influence its antiviral activity, an idea which will be discussed throughout this thesis. Image adapted from [10].

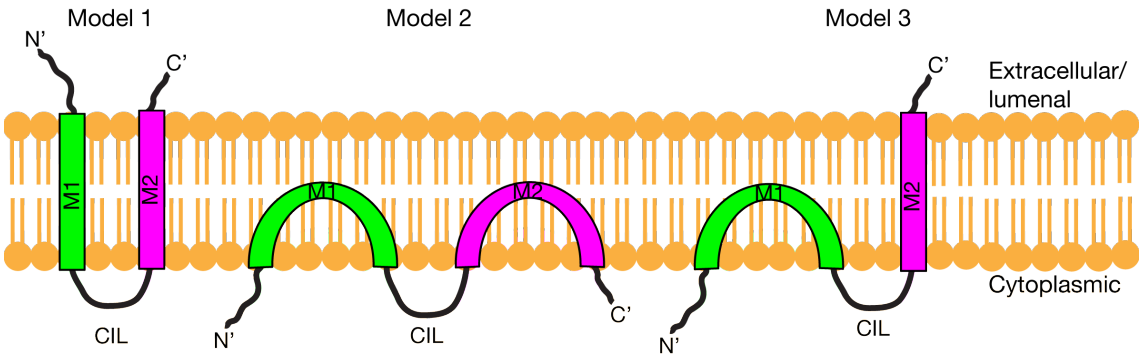

Figure 1.8: **Topology models of the IFITM proteins.** Model 1: The initially proposed model for IFITM membrane topology placed both the N- and C-terminal domains (NTD and CTD) on the extracellular/lumenal side of cellular membranes. The two termini are connected by two transmembrane domains (M1 and M2) and a conserved intracellular loop (CIL). Model 2: The second proposed model for IFITM membrane topology placed both the NTD and CTD on the cytoplasmic side of membranes, connected by M1, CIL and M2. This model necessitated M1 and M2 enter into but do not cross the lipid bilayer. Model 3: The most recently proposed model suggests that the NTD is cytoplasmic, while the CTD is extracellular/lumenal. M1 has enters into, but does not cross the bilayer, while M2 is transmembrane.

1 [185]. The exact functional significance of the CTD and the potential di-basic motif remains unclear, and will be discussed further in Chapter 6.

As previously alluded to, one outstanding question regarding the localisation of the IFITM proteins is what role, if any, this plays in their antiviral action. This will be a topic of discussion in Chapter 6.

Membrane topology

Another controversial aspect of IFITM proteins has been their membrane topology. When the IFITM proteins were initially identified, they were characterised as dual-pass transmembrane proteins, with the membrane associated domains connected by a conserved intracellular loop (CIL). Both the NTD and CTD were suggested to be in the extracellular/lumenal space (Fig. 1.8; model 1). Early studies on the IFITM proteins pointed towards the presence of extracellular regions of the proteins based on the binding of antibodies and functions potentially necessitating extracellular domains [114–116]. This model was further supported by the initial work of Brass *et al.* which suggested that both termini were extracellularly available [7].

However, subsequent work identified multiple PTMs in the NTD of IFITM3 ([151, 163],

and see Section 1.3.3), suggesting this part of the protein must be cytosolic. There was less data regarding the localisation of the CTD. Using engineered murine Ifitm3 constructs, Yount *et al.* suggested that a CTD NxT motif (H136T mutation) was not glycosylated in the ER and that the CTD could be prenylated by addition of a CLVL motif [151]. The argument was therefore made that the CTD resided on the cytosolic side of membranes. Little other data was generated, but a second model was proposed in which both the NTD and CTD resided in the cytoplasm, the CIL connects the two membrane domains, which were suggested to enter into, but not cross the lipid bilayer (Fig. 1.8; model 2).

In Chapter 3 work is presented that characterised the membrane topology of human IFITM proteins and suggested a third model (Fig. 1.8; model 3). This work is re-introduced at the start of the chapter, and is the source of discussion in Chapter 6. As such, greater detail on the membrane topology of the IFITM proteins can be found there.

Post-translational modifications

Not long after the IFITM proteins were identified as antiviral factors, PTMs started to be detected and were suggested to regulate the function of the proteins. Thus far, IFITM proteins have been shown to be subject to palmitoylation, phosphorylation, ubiquitination and methylation.

Palmitoylation

The first study that demonstrated PTM of IFITM3 was initially designed to identify lipid modified proteins with functions in the immune response using a murine dendritic cell line (DC2.4 cells) and mass-spectrometry. One of the hits detected in this screen as being S-palmitoylated was Ifitm3 [150]. S-palmitoylation involves the covalent attachment of palmitic acid to proteins, through thioester bonding to cysteine (C) residues. Ifitm3 was found to be palmitoylated at three highly conserved cysteine residues in membrane proximal regions (C71, 77 and 105). Mutation of all three residues to alanine (C-A) resulted in more diffuse immunofluorescence staining for Ifitm3, and caused a loss of antiviral activity against IAV, suggesting there is a need for lipid modification of Ifitm3 for antiviral activity [150]. Interestingly, the addition of an NTD myristolyation site (GARASVLS) and CTD prenylation site (CLVL), in the context of the triple C-A mutant Ifitm3, restored the clustered localisation of the protein and antiviral activity against IAV. Additionally,

murine Ifitm1 was found to be palmitoylated at a non-conserved CTD C residue, and this modification was necessary for stability and anti-IAV function of the protein [155]. It therefore appears that lipid modifications are necessary to promote IFITM clustering and antiviral activity.

Phosphorylation

Both human and murine IFITM3 have been found to be phosphorylated on NTD tyrosine residues [158, 163]. In human IFITM3, Y20 is the only site of phosphorylation [158], with this residue forming part of the Yxxϕ sorting motif discussed previously. Murine Ifitm3 is additionally phosphorylated at an non-conserved Y27 [158]. Fyn was identified as the kinase responsible for phosphorylation of Y20 [163]. It was subsequently demonstrated that increased phosphorylation at this site, by Fyn overexpression, can result in accumulation of IFITM3 at the plasma membrane [158], suggesting disruption of the interaction with AP-2 [143]. Since IFITM3 with a Y20A mutation, which cannot interact with AP-2 and localises to the plasma membrane, has been suggested to have reduced anti-IAV and HIV-1 activity [143, 158, 163, 174], it would appear that phosphorylation of IFITM3 Y20 may regulate antiviral function. In order to detect phophorylation of IFITM3 it was necessary to treat cells with phosphatase inhibitors such as sodium orthovadate [158, 163], suggesting dynamic regulation of IFITM3 phosphorylation. How, and whether this IFITM3 phosphorylation is modulated during IFN stimulation or infection, remains to be explored.

Ubiquitination

IFITM3 has also been detected to be modified by ubiquitination at any of 4 lysine (K) residues [150, 158]. The most strongly modified residue is K24 [150], which is located close to a PPxY motif (17-PPNY-20) in the IFITM3 NTD. This motif was shown to interact with the E3 ubiquitin ligase NEDD4 [160]. The other three residues are found in the CIL (K83, 88 and 104). Along with mono- and di-ubiquitination that was detected by overexposure of western blots, IFITM3 can also be poly-ubiquitinated with K48- and K63-linked ubiquitin chains [150]. K48-linked chains are generally associated with targeting proteins for proteasomal degradation, while K63-linked chains play non-degradative roles, suggesting potential for ubiquitin-mediated regulation of IFITM3 function. It appears that ubiquitination of IFITM3 is important for turnover of the protein since mutation of the K

residues to A increased protein stability and enhanced anti-IAV activity [150, 160], most likely as a consequence of decreased degradation. Interestingly, there appears to be an interplay between IFITM3 phosphorylation and ubiquitination as it has been demonstrated that overexpression of Fyn kinase reduced the level of ubiquitinated IFITM3 [158]. Since phosphorylation of Y20 can block IFITM3 endocytosis from the plasma membrane, this may play a role in the reduced ubiquitination, and indeed, Y20A mutant IFITM3 has a reduced level of ubiquitination compared to wild type [150]. However, it may also be the case that phosphorylation of Y20 disrupts NEDD4 association with the 17-PPxY-20 motif. Again, how, and whether ubiquitination is regulated during infection remains to be explored.

Methylation

The final PTM that has been proposed for IFITM3 is methylation, which was suggested to negatively regulate the antiviral activity of IFITM3 against IAV and VSV [157]. Monomethylation of IFITM3 was found to be controlled by the lysine methyltransferase Set7 which targets K88 [157]. IFN treatment of cells resulted in a decreased level of IFITM3 methylation, whereas infection with IAV or VSV appeared to enhance methylation. How viral infection modulates the interaction of Set7 and IFITM3 remains unclear. In the work of Shan *et al.* infection with VSV at a multiplicity of infection (MOI) of 0.02 appeared to give a marked increase in the level of methylated IFITM3 at a population level, even within the first 4 h of infection [157]. How infection at such a low MOI can modulate IFITM3 methylation status across a cell population is unclear. It also remains unknown how methylation and ubiquitination at K88 may be interacting to modulate IFITM3 function. Further work is required to define the importance of IFITM3 methylation.

Overall, it is clear that there are various PTMs that modulate IFITM cell biology and antiviral function. The vast majority of work to analyse these PTMs has focused on IFITM3, with much of that focusing on murine Ifitm3. The target residues for the PTMs are largely conserved in the IFITMs, with the exception of the lack of a PPxY and NTD phosphorylation site (Y20 of IFITM3) in IFITM1 because of the shorter NTD. Since IFITM2 shares all of the sites of PTMs as IFITM3, and IFITM1 shares all but the NTD sites, this suggests IFITM1 and IFITM2 are probably regulated in similar ways, though this remains poorly defined. Additionally, as mentioned throughout, how these PTMs are

modulated through an infection remains to be clearly established.

1.4 Summary

Much has been learnt about the breadth of antiviral function of IFITM proteins. However, for the majority of viruses, there is a lack of detailed understanding over how the IFITM proteins inhibit infection. IAV is the best characterised virus, with data pointing heavily towards an inhibition of viral-cell membrane fusion; but there is debate over whether IFITM proteins inhibit prior to, or after hemifusion has been established. Moreover, it remains unclear whether all viruses are inhibited through the same mechanism(s) as IAV. Infection by IAV in the presence of IFITM3 is modulated by AmphoB treatment, as is the infection of SIVagm [156, 168]. In contrast, infection by EBOV is not modulated by AmphoB treatment [142], perhaps suggesting different underlying mechanisms of antiviral action (discussed in more detail in Chatper 6). Moreover, mutational analysis has suggested that alteration to certain residues of IFITM3 can modulate anti-IAV activity, without altering anti-DENV activity, and vice versa [154].

There are also questions regarding aspects of IFITM cell biology. A major point of contention has been the membrane topology of the IFITM proteins, with two models being debated when the work presented in this thesis was started. A third model has since been proposed. Perhaps related to a lack of understanding about topology, there has also been a lack of full understanding of cellular distribution of the IFITM proteins, and what, if any, impact the different localisation of the IFITM isoforms may have on their antiviral function and breadth.

The work presented in this thesis therefore aims to better characterise aspects of IFITM cell biology and antiviral function. An investigation into the membrane topology has been conducted and produced a model in which the NTD resides in the cytosol, while the CTD resides in the extracellular or lumenal space. The first membrane segment enters into, but does not cross lipid bilayers, while the second membrane domain is a transmembrane segment ([15] and see Fig. 1.8; model 3). Building on the knowledge of the topology, an evaluation of IFITM localisation was made and defined IFITM1 to be localised at the plasma membrane, while IFITM2 and IFITM3 appeared to be dispersed throughout the

endosomal system. IFITM3 appeared to be more localised to early endosomal compartments than IFITM2, which conversely was more localised to late endosomal compartments than IFITM3. For the first time, alphaviruses were shown to be inhibited by IFITM proteins, extending the breadth of IFITM antiviral activity. Using SFV, it was determined that IFITM3 did not inhibit any aspect of viral entry into cells, up until the point of capsid release into the cytosol, suggesting that, as with IAV, membrane fusion is being inhibited [16]. Again, similarly to results with IAV, AmphoB treatment was found to modulate the anti-SFV activity of IFITM3, suggesting that type I and type II fusion machineries may be inhibited by similar mechanisms, at least between IAV and SFV. This work therefore defines SFV as a new model virus system to work with to understand IFITM-mediated inhibition of viral entry.

In contrast to many other viruses (Tables 1.1 and 1.2), alphaviruses were not inhibited by IFITM1. However rather than this necessarily being as a result of the localisation of IFITM1 compared to IFITM3, the data suggested there may be intrinsic differences in the anti-SFV activity of IFITM1 and IFITM3. A comparison between the antiviral function of IFITM proteins against SFV and flaviviruses was also made. These experiments further argued that protein localisation may not be the main determining feature of antiviral action. Flaviviruses enter cells through CME and have pH-dependent fusion in endosomes, but were found to be inhibited by all IFITMs, even the plasma membrane localised IFITM1, which did not inhibit SFV. AmphoB treatment did not modulate the antiviral function of IFITM proteins against flavivirus infection. An argument is made that the difference in IFITM-sensitivity and the impact of AmphoB treatment on alphavirus and flavivirus infection may be as a result of the membrane lipids required for viral fusion. Finally, the archetypal poxvirus, VACV, was tested for IFITM-mediated inhibition and found to be insensitive, further demonstrating that not all viruses entering cells through the endocytic pathway are targets for IFITM inhibition. However, the work with VACV did point towards a potentially interesting side effect of high IFITM protein expression, in that cells appear to become more motile.

In toto, the work presented in this thesis develops a better understanding of IFITM membrane topology and localisation. The previously unexplored alphavirus family is shown to be inhibited by IFITM proteins and a precise definition of the stage of en-

try inhibited is developed. A comparison is made between the inhibition of alphaviruses and flaviviruses, which suggested there could be intrinsic differences in the sensitivity of different viruses to the IFITM isoforms, and that this could be related to the lipid dependences for viral-cell membrane fusion. Combined, these data further the understanding of IFITM cell biology and antiviral function.

Chapter 2

Materials and Methods

2.1 Reagents

Below follows a list of the reagents used throughout this work along with a list of the abbreviations through which they are referred to. Numbers in brackets refer to notes which can be found after the table.

Reagent name	**Abbreviation**	**Supplier**
Ammonium chloride	NH_4Cl	Sigma-Aldrich
Ammonium persulfate	APS	Sigma-Aldrich
Amphotericin B	AmphoB	Amresco
Bovine serum albumin	BSA	Life Technologies (1) and Sigma-Aldrich (2)
Bafilomycin A1	Baf A	Sigma-Aldrich
Bromophenol blue	-	Sigma-Aldrich
Calcium chloride	$CaCl_2$	Fisons
Carboxymethylcellulose	CMC	VWR Chemicals
Complete protease inhibitor cocktail	PIC	Roche
Crystal violet	-	Sigma-Aldrich
DL-Dithiothreitol	DTT	Sigma-Aldrich
Dulbecco's modified Eagle medium	DMEM	Life Technologies
Ethanol	-	Fisher Scientific

Ethylenediaminetetraacetic acid	EDTA	Life Technologies
Epon resin	-	TAAB
EZ-Link Sulfo-NHS-SS-Biotin*	-	Thermo Scientific
Foetal calf serum	FCS	Life Technologies
FuGENE 6	F6	Promega
Gelatin	-	MP Biomedicals
Glasgow's minimum essential medium	GMEM	Life Technologies
Glutaraldehyde	-	TAAB
Glycerol	-	Sigma-Aldrich
Glycine	-	Sigma-Aldrich
Ham's F12 nutrient mixture	F12	Life Technologies
Hepes	-	Life Technologies (3) and Sigma-Aldrich (4)
Hoechst 33258	Hoechst	Sigma-Aldrich
Interferon beta	IFN-β	Rebif
Leibovitz-15 medium	L-15	Life Technologies
Lead nitrate	-	TAAB
Magnesium chloride	$MgCl_2$	Sigma-Alrdrich
Medium 199	M199	Life Technologies
Methanol	MeOH	Fisher Scientific
Minimum essential medium	MEM	Life Technologies
Mowiol	-	Sigma-Aldrich
Methylcellulose	-	Sigma
MES	-	Sigma-Aldrich
NeutrAvidin agarose beads	-	Thermo Scientific
Non-essential amino acids	NEAA	Life Technologies
Opti-minimum essential media	Opti-MEM	Life Technologies
Osmium tetraoxide	-	TAAB
Penicillin/streptomycin	Pen/Step	Life Technologies
Paraformaldehyde	FA	TAAB (5), TAAB (6) and Sigma-Aldrich (7)
Phenylmethylsulfonyl fluoride	PMSF	Sigma-Aldrich
Potassium ferricyanide	-	Sigma
Proteinase K	ProtK	Sigma-Aldrich

ProtoGel (30%)	ProtoGel	National Diagnostics
Roswell Park Memorial Institute medium	RPMI	Sigma-Aldrich (8)
Saponin	-	Sigma-Aldrich
Skimmed milk powder	-	Marvel
Sodium cacodylate	-	TAAB
Sodium chloride	NaCl	Fisons
Sodium citrate	-	Sigma
Sodium dodecyl sulfate	SDS	Sigma-Aldrich
Sodium pyruvate	-	Life Technologies
Soy bean trypsin inhibitor	SBTI	Sigma-Aldrich
Sucrose	-	Sigma
Subtilisin	-	Sigma-Aldrich
Tannic acid	-	TAAB
Tetramethylethylenediamine	TEMED	Sigma-Aldrich
Triton X-100	Tx100	Sigma-Aldrich
Trizma Base	Tris	Sigma-Aldrich
Trypsin	-	Sigma-Aldrich
Tryptose phosphate broth	TPB	Sigma-Aldrich
Tween-20	-	VWR Chemicals
Uranyl acetate	-	Agar Scientific

Table 2.1: Reagents and supplier details. * NHS-SS-Biotin; N-hydroxysulfosuccinimide-ester biotinylation reagent containing a disulfide bond. (1) Life Technologies supplied BSA was a 7.5% (w/v) solution. (2) Sigma-Aldrich supplied BSA was a powder. (3) Life Technologies supplied Hepes was a 1 mM solution. (4) Sigma-Aldrich supplied Hepes was a powder. (5) TAAB supplied FA was a 36% (w/v) 'EM-grade stock.' This was used for all fixation with the ensuing exceptions: (6) An additional TAAB supplied FA stock of 16% (w/v) described as 'MeOH free,' which was used for fixation before staining intact cell (referenced when used), (7) Sigma-Aldrich supplied FA was a 36% (w/v) stock and used only for making crystal violet stain. (8) RPMI with no bicarbonate supplied as a powder by Sigma-Aldrich.

2.2 Buffer recipes

Below follows a list of the buffers used throughout this work and their composition. Where applicable, abbreviations of solutions have been give which will be used throughout the

rest of this thesis.

- 3x Laemmli sample buffer (LSB)
  - 188 mM Tris pH 6.8
  - 6% (w/v) SDS
  - 30% (v/v) glycerol
  - 0.0006% (w/v) Bromophenol blue
  - 100 mM DTT (for reducing buffer)
- 6x Laemmli sample buffer (LSB)
  - 300 mM Tris pH 6.8
  - 12% (w/v) SDS
  - 60% (v/v) glycerol
  - 0.0006% (w/v) Bromophenol blue
  - (only used as non-reducing)
- Crystal violet stain
  - 0.1% (w/v) crystal violet
  - 2% (w/v) FA
- Dulbecco's phosphate buffered saline (DPBS)
  - PBS
  - 1 mM $CaCl_2$
  - 0.5 mM $MgCl_2$
- Infection media
  - Ham's F-12 nutrient mixture (GluaMAX) media
  - 10 mM Hepes (from 1 mM [pH 7] stock)
  - 0.2% BSA (from 7.5% stock)

- Overlay media
  - 1.5% (w/v) CMC
  - 1 x MEM
- SFV binding media (BM)
  - RPMI media (without bicarbonate)
  - 0.2% (w/v) BSA
  - 10 mM Hepes (powdered stock)
  - 10 mM MES
  - pH 6.8 (also adjusted to pH 5.5)
- TE buffer
  - 10 mM Tris
  - 5 mM EDTA
- TN buffer
  - 100 mM NaCl
  - 50 mM Tris
  - pH 7.6
- Tris buffered saline (TBS)
  - 20 mM Tris
  - 137 mM NaCl
  - pH 7.6
- TBS-Tween (TBST)
  - TBS (as above)
  - 0.05% (v/v) Tween-20
- Triton-X100 lysis buffer (Tx100 lysis buffer)

  - 1% (v/v) Tx100
  - 150 mM NaCl
  - 50 mM Tris
  - pH 8

- Western blot resolving gel (15%)
  - 2.3 ml ddH_2O
  - 2.5 ml 1.5 mM Tris pH 8.8
  - 5 ml Protogel
  - 100 μl 10% SDS
  - 100 μl APS
  - 4 μl TEMED

- Western blot resolving gel (10%)
  - 4 ml ddH_2O
  - 2.5 ml 1.5 mM Tris pH 8.8
  - 3.3 ml Protogel
  - 100 μl 10% SDS
  - 100 μl APS
  - 4 μl TEMED

- Western blot stacking gel (4%)
  - 7.18 ml ddH_2O
  - 1.25 ml 1 mM Tris pH 6.8
  - 1.36 ml Protogel
  - 100 μl 10% SDS
  - 100 μl APS
  - 8 μl TEMED

- Western blot running buffer (purchased through SLS Life Science)
  - 25 mM Tris
  - 192 mM Glycine
  - 0.1% (w/v) SDS
- Western blot transfer buffer
  - 25 mM Tris
  - 192 mM glycine
  - 20% (v/v) MeOH
  - 0.005% (w/v) SDS

2.3 Cell Culture

2.3.1 Cell lines

A549 cells stably expressing individual C-terminally HA-tagged IFITM proteins were acquired from the Kellam Lab (Sanger Institute, Cambridge, UK) and were produced by Sarah Smith, Rachael Wash and Carmen Diaz-Soria. Stable protein expression was achieved through lentiviral transfection (discussed in Section 2.3.2), and selected in two different ways. There were three sets of stable A549 cells which are denoted as original set (OS), puromycin 1 and puromycin 2 (P1 and P2, respectively). Transfected cells in the OS set were selected by single cell cloning as described [134]. Transfected P1 and P2 cells were selected by virtue of a puromycin resistance gene cassette within the lentiviral vector. See Table 2.2 for the different cells within each group.

Original Set (OS)	Puromycin 1 (P1)	Puromycin 2 (P2)
A549	A549 empty puro.	A549 GFP
IFITM1	IFITM1	-
IFITM2	IFITM2	-
IFITM3	IFITM3	IFITM3
-	-	IFITM3-Y20A

Table 2.2: Composition of OS, P1 and P2 IFITM cell groups

Cell line	Culture media	FCS (v/v)	Pen/Strep (v/v)	Additional (v/v)
A549	Ham's F12	10%	1%	-
BSC-40	DMEM	10%	1%	1% NEAA and sodium pyruvate
C6/36	L15	10%	1%	10% TPB
BHK-21	GMEM	5%	1%	5% TPB
HEK293T	DMEM	10%	1%	-
Vero E6	M199	10%	1%	-

Table 2.3: Cell culture conditions. All media was Life Technologies 'GlutaMAX' media. All % values are (v/v).

Cell culture conditions are displayed in Table 2.3. Cells were maintained on plastic 10 cm dishes (Corning), 15 cm dishes (Sigma-Aldrich) or tissue culture flasks of various sizes (Corning) as stated where appropriate through this chapter. Cells were also cultured in 6 x 35 mm well dishes, 24 x 1.5 mm well dishes (both Thermo Scientific) or black 96 well plates (PerkinElmer). Any other culture conditions are discussed where appropriate. Cells were maintained at 37℃ and 5% CO_2.

2.3.2 Stable cell line production

Stable cell lines were produced through lentiviral (HIV based) transduction (as described [134]). Lentivirus particles were produced by transient transfection of HEK293T cells with the p8.9, pMDG2 and pSIN vectors. pSIN vectors were used to carry the gene of interest while p8.9 provides the structural proteins for producing HIV particles and pMDG2 encodes the vesicular stomatitis virus glycoprotein (VSV-G) to mediate viral entry into cells (all constructs were kind gifts from the Kellam Lab [Sanger Institute]). HEK293T cells were plated at a density of 2 x 10^6 in 10 cm dishes and incubated overnight. The following day, cells were transfected with the three constructs in DMEM (transient transfection further detailed in Section 2.3.3 and Table 2.4); 1 μg of p8.9 and pMDG2 and 1.5 μg pSIN (DNA concentrations optimised by members of the Kellam Lab) and incubated for 24 hours (h). Subsequently, media were changed for fresh 10% FCS supplemented DMEM (with no Pen/Strep) and incubated for a further 24 h. After 48 h transfection, media were collected from the cells, filtered through 0.45 μm pores and stored at -80℃ prior to use.

2.3.3 Transfection

For all transfections FuGENE 6 (F6) transfection reagent was used. Cells were cultured overnight on 6 x 35 mm well dishes or 10 cm dishes depending on the assay. Cells were plated to achieve roughly 60-70% confluency as per the Promega F6 instruction. For all transient transfections, a F6 and OptiMEM transfection mix was made (see Table 2.4) and incubated for 5 minutes (min) at room temperature (RT). DNA was added to the transfection mix at an appropriate concentration (see Table 2.4). The F6:OptiMEM:DNA ratio for a 6 x 35 mm dish was suggested by Promega F6 instructions and scaled up based on plate area for 10 cm dishes (with the exception of the mix to produce lentiviruses as discussed in Section 2.3.2). The F6:OptiMEM:DNA mix was incubated for 20 min at room temperature (RT) prior to addition to cells in 10% FCS supplemented DMEM with no Pen/Strep. Cells were then incubated for either 24 or 48 h prior to use. For all transient transfections, the pcDNA3.1 vector was used. All constructs were provided by the Kellam Lab (Sanger Institute), having been purchased from GeneArt (Thermo Scientific).

Culture plate	FuGENE 6	OptiMEM	DNA
6 x 35 mm	6 μl	200 μl	2 μg
10 cm	39 μl	1.3 ml	13 μg
10 cm (lenti.)	10 μl	200 μl	1 μg p8.9
			1 μg pMDG2
			1.5 μg pSIN

Table 2.4: Transfection reagent mixes.

2.3.4 Scratch assay

Cells were plated onto glass coverslips (LabTech glass coverslip chambers, 8 well) and cultured overnight to form a confluent monolayer. Cells were imaged on an inverted microscope, a scratch was made through the middle of the monolayer with a sterile plastic P200 pipette tip, and were then imaged again. Cells were then incubated for various times and closure of the wound monitored by further imaging.

2.4 Antibodies

Details of primary antibodies and usage can be found in Table 2.5. WB: western blot, IF: immunofluorescence, EM: electron microscopy. Details of secondary antibodies can be found in Table 2.6. AF: AlexaFluor and abbreviations as above.

Target	Supplier	Cat. no.	Species	MAb/Ab	Conc.	WB	IF	EM
HA	Roche	1867423	Rat	MAb	100 μg/ml	1:1000	1:100	-
HA	Covance	MMS-101P	Mouse	MAb	1 mg/ml	1:1000	1:1000	1:400
IFITM1-NTD	Sigma	HPA004810	Rabbit	Ab	100 μg/ml	1:1000	1:200	1:100
IFITM3-NTD	Abgent	AP1153a	Rabbit	Ab	100 μg/ml	1:500	1:200	-
SFV E1/E2	MRC LMCB [97]	N/A	Rabbit	Ab	N/A	1:1000	1:500	1:50
SFV capsid	MRC LMCB [97]	N/A	Rabbit	Ab	N/A	1:500	-	-
DENV E protein	Thermo Sci.	MA1-27093	Mouse	MAb	1 mg/ml	1:500	-	-
YFV	Santa Cruz	sc-58083	Mouse	MAb	100 μg/ml	-	1:100	-
ZIKV	Merck Millipore	MAB10216	Mouse	MAb (D1-4G2-4-15	?	-	1:500	-
TfR	Abcam	ab1086	Mouse	MAb (MEM-189)	1 mg/ml	-	1:200	-
EEA1	BD Bio.	610457	Mouse	MAb (14/EEA1)	250 μg/ml	-	1:200	-
CD63	MRC LMCB [188]	N/A	Mouse	MAb (1B3)	N/A	-	1:10000	-
LAMP1	BD Bio.	555798	Mouse	MAb (H4A3)	500 μg/ml	-	1:500	-
Calreticulin	Thermo Sci.	PA3-900	Rabbit	Ab	N/A	1:5000	-	-
Tubulin	Sigma	T9026	Mouse	MAb (DM1A)	1 mg/ml	1:500	1:100	-
Tubulin	Sigma	ab184613	Mouse	MAb (GT114)	1 mg/ml	1:500	-	-
VDAC	Abcam	ab15895	Rabbit	Ab	1 mg/ml	1:3000	-	-
GFP	MRC LMCB*	N/A	Rabbit	Ab	N/A	-	1:500	-

Table 2.5: Primary antibodies. MAb/Ab denotes whether antibodies were monoclonal antibodies (MAb) or polyclonal antibodies (Ab). Antibody concentrations were either as supplied or manufacturer recommended dilutions. Usage conditions were either from manufacturer recommendations or optimisation. Any details with a '?' were not stated by manufacturer. * Anti-GFP antibody was a kind gift from Dr. Jason Mercer.

Antibody	Supplier	Cat. no.	Conjugate	Concentration	Usage
Goat anti-mouse	Life Technologies	A11029	AF488	2 mg/ml	IF: 1:500
Goat anti-mouse	Life Technologies	A21235	AF647	2 mg/ml	IF: 1:500
Goat anti-mouse	Li-COR	926-32210	IR-Dye 800	1 mg/ml	WB: 1:10000
Goat anti-rabbit	Life Technologies	A11034	AF488	2 mg/ml	IF: 1:500
Goat anti-rabbit	Life Technologies	A11037	AF594	2 mg/ml	IF: 1:500
Goat anti-rabbit	Life Technologies	A21244	AF647	2 mg/ml	IF: 1:500
Goat anti-rabbit	Li-COR	926-68071	IR-Dye 680	1 mg/ml	WB: 1:10000
Goat anti-rat	Life Technologies	A11006	AF488	2 mg/ml	IF: 1:500
Goat anti-rat	Life Technologies	A21247	AF647	2 mg/ml	IF: 1:500
Goat anti-mouse	Life Technologies	G21040	HRP	1 mg/ml	IF: 1:500

Table 2.6: Secondary antibodies. AF: AlexaFluor. Antibody concentrations were either as supplied or manufacturer recommended dilution. All usage conditions are from manufacturer recommendations.

2.5 Viruses Stock Preparation

2.5.1 Alphaviruses

Semliki Forest (SFV) and Sindbis virus (SINV) stocks were prepared from the CB3 and AR339 virus preparations, respectively (SFV CB3 was produced by Prof. Mark Marsh, SINV AR339 was a kind gift from Dr. Penny Powell, University of East Anglia, Norwich, UK). Stocks for both alphaviruses were prepared in the same way. BHK-21 cells were grown in T75 or T175 flasks for 2 days to form a confluent monolayer and infected with 0.05 pfu/cell (in GMEM supplemented with 0.2% [w/v] BSA and 10 mM Hepes [from powder, pH 7] containing Pen/Step). Cells were incubated with virus for 1 h at 37℃, prior to removal of media and replacement with fresh GMEM (supplemented as before). Cells were cultured at 37℃ to allow infection for 22 h. Following incubation, flasks were placed on ice for 30 min and media were collected to polypropylene Falcon tubes. Cellular debris was removed by centrifugation for 15 min at 2500 x g (4℃). Supernatant was collected and subject to ultracentrifugation for 2.5 h at 100000 x g (4℃). Following ultracentrifugation, supernatant was removed and the pellet placed on ice. The virus pellet was re-suspended in TN buffer and centrifuged for 5 min at 200 x g (RT) to remove any large clumps of virus. Samples were snap frozen with liquid nitrogen and stored at -80℃. Virus titre was determined by serial dilution plaque assay on BHK-21 cells (see Section 2.6.1).

2.5.2 Flaviviruses

Dengue (serotype 2; DENV), Zika (African strain; ZIKV) and yellow fever (17D strain; YFV) virus stocks were all produced by Dr. Michela Mazzon (MRC LMCB).

Dengue virus

C6/36 mosquito cells were grown in T175 flasks overnight, to ∼80% confluency, and infected with 0.5 pfu/cell (in L-15 media supplemented with 10% TPB and 2% FCS; referred to as '2% L15'). Cells were incubated with virus for 2 h at 37℃, prior to removal of media and replacement with fresh 2% L-15. Cells were incubated for 3 days before harvesting. The media were collected from flasks (and replaced) twice a day (morning and evening) for 2 days. At each collection, cellular debris was pelleted by centrifugation at 300 x g

for 10 min, filtered through 0.45 μm pores and stored at 4℃. After the final collection, all media were pooled and concentrated by centrifugation (Vivaspin column 20) at 4℃ for 1 h at 600 x g. The concentrated supernatant was transferred to ice and the concentrator rinsed with 2% L-15. Hepes (pH 7) was added to a final concentration of 25 mM (from 1 mM solution) and samples were snap frozen with liquid nitrogen prior to storage at -80℃.

DENV titre was determined by immunofocus assay (performed by Dr. Michela Mazzon). Vero cells were plated on 24 x 1.5 mm dishes and grown overnight, to ∼90% confluency, then infected with DENV across a 10 fold dilution series of appropriate range for the expected virus yield. Virus was added to cells in MEM supplemented with 2% FCS and incubated for 1 h at 37℃. Media were then removed and a CMC overlay was added. Cells were incubated for 3 days at 37℃. Following this period, the overlay was removed and the wells were washed with PBS. The cells were fixed with 5% (v/v) FA in PBS for 30 min at RT. Cells were permeabilised with 2% (v/v) Tx100 in PBS and incubated for 5 min at RT. Samples were then blocked with 2% (w/v) skimmed milk in PBS (blocking solution) for 30 min at RT. The blocking solution was removed and replaced with anti-DENV antibody diluted in blocking solution and incubated for 1 h at 37℃. Samples were washed 3x with PBS, to remove unbound antibody and subsequently incubated with HRP-conjugated anti-mouse secondary antibody, diluted in blocking buffer, for 1 h at RT. Wells were washed 4x with PBS to remove unbound antibody. Single SIGMAFAST tablets (SIGMAFAST 3-3-Diaminobenzidine tablet, D44418-50 Set) were diluted in 15 ml ddH_2O and at least 200 μl was added to each well and incubated at room temperature until well defined foci were visible. Plaques were then counted to determine the viral titre.

Yellow fever virus

Vero cells were grown in T75 flasks overnight to be about 70% confluent and infected with YFV (in M199 media supplemented with 2.5% FCS). The YFV stock was a kind gift from Dr. Joachim Bugert (University of Cardiff, UK), 300 μl was provided, and 150 μl was used for the innoculum (titre not determined). Cells were incubated with virus for 2 days. Media were collected and centrifuged at 600 x g for 8 min and filtered through 0.45 μm pores. Hepes (pH 7) was added to a final concentration of 25 mM (from 1 mM stock) and virus stored at -80℃. Virus titre was determined by infection and immunofluorescence

staining of A549 cells (see Section 2.8 for details on immunofluorescence).

Zika virus

ZIKV stocks were prepared and titre determined in the same way as YFV.

2.5.3 Vaccinia virus

VACV Western Reserve (WR) strain and VACV WR expressing EGFP from an early/late fusion promoter were a kind gift from Dr. Jason Mercer (MRC LMCB).

2.6 Virus Infections

2.6.1 Plaque assay

To determine alphavirus titre, serial dilution plaque assays were performed. BHK-21 cells were grown for 1 day in 6 x 35 mm well dishes to form a confluent monolayer. Virus stocks were diluted in GMEM supplemented with 10 mM Hepes (from powder) and 0.2% (w/v) BSA and a 10 fold dilution series made, over an appropriate range for the expected virus yield. Cells were inoculated with 0.5 ml virus containing media and incubated at 37℃ for 2 h with occasional manual agitation to ensure no cells dried out. After 2 h, virus containing media were removed and 2 ml CMC overlay media was added to the cells, before incubating at 37℃ for 2 days with minimal movement. Following infection, overlay media was removed and 1 ml crystal violet stain was added to cells and incubated for 30 min at RT. Crystal violet stain was removed following incubation and the plates washed in tap water. Crystal violet stains live cells. Plaques were detected, and counted, as clear areas within each well to determine viral titre.

VACV titres were also determined by serial dilution plaque assay with a slightly adjusted protocol. BSC-40 cells were grown overnight in 6 x 35 mm well dishes to form a confluent monolayer. Virus was diluted in unsupplemented DMEM across a 10 fold dilution series, over an appropriate range for the expected virus yield. Virus was incubated with cells for 30 min at 37℃, prior to removal of inoculation media and addition of 2 ml DMEM (supplemented as for maintenance of BSC-40 cells; see Table 2.3). Infection was

allowed to proceed for 2 days prior to crystal violet staining as above.

2.6.2 Alphavirus and flavivirus infections

Cells were grown overnight in various cell culture dishes to achieve 70-80% confluency. For infection of A549 cells, virus was diluted to the required MOI (listed for each experiment) in F-12 infection media. Cells were incubated for 5.5 - 6 h to allow infection prior to fixation with 3% FA for 15 min at RT for the alphaviruses. For flaviviruses, cells were infected using the same media as for alphaviruses and incubated for 27 h prior to fixation. Following fixation, infection level was determined by immunofluorescence staining for the E1/E2 envelope proteins of the alphaviruses or antibodies against the flaviviruses (see Table 2.5 for antibody details, Section 2.8 for details on immunofluorescence staining and Section 2.6.8 for details on infection quantification).

2.6.3 SFV binding to the cell surface

Many of the experiments subsequently described required SFV to be bound to the cell surface, without being internalised through endocytosis. This was achieved by adding virus at 4°C, which blocks endocytic uptake and therefore viral entry. Virus could then be allowed to enter cells by synchronous endocytic uptake (as described in Section 2.6.4) or experimentally induced to infect cells by fusion with the plasma membrane (as described in Section 2.6.7). Cells were grown on plastic plates of various size, or glass coverslips (VWR International) overnight to be 80-90% confluent. After overnight culture, cells were washed 1x with 4°C binding media (BM) and placed on ice. Virus was diluted to the required MOI (as indicated) in 4°C BM, added to cells and incubated for 1 h, on ice and at 4°C, with gentle agitation. Subsequently, the media were removed and the cells rinsed twice with 4°C BM to remove unbound virus. Appropriate further treatments were then performed (detailed below).

2.6.4 SFV internalisation

In order to analyse SFV internalisation into cells, biochemical immunofluorescence microscopy or electron microscopy (EM) were used. Virus was added to cells at an MOI of

50 or 200 pfu/cell (as indicated) for IF analysis, and 1000 or 5000 pfu/cell for EM analysis, and allowed to bind at the cell surface. Endocytosis of virus was stimulated by incubating cells in 37℃ infection media for the indicated times. Cells were fixed with 3% FA and processed for immunofluorescence microscopy (Section 2.8).

Subtilisin resistance assay

To investigate SFV internalisation biochemically, a protease resistance assay was used. Virus was added to cells at an MOI of 200 pfu/cell and allowed to bind at the cell surface for 1 h, then allowed to internalise for the indicated times. Cells were returned to ice and treated with 2 mg/ml subtilisin in PBS for 1 h at 4℃ with gentle shaking. Subtilisin can remove virus remaining at the surface without impacting intracellular pools. Subtilisin was inactivated by addition of 1 mM PMSF and 30 mg/ml BSA in PBS (containing 1x complete PIC). Cells were collected (by scraping for samples not treated with protease), and centrifuged to form a pellet (300 x g for 5 min at 4℃.) The supernatant was removed and the cell pellet resuspended in 0.2% BSA in PBS to wash. Cells were again pelleted under the same centrifuge conditions and washed a final time in PBS. After removing the final wash, cells were lysed with Tx100 lysis buffer and analysed by SDS-PAGE and western blot (see Section 2.7) for the E1/E2 proteins, to determine the amount of cell-associated virus.

2.6.5 Time course of SFV penetration

The kinetics of SFV endosomal penetration were determined in A549 cells. SFV was bound to the surface of cells. Media at 37℃ were then added to cells to allow endocytic uptake of virus. The pre-warmed F12 infection media added to cells contained DMSO or 10 μM monensin. Monensin is an ionophore which dissipates low pH gradients thus inhibiting SFV fusion with endosomes. Addition of monensin can therefore be used to determine the time at which SFV passes the acid-sensitive stage of entry. At time points between 3 and 30 min, media containing DMSO were removed and replaced with media containing monensin. Cells were then incubated for 5.5 - 6 h at 37℃ to allow infection, prior to fixation and immunofluorescence analysis of infection (Section 2.8 and Section 2.6.8).

2.6.6 SFV E1 trypsin insensitivity

Cells were grown in 6 x 35 mm well plates overnight and pre-incubated with DMSO or 100 nM Baf A in BM for 15 min at 37°C. Cells were then placed on ice and washed with cold BM containing DMSO or Baf A to match the pre-incubation (as in all subsequent steps) prior to addition of SFV (200 pfu/cell). Virus was incubated with cells for 1 h on ice to allow binding to the cell surface. Subsequently, unbound virus was removed by washing with cold BM. Cells were then either incubated with 37°C BM for the indicated times to allow virus internalisation, incubated at 37°C with BM adjusted to pH 5.5, or left on ice as control. Cells were washed twice with ice cold PBS and lysed with 60 μl/well 1% (v/v) Tx100 in PBS for 15 min on ice. Nuclei were removed by centrifugation (16000 x g, 20 min, 4°C) and lysate was aliquoted to 2 x 20 μl samples. One sample was mixed with 20 μl trypsin at 800 μg/ml in 1% Tx100, while the other was mixed with 20 μl 1% Tx100, and incubated for 10 min at 37°C. Both samples were mixed with 20 μl soy bean trypsin inhibitor, to inactivate the enzyme, at 2 mg/ml in 1% Tx100. Finally, 6x non-reducing LSB was added to a final concentration of 1x. The samples were not heated as this can dissociate the E1 homotrimer. An equal volume of each sample was separated by SDS-PAGE and analysed by western blot (Section 2.7).

2.6.7 SFV plasma membrane fusion

Cells were grown overnight in 96 well plate format and pre-incubated with DMSO or 100 nM Baf A prior to adding SFV (5 pfu/cell) as described for SFV E1 trypsin insensitivity. Unbound virus was removed by washing with cold BM (2 washes) and the cells were then treated with 37°C BM adjusted to pH 5.5 to activate the virus fusion machinery (or as control, remaining at pH 6.8) and incubated at 37°C for 3 min. Media were removed and replaced with F-12 infection media (pH 7) containing DMSO or Baf A and incubated for 5.5 - 6 h to allow infection, prior to fixation and analysis of infection by immunofluorescence microscopy (Section 2.8 and Section 2.6.8).

2.6.8 Infection quantification

Two approaches were used to detect the percentage of infected cells, both using immunofluorescence staining and microscopy (see Section 2.8). Either, cells were imaged using an Opera automated, high-throughput confocal microscope system (PerkinElmer): Cells were detected and counted based on Hoechst staining and infected cells were detected and counted based on viral protein staining by the Columbus software (PerkinElmer), allowing calculation of percentage infected cells. The Opera microscope was set up to image 12 fields of view at 20x magnification for each well. Or, cells were imaged with a Leica DMIRB epifluorescence microscope (also see Section 2.8.4 for further detail) and total cells and total infected cells were detected using ImageJ software. For this quantification of infection, 3 random fields of view were collected at 20x magnification per well. The images were separated to their component channels to give images of nuclei and staining of viral protein to mark infected cells. Nuclei were segmented and counted to determine the total number of cells per field of view. The segmented nuclei were then super-imposed on the image of the fluorescent channel for infected cells and a ring of 10 pixels was expanded around each nucleus area. The fluorescence intensity within this area was then used to score cells as infected or uninfected and the percentage of infected cells determined. The second approach was used as the Opera system was not always available. A direct comparison indicated very little difference in the data generated by the two methods. GraphPad Prism software was used for significance testing.

2.7 Western blotting

To produce whole cell lysates, cells were rinsed twice with ice cold PBS prior to addition of Tx100 lysis buffer (unless otherwise indicated) and incubated for 15 min on ice. Cells were scraped in order to collect all sample. Nuclei were pelleted by centrifugation (16000 x g, 20 min, 4℃) and the supernatant collected. Protein content was determined using the bicinchoninic acid method (Thermo Scientific), as per the manufacturer's instructions. Unless indicated otherwise, 20 μg of protein was used in each gel and mixed with 3x reducing or non-reducing LSB (final concentration of 1x), heated at 95℃ for 5 min. Proteins were separated by SDS-PAGE with constant voltage, using either 10% or

15% gels depending on the molecular weight of the protein being analysed. Proteins were transferred to PVDF membrane (Immobilon-FL, Millipore; activated with MeOH as per the manufacturers instructions) with constant current using a semi-dry approach (BioRad Trans Blot SD Semi-Dry Transfer Cell). Membranes were dried at 37℃ for 30 min, then re-wetted by 15 s incubation in MeOH, followed by washing with water for 2 min and TBST for 2 min. Membranes were then blocked using 5% (w/v) skimmed milk in TBST (block buffer) for 1 h and incubated with primary antibody (diluted in block buffer) at 4℃ overnight. Membranes were washed 3 x 5 min with TBST and incubated with Li-COR secondary antibodies diluted in block buffer for 1 h at RT. Membranes were washed 6 x 5 min with distilled water and dried by 30 min incubation at 37℃ prior to imaging on a Li-COR Odyssey system. Quantification of band intensity was performed using the Odyssey software.

2.7.1 Protease cleavage assays to investigate topology

A trypsin cleavage assay was performed to analyse IFITM1 topology. Cells were grown overnight on 6 x 35 mm well plates to be 80-90% confluent, washed twice with PBS at RT and treated with 100 μg/ml trypsin in PBS for 5-30 min at 37℃. Cells in suspension were collected and transferred to microcentrifuge tubes, on ice. The wells were rinsed with 1 mg/ml soy bean trypsin inhibitor (SBTI) in PBS, to collect any remaining cells, and this rinse was added to the microcentrifuge tubes on ice to inactivate the trypsin. The untreated control cells were incubated with PBS for 30 min at 37℃, prior to scraping to detach cells which were then collected into microcentrifuge tubes on ice. Wells were similarly washed with SBTI. As a further control, samples were incubated with inactivated trypsin (1:1 mix between trypsin and SBTI) for 30 min at 37℃ and collected as for the untreated control samples. Cells were pelleted by centrifugation (600 x g, 5 min, 4℃), washed with soy bean trypsin inhibitor then directly lysed in 1x reducing LSB (diluted from the 3x LSB stock - see Section 2.2) prior to SDS-PAGE and western blotting.

A similar protease cleavage assay was used to investigate the topology of IFITM3-Y20A, however IFITM3 lacks trypsin cleavage sites in the CTD. As a consequence proteinase K (ProtK) was used instead. Cells were set up as for the trypsin cleavage assay and treated with 500 μg/ml ProtK in DPBS for 10 or 30 min at 37℃ (DPBS used as

ProtK requires calcium ions for activity). PMSF was added (1 mM final) following each incubation to terminate the reaction. Cells in suspension were collected and transferred to microcentrifuge tubes on ice. Wells were rinsed with 1 mM PMSF in PBS, to collect any remaining cells, and this rinse was added to the microcentrifuge tube. Untreated control cells were incubated with DPBS for 30 min at 37℃, prior to collection by scraping; PMSF was added (1 mM final) and wells were similarly rinsed as for collection of other samples. For the inactivated control sample, PMSF was added to ProK (1 mM final) in DPSB prior to addition to cells and incubation for 30 min at 37℃. This inactivated control was collected in the same way as the untreated control. Cells were pelleted as above and washed with 1 mM PMSF then lysed with Tx100 lysis buffer prior to analysis by western blotting.

2.7.2 Biotin labelling and pulldown

HEK293T cells were grown on 10 cm dishes and transfected with pcDNA3.1 plasmids containing untagged IFITM1 or IFITM1-Vstop (Section 2.3.3). The cells were incubated for 24 h then detached with 5 mM EDTA and re-plated on 6 x 35 mm well plates. After a further 24 h, the cells were washed twice with PBS then labelled for 45 min at 37℃ with 1 mg/ml EZ-link Sulfo-NHS-SS-Biotin. The label was washed off with TBS and the cells were lysed with 100 μl Tx100 lysis buffer. Whole cell lysate (70 μl) was added to 25 μl of NeutrAvidin agarose beads and rotated for 3 h at 4℃. The beads were then pelleted by centrifugation (200 x g, 1 min) and the supernatant collected to assess the unbound material. The pelleted beads were washed with Tx100 lysis buffer, TBS and TE buffer, pelleting and removing the supernatant between each wash. Proteins were eluted from the beads by addition of 70 μl of 1x reducing LSB (diluted from 3x LSB stock) and heating at 95℃ for 10 min. The beads were again pelleted and the supernatant containing the eluted proteins was collected. A second round of elution was performed to ensure all protein had been collected. Equivalent volumes of the remaining whole cell lysate, unbound material and both protein elutions were separated by SDS-PAGE and analysed by western blot.

2.8 Immunofluorescence and Flow Cytometry

2.8.1 Immunofluorescence staining of permeabilised cells

Cells were cultured on glass coverslips, or plastic tissue culture dishes prior to any immunofluorescence staining. All processing was performed at RT. Cells were fixed for 15 min with 3% FA diluted in PBS. Samples were rinsed with PBS and free aldehyde was quenched by incubation with 50 mM NH_4Cl in 0.2% (w/v) BSA in PBS (PBS/BSA) for 15 min. Cells were again rinsed with PBS and then permeabilised with 0.05% saponin in PBS/BSA (permeabilisation buffer [PB]), and incubated for 30 min. Samples were subsequently incubated with appropriate primary antibodies diluted in PB for 1 h, prior to washing to remove any unbound antibody (3 x 5 min washes with PB). Secondary antibodies were similarly diluted in PB and incubated with samples for 45 min prior to washing (4 x 5 min). Details of all antibodies and their usage are given in Tables 2.5 and 2.6. Nuclei were labelled by 5 min incubation with 5 μg/ml Hoechst (in PB). Samples were finally washed 3 x 5 min in PBS and mounted to glass slides (Thermo Scientific or VWR International) in Mowiol prior to imaging. All samples in culture dishes were left in PBS.

For detection of flavivirus infection and SFV capsid by immunofluorescence staining, the above procedure was altered to use 0.1% (v/v) Tx100 in PBS for permeabilisation. In this variation, permeabilisation was carried out for 10 min, and PBS/BSA (without Tx100) was used for all subsequent steps.

2.8.2 Immunofluorescence staining of intact cells

Where indicated immunofluorescence staining was performed on intact cells using one of two approaches. For the first approach, cells were incubated on ice with cold PBS/BSA for 10 min prior to incubation with primary antibody diluted in ice cold PBS/BSA for 1 h. Unbound antibody was removed by washing with cold PBS/BSA (3 x 5 min) and the cells were fixed with cold 3% FA for 1 h (30 min on ice and 30 min at RT). Subsequent steps were performed as for permeabilised immunofluorescence, using PBS/BSA for diluting all reagents. An alternative approach was to fix cells with 3% MeOH free FA and perform all steps at RT, as described for permeabilised immunofluorescence, in the absence of

detergent (PBS/BSA for all steps).

2.8.3 Antibody feeding

Cells were cultured on coverslips overnight and incubated with 5 μg/ml rat anti-HA antibody for 3 h at 37℃ (diluted in culture media). Unbound antibody was removed by rinsing the cells 2x with media and 1x with PBS prior to fixation with 3% FA. Cells were then processed for immunofluorescence staining with permeabilisation (Section 2.8.1).

2.8.4 Microscopy

For imaging cells in tissue culture dishes, a Leica DMIRB epifluorescence microscope connected to a Hammamatsu C4742-95 Orca CCD camera was used. Images were acquired using OpenLab software (PerkinElmer). Cells on coverslips were imaged using either epifluorescence or confocal microscopy. For epifluorescence microscopy either a Zeiss AxioImager (connected to a QImaging Retiga EXi camera), or a Zeiss Axioplan (connected to a QImaging QIClick camera) were used, with images acquired through OpenLab software. For confocal microscopy a Leica SPE system was used with images acquired through the LAS AF software (Leica). As discussed in Section 2.6.8, an Opera automated, high-throughput confocal microscope system (PerkinElmer) was also used for analysis of infection percentages.

2.8.5 Flow cytometry

Samples were prepared as described for the immunofluorescence staining with the alterations described subsequently. Flow cytometry was performed with an LSR-II (BD Bioscience) with cells being gated on forward and side scatter and analysed for fluorescence intensity. Data was processed with FlowJo software (TreeStar).

Cell surface IFITM staining and flow cytometry

Cells grown on 6 x 35 mm dishes were detached by incubation at 37℃ with 5 mM EDTA in PBS. The detached cells were collected, pelleted by centrifugation (600 x g 5 min at RT) and the supernatant removed. Cell pellet was resuspended in 3% FA and incubated

at RT for 15 min to fix. Cells were again pelleted by centrifugation, and resuspended in 50 mM NH_4Cl and incubated at RT for 15 min (as described for cells on coverslips in Section 2.8). Samples were then either permeabilised with 0.05% saponin or left intact by incubation with PBS/BSA only (30 min incubation). Cells were labelled with rat anti-HA antibody followed by appropriate secondary antibody. The staining procedure was carried out to mimic that of cells on coverslips as described in Section 2.8, with centrifugation and supernatant removal at each step. As controls, samples were either incubated without antibodies present (PBS/BSA only) or incubated with secondary antibody only.

HA-tag trypsin cleavage and flow cytometry

Cells were grown in 6 x 35 mm dishes and treated with trypsin for 10 or 30 min (as described in Section 2.7.1). Cells were collected and processed as above.

2.9 Image analysis

2.9.1 Co-localisation analysis

All microscope image analysis was performed using ImageJ. For calculation of Pearson's R-value and Mander's correlation coefficients M1 and M2, individual cells were manually segmented and analysed using the JACoP plugin [189]. For the M1 and M2 values a Costes's automatic threshold was applied, as described [189]. The process of calculating relative areas of overlap is detailed in Fig. 2.1. All significance testing was performed used GraphPad Prism software.

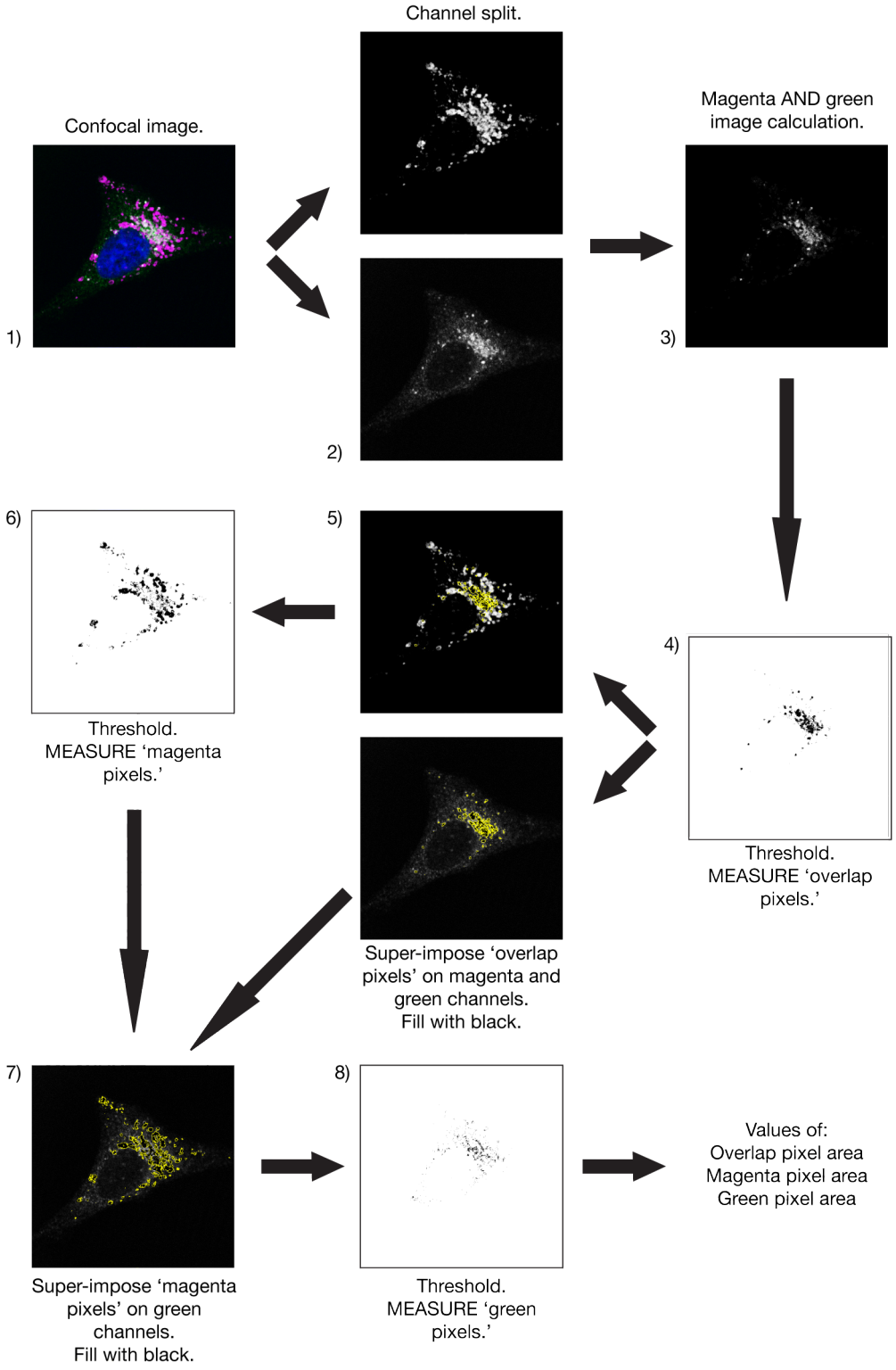
Channel split.
Confocal image.
Magenta AND green image calculation.
1)
2)
3)
4)
5)
6)
Threshold. MEASURE 'magenta pixels.'
Threshold. MEASURE 'overlap pixels.'
Super-impose 'overlap pixels' on magenta and green channels. Fill with black.
7)
8)
Super-impose 'magenta pixels' on green channels. Fill with black.
Threshold. MEASURE 'green pixels.'
Values of: Overlap pixel area Magenta pixel area Green pixel area

Figure 2.1: **Work flow for co-localisation analysis.** 1) To analyse co-localisation, single confocal sections were acquired through the centre of cells. 2) The component channels of the image were separated and the nuclei (blue channel) were discarded, leaving magenta and green channels. 3) An 'AND' function was performed on the two channels to produce a new image made up of pixels containing both magenta and green signal. 4) A threshold was set to remove background signal and the area of the magenta and green ('overlap') pixels was measured. 5) 'Overlap' pixels were removed from the individual magenta and green channels. 6) As in 4, a threshold was set to remove background and measure the magenta only pixels. 7) Magenta only pixels were removed from the green channel. 8) The remaining green pixel area was measured. Three values were therefore produced per confocal section, overlap pixel area, magenta only pixel area and green only pixel area. These values were set relative to total pixel area and analysed across multiple images to determine co-localisation.

2.9.2 Analysis of cytosolic SFV capsid immunofluorescence staining

All microscope image analysis was performed using ImageJ. The process of quantifying the immunofluorescence associated with SFV capsid release into the cytosol is detailed in Fig. 2.2. GraphPad Prism software was used for significance testing.

2.10 Statistical analysis

All statistical analysis was performed using GraphPad Prism software. All analyses were performed as unpaired student's t-tests to compare difference between control A549 cells and IFITM expressing cells, or drug treated cells and untreated cells.

2.11 Electron Microscopy

All sample preparation for EM was performed by Dr. Ian White (MRC LMCB). All samples were imaged using a transmission electron microscope (Tecani T12; FEI), equipped with a charge-coupled device camera (SIS Morada; Olympus).

Epon section EM

Cells were grown on coverslips overnight prior to addition of SFV (1000 pfu/cell) for cell surface binding and internalisation as described in Section 2.6.3. Cells were fixed

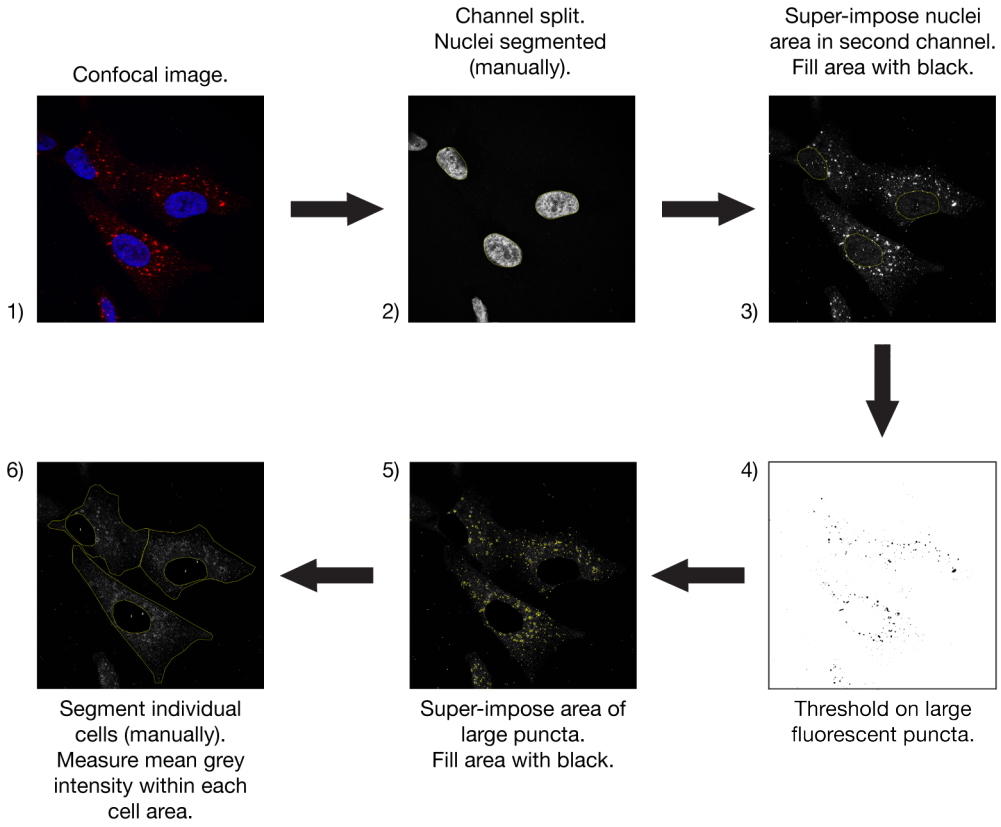

Figure 2.2: **Work flow for analysis of cytosolic capsid fluorescence.** 1) To analyse cytosolic capisd fluorescence, single confocal sections were acquired through the centre of cells. 2) The component channels were split and nuclei areas were manually segmented. 3) Any fluorescence in the capsid channel associated with the nuclei area was deemed to be background and was therefore removed. 4) A threshold was set to detect the large fluorescent puncta. 5) The large puncta were judged to be virus particles within endosomes, rather than staining of capsid in the cytosol and as such, these pixels were also removed. 6) Individual cell areas were segmented and the mean grey value within each area was measured to determine cytosolic fluorescence intensity.

with EM-grade 2% FA / 2% glutaraldehyde in 0.1 M sodium cacodylate (pH 7.4) for 30 min. Samples were further fixed for 1 h in 1% osmium tetraoxide/1.5% potassium ferricyanide at 4℃ then treated with 1% tannic acid in 0.1 M sodium cacodylate for 45 min at RT. Samples were dehydrated in sequentially increasing concentrations of ethanol and embedded in Epon resin. The coverslips were inverted onto prepolymerised Epon stubs and polymerised by baking at 60℃ overnight. A Diatome 45° diamond knife and an ultramicrotome (UC7; Leica) were used to cut 70 nm ultrathin sections. These sections were collected on 1 x 2 mm formvar-coated slot grids and stained with Reynolds lead citrate [190].

Immunogold labelling of cryosections and EM

When analysing SFV internalisation by immunogold labelling, virus was added to cells at 5000 pfu/cell for binding at the plasma membrane, prior to warming to allow internalisation (as described in Section 2.6.4), prior to fixation. Alternatively, cells were grown on coverslips overnight prior to fixation. Cells were fixed with 4% FA in 0.1 M phosphate buffer (pH 7.4), infused with 2.3 M sucrose, supported in 12% (w/v) gelatin and frozen in liquid nitrogen. Ultrathin (70 nm) cryosections were cut at -120℃ and picked up in 1:1 2% sucrose:methylcellulose. Sections were labelled with primary antibodies (detailed in Table 2.5) and where necessary a bridging antibody (rabbit anti-mouse intermediate [1:180; DAKO] - required for detection of mouse anti-HA antibody) and protein A-gold. For double labelling experiments, sections were treated with 1% glutaraldehyde in PBS after the first protein A-gold incubation then quenched in 15 mM glycine before repeating the single labelling procedure with the second primary antibody and different sized protein-A gold [191]. The antibody order was anti-HA followed by anti-E1/E2. Sections were contrast stained in a 1:9 solution of 4% uranyl acetate:2% methylcellulose pH 4.0.

Chapter 3

IFITM Protein Membrane Topology and Localisation

3.1 Introduction

When the IFITM proteins were identified as having antiviral function by Brass *et al.* [7], their data suggested that the IFITMs had a dual-pass transmembrane topology. The N- and C-terminal domains (NTD and CTD) were both suggested to reside in the extracellular/lumenal space, connected by two transmembrane domains and the conserved intracellular loop (CIL; Fig. 3.1; model 1). This model was in agreement with older suggestions of IFITM membrane topology [114–116]. However, subsequent studies were published suggesting that both the NTD and CTD were in fact on the cytoplasmic side of cellular membranes, necessitating two intramembrane loops (Fig. 3.1; model 2; [150, 163]).

At the commencement of this work, there was debate over the topology of the IFITMs. Therefore, biochemical and cell biological experiments were performed to define the membrane topology in a stable A549 cell system. These investigations produced data to suggest a third membrane topology model in which the NTD is on the cytoplasmic side of membranes, while the CTD is on the extracellular/lumenal side (Fig. 3.1; model 3). Our work was published [15], and much of the data presented in this chapter can also be found there. During the course of our studies, the same topology model was proposed for murine Ifitm3 [153]. Another more recent study has further supported this topology

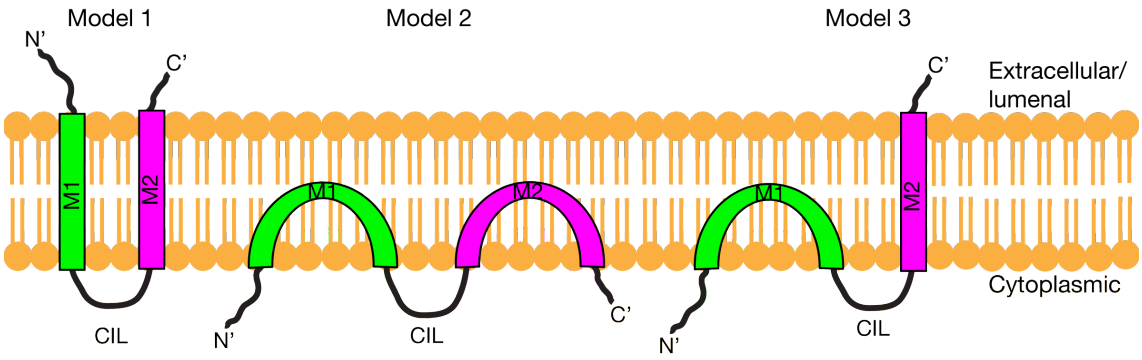

Figure 3.1: **Topology models of the IFITM proteins.** Model 1: The initially proposed model for IFITM membrane topology placed both the N- and C-terminal domains (NTD and CTD) on the extracellular/lumenal side of cellular membranes. The two termini are connected by two transmembrane domains (M1 and M2) and a conserved intracellular loop (CIL). Model 2: The second proposed model for IFITM membrane topology placed both the NTD and CTD on the cytoplasmic side of membranes, connected by M1, CIL and M2. This model necessitated M1 and M2 enter into but do not cross the lipid bilayer. Model 3: The most recently proposed model suggests that the NTD is cytoplasmic, while the CTD is extracellular/lumenal. M1 enters into, but does not cross the bilayer, while M2 crosses the bilayer. (N.B. This figure has previously been displayed in Chapter 1 and is repeated here as an aide-memoire).

model for human IFITM3 using the methods of nuclear magnetic resonance (NMR) and electron paramagnetic resonance (EPR; [192]). Defining a membrane topology in which the CTD resides in extracellular/lumenal spaces has implications for understanding the distribution of IFITM proteins within the endosomal system. Consequently, work is presented analysing the cellular distribution of the IFITM proteins by immunofluorescence microscopy with antibodies against the NTD. Developing an understanding of the topology and localisation may also have implications for understanding the antiviral activity of the proteins, as will be discussed in subsequent chapters.

3.2 Results

3.2.1 The IFITM1 C-terminal domain resides in the extracellular space

To investigate the topology and cellular distribution of the IFITM proteins, A549 cells stably expressing C-terminally HA-tagged proteins were analysed by immunofluorescence microscopy. When cells were permeabilised with saponin and labelled with anti-HA anti-

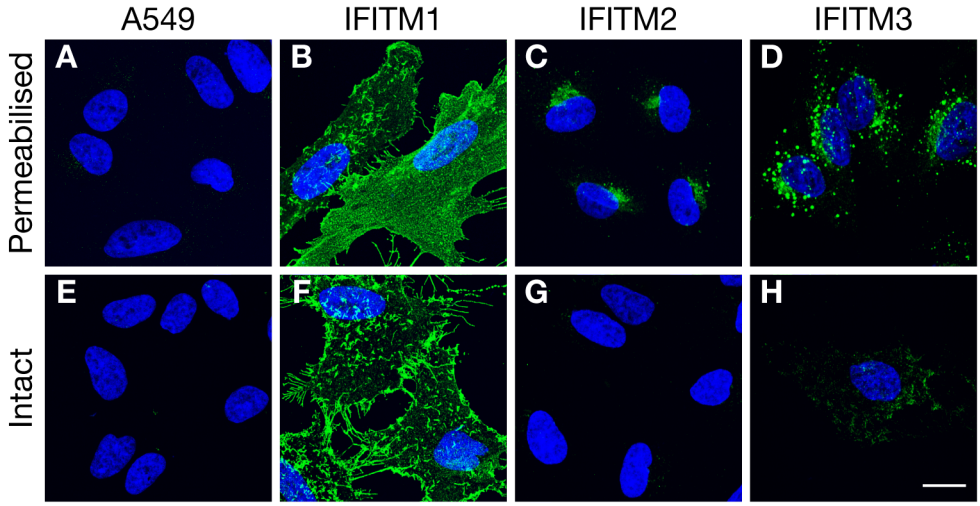

Figure 3.2: **Cellular distribution of the IFITM proteins and HA-tag localisation.** Control A549 and C-terminally HA-tagged IFITM1, 2 and 3 expressing cells were labelled with an anti-HA antibody following saponin permeabilisation or with intact cell membranes (antibody added on ice prior to fixation). The anti-HA antibody was visualised with anti-rat AF488 antibody. A and E) Permeabilised and intact A549 cells showed no specific staining for HA. B-D) In permeabilised cells, the HA-tag could be detected and the labelling showed that IFITM1, 2 and 3 have distinct distributions. F) The HA-tag was accessible on intact IFITM1 expressing cells. G) Intact IFITM2 expressing cells show no specific staining. H) A minority (<1%) of intact IFITM3 expressing cells had low level HA signal detectable at the plasma membrane. Nuclei were labelled with Hoechst. All images are maximum intensity projections of confocal sections through the depth of the cells. All images were acquired with the same microscope settings and brightness and contrast have been adjusted uniformly. Scale bar represents 15 μm.

body, all three IFITM proteins were found to have distinct distributions (Fig. 3.2 B-D). There was no background staining in the control A549 cells (Fig. 3.2 A). IFITM1 appeared to be primarily at the plasma membrane, while IFITM2 and IFITM3 were mostly seen in punctate, intracellular compartments. Intact cells were also stained to assess the extracellular availability of the C-terminal HA-tags. In order to ensure the integrity of the plasma membrane, anti-HA antibody was added to cells on ice prior to fixation. IFITM1 could be detected on intact cells (Fig. 3.2 F), and the staining appeared very similar to that seen on saponin treated cells. There was no detection of IFITM2, probably as a result of localisation to intracellular membrane compartments (Fig. 3.2 G). A small fraction (<1%) of IFITM3 expressing cells showed some signal at the plasma membrane, however most cells lacked any positive staining (Fig. 3.2 H). These data suggested that IFITM1 (and perhaps IFITM3) have a CTD HA-tag that is exposed in the extracellular space.

To ensure that cytoplasmic antigens were not being labelled, the integrity of the plasma membrane to antibodies was assessed. Tubulin could be detected in saponin permeabilised cells (Fig. 3.3 A), and IFITM1-3 showed the same distributions displayed in Fig. 3.2. However, when antibodies were added on ice prior to fixation there was no detectable tubulin staining (Fig. 3.3 B). Comparatively, IFITM1 could be detected and a low percentage of IFITM3 expressing cells again stained positively (Fig. 3.3 B). These data suggest that intracellular antigens are not detected under the 'intact' condition, suggesting the HA-tag is extracellularly exposed.

Finally, to test the apparent plasma membrane localisation of IFITM1 and a minority of IFITM3, intact cells were co-labelled with wheat germ agglutinin conjugated to a fluorophore. These results suggest that IFITM1 and IFITM3 are indeed at the plasma membrane (Fig. 3.4). Overall, the data suggest that in A549 cells, IFITM1 is localised at the plasma membrane and the CTD HA-tag is extracellularly accessible to antibody labelling. IFITM2 and IFITM3 are predominantly found within internal membrane compartments, however, on a low number of cells the CTD HA-tag of IFITM3 could be detected at the plasma membrane, suggesting that similarly to IFITM1, the CTD is in the extracellular space.

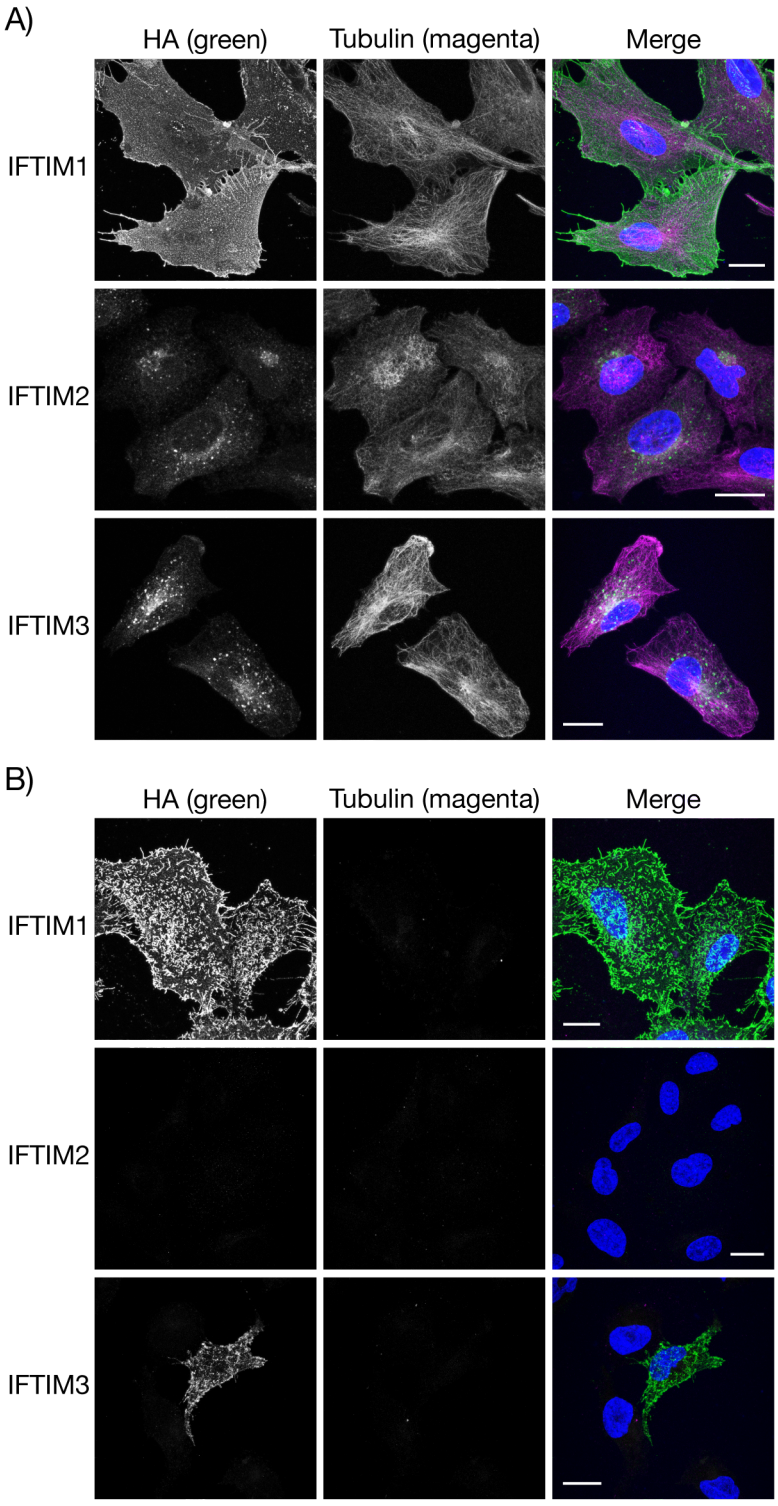
A)
HA (green)
Tubulin (magenta)
Merge
IFTIM1
IFTIM2
IFTIM3
B)
HA (green)
Tubulin (magenta)
Merge
IFTIM1
IFTIM2
IFTIM3

Figure 3.3: **IFITM1 and IFITM3 can be labelled on intact cells, while tubulin cannot.** C-terminally HA-tagged IFITM1, 2 or 3 expressing cells were co-stained for the HA-tag and tubulin following saponin permeabilisation or in intact conditions. The HA-tag was visualised with AF488 (green), while tubulin was visualised with AF594 (magenta). A) Permeabilised cells showed positive labelling for tubulin and all three IFITMs. B) When antibodies were added to cells on ice, prior to fixation to maintain the integrity of the plasma membrane, no tubulin was detected. Conversely, IFITM1 and a minority of IFITM3 expressing cells were positive for HA. No IFITM2 was detected in the absence of permeabilisation. Nuclei were labelled with Hoechst. All images are maximum intensity projections of confocal sections through the depth of the cells. All images were acquired with the same microscope settings and brightness and contrast have been adjusted uniformly. Scale bar represents 15 μm. (Immunofluorescence staining and microscopy was performed by Stephanie Czieso).

3.2.2 Analysis of IFITM localisation and HA-tag orientation by electron microscopy

To further define the localisation of the IFITM proteins, ultrathin (70 nm) cryosections of IFITM expressing cells were prepared and labelled using antibodies against the HA-tag and protein A-gold and analysed by electron microscopy (EM). The majority of IFITM1 labelling was detected at the plasma membrane (Fig. 3.5), supporting the immunofluorescence data (Fig. 3.2). It also appeared that many of the gold particles were on the extracellular side of the plasma membrane, further suggesting the extracellular localisation of the CTD. Additional IFITM1 labelling was detected in endosomes and multivesicular bodies (MVBs; Fig. 3.5B and C) and the Golgi apparatus (Fig. 3.5 D), indicating the presence of protein in the endocytic and biosynthetic pathways.

There was generally low labelling for the HA-tag in IFITM2 expressing cells. The labelling that was seen appeared to be predominantly on MVBs, with much of that labelling being on intra-lumenal vesicles (ILV), rather than on the limiting membrane (Fig. 3.6 B). In contrast to IFITM1, only a low level of IFITM2 HA labelling was detected at the plasma membrane (Fig. 3.6 A). Similarly to IFITM1, IFITM2 HA labelling was also found at the Golgi apparatus (Fig. 3.6 C).

Some IFITM3 HA labelling could be detected at the plasma membrane (Fig. 3.7 A). This was less common than seen for IFITM1, but more common than seen for IFITM2. Similarly to IFITM2, the majority of IFITM3 HA labelling was found on MVBs, and specifically the ILVs (Fig. 3.7 B). Labelling was again observed at the Golgi apparatus (Fig. 3.7 C). Similarly to IFITM1, in IFITM3 expressing cells, plasma membrane localised gold particles appeared to be predominantly on the extracellular side of membranes (Fig. 3.7 A).

Overall, the data from the EM further defines that IFITM1 is predominantly found at the plasma membrane, while IFITM2 and IFITM3 are mostly found within intracellular compartments, particularly MVBs. However, these localisations are not exclusive as protein was found in compartments of the endocytic and biosynthetic pathways. It is therefore possible to infer some details of IFITM protein trafficking. IFITM proteins may traffic through the Golgi apparatus and the secretory pathway to reach the plasma membrane, from where they may be internalised to endocytic compartments. Alternatively,

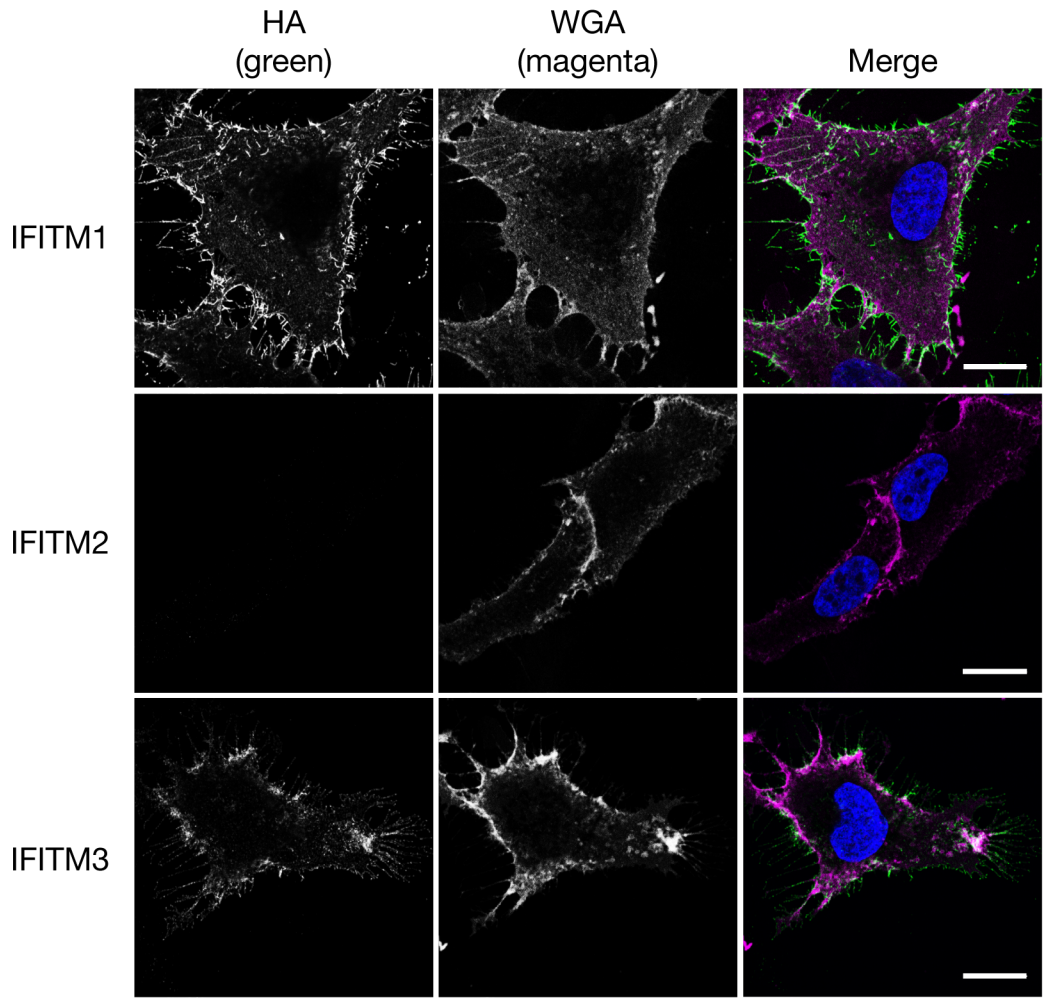

Figure 3.4: **IFITM1 and IFITM3 labelling on intact cells co-localises with wheat germ agglutinin.** IFITM expressing cells were co-labelled with anti-HA antibody (detected with AF488; green) and wheat germ agglutinin (WGA) directly conjugated to AF647 (magenta). WGA labels the plasma membrane, under these intact conditions, and acts as a marker to show that the C-terminal HA-tag of IFITM1 and IFITM3 can be detected at the cell surface of intact cells. There was no HA-tag detection on the IFITM2 expressing cells. Images are single optical sections. Nuclei were labelled with Hoechst. Scale bars represent 15 μm.

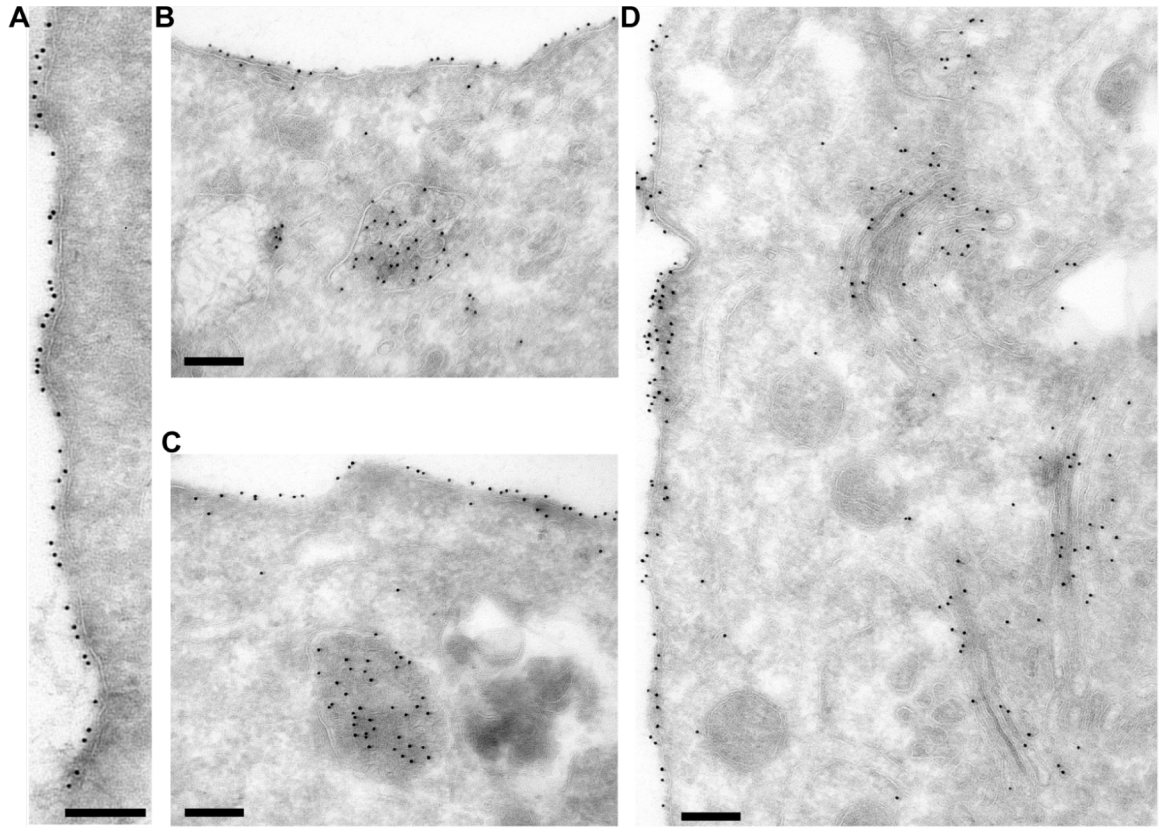

Figure 3.5: **IFITM1 localisation analysed by electron microscopy.** Cryo-sections of IFITM1 expressing cells were labelled with anti-HA antibody and Protein A-gold and analysed by electron microscopy. A) Labelling for IFITM1 localised at the plasma membrane. B and C) IFITM1 labelling at the plasma membrane and within multivesicular bodies. D) Further plasma membrane labelling and Golgi apparatus labelling. As suggested from the images, the majority of IFITM1 protein was found at the plasma membrane, but some protein was also localised in intracellular compartments. Scale bars represent 200 nm. (Sample preparation and microscopy were performed by Dr. Ian White).

there could be direct trafficking from the Golgi apparatus to compartments of the endocytic pathway. Additionally, the immuno-gold labelling of the HA-tag appears to support the notion that this C-terminal epitope is on the extracellular face of membranes.

3.2.3 The IFITM1 N-terminal domain resides intracellularly

Having determined that the CTD of IFITM1 was accessible at the plasma membrane on intact cells, the topology of the IFITM proteins was further analysed through the use of antibodies targeting the NTD. Two commercially available antibodies that were raised against the 'IFITM1-NTD' or the 'IFITM3-NTD' were used. The anti-IFITM1-NTD

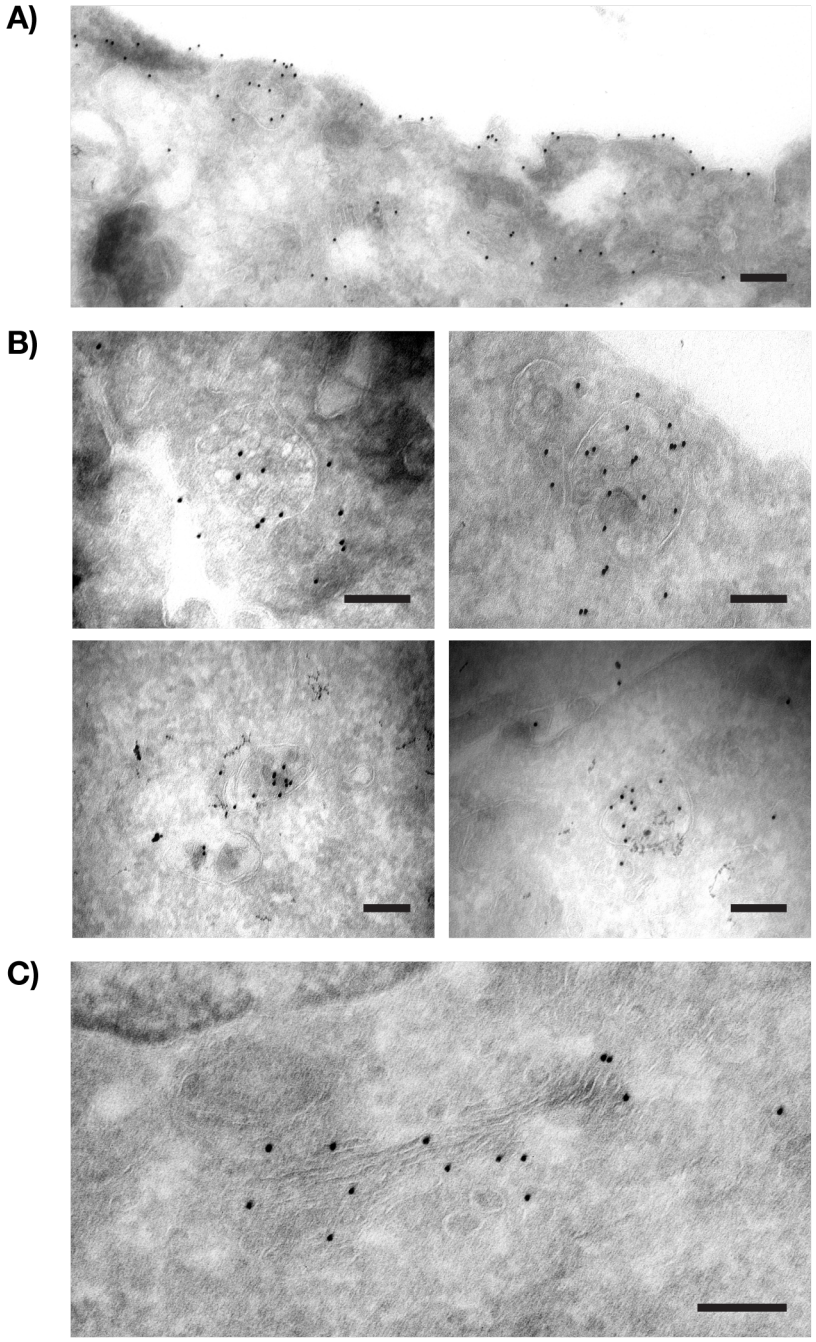

Figure 3.6: **IFITM2 localisation analysed by electron microscopy.** Cryo-sections of IFITM2 expressing cells were labelled with anti-HA antibody and Protein A-gold and analysed by electron microscopy. A) A rare example of plasma membrane localised labelling for IFITM2. B) Four examples of IFITM2 labelling in endosome and multivesicular bodies. Most of IFITM2 labelling was seen on such compartments. C) Labelling of IFITM2 in the Golgi apparatus. Scale bars represent 200 nm. (Sample preparation and microscopy were performed by Dr. Ian White).

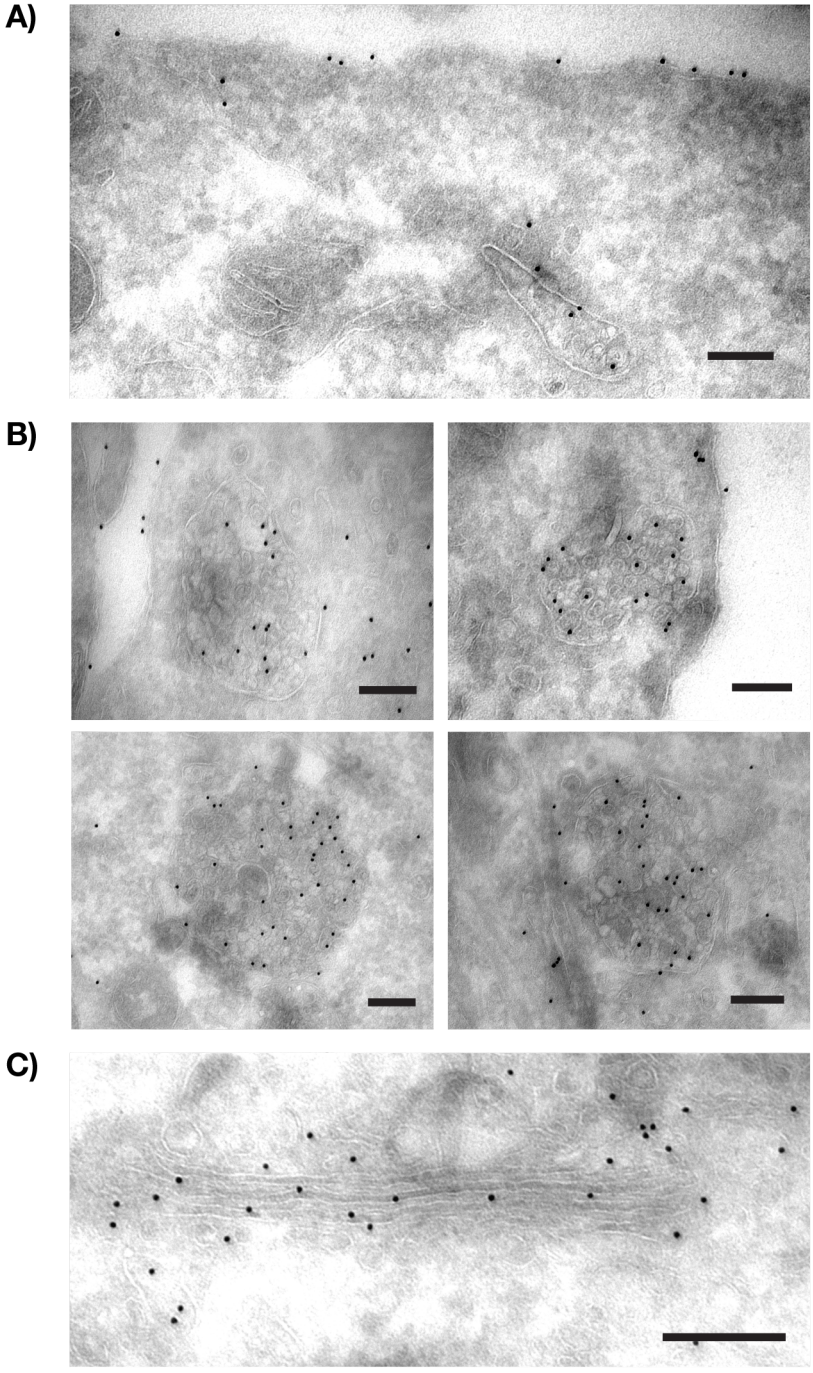

Figure 3.7: **IFITM3 localisation analysed by electron microscopy.** Cryo-sections of IFITM3 expressing cells were labelled with anti-HA antibody and Protein A gold and analysed by electron microscopy. A) Labelling for IFITM3 at the plasma membrane and an internal membrane compartment. Compared to IFITM2 (Fig. 3.6), more examples of IFITM3 at the plasma membrane were seen. B) Four examples of IFITM3 labelling on multivesicular bodies. Most of the IFITM3 labelling was seen in such compartments. C) Labelling of IFITM3 in the Golgi apparatus. Scale bars represent 200 nm. (Sample preparation and microscopy were performed by Dr. Ian White).

antibody was raised against the first 35 amino acids of IFITM1. This region has 69% and 75% amino acid identity with IFITM2 and IFITM3, respectively (see Fig. 1.6 [page 44], for sequence alignments). The anti-IFITM3-NTD antibody was raised against the first 30 amino acids of IFITM3. There is 90% amino acid identity between IFITM2 and IFITM3 in the first 30 amino acids, however IFITM1 has a 21 amino acid truncation compared to IFITM3 and therefore has only 9 amino acids overlapping with this sequence (Fig. 1.6).

The two antibodies were tested for cross-reactivity against the three IFITM proteins by western blotting whole cell lysates from each of the stable cell lines, and by immunofluorescence. By western blot, the anti-IFITM1-NTD antibody was found to cross-react with IFITM3, but did not detect IFITM2 (Fig. 3.8), while the anti-IFITM3-NTD antibody showed cross-reactivity with IFITM2 but not IFITM1 (Fig. 3.8). Multiple bands were seen in the range of 12-17 kDa when analysing the NTD, while only one band was seen for the HA-tag. This suggested that there could be some form of post-translational modification of the protein (discussed further in Section 3.2.6). When the two NTD antibodies were used for immunofluorescence on permeabilised cells, the labelling largely matched the western blot results. The anti-IFITM1-NTD antibody detected IFITM1 and IFITM3, and there was only minimal detection of IFITM2 (Fig. 3.9 B-D). No staining was observed in control A549 cells (Fig. 3.9 A). The anti-IFITM3-NTD antibody did not detect IFITM1, but did detect IFITM3 and IFITM2 (Fig. 3.9 F-H). Some background fluorescence was seen in control A549 cells using the anti-IFITM3-NTD antibody (Fig. 3.9 E), but this was clearly lower than when IFITM proteins were stably expressed.

Using the NTD antibodies for immunofluorescence microscopy on permeabilised cells showed distributions of IFITM proteins that matched those seen when using antibodies against the HA-tag (Fig. 3.2). There was more, and brighter labelling for IFITM2 with the anti-IFITM3-NTD than the HA-tag (discussed in further Section 3.2.6). When intact cells were labelled with anti-IFITM1-NTD antibody neither IFITM1 nor IFITM3 could be detected, unlike results seen after labelling for the HA-tag (Fig. 3.9 J and L, compared to Fig. 3.2 F and H). These data therefore suggest a topology in which the NTD is on the cytosolic side of membranes, while the CTD is in the extracellular space.

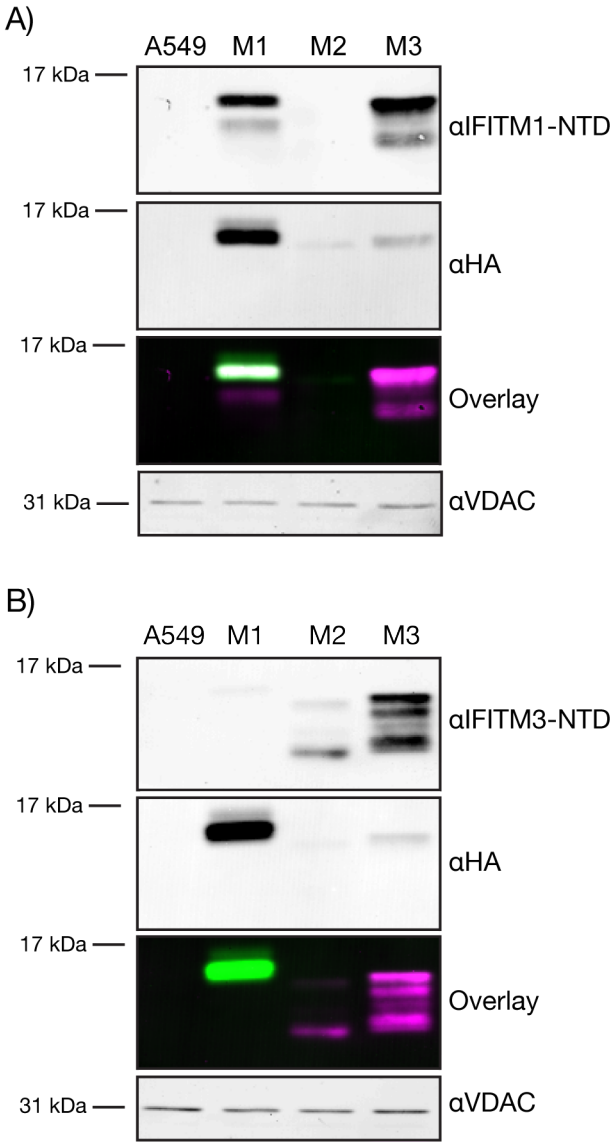

Figure 3.8: **Analysis of IFITM NTD antibodies by western blot.** Two commercially available antibodies were tested for their cross-reactivity between IFITM proteins by western blot of whole cell lysates from A549 cells, or IFITM1-3 expressing A549 cells (M1, M2 and M3). Equivalent amounts of protein were separated by SDS-PAGE on 15% gels, transferred to PVDF membranes and western blotted with antibodies against the IFITM-NTD, HA-tag and VDAC (as a loading control). Blots were imaged using the Li-COR Odyssey system that uses far-red fluorophore conjugated secondary antibodies, displayed in magenta (NTD) and green (HA). A) Anti-IFITM1-NTD probed western blots show this antibody detects IFITM1 and cross-reacts with IFITM3. B) Anti-IFITM3-NTD probed western blots show this antibody detects IFITM3 and cross-reacts with IFITM2.

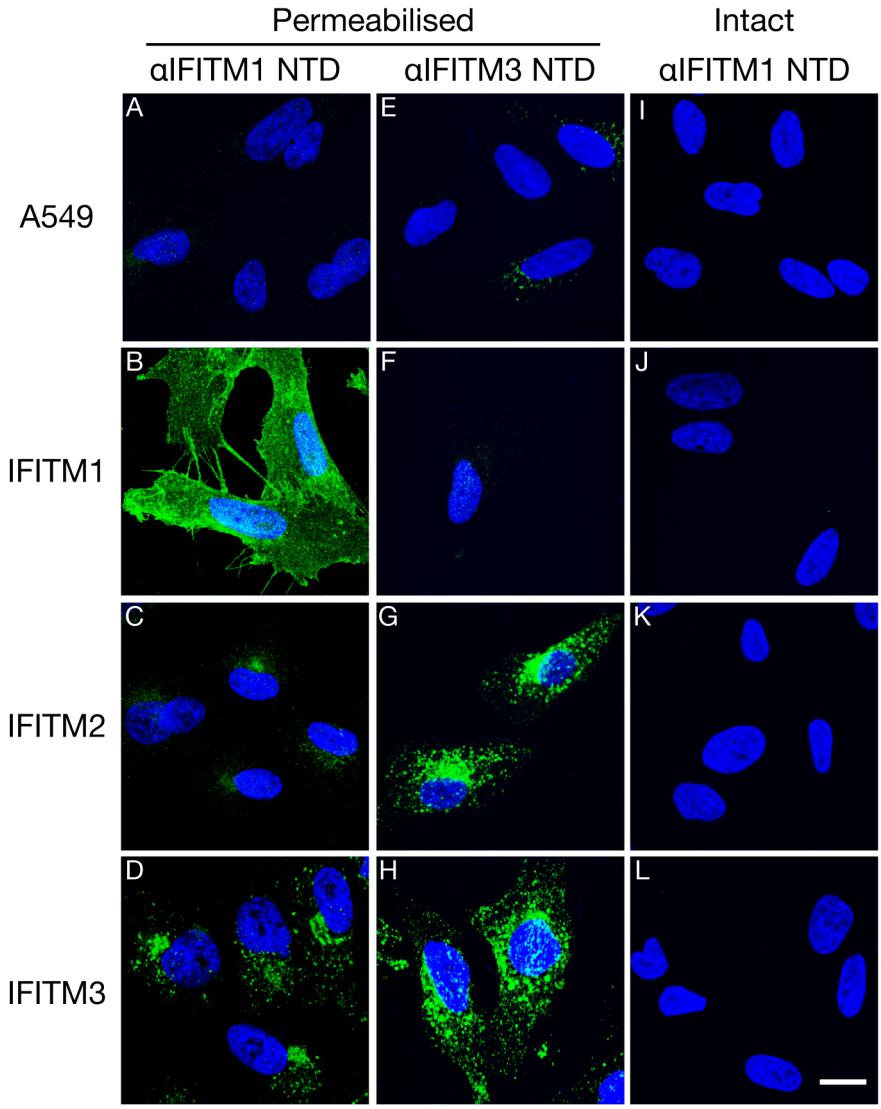

Figure 3.9: **Cellular distribution of IFITM proteins and NTD localisation.** Immunofluorescence microscopy of control A549 cells, or cells expressing IFITM1-3 using anti-IFITM1-NTD or anti-IFITM3-NTD antibodies. A) Saponin permeabilised A549 cells show no specific staining with the anti-IFITM1-NTD antibody. B-D) IFITM1, 2 and 3 can be detected with the anti-IFITM1-NTD antibody and have distinct cellular distributions, when cells were permeabilised. E and F) The anti-IFITM3-NTD antibody detects a low level of background protein in permeabilised A549 and IFITM1 expressing cells. G and H) IFITM2 and IFITM3 were detected by the anti-IFITM3-NTD antibody in permeabilised cells. I-L) No specific staining was detected with the anti-IFITM1-NTD antibody when cell membranes were intact. Hoechst was used to label the nuclei. All images are maximum intensity projections of confocal sections through the depth of the cells. All images were acquired using the same microscope settings and brightness and contrast have been adjusted uniformly. Scale bar represents 15 μm.

3.2.4 The IFITM1 C-terminal domain is accessible to extracellular proteases

The data have shown that IFITM1 is predominantly localised at the plasma membrane making it highly amenable to further analysis of its membrane topology. The hypothesis was made that because the HA-tag was accessible to antibodies, it would also be accessible to extracellular proteases. The IFITM1 CTD amino acid sequence was analysed with the ExPASy Peptide Cutter tool (`http://web.expasy.org/peptide_cutter/`). There are two trypsin cleavage sites in the IFITM1 CTD (Fig. 3.10 A) and there is a suitable inhibitor to terminate trypsin activity (soy bean trypsin inhibitor; SBTI); trypsin was therefore chosen as an appropriate enzyme to test accessibility of the HA-tag.

IFITM1 expressing cells were incubated with trypsin for between 5 and 30 min at 37°C, or incubated for 30 min with PBS alone. The reaction was terminated by addition of SBTI after each incubation period. Samples were then collected, lysed, separated by SDS-PAGE and analysed by western blot for loss of HA signal, and a change in the molecular weight (MW) of the protein. As previously seen in Fig. 3.8, untreated IFITM1 displayed two bands when detected with anti-IFITM1-NTD antibody. The high MW band corresponded to the HA-tagged form of the protein, based on overlap of the bands (Fig. 3.10 Bi-iii). Following treatment with trypsin, the intensity of the HA band decreased, and there was a concomitant increase in the intensity of the lower MW NTD band (Fig. 3.10 Bi and ii). By 30 min there was ∼8% of the HA-tag signal remaining, compared to the untreated control. This incomplete loss of the HA-tagged form of the protein was probably due to the intracellular pool that was inaccessible to the enzyme (Fig. 3.5). When trypsin was mixed with SBTI prior to addition to cells there was no cleavage of the HA-tag, indicating the reaction was effectively terminated and there was no cleavage following lysis of the cells (Fig. 3.10 B). The NTD and the CIL of IFITM1 both have trypsin cleavage sites (2 and 5 sites, respectively), therefore if either of these were extracellularly available, more fragments of IFITM1 would be expected on the western blots. These results further suggest that IFITM1 has a topology in which the CTD HA-tag is accessible at the cell surface, while the NTD is located on the cytoplasmic side of membranes.

Cleavage of the IFITM1 HA-tag was also assessed by flow cytometry. Cells were incubated with trypsin for 10 or 30 min, and the enzyme was inactivated by addition

of SBTI. Cells were subsequently fixed and labelled with anti-HA antibody, which was detected with fluorophore-conjugated secondary antibody. Untreated IFITM1 expressing cells showed clear HA labelling, compared to A549 control cells, as judged by the higher mean fluorescence intensity (MFI) and shift in peak fluorescence intensity (Fig. 3.10 C and D). When cells were treated with trypsin, there was a lower peak fluorescence intensity and reduced MFI, with greater reduction at 30 min than 10 min of treatment (Fig. 3.10 C and D). Overall, the data from trypsin cleavage experiments argue that the IFITM1 C-terminal HA-tag is accessible to extracellular proteases, while the NTD and CIL are protected.

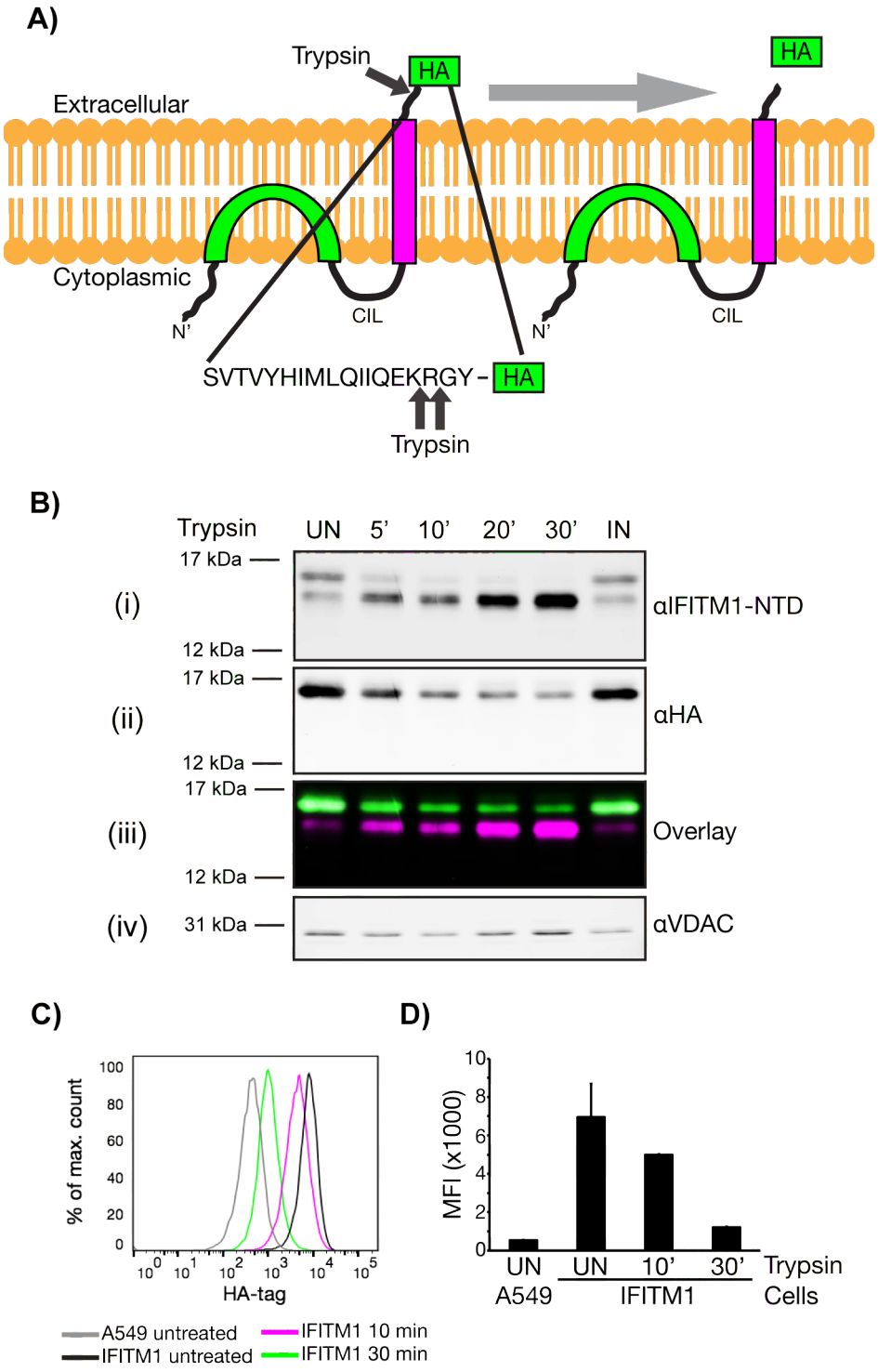
A)
Trypsin
HA
HA
Extracellular
Cytoplasmic
N'
CIL
N'
CIL
SVTVYHIMLQIIQEKRGY-
HA
Trypsin
B)
Trypsin
UN
5'
10'
20'
30'
IN
17 kDa
12 kDa
(i)
αIFITM1-NTD
17 kDa
12 kDa
(ii)
αHA
17 kDa
12 kDa
(iii)
Overlay
(iv)
31 kDa
αVDAC
C)
% of max. count
100
80
60
40
20
0
HA-tag
A549 untreated
IFITM1 untreated
IFITM1 10 min
IFITM1 30 min
D)
MFI (x1000)
10
8
6
4
2
0
UN
UN
10'
30'
Trypsin
A549
IFITM1
Cells

Figure 3.10: **Trypsin cleavage of HA-tagged IFITM1.** A) Schematic representation of the trypsin cleavage assay and the predicted cleavage sites in the IFITM1 CTD. B) IFITM1 expressing cells were treated with trypsin (100 μg/ml) for up to 30 min at 37℃. The reaction was terminated by addition of soy bean trypsin inhibitor (SBTI; 1 mg/ml) at each time point. Cells were lysed and samples separated by SDS-PAGE. Proteins were detected by western blot using antibodies against the IFITM1-NTD (i), the HA-tag (ii) and VDAC (iv; as a loading control). Secondary antibodies conjugated to far-red fluorophores were used for visualisation and allowed overlay of the IFITM1-NTD (magenta) and HA (green) labelling (iii). Control samples were untreated (UN; PBS only) or samples treated with SBTI-inactivated trypsin (IN; 1:1 mix of trypsin and SBTI), and both were incubated with cells at 37℃ for 30 min. C) IFITM1 expressing cells were treated with trypsin for 10 or 30 min, at 37℃, fixed and immunofluorescence stained for the HA-tag prior to analysis by flow cytometry. The anti-HA labelling was detected with anti-rat AF647. A representative histogram is displayed with the fluorescence intensity of HA labelling being plotted against cell count. D) Mean fluorescence intensity (MFI) of HA labelling with data averaged from two independent experiments. Error bars represent standard deviation.

3.2.5 Topology of untagged IFITM1

To exclude the possibility that the addition of a CTD epitope influenced the topology of IFITM1, we made use of C-terminal residues amenable to biotinylation (Fig. 3.11 A). HEK293T cells were used for transient expression of untagged IFITM1 and were chosen by virtue of their ease of transfection, high protein expression and lack of background IFITM protein when using the anti-IFITM1-NTD antibody (Fig. 3.11 Biii). Following transfection, cells were incubated with the membrane impermeable Sulfo-NHS-SS-Biotin for 45 min at 37℃. This incubation period was used in an attempt to allow for effective labelling at the plasma membrane, and may also label some intracellular pools of protein. Following labelling, cells were lysed and incubated with NeutrAvidin beads to precipitate biotinylated protein. There was no dilution of the sample added to the beads, allowing analysis of bound and unbound material. Samples were eluted from the beads and analysed by western blot using the anti-IFITM1-NTD antibody. Following the labelling procedure it was possible to elute IFITM1 protein from the beads as seen in the pulldown lane (PD; Fig. 3.11 Bi). The elution procedure appeared to be efficient as a second round of elution did not retrieve any additional protein (PD2). While it was possible to collect IFITM1 from the NeutrAvidin beads, a large proportion of the protein was detected in the unbound fraction (UB; Fig. 3.11 Bi). The pulldown appeared to be specific for biotinylated IFITM1 as no bands were detected in the pulldown fraction of unlabelled samples, but there was

high recovery of protein in the unbound fraction (Fig. 3.11 Bii).

The low level of pulldown could have been a result of IFITM1 not being localised at the plasma membrane in HEK293T cells, in contrast to results seen in A549 cells; but this did not appear to be the case by immunofluorescence microscopy (Fig. 3.11 C). The immunofluorescence staining of IFITM1 in HEK293T cells appeared very similar to that seen in A549 cells (Fig. 3.2 and 3.9). In the A549 cells, intracellular pools of protein were found by EM (Fig. 3.5) and similar pools may exist in HEK293T cells. Therefore the relatively low level of protein pulldown could arise from a combination of some intracellular pools of IFITM1 that are inaccessible to the cell impermeable biotin labelling reagent and/or inefficiencies in labelling and precipitation. It can also not be ruled out that there may be forms of the protein with a topology in which the CTD is on the cytoplasmic side of cell membranes.

To further control for the specificity of the observed IFITM1 biotin labelling, a CTD truncation mutant of IFITM1 was used. This mutant form of IFITM1 has a stop codon after valine 109 (IFITM1-Vstop), thus removing residues that could be biotinylated (Fig. 3.11 A). When IFITM1-Vstop was transiently expressed in HEK293T cells there was a clear difference in MW compared to wild type IFITM1, indicative of the protein being truncated (Fig. 3.11 D). When HEK293T cells expressing IFITM1-Vstop were incubated with Sulfo-NHS-SS-Biotin and subject to the previously described pulldown assay, no IFITM1-Vstop was detected as being eluted from NeutrAvidin beads (Fig. 3.11 E). These results suggest that precipitation of IFITM1 seen in Fig. 3.11 B is specifically due to labelling of amino acid residues in the CTD, beyond valine 109. Moreover, since there are residues in the NTD that could be biotinylated, the lack of IFITM1-Vstop precipitation additionally suggests that the NTD is not exposed on the extracellular side of membranes. Overall, these biotinylation and pulldown experiments suggest that untagged IFITM1 has a topology in which the CTD can be extracellularly accessible, and therefore that the HA epitope does not influence membrane topology. However, in HEK293T cells, there appears to be a large pool of protein that is inaccessible to biotinylation.

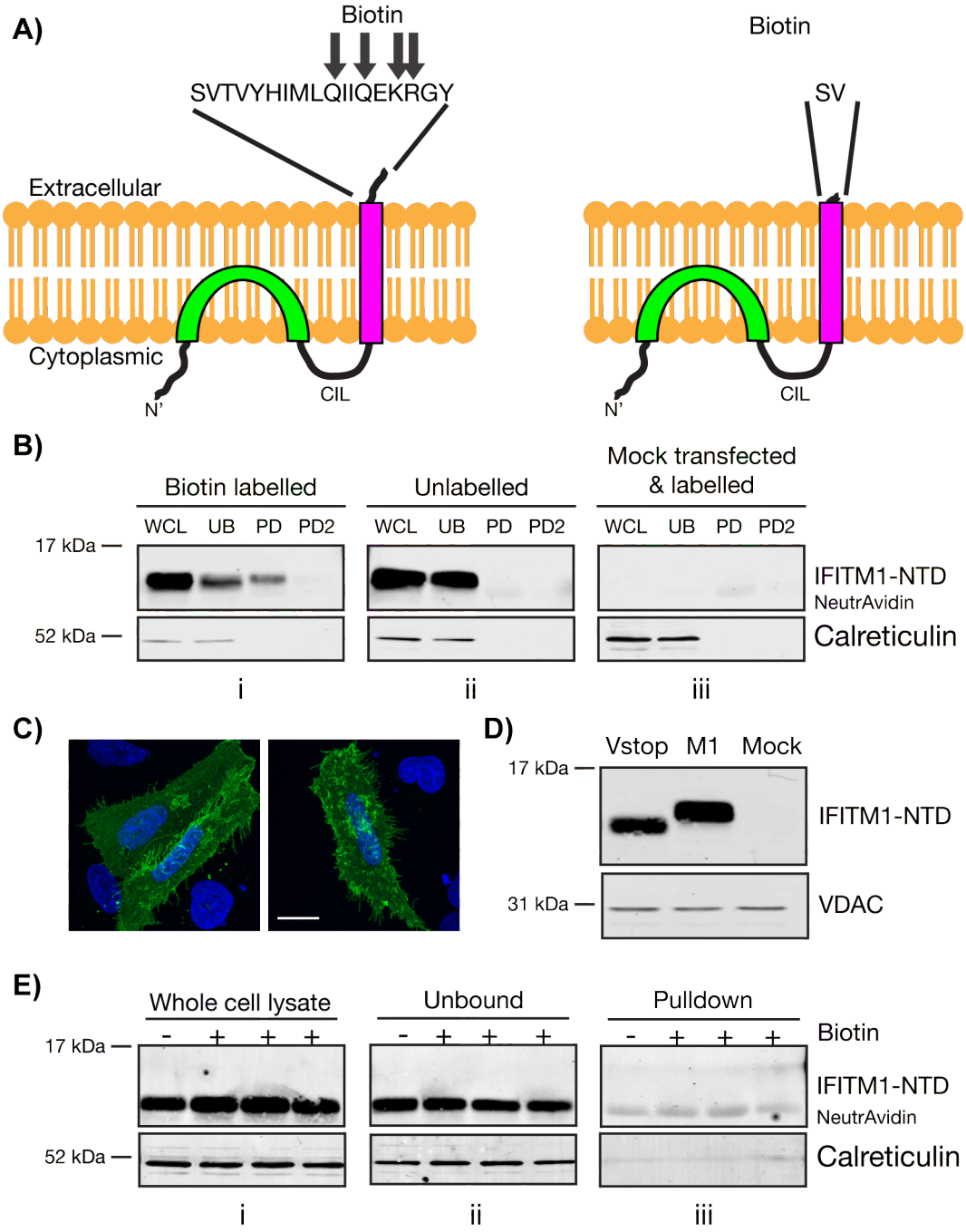
A)
Biotin
SVTVYHIMLQIIQEKRGY
Extracellular
Cytoplasmic
N'
CIL
Biotin
SV
N'
CIL
B)
Biotin labelled
Unlabelled
Mock transfected & labelled
WCL UB PD PD2
WCL UB PD PD2
WCL UB PD PD2
17 kDa
52 kDa
IFITM1-NTD
NeutrAvidin
Calreticulin
i
ii
iii
C)
D)
Vstop M1 Mock
17 kDa
31 kDa
IFITM1-NTD
VDAC
E)
Whole cell lysate
Unbound
Pulldown
- + + +
- + + +
- + + +
17 kDa
52 kDa
Biotin
IFITM1-NTD
NeutrAvidin
Calreticulin
i
ii
iii

Figure 3.11: **Biotin labelling and pulldown of untagged IFITM1.** Untagged wild type IFITM1 or IFITM1-Vstop expression plasmids were transfected into HEK293T cells. After 2 days the cells were labelled with membrane impermeable Sulfo-NHS-SS-Biotin for 45 min at 37℃. Excess labelling reagent was washed out with Tris buffered saline. Whole cell lysates were produced and incubated with NeutrAvidin agarose beads (without any dilution) to precipitate biotinylated proteins. The unbound material was collected from the beads and precipitated proteins were eluted by incubation with reducing Laemmli sample buffer. A) A schematic representation of the IFITM membrane topology to show the hypothesised exposed CTD residues of IFITM1 and IFITM1-Vstop. B) Western blots were probed with anti-IFITM1-NTD; WCL - whole cell lysates, UB - unbound material following incubation with NeutrAvidin beads, PD and PD2 - two rounds of elution from the NeutrAvidin beads. Gel i - samples from biotinylated cells. Gel ii - samples from unlabelled cells. Gel iii - samples from mock transfected biotinylated HEK293T cells. The elution step detached some NeutrAvidin monomers from the beads which have a molecular weight of ∼14 kDa, this background has been labelled. Calreticulin was used as a loading control and negative control for the pulldown. C) HEK293T cells, transfected with IFITM1 were fixed, permeabilised and labelled for the presence of IFITM1 using the anti-IFITM1-NTD antibody (detected with AF488). Two representative images are shown, both being maximum intensity projections of confocal sections through the depth of the cells. Scale bar represents 15 μm. D) Western blot comparing wild type IFITM1 (M1), IFITM1-Vstop and mock transfected HEK293T cells. E) HEK293T cells transfected with IFITM1-Vstop and subject to the same biotinylation procedure. Four independent transfection samples are displayed, one of which is unlabelled. Gel i - whole cell lysate samples from the four transfections. Gel ii - samples retrieved from the unbound fraction. Gel iii - samples eluted from the NeutrAvidin beads. As previously NeutrAvidin monomers were eluted, which run at ∼14 kDa. The NeutrAvidin monomers have a very similar molecular weight to IFITM1-Vstop, but due to the presence of a band in the unlabelled sample in Gel iii, these bands are considered to be background, not IFITM1-Vstop.

3.2.6 Conservation of the IFITM1 topology in IFITM2 and IFITM3

IFITM1 is localised at the plasma membrane in A549 cells, making it highly amenable to the experiments used to define the topology. In comparison, IFITM2 and IFITM3 appear to be mostly associated with intracellular membrane compartments, necessitating alternative approaches to investigate if the topology observed for IFITM1 is conserved.

Antibody feeding

To test the topology of IFITM2 and IFITM3 and to investigate certain aspects of protein trafficking, an antibody feeding assay was used. Live cells were cultured in media containing anti-HA antibody for 3 h, prior to washing, fixation, permeabilisation and la-

belling with secondary antibody for immunofluorescence microscopy. In this experiment, if IFITM2 or IFITM3 traffic to the plasma membrane, and have an extracellularly exposed HA-tag, this should bind antibody. IFITM2 or IFITM3 may then be detectable at the plasma membrane, or within internal compartments following internalisation of antibody bound protein. Control A549 cells showed no labelling when incubated with anti-HA antibody for 3 h, suggesting that there was no non-specific uptake of antibody (Fig. 3.12 A). As a negative control, IFITM3 expressing cells were incubated for 3 h in media without anti-HA antibody. These cells were then fixed, permeabilised and labelled with a fluorescent secondary antibody, but showed no fluorescence signal (Fig. 3.12 C), suggesting there was no non-specific labelling with the secondary antibody. IFITM1 expressing cells acted as a positive control as the protein is localised at the plasma membrane and the HA-tag is accessible at the cell surface (Fig. 3.12 B).

When IFITM2 and IFITM3 cells were incubated with anti-HA antibody for 3 h, the majority of cells had little, if any staining for HA. However, ∼25% of IFITM3 and ∼10% of IFITM2 expressing cells did have punctate fluorescence (Fig. 3.12 D and E; values calculated from 30 random fields of view at 40x magnification). This suggested that, in some cells, the IFITM2 and IFITM3 proteins are trafficked to the plasma membrane, where the extracellularly available HA-tag can bind anti-HA antibody. Both proteins appear to then be internalised, along with antibody.

HA-tag loss

IFITM2 and IFITM3 are found in puncta within cells when assessed by immunofluorescence microscopy (Fig. 3.2 and 3.9) and appear to localise to MVBs by EM (Fig. 3.6 and 3.7), strongly suggesting predominant localisation within the endosomal system. If the topology observed for IFITM1 is conserved in the other two IFITM proteins, this would suggest that the C-terminal HA-tags reside in the lumen of endosomal compartments. It was therefore hypothesised that the HA-tag could be subject to cleavage by endosomal/lysosomal proteases, similar to the exogenous addition of trypsin for cleavage of the HA-tag from IFITM1 (Fig. 3.10). This hypothesis was supported by western blots that showed lower levels of HA labelling for IFITM2 and IFITM3 than IFITM1 (Fig. 3.8). Moreover, these western blots showed multiple bands when probed with anti-NTD

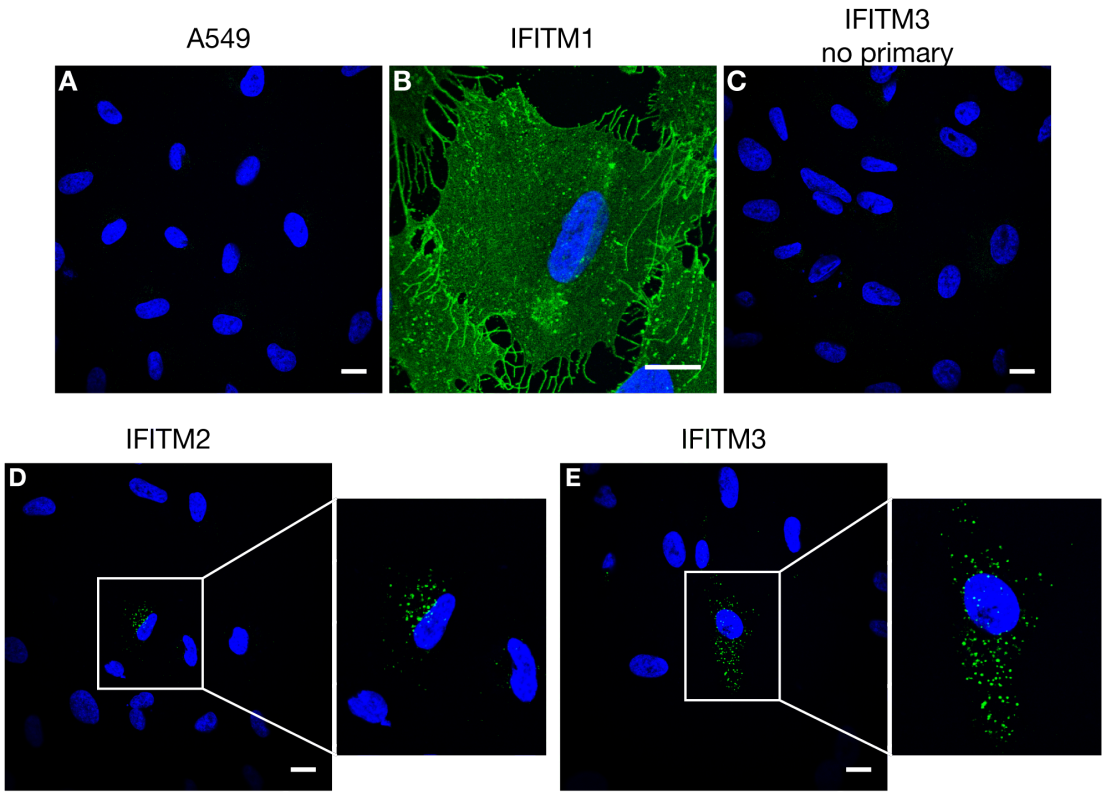

Figure 3.12: **Antibody feeding of IFITM expressing cells.** Live IFITM expressing cells were incubated with anti-HA antibody (5 μg/ml) for 3 h at 37°C. This incubation should allow antibody to bind to any extracellularly exposed HA epitopes and potentially be internalised to cells by endocytosis. Following the feeding period, cells were fixed, permeabilised with saponin and incubated with anti-rat AF488 to detect any anti-HA antibody. A) Control A549 cells show no specific HA labelling, suggesting no non-specific uptake of antibody. B) The majority of IFITM1 HA labelling is at the cell surface. C) IFITM3 expressing cells not incubated with anti-HA antibody, but labelled with secondary antibody show no staining, acting as a control for the specificity of the secondary antibody. D and E) For the majority of IFITM2 and IFITM3 expressing cells no staining was seen. However, ~10% of IFITM2 and ~25% of IFITM3 cells (each counted from 30 random fields of view at 40x magnification. Counted data are from n = 1 experiment, representative of two individual experiments) showed punctate labelling, suggesting binding of anti-HA antibody and internalisation. Nuclei were labelled with Hoechst. All images were acquired using the same microscope settings and brightness and contrast have been adjusted uniformly. Scale bars represent 15 μm. (Experiment and microscopy was performed by Stephanie Czieso).

antibodies, suggesting forms of the protein that may have lost the HA-tag (Fig. 3.10).

To test for loss of the HA-tag from IFITM2 and IFITM3, cells were co-labelled with antibodies against the HA-tag and the NTD and analysed by immunofluorescence microscopy. Since the IFITM proteins are relatively small (125, 132 and 133 amino acids for IFITM1, 2 and 3, respectively), it would be expected that labelling the NTD and CTD should have a high degree of overlap. This was indeed seen to be the case for IFITM1 expressing cells where ∼70% of pixels were detected as overlapping and there was a high value for the Mander's correlation coefficients M1 and M2 (Fig. 3.13 and Table 3.1). The lack of complete overlap may in part be explained by some endosomal IFITM1, as visualised by EM (Fig. 3.5), where the HA-tag may be lost.

In contrast to IFITM1, IFITM2 expressing cells had a lower proportion of overlapping pixels (∼49%) and lower M1 and M2 values (Table 3.2). This is best seen with the anti-IFITM3-NTD antibody (Fig. 3.14) because the anti-IFITM1-NTD antibody has low detection of IFITM2 (Fig. 3.8, Fig. 3.13 and Table 3.1). Similarly, IFITM3 had a lower proportion of overlapping pixels between the NTD and HA-tag than IFITM1, when either of the NTD antibodies were used (Fig. 3.13, 3.14, Table 3.1 and Table 3.2). Importantly, in both IFITM2 and IFITM3 expressing cells there were distinct magenta only puncta, indicative of compartments in which the NTD is intact, but the HA-tag has been lost. Through image quantification it was also seen that there was an increased proportion of magenta (NTD) only pixels in IFITM2 and IFITM3 expressing cells compared to IFITM1 expressing cells. This higher level of magenta only pixels for IFITM2 and IFITM3 is indicative of a larger extent of HA-tag loss, presumably as a result of the predominant endosomal distribution of these proteins, compared to the predominant plasma membrane localisation of IFITM1. It is also noted that green only pixels were detected. It is unclear whether this was due to antibody accessibility issues, issues with the image analysis or as a consequence of protein that has an intact CTD but an NTD that could not be detected by antibody.

Overall, these results suggest that IFITM2 and IFITM3 have a topology that allows for extracellular binding of anti-HA antibodies and that there are pools of protein in which the HA-tag has been lost from the CTD, but the NTD is intact. The interpretation of this loss is that the epitope tag faces the lumen of endocytic organelles where it can be cleaved

in the acidic/proteolytic environment. Therefore it appears that the topology displayed for IFITM1 may be conserved in IFITM2 and IFITM3.

Cell line	# of cells imaged	Pearson's R value	Mander's M1	Mander's M2
IFITM1	58	0.85 (±0.05)	0.97 (±0.12)	0.99 (±0.01)
IFITM2	53	0.60 (±0.10)	0.83 (±0.17)	0.82 (±0.12)
IFITM3	57	0.81 (±0.05)	0.75 (±0.19)	0.77 (±0.19)

Table 3.1: **Image analysis of anti-IFITM1-NTD antibody and anti-HA antibody co-staining.** Individual cells were segmented and analysed to assess the Pearson's R-value and Mander's correlation coefficients. The data are collected from two independent experiments and the mean values and standard deviation across cells are displayed. The Pearson's R-value assesses the correlation between intensity of magenta (NTD) and green (HA) fluorescent signals. The Mander's correlation coefficients, M1 and M2, represent the proportion of magenta pixels in pixels that are green, and the proportion of green pixels in pixels that are magenta, respectively. See also Fig. 3.13 for example images and further image analysis.

Cell line	# of cells imaged	Pearson's R value	Mander's M1	Mander's M2
IFITM2	57	0.73 (±0.13)	0.85 (±0.16)	0.86 (±0.14)
IFITM3	49	0.72 (±0.04)	0.75 (±0.21)	0.77 (±0.17)

Table 3.2: **Image analysis of anti-IFITM3-NTD antibody and anti-HA antibody co-staining.** Individual cells were segmented and analysed to assess the Pearson's R-value and Mander's correlation coefficients. The data are collected from two independent experiments and the mean values and standard deviation across cells are displayed. The Pearson's R-value assesses the correlation between intensity of magenta (NTD) and green (HA) fluorescent signals. The Mander's correlation coefficients, M1 and M2, represent the proportion of magenta pixels in pixels that are green, and the proportion green pixels in pixels that are magenta, respectively. See also Fig. 3.14 for example images and further image analysis.

3.2.7 The IFITM3-Y20A C-terminal domain resides in the extracellular space

IFITM3 is predominantly found within endosomal compartments (see Section 3.2.8). This endosomal localisation is in part determined by the presence of a Yxxϕ sorting motif (where Y is a tyrosine, x is any amino acid and ϕ represents a hydrophobic residue) present in the NTD (20-YEML-23), which has been shown to interact with the clathrin adaptor AP-2 [143]. IFITM2 has a similar Yxxϕ motif in the NTD (19-YEML-22), but IFITM1 does not because of a 21 amino acid truncation at the NTD (compared to IFITM3, see Fig. 1.6 [page 44], for sequence alignment). The difference in the presence of the Yxxϕ motif may explain the differences in localisation of IFITM2 and IFITM3 compared to IFITM1. That

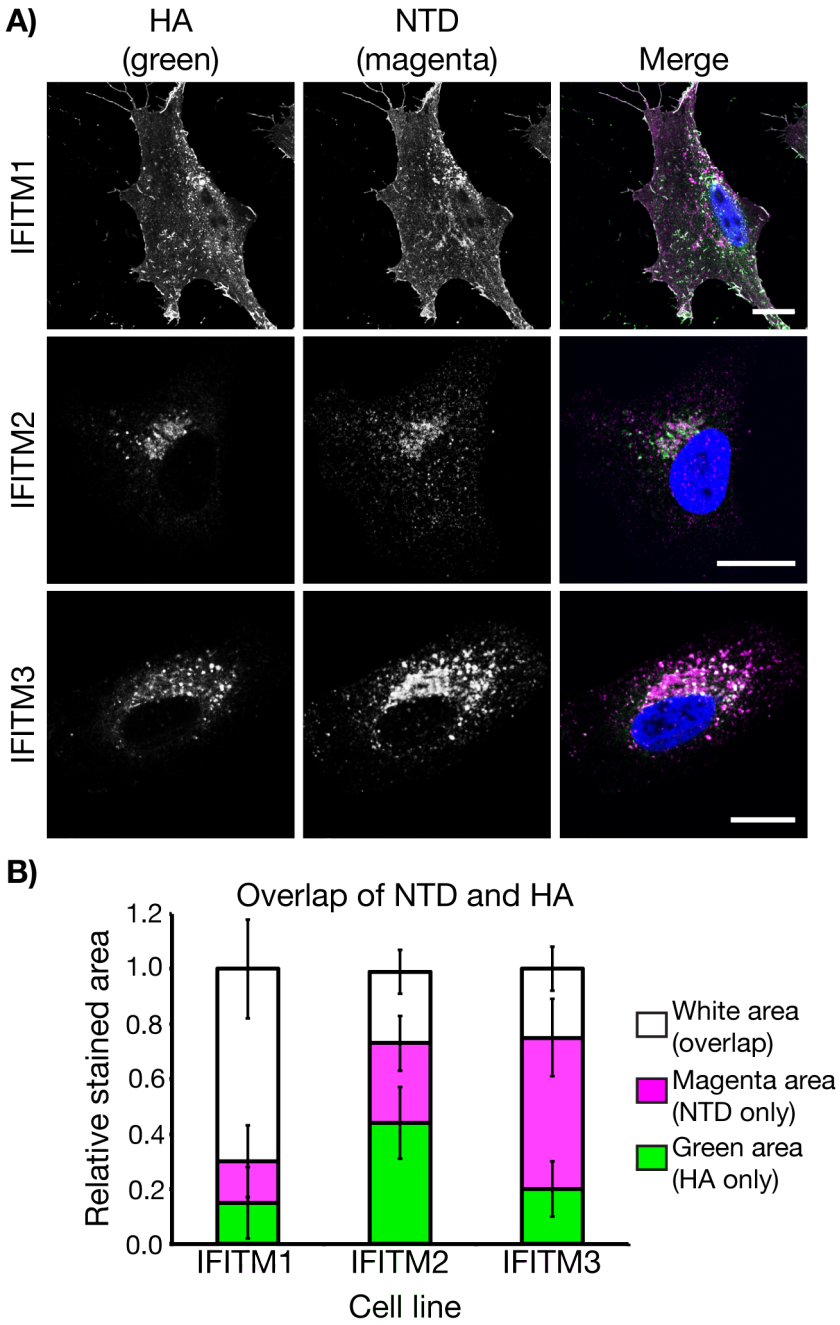

Figure 3.13: **Co-staining of IFITM expressing cells with anti-IFITM1-NTD and anti-HA antibodies indicates HA-tag loss.** A) IFITM1, 2 and 3 expressing cells were saponin permeabilised and labelled with the anti-IFITM1-NTD antibody and anti-HA antibody, which were detected with AF647 (magenta) and AF488 (green), respectively. Images are single optical sections. Nuclei were stained with Hoechst. Scale bars represent 15 μm. B) Quantification of relative pixel areas across 14 (IFITM1 and IFITM2) and 15 (IFITM3) random fields of view at 63x magnification, collected from 2 independent experiments. A total of 58 IFITM1, 53 IFITM2 and 57 IFITM3 expressing cells were analysed. Values plotted are relative mean area and error bars are standard deviation across images. (N.B. see Table 3.1 for further image analysis of the same data set).

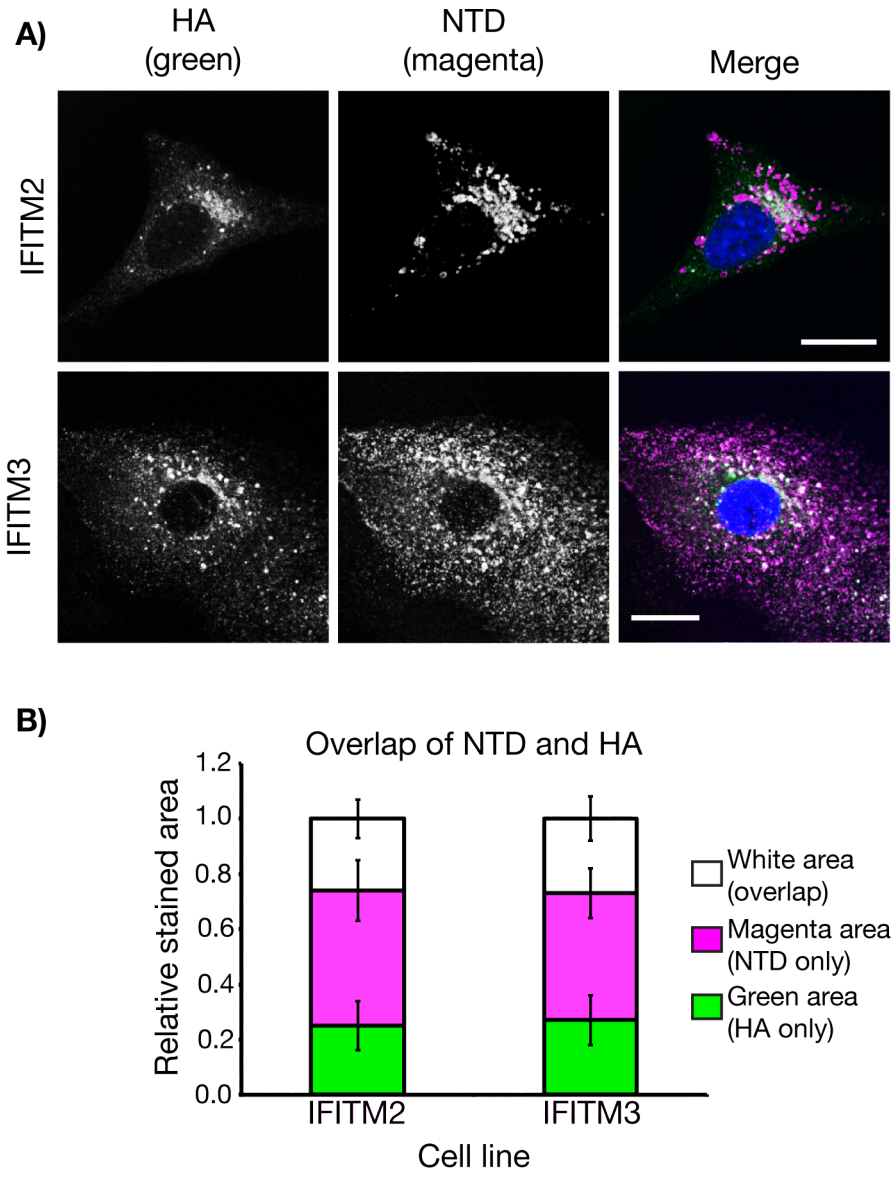

Figure 3.14: **Co-staining of IFITM expressing cells with anti-IFITM3-NTD and anti-HA antibodies indicates HA tag loss.** A) IFITM2 and IFITM3 expressing cells were saponin permeabilised and labelled with anti-IFITM3-NTD and anti-HA antibodies, which were detected with AF647 (magenta) and AF488 (green), respectively. Images are single optical sections. Scale bars represent 15 μm. B) Quantification of relative pixel areas across 13 (IFITM2) and 14 (IFITM3) random fields of view at 63x magnification, collected from 2 independent experiments. A total of 57 IFITM2 and 49 IFITM3 expressing cells were analysed. Values plotted are relative mean area and error bars are standard deviation across images. (N.B. see Table 3.2 for further image analysis of the same data set).

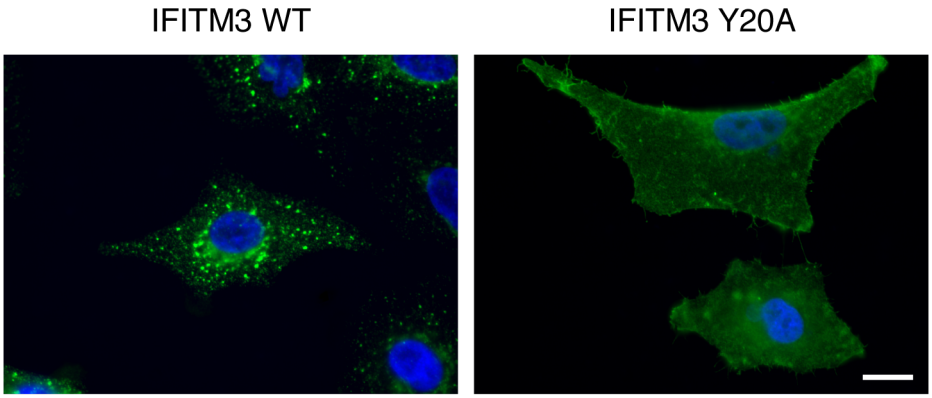

Figure 3.15: **IFITM3-Y20A localises to the plasma membrane.** P2-IFITM3 and Y20A cells were saponin permeabilised and labelled with anti-IFITM1-NTD antibody which was detected with AF488. Images were collected on an epifluorescence microscope with equivalent exposure time. Nuclei were labelled with Hoechst. Scale bar represents 15 μm.

20-YEML-23 of IFITM3 acts as a functional sorting motif has been shown by the fact that when Y20 was replaced with an alanine (A) residue (Y20A), this mutant IFITM3 accumulated at the plasma membrane and could no longer interact with AP-2 [143, 163]. In the work presented here, a cell line was produced that stably expresses IFITM3-Y20A and is part of the P2 cell set, which also contains a cell population expressing wild type IFITM3 (see Materials and Methods; Table 2.2 [page 72]). To confirm published data, the mutant IFITM3 was tested by immunofluorescence staining of permeabilised cells. As expected, IFITM3-Y20A appeared to be primarily localised at the plasma membrane (Fig. 3.15), while wild type IFITM3 was found in an intracellular punctate distribution. Owing to the plasma membrane localisation, the Y20A protein acts as a tool to further investigate IFITM3 topology.

It was previously seen that the CTD HA-tag of IFITM1 was accessible at the cell surface, such that cells could be labelled for immunofluorescence microscopy in the absence of permeabilisation. A similar approach was used to test the extracellular availability of the CTD HA-tag on IFITM3-Y20A expressing cells. The previous protocol was slightly altered to fix cells with methanol free formaldehyde prior to addition of antibodies (i.e. cells were not incubated on ice at any point). It was found that fixation before addition of antibody resulted in a degree of background fluorescence for both tubulin and the

IFITM NTD (potentially non-specific), but the HA-tag still clearly showed extracellular availability for both IFITM1 and IFITM3-Y20A (Fig. 3.16 A). It therefore appears that like IFITM1, IFITM3-Y20A has a CTD HA-tag that is available to antibody binding at the cell surface, while the NTD appears to be on the cytosolic side of membranes.

To further assess the topology of IFITM3-Y20A, a protease cleavage assay was performed, as for IFITM1 (Fig. 3.10). IFITM3 lacks trypsin cleavage sites in the CTD, therefore proteinase K (ProtK) was used instead (Fig. 3.16 Bi). ProtK treatment of IFITM3-Y20A cells for 10 or 30 min resulted in a clear weight shift when detected by the anti-IFITM1-NTD antibody (Fig. 3.16 Bii). After each time point phenylmethylsulfonyl fluoride (PMSF) was added to inactivate ProtK. The observed weight shift was not seen when ProtK was inactivated by addition of PMSF prior to incubating with cells for 30 min, suggesting that the cleavage did not occur following lysis of the cells (Fig. 3.16 Bii). As was the case with IFITM1 and trypsin, ProtK has multiple cleavage sites in both the NTD (26 sites) and CIL (12 sites) of IFITM3, suggesting that both of these domains are protected from proteolytic cleavage as more fragments of IFITM3-Y20A would be expected otherwise.

Overall these data suggest that IFITM3-Y20A has the same type II transmembrane topology as IFITM1. This, coupled with the data on IFITM2 and wild type IFITM3 suggests that the type II transmembrane topology may be conserved across the human IFN-inducible IFITM proteins.

3.2.8 IFITM3 preferentially localises to early endosomes and IFITM2 to late endosomes

Having observed that the CTD HA-tag on IFITM2 and IFITM3 can be lost in endosomal compartments, any analysis of the localisation based on immunostaining the epitope tag would most likely miss pools of protein that may be functionally important. Therefore, an analysis of the localisation of IFITM2 and IFITM3 was performed to better define their distribution within the endosomal system using anti-NTD antibody. Cells were co-stained for the IFITM protein, using the anti-IFITM3-NTD antibody, and markers of early and recycling endosomes (early endosomal antigen 1 [EEA1] and transferrin receptor [TfR]) or late endosomes and lysosomes (CD63 and lysosomal associated protein 1 [LAMP1]),

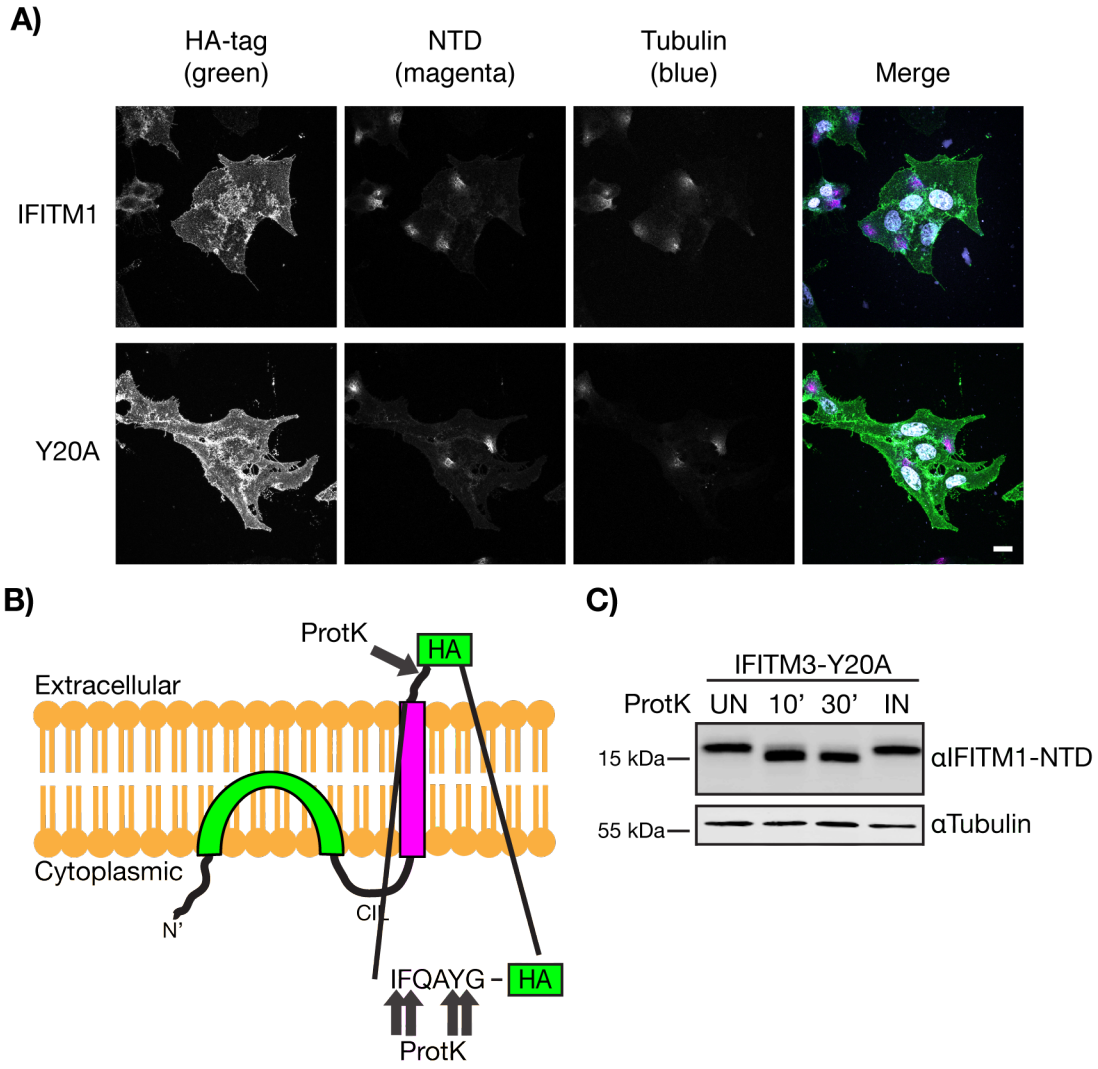

Figure 3.16: **IFITM3-Y20A has an extracellular CTD HA-tag.** A) IFITM1 or IFITM3-Y20A cells were fixed with methanol free formaldehyde prior to labelling with anti-HA, anti-IFITM1-NTD and anti-tubulin antibodies without permeabilisation. Primary antibodies were detected with AF488 (HA; green), AF594 (NTD; magenta) and AF647 (tubulin; blue) conjugated secondary antibodies. Anti-IFITM1-NTD and anti-tubulin antibodies acted as controls for permeabilisation from fixation and show some background, but no specific staining, suggesting the plasma membrane was largely intact. Nuclei were labelled with Hoechst and are displayed in white. Images are confocal sections. Scale bar represents 15 μm. B) Schematic of the Proteinase K (ProtK) cleavage assay showing the predicted cleavage sites in the IFITM3 CTD. C) IFITM3-Y20A expressing cells were treated with ProtK (500 μg/ml) for 10 or 30 min at 37°C. The reaction was terminated by addition of 1 mM PMSF. Samples were western blotted for IFITM3-Y20A using the anti-IFITM1-NTD antibody and tubulin as a loading control. Control samples were either untreated (UN) or treated with ProtK that was inactivated (IN) with 1 mM PMSF prior to incubation with cells for 30 min.

and analysed by confocal microscopy. IFITM3 was found to have greater overlap with the early/recycling endosomal markers than IFITM2, while IFITM2 had greater overlap with the markers of late endosomes and lysosomes than IFITM3. Images were analysed to quantify these differences. A large fraction of each IFITM does not overlap with any single endosomal marker, suggesting that the proteins are distributed throughout the endosomal system and other compartments (such as the plasma membrane and Golgi apparatus as seen by EM, Fig. 3.6 and 3.7). Accepting that early endosomes are heterogeneous and neither EEA1 nor TfR mark the entire population, and that IFITM2 and IFITM3 have somewhat overlapping distribution, the conclusions from these analyses are that IFITM3 shows greater association with markers of early endosomal compartments, while IFITM2 shows greater association with markers of late endosomal and lysosomal compartments.

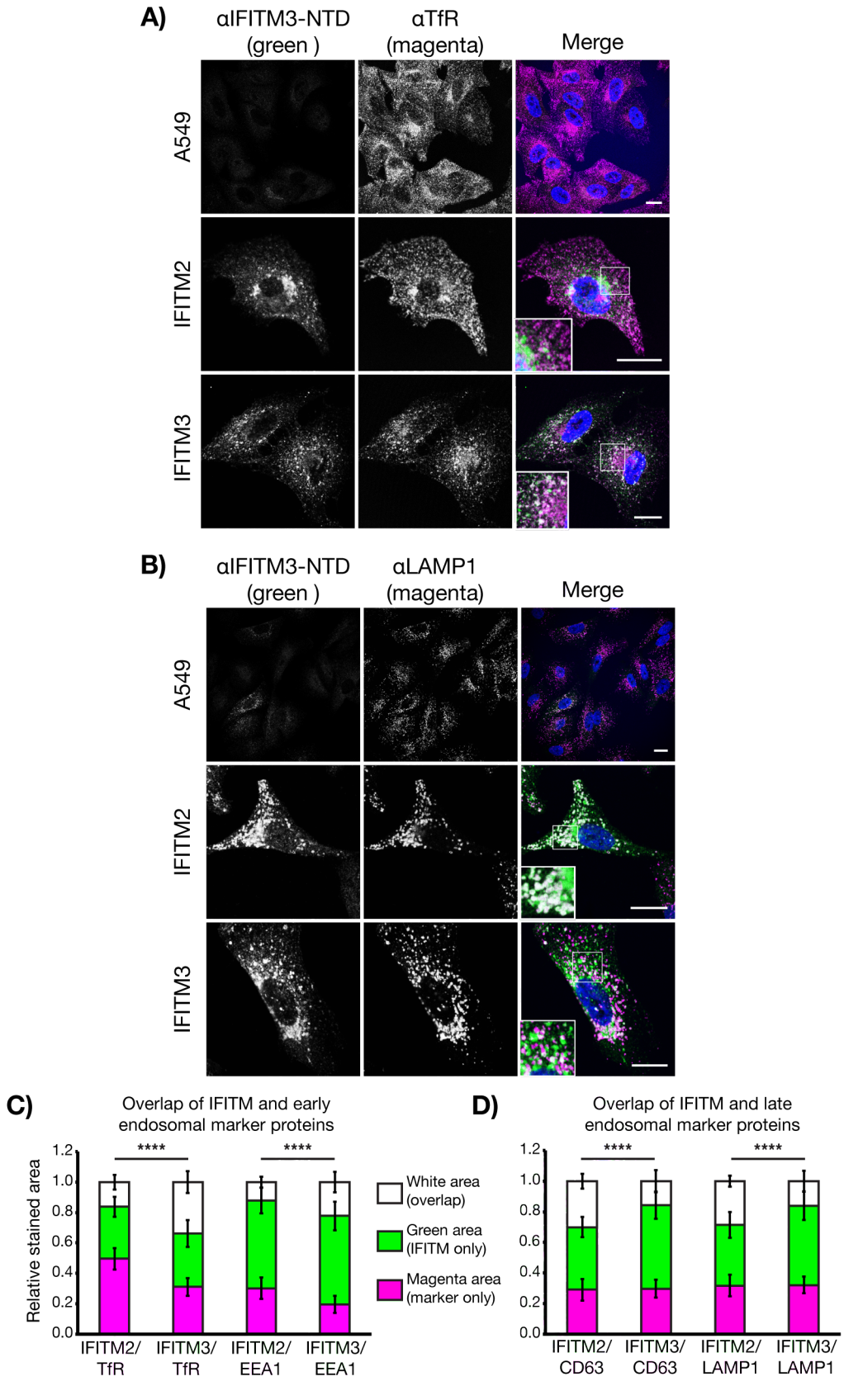
A)
αIFITM3-NTD (green)
αTfR (magenta)
Merge
A549
IFITM2
IFITM3
B)
αIFITM3-NTD (green)
αLAMP1 (magenta)
Merge
A549
IFITM2
IFITM3
C)
Overlap of IFITM and early endosomal marker proteins
Relative stained area
1.2
1.0
0.8
0.6
0.4
0.2
0.0
****
****
IFITM2/ TfR
IFITM3/ TfR
IFITM2/ EEA1
IFITM3/ EEA1
White area (overlap)
Green area (IFITM only)
Magenta area (marker only)
D)
Overlap of IFITM and late endosomal marker proteins
****
****
IFITM2/ CD63
IFITM3/ CD63
IFITM2/ LAMP1
IFITM3/ LAMP1

Figure 3.17: **Endosomal distribution of IFITM2 and IFITM3.** IFITM2 and IFITM3 expressing cells were fixed and permeabilised with saponin prior to labelling with anti-IFITM3-NTD antibody and endosomal markers. A) Confocal sections of cells co-stained for IFITM protein and transferrin receptor (TfR) as a marker of early and recycling endosomes. IFITM protein were detected with AF488 (green) and TfR with AF647 (magenta). B) Confocal sections of cells co-stained for IFITM protein (green) and LAMP1 (magenta) as a marker of late endosomes and lysosomes. Nucleic were detected with Hoechst. A549 cells are displayed as a control for lack of IFITM protein expression. Scale bars represent 15 μm. C and D) Analysis of the overlap between green and magenta pixels of IFITM2 or IFITM3 with markers of early/recycling endosomes (C; EEA1/TfR) and late endosomes/lysosomes (D; CD63/LAMP1). Data are from three independent experiments with between 18 and 21 fields of view collected at 63x magnification (displaying a total of between 155 and 308 cells in each staining condition). In all cases there are pixels that are only green or only magenta, indicating the IFITM proteins do not occupy a single compartment. However, overlap is detected and there are significant differences between the co-localisation of IFITM2 and IFITM3 with early or late endosomal markers. IFITM3 has greater overlap with early markers, while IFITM2 has greater overlap with late markers. Bars show the relative mean pixel area and error bars are standard deviation between images. Significance test relates to the difference in overlap area between IFITM2 and IFITM3. **** $p < 0.0001$.

3.3 Conclusions and Discussion

The membrane topology of the IFITM proteins had been a contentious issue. The IFITMs had initially been suggested to be dual-pass transmembrane proteins with extracellular NTDs and CTDs (Fig. 3.1 model 1; [7, 114–116]). However, later work suggested that the proteins could be post-translationally modified by intracellular enzymes, placing the terminal domains on the cytoplasmic side of membranes (Fig. 3.1 model 2; [150, 163]). Experimental data for the localisation of the CTD was generally lacking, however murine Ifitm1 was shown to have a non-conserved cysteine residue in the CTD which could be palmitoylated, suggesting cytosolic localisation [155]. The work presented here was designed to better understand the membrane topology of the human IFITM proteins; a third membrane topology model (Fig. 3.1) has since been proposed by ourselves and others [15, 153, 192].

The work of Bailey *et al.* first defined the type II transmembrane topology model using murine Ifitm3 [153]. Their work used similar approaches to those presented here. As with our own experiments, it was demonstrated that epitope tags at the C-terminal end of Ifitm3 were exposed extracellularly and could be detected on intact cells using immunoflu-

orescence microscopy and flow cytometry. The work of Bailey *et al.* also demonstrated that the CTD of Ifitm3 enters into the lumen of the ER as the addition of a KDEL motif resulted in ER retention. As with work presented here (Fig. 3.13 and 3.14), epitope tags at the C-terminal end of Ifitm3 were localised to the lumen of lysosomes, and consequently lost [153]. Finally, Bailey *et al.* demonstrated that the constructs they analysed had antiviral activity against IAV and VSV, arguing that the proteins with this topology were functionally active. In Chapters 4 and 5, the IFITM proteins analysed in this work are also displayed to have antiviral function. Ling *et al.* took the analysis of IFITM3 membrane topology further by reconstituting the protein in artificial lipid membranes and used the approaches of NMR and EPR for structural analysis [192]. These approaches demonstrated the presence of an α helical transmembrane domain at the C-terminal end of the protein, and a membrane interacting domain made of two α helices that did not cross lipid bilayers at the N-terminal end [192]. These structural data thus support the type II transmembrane topology shown through biochemical and cell biological approaches used by Bailey *et al.* [153] and ourselves ([15] and results in this chapter).

Our experiments largely focused on defining the topology of human IFITM1 as this protein was found to be localised predominantly at the plasma membrane when expressed in A549 cells, making it easily accessible. The IFITM1 C-terminal HA-tag could be labelled with antibody at the surface of non-permeabilised cells (Fig. 3.2) and be proteolytically removed by addition of trypsin (Fig. 3.10). Conversely, an antibody targeting the IFITM1 NTD could only label the protein following saponin permeabilisation (Fig. 3.9). Moreover, based on the molecular weight shift seen by western blot following trypsin treatment of cells, the NTD appeared to be protected, suggesting cytosolic localisation (Fig. 3.10).

Much of the experimental data was generated using cells that stably expressed IFITM1 with a C-terminal HA-tag, which acted as a good substitute for the lack of CTD targeting antibodies. However, data was presented suggesting that it was possible to biotin label C-terminal residues of untagged IFITM1, when transiently expressed in HEK293T cells, arguing that the tag does not influence the topology (Fig. 3.11). Relatively little IFITM1 was precipitated with NeutrAvidin beads in these experiments which is thought to be due to a combination of intracellular protein that may not be biotinylated (seen by EM in A549 cells [Fig. 3.5], and expected to be present in HEK293Ts), and potential label accessibility

issues at the plasma membrane, possibly due to the short CTD length of IFITM1.

Interestingly, experimental data appears to suggest that murine Ifitm1 may adopt a different topology to human IFITM1. The work of Hach *et al.* demonstrated that a cysteine residue present in the murine Ifitm1 CTD could be palmitoylated; this residue is not conserved in the human orthologue of the protein [155]. The enzymes responsible for palmitoylation are thought to be cytosolic, suggesting that the murine Ifitm1 CTD faces the cytosol. Murine Ifitm1 was shown to have antiviral activity against IAV [155], and multiple studies have demonstrated human IFITM1 has antiviral activity (see Tables 1.1 and 1.2). Furthermore, results presented in Chapter 5 demonstrate that human IFITM1 can inhibit infection by three different flaviviruses in this A549 cell system. What impact the apparent different topology of human and murine IFITM1 has on antiviral activity remains to be explored.

The topology proposed for IFITM1 appears to be conserved in IFITM2 and IFITM3, though these proteins were harder to assess due to their predominant intracellular localisation. Antibody feeding assays and analysis of HA-tag loss suggested that for both IFITM2 and IFITM3 the HA-tag may face the extracellular space and the lumen of cellular organelles (Fig. 3.12, 3.13, 3.14). Additionally, the mutant form of IFITM3, IFITM3-Y20A, which localises to the plasma membrane, gave very similar results in experiments used to define IFITM1 membrane topology (Fig. 3.16). The work of Ling *et al.*, discussed above, independently supports the suggestion that human IFITM3 has a topology with a transmembrane domain present at the second membrane interacting domain.

Since it appeared that the C-terminal HA-tag can be lost from IFITM2 and IFITM3 (Fig. 3.13 and 3.14), any analysis of the localisation of these proteins using C-terminal tags has the potential to not detect pools of protein that may be functionally important. Therefore, immunofluorescence experiments were used to define the endosomal localisation of IFITM2 and IFITM3 by co-staining the NTD with various markers of early and late endosomes (Fig. 3.17). These experiments suggest that there is more IFITM3 associated with early endosomes, and more IFITM2 associated with late endosomes and lysosomes, as compared with each other. With IFITM1 localised at the plasma membrane, it therefore appears that the three different IFITM proteins occupy the main membrane compartments that need to be crossed by different viruses to enter cells (see Fig. 3.18). Understanding

IFITM localisation may aid in understanding the antiviral activity, which will be discussed in more detail in subsequent chapters.

An important caveat should be noted; these localisations have been determined in cells expressing each IFITM protein in isolation. During an IFN response, it is likely that all three antiviral IFITM proteins will be expressed. It has been suggested that IFITM proteins form homo- and heteromeric complexes [154]; what impact expression of multiple IFITM proteins may have on their cellular distribution and antiviral activity remains to be fully explored. However, investigating the function of the IFITM proteins individually provides a simpler system for analysis which can then be built upon to better understand any changes that occur as a consequence of expression of multiple proteins.

In summary, the work presented in this chapter suggests that the IFITM proteins have a type II transmembrane topology in which the NTD faces the cytoplasm while the CTD faces the extracellular/lumenal space. The two terminal domains are connected by two membrane interacting regions and the CIL. The precise functional consequence of this topology remains unclear, and will be discussed in greater detail in Chapter 6. IFITM1 is predominantly localised at the plasma membrane while IFITM2 and IFITM3 are predominantly found within intracellular compartments. Having developed an understanding of the membrane topology, a more thorough analysis of IFITM2 and IFITM3 localisation could then be performed, suggesting these proteins are found throughout compartments of the endosomal system. It is hypothesised that these differences in distribution may influence the antiviral function of the IFITM proteins, which will be the topic of the following chapters.

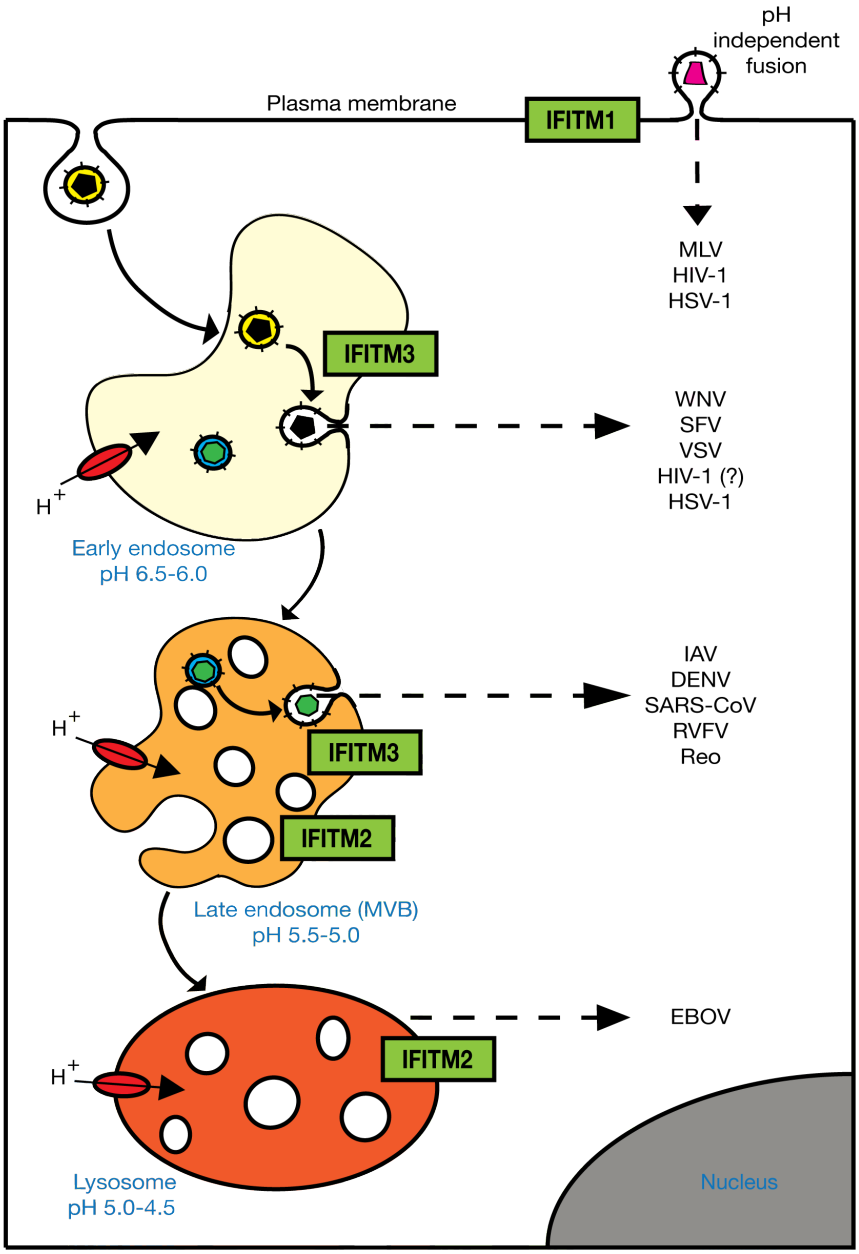

Figure 3.18: **IFITM cellular distribution and select viral entry sites.** When expressed individually in A549 cells, the IFITM proteins are found to occupy various cellular membrane compartments. As displayed in this chapter and [15, 16], IFITM1 is predominantly localised at the plasma membrane, while IFITM2 and IFITM3 are dispersed through the endosomal system. IFITM3 appears to have greater localisation to early endosomal compartments than IFITM2, while IFITM2 appears to have greater localisation to late endosomal compartments than IFITM3. Many different viruses (some examples provided here) penetrate into the cytosol through the different membrane compartments the IFITM proteins are found to be predominantly located in. It could therefore be hypothesised that the localisation of the IFITM protein may influence its antiviral activity, an idea which will be discussed throughout this thesis. Image adapted from [10]. (N.B. This figure has previously been displayed in Chapter 1 and is repeated here as an aide-memoire).

Chapter 4

Alphavirus restriction by IFITM proteins

4.1 Introduction

A precise understanding of the mechanism(s) of IFITM-mediated antiviral activity remain elusive. Alphaviruses, particularly Semliki Forest virus (SFV), have been used extensively to study clathrin-mediated endocytosis and pH-dependent virus entry into cells [45, 47, 85]. Due to the wealth of experimental data on SFV entry, this virus is an attractive model system to study IFITM-mediated inhibition of viral infection. While the majority of viruses shown to be inhibited by the IFITM proteins enter cells through similar pathways to SFV, there had been little study as to whether IFITMs inhibit alphavirus infection. An overexpression screen suggested IFITMs inhibit Chikunguna virus (CHIKV), but have limited impact on Venezuelan equine encephalitis virus (VEEV) [3]. Additionally, it has been suggested that IFITM1 and IFITM3 can inhibit cell-cell fusion driven by cellular expression of the SFV E1/E2 envelope glycoproteins [13]. Nevertheless, there was also a view that alphaviruses are not inhibited by IFITM proteins [9, 11].

The work presented in this chapter shows that IFITM3, and to a lesser extent IFITM2, can inhibit SFV and Sindbis virus (SINV, another alphavirus) when virus enters through the endocytic pathway, and that IFITM1 had no effect. Focusing on SFV, IFITM3 was found to block capsid release from endosomal compartments, without any inhibition of earlier events in the entry pathway. When SFV fusion was triggered directly at the plasma

membrane, IFITM1 could inhibit infection to a minor extent. However, surprisingly, the predominantly endosomal localised IFITM3 could still potently inhibit infection when virus was fused at the cell surface, even though there are low levels of the protein at this site, especially compared to IFITM1. In Chapter 3, it was speculated that the different localisation of the IFITM proteins may influence the range of viruses they inhibit, however, from the data presented here, the conclusion made is that IFITM3 can inhibit alphavirus infection more potently than IFITM1, regardless of localisation. This suggests intrinsic differences in IFITM1 and IFITM3. Much of the work presented in this chapter has been published in [16].

4.2 Results

4.2.1 IFITMs can restrict alphavirus infection

To initially investigate whether IFITM proteins inhibit alphavirus infection, stably expressing A549 cells were used (as in Chapter 3). Cells were infected with SFV or SINV at a range of input between 0.1 and 1000 pfu/cell for 5.5 - 6 h. Cells were then fixed and labelled for newly synthesised envelope glycoproteins (E1/E2) as a read-out of infection. IFITM3 inhibited infection by both viruses (Fig. 4.1). At 1 pfu/cell, ∼80% of A549 cells were positive for E1/E2, but only ∼3% of IFITM3 expressing cells were infected ($p < 0.0001$). A549 cells seemed less permissive to SINV than SFV with ∼40% of cells infected at 10 pfu/cell. IFITM3 inhibited SINV infection, with only ∼5% infection at 10 pfu/cell ($p < 0.0001$). IFITM3-mediated inhibition of both viruses was reduced at higher input of virus with ∼20% inhibition at 100 pfu/cell (still a statistically significant difference compared to A549 cells; $p < 0.0001$) and <10% inhibition at 1000 pfu/cell ($p = 0.0155$) for SFV, and ∼10% inhibition at 100 pfu/cell for SINV ($p = 0.0008$). IFITM2 also inhibited SFV infection, though not as efficiently as IFITM3 (∼50% inhibition at 1 pfu/cell [$p = 0.0006$], compared to ∼95% with IFITM3), but showed no statistically significant inhibition of SINV infection. IFITM1 did not inhibit either virus.

These data indicate that IFITM3, and to a lesser extent IFITM2, can restrict alphavirus infection of A549 cells, while IFITM1 has no apparent inhibitory effect. This restriction seemed to become saturated as the level of input virus was increased.

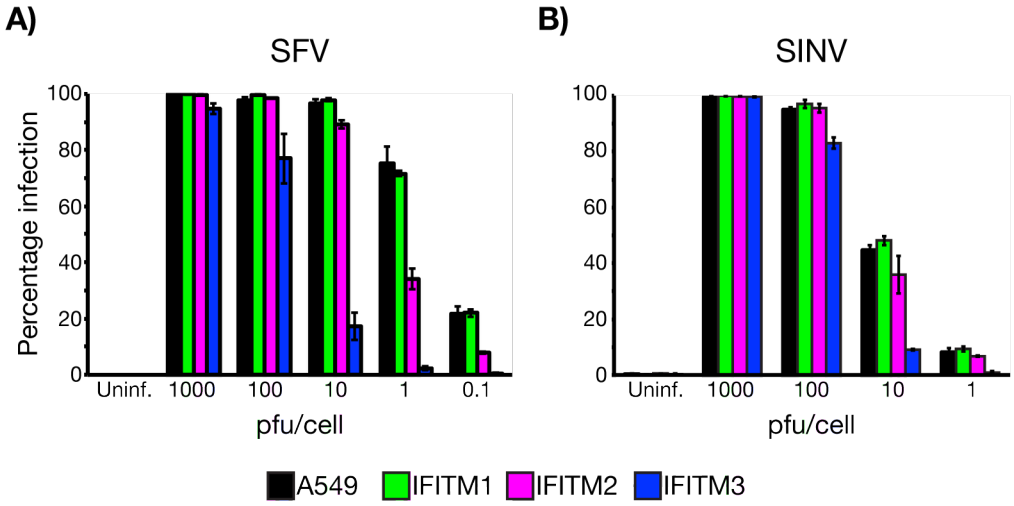

Figure 4.1: **Alphavirus infection is inhibited by IFITM proteins.** A549 cells stably expressing HA-tagged IFITM1, 2 or 3 were infected with SFV (A) or SINV (B). Cells were infected at the indicated level of input virus for 5.5 - 6 h, then fixed and labelled for the production of the respective viral envelope glycoproteins as a marker of infection. The percentage of infected cells was determined by immunofluorescence microscopy using a high-throughput Opera confocal microscope. SINV did not infect A549 cells as efficiently as SFV, however both viruses show reduced infection when IFITM3 was expressed. IFITM2 expression had some inhibitory effect on SFV, but little impact on SINV infection. IFITM1 had no apparent affect on either virus. These data are from a representative experiment (n = 3 for SFV and 2 for SINV) performed in 96 well plate format with triplicate wells of infection. Each bar shows the mean infection percentage with error bars representing the standard deviation between the three wells.

4.2.2 IFITM3 endosomal localisation and expression levels impact on antiviral activity

The IFITM expressing cell lines used in Fig. 4.1 were produced through single cell cloning of lentivirally transduced cells (OS cells - see Materials and Methods Table 2.2 [page 72]). To further define SFV restriction by IFITM proteins, and rule out the potential for inhibition being a consequence of using clonal cells, two further groups of stable IFITM expressing cells, produced through puromycin selection, were tested (P1 and P2 cell groups - Table 2.2 [page 72]).

Initially, the IFITM expression levels in each of the different cells were tested by western blot (Fig. 4.2 A). Antibodies against the NTD were used, as the HA-tag can be lost in endosomal compartments (Fig. 3.13 and 3.14, pages 120 and 121). The OS cell group had the highest levels of IFITM expression. P1 and P2 cells had expression levels that were similar to each other. OS- and P1-IFITM1 had similar expression levels. OS- and P1-IFITM2 had low expression or poor detection with the anti-IFITM3-NTD antibody. The expression levels for the three groups of cells were compared to the expression level induced by interferon (IFN)-β treatment of A549 cells. It appears that the majority of IFITM protein produced in A549 cells following IFN-β treatment is IFITM1 (Fig. 4.3); a band was detected using the anti-IFITM1-NTD antibody but there was only a weak protein band detected with the anti-IFITM3-NTD antibody (which does not detect IFITM1; Fig. 3.8 [page 107]). The apparent IFITM1 band that was detected by IFN-β treatment of A549 cells suggests that the P1 and P2 cells have IFITM expression levels closest to the levels induced in A549 cells (Fig. 4.3).

When infected with SFV, the P1-IFITM expressing cells showed a similar restriction pattern as OS-IFITMs. P1-IFITM3 inhibited infection most potently ($\sim$70% inhibition at 1 pfu/cell [$p < 0.0001$]), with IFITM2 having some inhibitory affect ($\sim$50% inhibition at 1 pfu/cell [$p = 0.0001$]), while IFITM1 did not inhibit infection (Fig. 4.2 B). P1-IFITM3 was less restrictive of SFV infection than OS-IFITM3, with inhibition only occurring between 0.1 - 10 pfu/cell, compared to 0.1 - 100 pfu/cell for OS-IFITM3. At 1 pfu/cell where OS-IFITM3 had $\sim$95% inhibition of infection, P1-IFITM3 inhibited infection by $\sim$70%. Similar levels of inhibition were seen with P2-IFITM3. These lower levels of restriction correlate with the lower expression level of IFITM3 in the P1 and P2 cells (Fig. 4.2 A),

matching with the apparent saturation of inhibition that occurs with higher input of virus (Fig. 4.1 and 4.2 B).

As previously discussed, IFITM3-Y20A is localised primarily to the plasma membrane (Fig. 3.15 [page 122]), similarly to IFITM1 (Fig. 3.2 [page 97] and Fig. 3.9 [page 108]). While endosomal localised IFITM3 inhibited SFV infection, IFITM3-Y20A did not (Fig. 4.2 B), matching IFITM1. Therefore it appears that the endosomal localisation of IFITM3 is essential for inhibition of SFV infection when the virus enters through the normal endosomal route.

For clarity, unless otherwise indicated, all work presented from here was performed with OS-IFITM cells.

4.2.3 IFITM3 expression does not block SFV binding or endocytosis

IFITM3 can inhibit SFV infection of cells, and the endosomal localisation of the protein is essential for this function. Since SFV enters cells by fusion in early endosomes, it was hypothesised that IFITM3 inhibited infection by blocking SFV entry. In order to enter and infect a cell, SFV must initially bind to the cell surface, prior to internalisation by clathrin-mediated endocytosis (CME). Once internalised, virus is trafficked to endosomes where the low pH environment triggers conformational changes in the E1/E2 glycoprotein complex that promotes fusion between viral and endosomal membrane, allowing release of the viral capsid into the cytosol. Each of these aspects of the entry pathway were tested to determine at which stage IFITM3 inhibits infection.

Initially, SFV binding to the cell surface of IFITM expressing cells was tested. Equal amounts of virus were added to IFITM expressing cells for 1 h at 4°C (conditions at which virus has been found to effectively bind to BHK-21 cells [45, 86]), prior to production of lysates which were separated by SDS-PAGE and analysed for the E1/E2 proteins by western blot. Similar amounts of E1/E2 were detected in lysates from A549 and IFITM1, 2 and 3 expressing cells, suggesting that IFITM expression does not impact on SFV binding to the cell surface (Fig. 4.4 A).

Following binding, SFV must be internalised by the cell through CME. To test whether IFITM3 inhibits CME of SFV particles, a protease resistance assay was used. Virus was

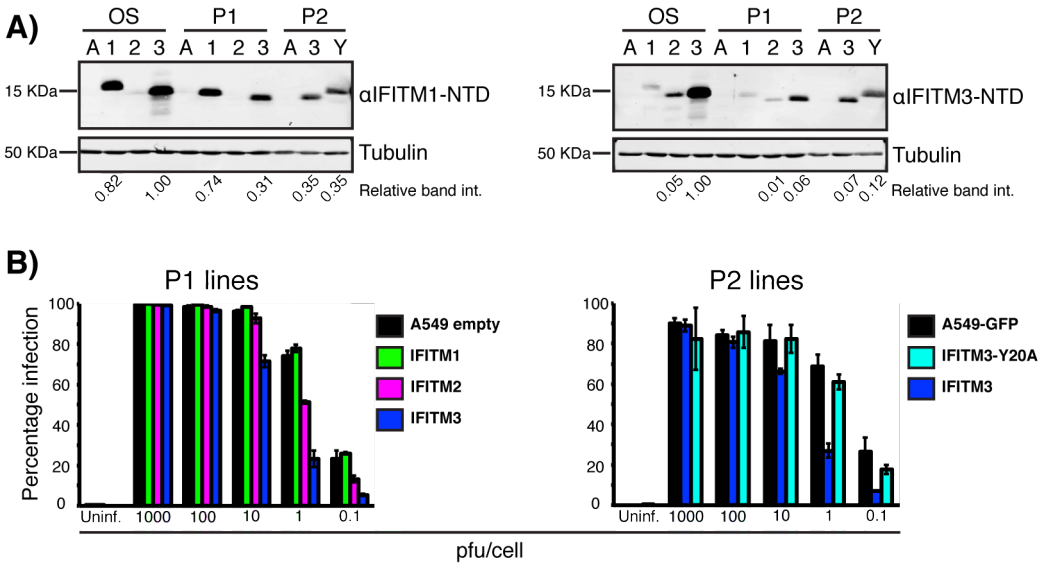

Figure 4.2: **IFITM expression level and endosomal localisation affect SFV restriction.** P1- and P2-IFITM expressing cell lines were analysed for IFITM expression levels and SFV restriction (see Materials and Methods Table 2.2 [page 72], for a description of the cells). A) Western blots to compare the IFITM expression levels of OS- (the original set used in Fig. 4.1), P1- and P2-IFITM cells. A, M1, M2, M3 denote A549, IFITM1, IFITM2 and IFITM3, respectively. The anti-IFITM1-NTD and anti-IFITM3-NTD antibodies were used to detected IFITM proteins (as described in Chapter 3). Tubulin was used as a loading control. Proteins were detected using secondary antibodies conjugated to far-red fluorophores and imaged on a Li-COR Odyssey system. The fluorescence intensity (int.) of the IFITM and tubulin bands was quantified using Li-COR Odyssey software. IFITM band intensities were normalised to the tubulin loading controls and set relative to the highest band intensity in each blot (OS-IFITM3 for both). B) P1- and P2-IFITM cells were infected with SFV at an input between 0.1 and 1000 pfu/cell. Cells were incubated for 5.5 - 6 h to allow infection, prior to fixation and labelling for production of *de novo* E1/E2 protein as a read-out of infection, which was analysed by immunofluorescence microscopy. Concomitantly with the lower expression in the P1- and P2-IFITM cells (A), there were reduced levels of SFV restriction compared to OS-IFITM cells (Fig. 4.1). The data are a representative experiment (n = 2) performed with triplicate wells in a 96 well plate format. Each bar shows the mean infection percentage of the three wells and errors bars are the standard deviation.

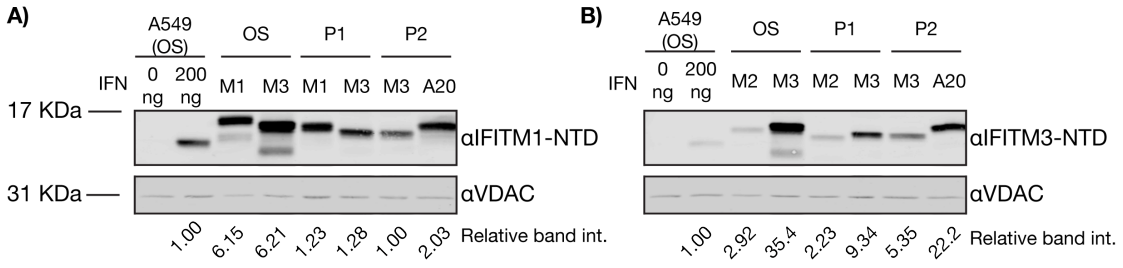

Figure 4.3: **IFN-β treatment induces IFITM expression in A549 cells.** OS-A549 cells were treated with 200 ng IFN-β for 24 h prior to production of whole cell lysates for western blotting. Samples were separated by SDS-PAGE and blotted with the anti-IFITM1-NTD (A) or anti-IFITM3-NTD (B) antibodies and for VDAC as a loading control. Lysates from IFN-β treated A549 cells were western blotted alongside samples produced from OS-, P1- and P2-IFITM cell sets (M1, M2, M3 and A20 denote IFITM1, IFITM2, IFITM3 and IFITM3-Y20A, respectively). Proteins were detected using secondary antibodies conjugated to far-red fluorophores and imaged on a Li-COR Odyssey system. The fluorescence intensity (int.) of the IFITM and VDAC bands was quantified using Li-COR Odyssey software. IFITM band intensities were normalised to the tubulin loading controls and set relative to the band intensity of IFN-β treated A549 samples. It appears that the majority of IFITM protein produced by A549 cells is IFITM1 as the band intensity is low with the anti-IFITM3-NTD antibody (which does not detect IFITM1), compared to the band intensity seen with the anti-IFITM1-NTD antibody.

bound to the surface of cells, which were then warmed to 37℃ for 5, 15 or 30 min, or left on ice. The shift from 4℃ to 37℃ promotes endocytosis of bound virus [45, 85]. After each period of warming, cells were shifted back to 4℃, to prevent further trafficking events, then treated with subtilisin for 1 h. Subtilisin treatment can remove virus particles bound at the cell surface, without impacting intracellular pools [193]. Thus, following subtilisin treatment, only virus particles internalised by endocytosis will remain associated with the cells, which can be analysed by western blot for the E1/E2 proteins. Without warming, subtilisin treatment removed ∼78% of bound virus from A549 cells (Fig. 4.4 B and C). Following warming, there was an increase in the amount of cell-associated E1/E2, which peaked at 15 min with >75% of virus internalised (Fig. 4.4 B and C). Very similar kinetics of uptake were observed on IFITM3 expressing cells (Fig. 4.4 B and C), indicating that IFITM3 does not inhibit SFV internalisation to A549 cells.

4.2.4 Internalised SFV co-localises with IFITM3

Seeing that SFV can be endocytosed to IFITM3 expressing cells, that IFITM3 localises primarily to endosomal membranes (Fig. 3.17 [page 127]), and with the knowledge that

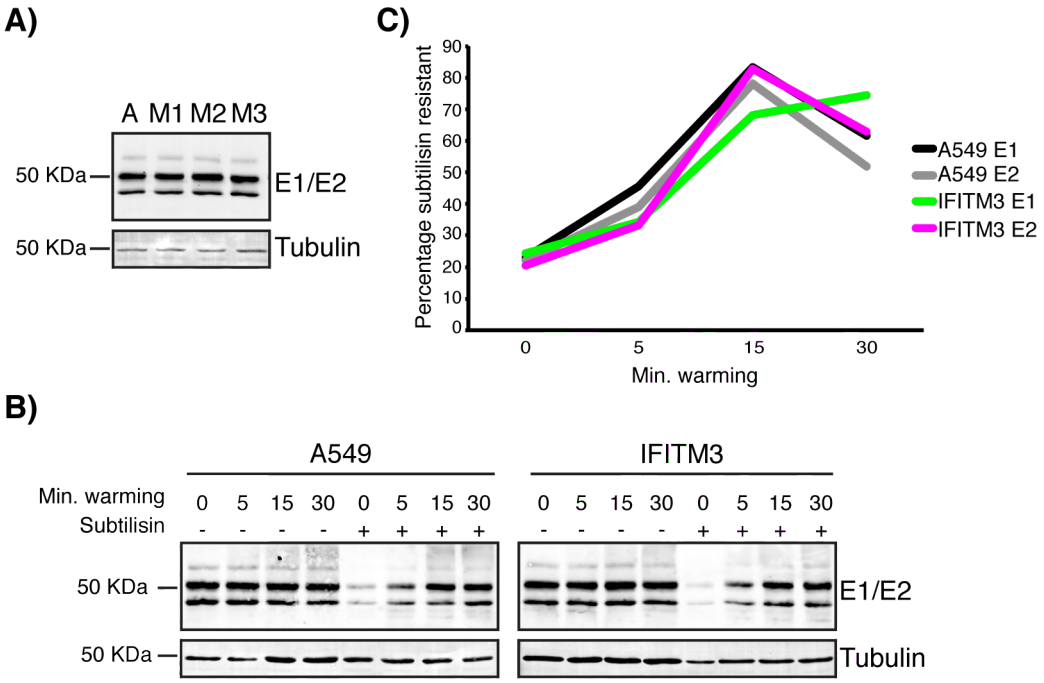

Figure 4.4: **SFV binding and internalisation into IFITM expressing cells.** A) Cell surface binding: SFV (200 pfu/cell) was added to A549 or IFITM expressing cells (A, M1, M2 and M3) at 4℃, and incubated for 1 h to allow virus binding to the cell surface. Cells were washed to remove unbound virus and lysed to analyse the level of viral protein (E1/E2) associated with cells by western blot. A representative western blot (n = 4) is displayed. Tubulin was used as a loading control. B) Virus endocytosis: SFV was bound to A549 or IFITM3 expressing cells as in (A). Cells were washed to remove unbound virus, media at 37℃ was added and the cells incubated at 37℃ for the indicated times to promote virus endocytosis. Cells were subsequently incubated with subtilisin at 4℃ to proteolytically remove any virus remaining at the plasma membrane, without impacting on internal pools. Cells were lysed and analysed for cell-associated viral protein (E1/E2) by western blot. Control samples that were not treated with subtilisin were analysed to indicate the total cell-associated virus. (The experiments were performed by Stephanie Czieso). C) Fluorescence intensity of E1 (bottom), E2 (top) and tubulin bands were measured to quantify the level of subtilisin resistant E1/E2 across 3 - 4 independent experiments (n = 4 for A549 and n = 3 for IFITM3). Band intensity of E1/E2 were adjusted based on tubulin loading. A measure of the total cell-associated virus was determined by averaging the band intensity for all untreated time points and setting the intensity of E1 or E2 at each treated time relative to this total. These relative intensities were averaged across all experiments and plotted to display the percentage E1/E2 that was subtilisin resistant at each time point.

SFV fusion occurs in these compartments, we investigated whether internalised SFV entered into IFITM3-positive endosomes. As described previously, virus was bound to the surface of cells grown on glass coverslips at 4℃ for 1 h and the cells then shifted to 37℃ to promote endocytic uptake of bound virus. At time points between 0 and 30 min, cells were fixed and processed for immunofluorescence microscopy. Cells were stained for SFV using antibodies directed against E1/E2, and the IFITM3 HA-tag (Fig. 4.5). While some pools of IFITM3 may be missed due to loss of the HA-tag in endosomes (Fig. 3.13 [page 120], and Fig. 3.14, [page 121]), it was necessary to use rat anti-HA antibody as both IFITM-NTD antibodies were rabbit polyclonal preparations, and the SFV E1/E2 anti-serum was also from rabbit. As a control, comparable experiments were performed in A549 cells, which were stained for E1/E2 and EEA1, as a marker of early endosomes (Fig. 4.7). On cells kept at 4℃, E1/E2 staining was seen as small puncta primarily around the periphery of cells, and there was little overlap with either IFITM3 (Fig. 4.5) or EEA1 (Fig. 4.7). After 10 min at 37℃ and at later time points, overlap was detected between E1/E2 and the cellular proteins (Fig. 4.5 and 4.7). The E1/E2 positive puncta also appeared to increase in size and fluorescence intensity suggesting particles may be accumulating within endosomes. An increase in the size and fluorescence intensity over time of warming was also observed for EEA1 (Fig. 4.7), but this was similarly seen in mock infected cells (data not shown), suggesting it is probably a consequence of cooling and warming, rather than an affect induced by SFV internalisation. The time dependent increase in overlap between SFV and IFITM3 (Fig. 4.6) or EEA1 (Fig. 4.8) was observed over multiple experiments. These data indicate that when SFV is taken up by CME, it is delivered into IFITM3-positive endosomes.

These observations were further confirmed by electron microscopy (EM). As before, virus particles were bound to cells and allowed to internalise, prior to processing for EM analysis. SFV particles were found within coated vesicles and multivesicular bodies in both A549 and IFITM3 expressing cells (Fig. 4.9 and 4.10), further supporting the suggestion that IFITM3 expression does not inhibit SFV internalisation or trafficking. As with the immunofluorescence experiments, SFV and IFITM3 were found in the same compartments by immuno-gold labelling of cryo-sections (Fig. 4.10 B), further arguing that virions are delivered to IFITM3-positive endosomes.

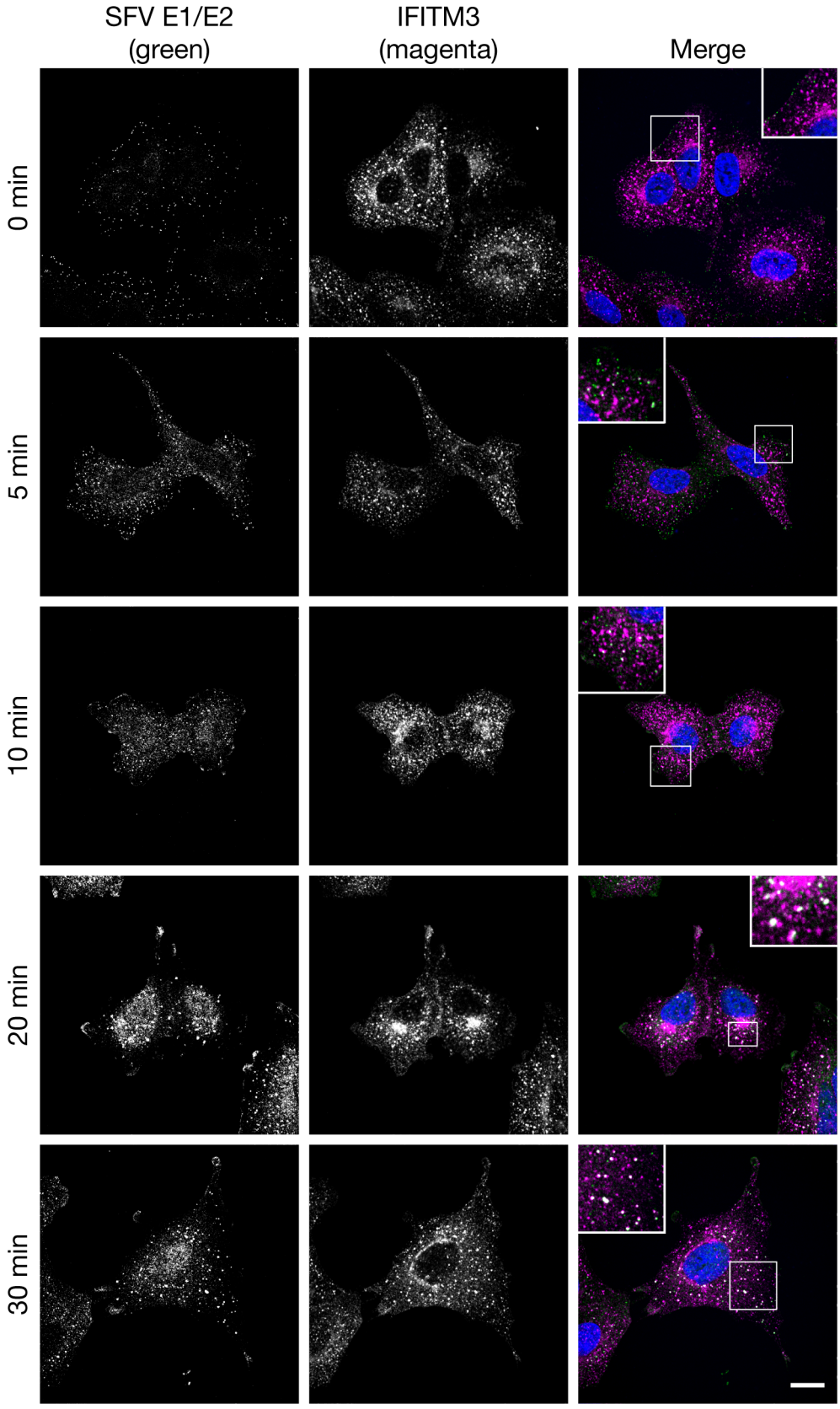
SFV E1/E2
(green)
IFITM3
(magenta)
Merge
0 min
5 min
10 min
20 min
30 min

Figure 4.5: **Internalised SFV co-localises with IFITM3.** SFV (50 pfu/cell) was added to IFITM3 expressing cells and allowed to bind for 1 h at 4℃. Unbound virus was removed by washing. Media pre-warmed to 37℃ was added to cells, which were then incubated for the indicated times to allow internalisation. Cells were then fixed and labelled with antibodies against SFV E1/E2 (detected with AF488; green) and HA (detected with AF647; magenta) following permeabilisation. Single confocal sections are displayed. E1/E2 labelling was seen as small puncta primarily around the periphery of cells after 0 and 5 min at 37℃, and had little overlap with HA. With longer periods of warming, larger and brighter puncta of E1/E2 were seen and overlap was observed with HA. Nuclei were detected with Hoechst. Scale bar represents 15 μm. All images were acquired with the same microscope settings and brightness and contrast have been adjusted uniformly. See Fig. 4.6 for analysis of the overlap between SFV and IFITM3 staining.

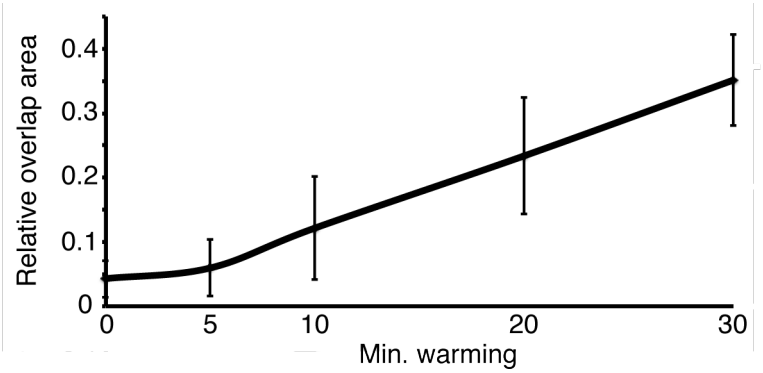

Figure 4.6: **Internalised SFV co-localisation with IFITM3 (quantification).** Analysis of overlap between E1/E2 (green) and HA (magenta) pixels as displayed in Fig. 4.5. Data were quantified over three independent experiments, with six images at 63x magnification for each sample per experiment (displaying a total of between 131 and 163 cells per condition). The average ratio of relative area of overlapping pixels to green only pixels is plotted, with error bars displaying the standard deviation (see Section 2.9.1 [page 89] for further detail).

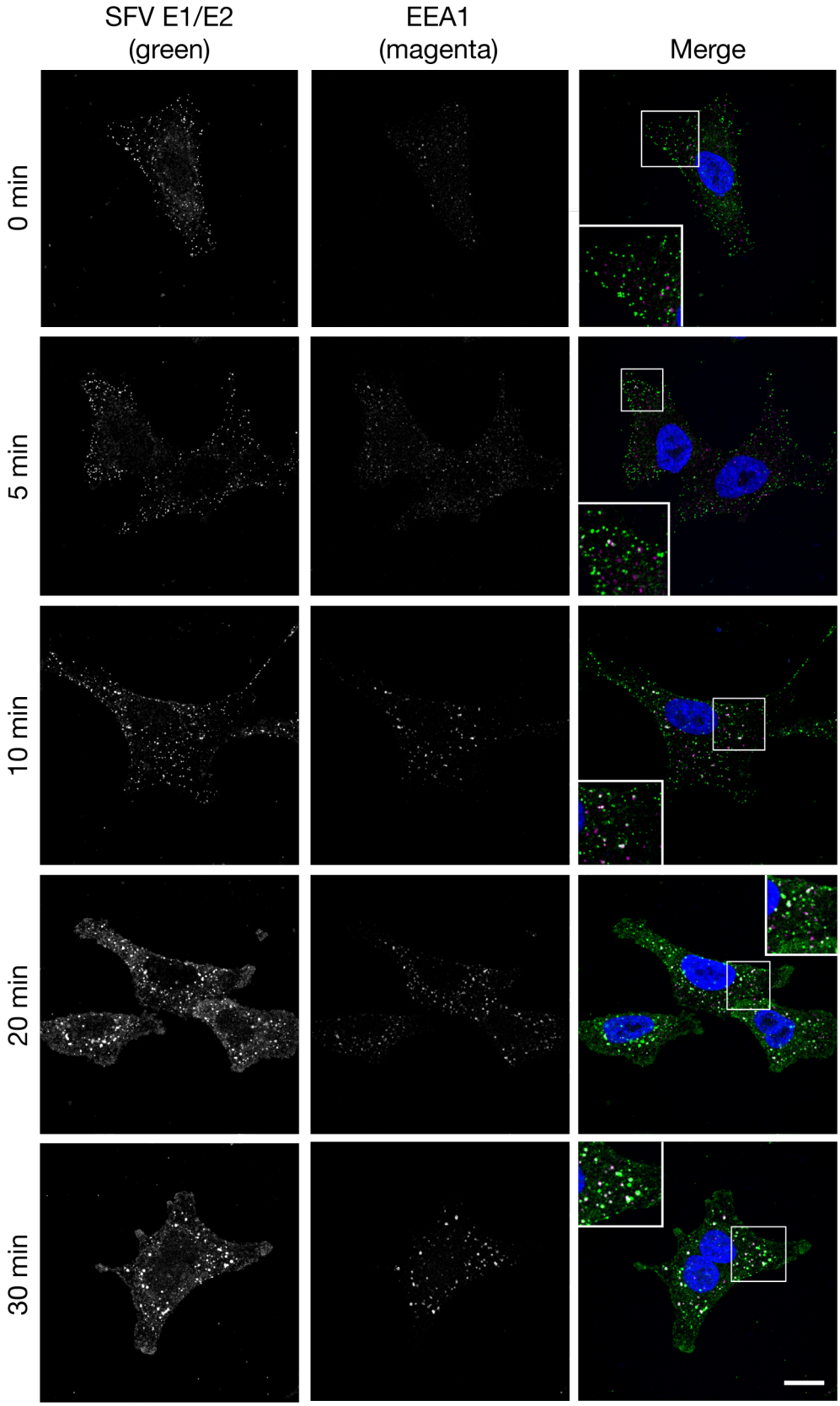
SFV E1/E2
(green)
EEA1
(magenta)
Merge
0 min
5 min
10 min
20 min
30 min

Figure 4.7: **Internalised SFV co-localises with EEA1.** SFV (50 pfu/cell) was added to A549 cells and allowed to bind for 1 h at 4℃. Unbound virus was removed by washing. Media pre-warmed to 37℃ was added to cells, which were then incubated for the indicated times to allow internalisation. Cells were then fixed and labelled with antibodies against SFV E1/E2 (detected with AF488; green) and EEA1 (detected with AF647; magenta) following permeabilisation. Single confocal sections are displayed. E1/E2 labelling was seen as small puncta primarily around the periphery of cells after 0 and 5 min at 37℃, and had little overlap with EEA1. With longer periods of warming, larger and brighter puncta of E1/E2 were seen and overlap was observed with EEA1. There also appeared to be an increase in the brightness of EEA1 puncta over time that was similarly seen in mock-infected samples (data not shown), and may be due to cooling and warming the cells. Nuclei were detected with Hoechst. Scale bar represents 15 μm. All images were acquired with the same microscope settings and brightness and contrast have been adjusted uniformly.

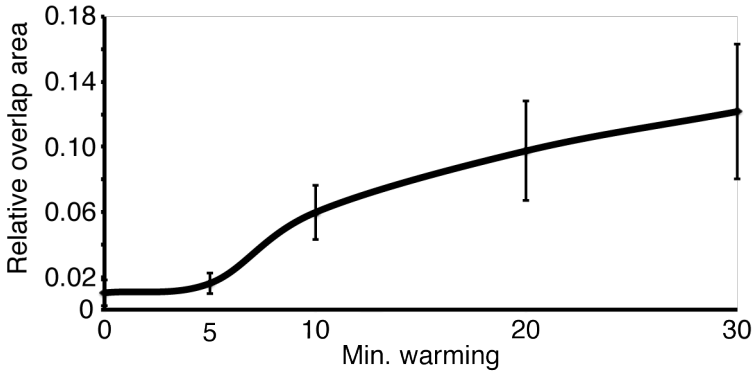

Figure 4.8: **Internalised SFV co-localisation with EEA1 (quantification).** Analysis of overlap between E1/E2 (green) and EEA1 (magenta) pixels as displayed in Fig. 4.5. Data were quantified over three independent experiments, with six images at 63x magnification for each sample per experiment (displaying a total of between 150 and 213 cells per condition). The average ratio of relative area of overlapping pixels to green only pixels is plotted, with error bars displaying the standard deviation (see Section 2.9.1 [page 89] for further detail).

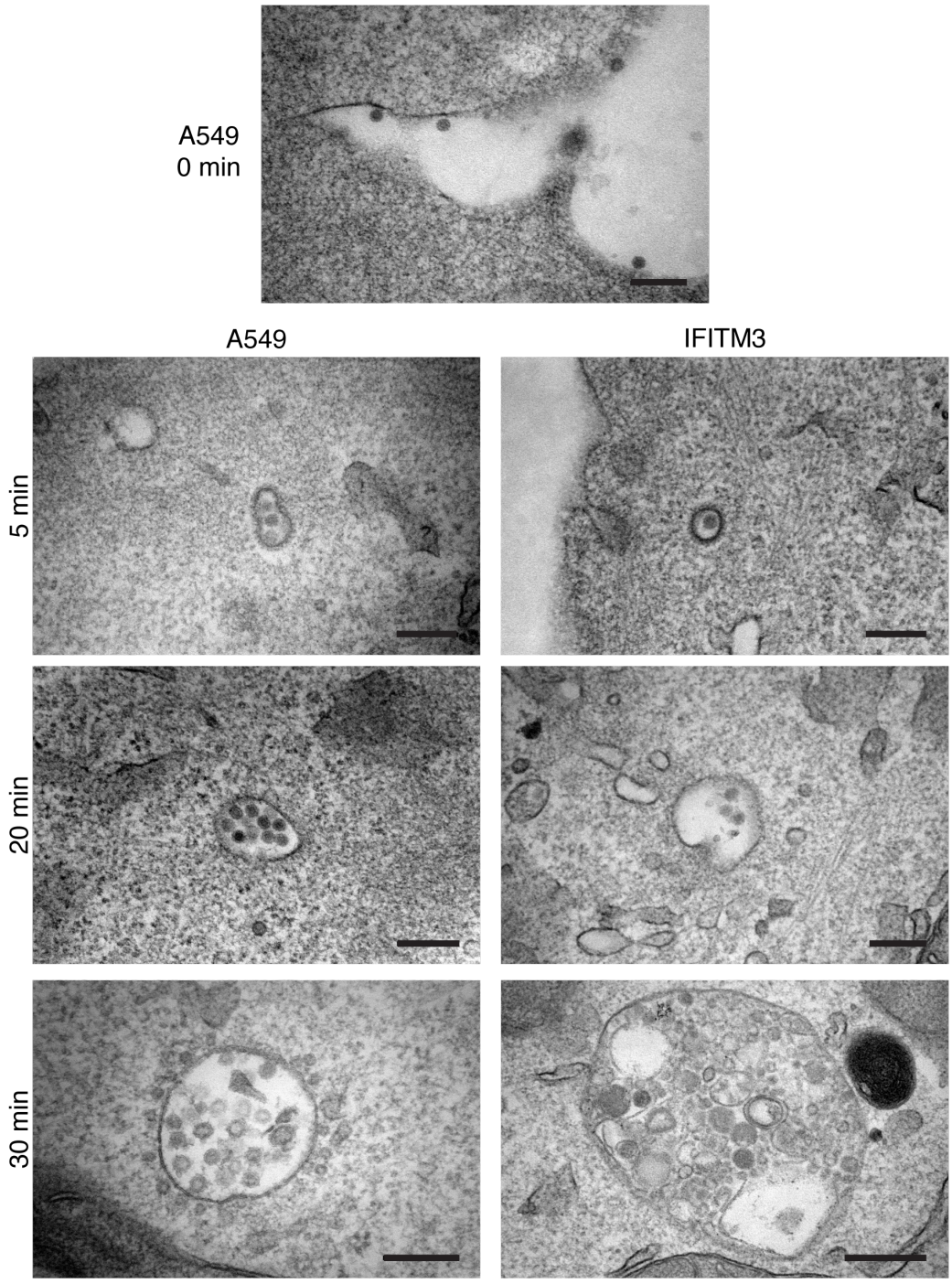
A549
0 min
A549
IFITM3
5 min
20 min
30 min

Figure 4.9: **Electron microscopy imaging of SFV uptake to A549 and IFITM3 expressing cells.** SFV (1000 pfu/cell) was added to A549 or IFITM3 expressing cells and allowed to bind for 1 h at 4℃. Unbound virus was removed by washing. Media pre-warmed to 37℃ was added to cells to allow internalisation of virus for the indicated times. Samples were fixed and processed for Epon section electron microscopy. After binding, virus particles could be detected at the plasma membrane (0 min), based on their characteristic morphology. With 5 min of warming virus particles could be detected in coated vesicles and at the plasma membrane. By 20 and 30 min, virus particles appeared in endosomal structures, but it became hard to differentiate virions form intralumenal vesicles, which have a similar size. These internalisation patterns appeared similar in A549 and IFITM3 expressing cells. Scale bars represent 200 nm. Sample preparation and imaging was performed by Dr. Ian White.

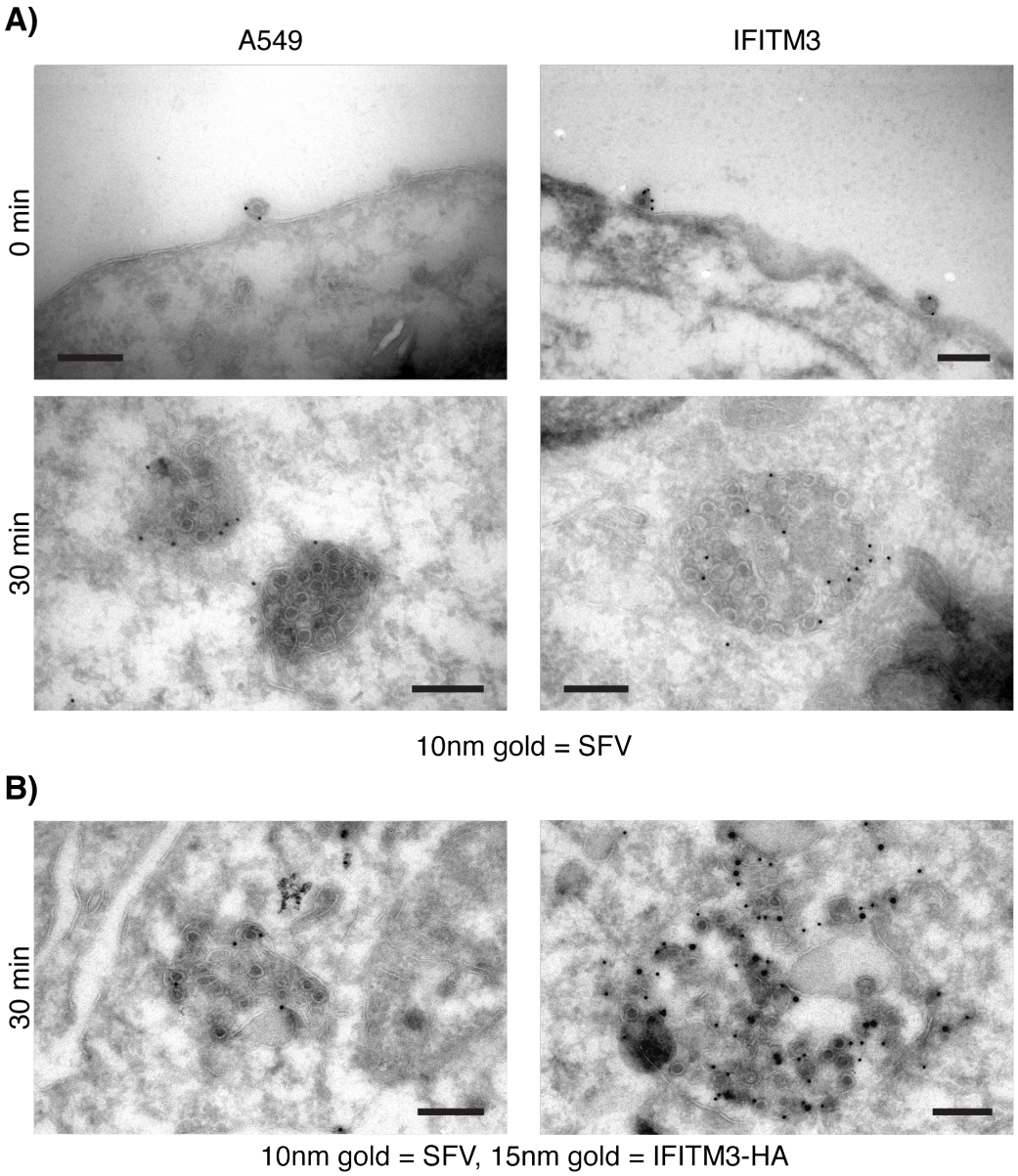
A)
A549
IFITM3
0 min
30 min
10nm gold = SFV
B)
30 min
10nm gold = SFV, 15nm gold = IFITM3-HA

Figure 4.10: **Immuno-gold labelling of cryo-sections and electron microscopy of SFV uptake to A549 and IFITM3 expressing cells.** SFV (5000 pfu/cell) was added to A549 or IFITM3 expressing cells and allowed to bind for 1 h at 4℃. Unbound virus was removed by washing. Media pre-warmed to 37℃ was added to cells for the indicated times to allow internalisation of virus. Samples were fixed and processed for cryo-sectioning and immuno-gold labelling. A) Sections were labelled with antibodies against SFV E1/E2. After binding, virus particles were detected at the cell surface. With 30 min of warming, gold particles were found within multivesicular bodies in both A549 and IFITM3 expressing cells. B) Sections were labelled with antibodies against SFV E1/E2 (detected with 10 nm colloidal gold) and the HA-tag (detected with 15 nm colloidal gold). Minimal background to the HA-tag was detected in A549 cells: The majority of labelling in IFITM3 expressing cells was found in multivesicular bodies (as seen in Chapter 3, Fig. 3.7). As in (A), SFV particles were detected in multivesicular bodies following 30 min internalisation, and were seen in the same compartments as IFITM3 (as based on the HA labelling). Scale bars represent 200 nm. Sample preparation and imaging was performed by Dr. Ian White.

4.2.5 Kinetics of SFV capid release into A549 cells

To ensure that the investigations of virus internalisation were at time points relevant to infection, the kinetics of SFV capsid release into A549 cells was determined. Delivery of the capsid into the cytosol is dependent on virion endocytosis and low pH-induced fusion in endosomes. Therefore, disruption of pH gradients can inhibit SFV infection, up until the point of membrane fusion. After membrane fusion, disruption of low pH gradients will not impact SFV infection of cells. To investigate the time for SFV penetration of endosomes to occur, the fast acting ionophore monensin was used to dissipate the low pH gradient across endosome membranes. Virus particles were bound at the cell surface and allowed to internalise by shifting cells to 37℃. Monensin was added at times between 0 and 30 min, and left through the 5.5 - 6 h infection period. E1/E2 production, as detected by immunofluorescence microscopy, was used as a read-out of infection (with infection being a surrogate of successful fusion with endosomes). The percentage of infected cells was then determined and compared to untreated control cells. When monensin was added at 0 min, there was nearly a complete loss of infection (Fig. 4.11). However, when added at later times an increasing number of cells were infected. Adding monensin at 30 min had almost no inhibitory affect (Fig. 4.11). These data suggest that the majority of infectious virus had penetrated cells by 30 min. Therefore the previous analysis of SFV internalisation within the first 30 min is relevant to infection in A549 cells.

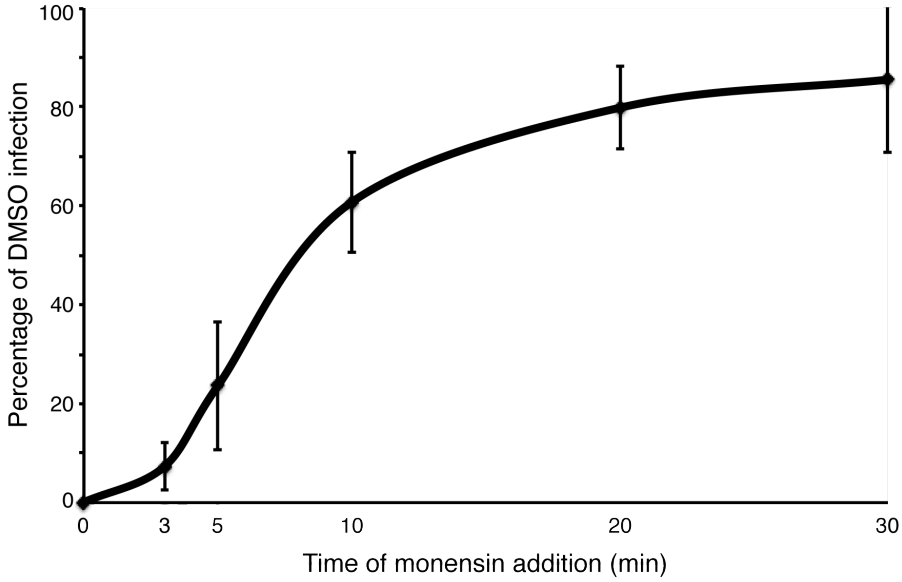

Figure 4.11: **Kinetics of SFV penetration into A549 cells.** SFV (5 pfu/cell) was added to A549 cells and allowed to bind for 1 h at 4℃. Unbound virus was removed by washing. Media pre-warmed to 37℃ containing DMSO (as control) or 10 μm monensin was added to the cells to allow internalisation of virus. At times between 3 and 30 min, control media were replaced with monensin-containing media. After 5.5 - 6 h infection, cells were fixed and analysed for infection by immunofluorescence microscopy. The data are presented as the percentage infected cells in monensin treated samples relative to control samples. The data are the mean infection percentage (relative to DMSO controls) from three independent experiments (containing duplicate wells). Error bars represent the standard deviation between experiments.

4.2.6 SFV is exposed to acidic pH in IFITM3 expressing cells

Since SFV was effectively endocytosed into IFITM3 expressing cells, the next question was whether virus particles were being delivered to low pH compartments to activate the fusion machinery. Following exposure to low pH, E1 undergoes conformational changes to form a homotrimer (HT) that is insensitive to SDS and digestion with trypsin [96], changes that can be seen by SDS-PAGE and western blotting. As a positive control for the acid-induced conformational changes, virus particles bound at the cell surface were treated with pH 5.5 media for 3 min at 37℃. To test for SFV delivery to acidic compartments of cells, virus was bound to the cell surface and allowed to internalise for 0, 5, 15 and 30 min at 37℃. As a negative control, cells were pre-treated with bafilomycin A1 (Baf A) for 15 min at 37℃, prior to virus binding at 4℃, and internalisation for 30 min, all in the presence of Baf A. Baf A is an inhibitor of the vacuolar ATPase proton pump and therefore inhibits endosomal acidification. After all treatments, cells were lysed, the lysates where split in two, and one half treated with trypsin. The E1/E2 proteins were then analysed by western blot. Heat can dissociate the E1 HT, so unlike in other western blots, the samples were not heated prior to SDS-PAGE.

With 0 min of internalisation, the monomeric forms of E1/E2 were detected with a molecular weight (MW) of ∼50 kDa (Fig. 4.12 lane 1). These monomeric forms of E1/E2 are sensitive to trypsin digestion as the bands became undetectable following incubation with the protease (lane 2). Treatment of surface bound virus with pH 5.5 media for 3 min prior to lysis induced the formation of a higher MW fragment, which was insensitive to trypsin digestion, and therefore concluded to be the E1 HT (lanes 3 and 4). This higher molecular weight, trypsin-insensitive band, was also detected when virus was internalised into A549 cells. The intensity of the band increased over the three time points, indicating a time-dependent increase in the appearance of the E1 HT (lanes 7 - 12). When virus was internalised for 30 min into cells that were treated with Baf A, the higher MW band was not detected (lanes 5 and 6), arguing that this band is indeed induced by an acidic environment. Virus internalised to IFITM3 expressing cells displayed the higher MW band of E1 with similar kinetics to those in A549 cells (lanes 13 - 18). It can therefore be concluded that IFITM3 does not interfere with endosomal acidification, SFV

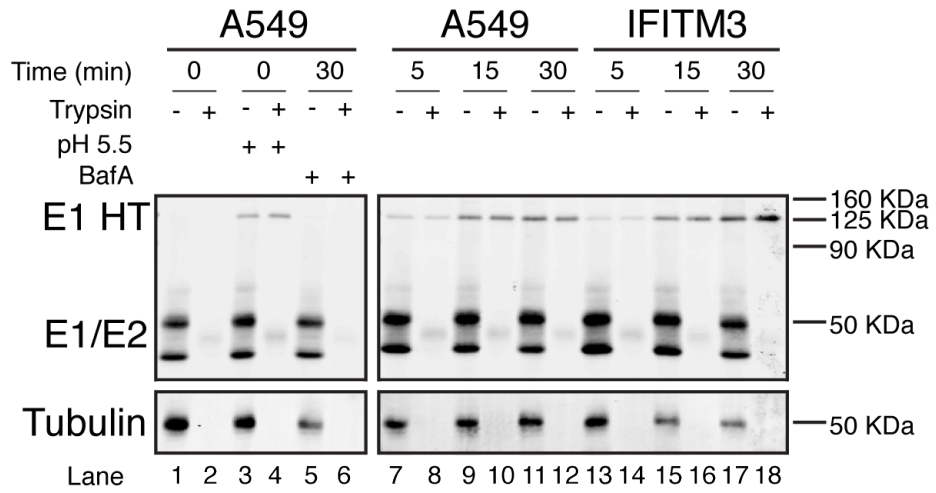

Figure 4.12: **SFV is exposed to acidic pH in IFITM3 expressing cells.** Cells were pre-treated at 37℃ for 15 min with media containing 100 nm bafilomycin A1 (Baf A) or untreated (DMSO control), prior to addition of media at 4℃ (containing Baf A or DMSO) and placing on ice. SFV (200 pfu/cell) was added to A549 (lanes 1 - 12) or IFITM3 expressing cells (lanes 13 - 18) for 1 h at 4℃. Unbound virus was removed by washing and pre-warmed media were added to the cells prior to incubation at 37℃ for the indicated times (lanes 5 - 18), or kept at 4℃ (lanes 1 - 4). In lanes 3 - 4, cells with bound virus were treated with pH 5.5 media for 3 min at 37℃. In lanes 5 - 6 cells were treated with 37℃ media, containing 100 nm bafilomycin A1 (Baf A), and incubated for 30 min. Cells were placed on ice and lysed with 1% Triton X-100 (Tx100) in PBS for 15 min. Nuclei were removed by centrifugation and the lysate was split into two aliquots and one sample was treated with 800 μg/ml trypsin in 1% Tx100. After 10 min incubation at 37℃, soy bean trypsin inhibitor (2 mg/ml) in 1% Tx100 was added to all samples to inactivate the protease. All samples were then analysed by non-reducing SDS-PAGE and western blotting for E1/E2, and tubulin as a loading control. Samples were not heated prior to SDS-PAGE as this can dissociate the E1 homotrimer (HT).

internalisation to these compartments, or conformational changes of E1/E2.

4.2.7 IFITM3 inhibits release of SFV capsid to the cytosol

SFV can be delivered into acidic compartments, and the E1 glycoprotein can undergo conformational changes in IFITM3 expressing cells. Therefore, it was investigated whether the viral capsid could be released from endosomes into the cytosol. To determine if capsid was being released from endosomes, virus was bound to cells and internalised for up to 60 min. At each time point, cells were fixed, peremeabilised with Triton X-100, and labelled with antibodies against the SFV capsid for analysis by immunofluorescence microscopy.

Between 0 and 20 min, in both A549 and IFITM3 expressing cells, the capsid staining was detected as small puncta initially around the cell periphery, then seemingly within

intracellular compartments, which were most likely endosomes (Fig. 4.13). The staining pattern observed with the capsid appeared to be very similar to that seen with E1/E2 at these earlier time points (Fig. 4.5 and 4.7). The labelling was generally weak, presumably owing to the tight packaging of the capsid protein within virions limiting access of anti-capsid antibodies. With 40 min of internalisation to A549 cells, diffuse cytosolic capsid fluorescence was seen that increased in intensity after 60 min warming (Fig. 4.13 and 4.14). This diffuse fluorescence was thought to be capsid protein that had been released from endosomes into the cytosol. Monensin raises the pH of acidic organelles and inhibits SFV infection by preventing membrane fusion (Fig. 4.11). When A549 cells were treated with monensin, the diffuse cytosolic fluorescence was not detected, supporting the idea that the cytosolic staining pattern was associated with capsid release into the cytosol (Fig. 4.13 and 4.14). Even though there was little difference in the capsid staining on A549 and IFITM3 expressing cells up to 20 min, at later time points, there was no detection of diffuse cytosolic fluorescence in the IFITM3 expressing cells (Fig. 4.13 and 4.14). The similar staining pattern between monensin treated A549 cells and IFITM3 expressing cells suggests that IFITM3 blocked capsid release into the cytosol, and therefore blocked infection.

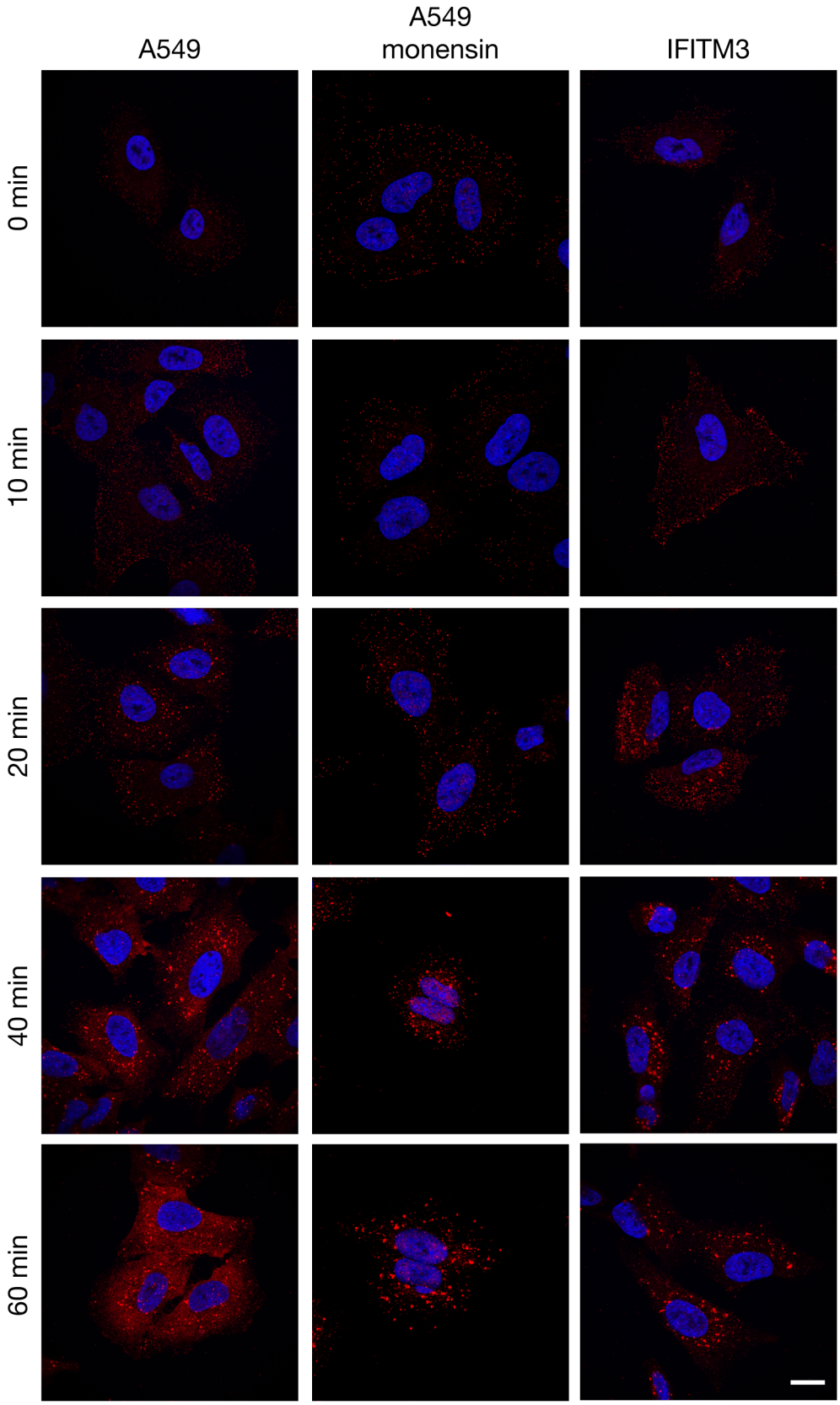
A549
A549
monensin
IFITM3
0 min
10 min
20 min
40 min
60 min

Figure 4.13: **IFITM3 expression inhibits SFV capsid release into the cytosol.** SFV (200 pfu/cell) was added to A549 or IFITM3 expressing cells and allowed to bind for 1 h at 4℃. Unbound virus was removed by washing. Media at 37℃ (containing 10 μM monensin where indicated) was added and cells incubated for up to 60 min. Cells were fixed, permeabilised with 0.1% Triton X-100 and labelled with rabbit anti-SFV capsid anti-serum (detected with AF594). With longer times of incubation at 37℃, staining for the SFV capsid was detected as increasingly bright puncta, indicative of virus trafficking to endosomes. In untreated A549 cells, by 40 min, diffuse cytosolic fluorescence was also seen, indicating release of the SFV capsid into the cytosol. Monensin treatment dissipates low pH gradients and inhibits SFV infection (see Fig. 4.11). In monensin treated A549s, the diffuse cytosolic fluorescence was not seen, even though puncta of SFV were, suggesting inhibition of capsid release into the cytosol. IFITM3 expressing cells showed a very similar staining pattern to monensin treated A549 cells, with endosomal puncta of SFV detected, but a lack of diffuse cytosolic fluorescence. Nuclei were detected with Hoechst. Scale bar represents 15 μm.

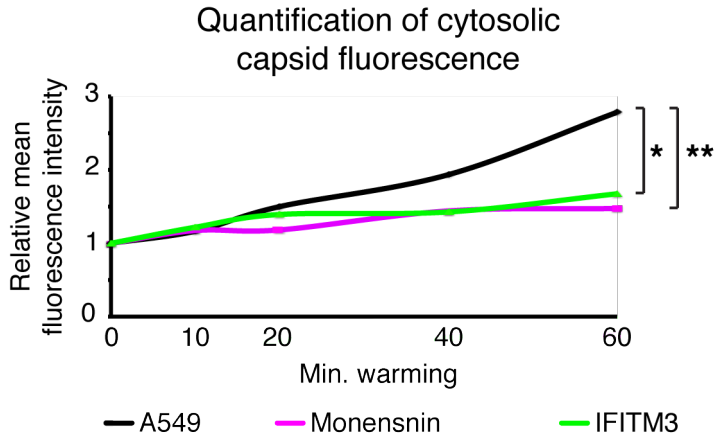

Figure 4.14: **IFITM3 expression inhibits SFV capsid release into the cytosol (quantification).** Quantification of cytosolic fluorescence associated with SFV capsid release from endosomes (as displayed in Fig. 4.13 and significance testing, as described in Chapter 2 (page 91). Briefly, nuclei were segmented and any fluorescence in the capsid channel associated with that area was removed as background. Large puncta of capsid staining were detected by application of a threshold and removed, as these were considered to be virus particles in endosomes. The remaining signal was deemed to be cytosolic, and the mean fluorescence intensity of individual cells determined. The mean average of these fluorescence intensity values was calculated from cells imaged across 3 independent experiments with 3 - 7 images at 63x magnification from each. A total of between 67 and 153 cells were analysed across all conditions. The plotted data are the averaged fluorescence intensity, normalised to background intensity at 0 min of warming. * $p < 0.05$, ** $p < 0.01$.

4.2.8 Amphotericin B treatment reduces IFITM3-mediated inhibition of SFV infection

IFITM3 has been shown to inhibit influenza A virus (IAV) infection by blocking fusion between viral and endosomal membranes [13, 14], and thus block nuclear translocation of the genetic material [12]. However, there is debate over the precise mechanisms underlying the block to membrane fusion [13, 14] (see Chapter 1 for more extensive discussion). The data presented thus far suggest that a similar mechanism may be associated with the restriction of SFV infection, since inhibition of membrane fusion can explain the lack of SFV capsid release into the cytosol. One characteristic of IFITM3-mediated IAV inhibition is that the antifungal drug amphotericin B (AmphoB) promotes IAV infection of IFITM3 expressing cells, without altering IFITM3 expression levels or distribution [156]. The precise mechanism(s) underlying this disruption are unclear, but AmphoB can bind to cholesterol, and was suggested to alter the properties of cellular membranes [156].

It was therefore tested whether IFITM3-mediated inhibition of SFV is similarly sensitive to AmphoB treatment. In the study of Lin *et al.* [156], it was reported that pre-treating cells with AmphoB for 1 h, prior to addition of virus, gave the greatest enhancement of IAV infection of IFITM3 expressing cells. To test the effects of AmphoB treatment in the context of SFV infection, cells were pre-treated with 1 μM AmphoB (as in [156]) at 37°C for 1 h prior to infection with SFV (in the presence of drug). Alternatively, there was no pre-treatment step, and SFV was added to cells with 1 μM AmphoB. Cells were incubated for 5.5 - 6 h to allow infection prior to immunofluorescence staining for production of E1/E2. Treatment of cells with AmphoB had very little impact on infection of A549 cells. However, with infection at 10 pfu/cell, the AmphoB treatment resulted in a small but statistically significant decrease in percentage of infected cells (Fig. 4.15). While AmphoB had little impact on infection of A549 cells, there was a large increase in the number of infected IFITM3 expressing cells (Fig. 4.15). When cells were pre-treated with AmphoB, there was a ∼6.5 fold increase in the percentage of IFITM3 infected cells (at 1 pfu/cell). When AmphoB was added with SFV, there was a ∼4.7 fold increase in infection (Fig. 4.15). These data suggest that the pre-treatment step, can to an extent enhance the impact of AmphoB treatment on IFITM3 expressing cells, although there was no statistically significant difference between the two treatments (Fig. 4.15). To further

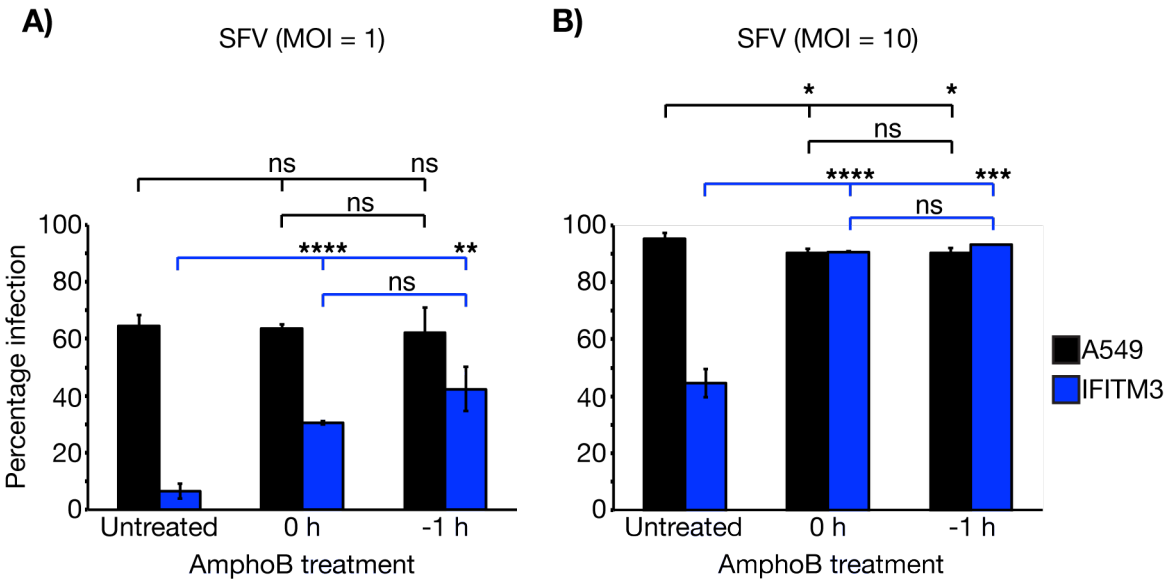

Figure 4.15: **Amphotericin B treatment enhances SFV infection of IFITM3 expressing cells.** A549 or IFITM3 expressing cells were treated with 1 μM AmphoB for 1 h at 37℃ prior to infection with SFV in the presence of AmphoB (-1 h), or 1 μM AmphoB was added to cells with SFV (0 h). Cells were incubated for 5.5 - 6 h to allow infection, prior to fixation and immunofluorescence staining for E1/E2 as a read-out of infection. The percentage of infected cells at 1 pfu/cell (A) and 10 pfu/cell (B) are displayed. The data are from a representative experiment (n = 2; the data are from an infection performed by Stephanie Czieso), performed in a 96 well plate format with triplicate wells for each condition. Bars represent the mean infection percentage across the three wells with error bars representing the standard deviation between these. Significance tests relate to the difference in mean infection percentage for each compared condition using student's unpaired t-tests. * $p < 0.05$, ** $p < 0.01$, *** $p < 0.001$, **** $p < 0.0001$.

confirm these results, the P1 and P2 cell groups were similarly treated with AmphoB and infected with SFV. As with OS-IFITM3 expressing cells, AmphoB treatment of P1- and P2-IFITM3 expressing cells enhanced SFV infection (Fig. 4.16), with no impact on infectivity of control A549 cells. In sum, it appears that AmphoB can indeed abrogate IFITM3-mediated inhibition of SFV, similarly to results previously seen with IAV [156].

Addition of AmphoB at the same time as virus (0 h; Fig. 4.15 and 4.16) gave a lower level of enhanced infection than when pre-incubated for 1 h. These data suggest that AmphoB may enhance SFV infection by altering IFITM3-mediated inhibition of entry. To further test this hypothesis, and investigate whether any later aspects of the SFV life cycle were impacted by AmphoB, a time of addition assay was used, as previously described with monensin (Fig. 4.11). SFV was bound to the cell surface at 4℃, prior to shifting cells to 37℃ to promote synchronous uptake of virus. AmphoB was added to cells

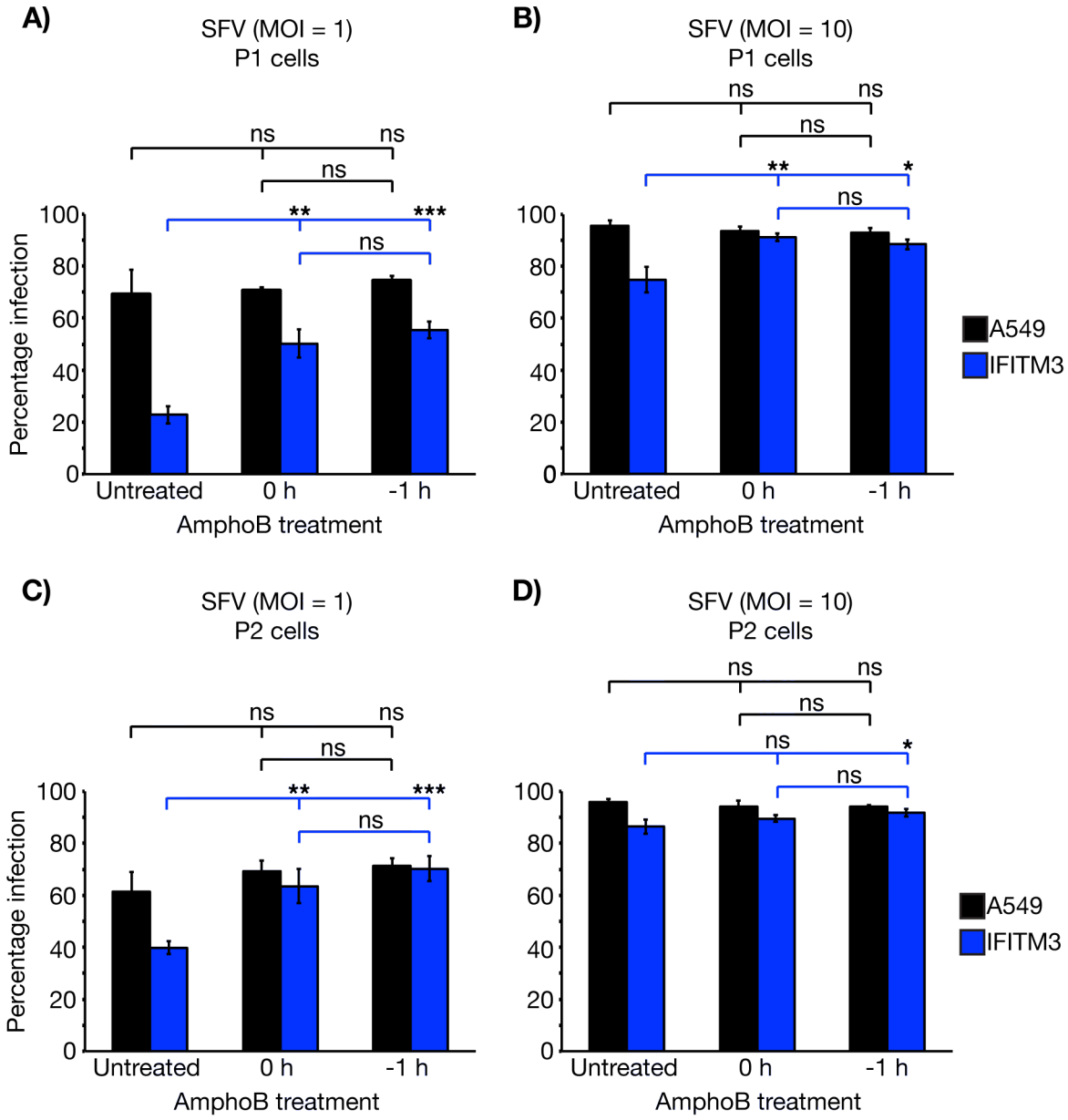

Figure 4.16: **Amphotericin B treatment enhances SFV infection of P1 and P2-IFITM3 cells.** P1- and P2-A549 or IFITM3 expressing cells were treated with 1 μM AmphoB for 1 h at 37℃ prior to infection with SFV in the presence of AmphoB (-1 h), or 1 μM AmphoB was added to cells with SFV (0 h). Cells were incubated for 5.5 - 6 h to allow infection, prior to fixation and staining for E1/E2 as a read-out of infection. The percentage of P1 cells infected with SFV at 1 pfu/cell (A) or 10 pfu/cell (B) and the percentage of P2 cells infected with SFV at 1 pfu/cell (C) or 10 pfu/cell (D) are displayed. The data are from one experiment (performed by Stephanie Czieso), in a 96 well plate format with triplicate wells for each condition. Bars represent the mean infection percentage across the three wells with error bars representing the standard deviation between these. Significance tests relate to the difference in mean infection percentage for each compared condition using student's unpaired t-tests. * $p < 0.05$, ** $p < 0.01$, *** $p < 0.001$.

either when first shifting to 37℃, or at time points between 10 min and 120 min after warming. While AmphoB could enhance SFV infection when added at 0 min, addition even after 10 min internalisation did not increase SFV infection of IFITM3 expressing cells (Fig. 4.17). These results suggest that 1 μM AmphoB enhances SFV infection by disrupting IFITM3-mediated inhibition of entry, and does not impact later stages of the virus life cycle.

To further examine the effect of AmphoB on IFITM3-mediated restriction of SFV, a range of concentrations were examined. Initially, 1 μM AmphoB was used as in [156], however it was noted that when treating IFITM3 expressing cells with this concentration the level of infection did not reach that seen in A549 cells (at 1 pfu/cell; Fig. 4.15 and 4.16). Higher concentrations of AmphoB were therefore examined to test if there was any further enhancement of infection. At higher concentrations of AmphoB (12.5 μM - 50 μM), SFV infection in both the IFITM3 expressing and A549 control cells was inhibited (Fig. 4.18). There were no clear signs of cytotoxicity when cells were examined by microscopy (data not shown), even at the highest concentration of AmphoB (this is further supported by data presented in Chapter 5), suggesting a drug-mediated inhibition of infection. Enhancement of SFV infection in the presence of IFITM3 was detectable across the range of 0.5 μM to 3.125 μM, therefore 1 μM as used previously appeared to be optimal for promoting SFV infection in the presence of IFITM3 (Fig. 4.18).

SFV requires cholesterol for fusion [100], therefore it was hypothesised that high concentrations of AmphoB were binding to the lipid and disrupting entry. This hypothesis was tested by performing another time of addition experiment. As above, virus was bound at the cell surface and allowed to enter cells by shifting to 37℃. At time points between 0 and 120 min, 50 μM AmphoB was added to the cells. Addition of the drug at all time points potently inhibited SFV infection (Fig. 4.19). These results are in stark contrast to monensin, which did not inhibit infection after the first 30 min at 37℃ (Fig. 4.11). Therefore, although high concentration AmphoB may inhibit entry, it may also have additional effects on later steps of the replication process.

Overall, AmphoB treatment of cells reduced the anti-SFV function of IFITM3, as has been published for anti-IAV activity, suggesting similarities in the mechanism of inhibition for both viruses. Following 10 min internalisation to cells, AmphoB no longer impacted

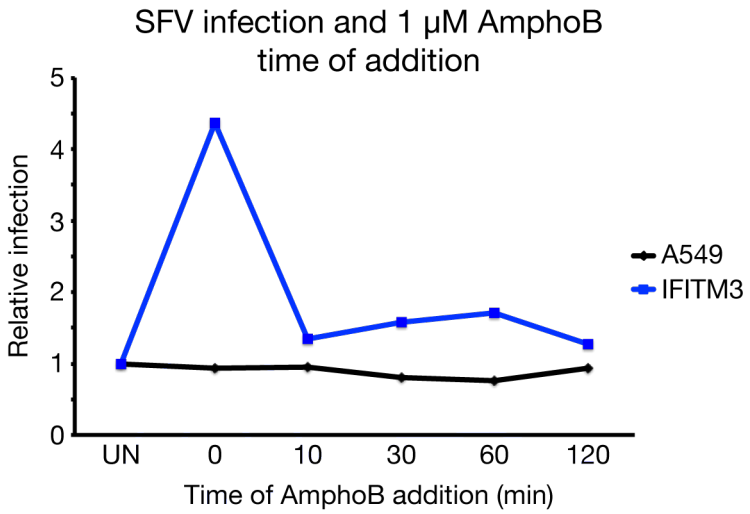

Figure 4.17: **Amphotericin B does not enhance SFV infection of IFITM3 expressing cells after virus internalisation.** SFV (5 pfu/cell) was added to A549 or IFITM3 expressing cells and incubated for 1 h at 4℃. Cells were washed to remove unbound virus and then treated with media pre-warmed to 37 ℃, with or without 1 μM AmphoB. At the indicated times between 10 and 120 min, media were replaced with media containing AmphoB. Cells were incubated for a total of 5.5 - 6 h to allow infection, prior to immunofluorescence analysis. Data presented are percentage of infected cells normalised to untreated cells (A549 ∼70%, IFITM3 ∼5% infection). Data is from one experiment performed in 96 well plate format using triplicate wells.

IFITM3-mediated inhibition of SFV, suggesting that even though AmphoB can act rapidly, once virus is internalised to cells, infection is inhibited by IFITM3. High concentrations of AmphoB can inhibit SFV infection, which was hypothesised to be as a result of the dependency of SFV on cholesterol for fusion. However it appears that AmphoB may disrupt later aspects of the SFV life cycle (potentially in addition to early aspects).

4.2.9 AmphotericinB does not appear to alter properties of SFV virions

It appears that AmphoB treatment has a negative impact on the antiviral function of IFITM3 against SFV and IAV [156]. A possibility that was not explored by Lin *et al.* is that AmphoB may have direct affects on virus particles, rather than IFITM3 expressing cells. An experiment was therefore set up to investigate whether AmphoB treatment was impacting SFV particles or having a cellular affect. For this experiment 1 μM AmphoB was used to boost SFV infection in the presence of IFITM3, while 1 nM was used as a concentration which was expected to have little impact (and indeed did not, see Fig.

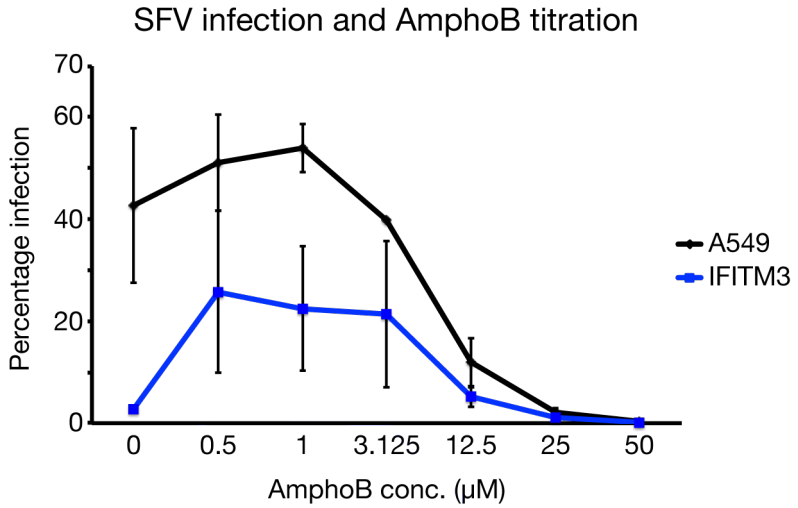

Figure 4.18: **Higher concentrations of AmphoB inhibit SFV infection.** A549 or IFITM3 expressing cells were pre-treated with AmphoB at concentrations between 0 and 50 μM for 1 h at 37℃. SFV was added to cells at 1 pfu/cell in the presence of AmphoB at the appropriate concentration. Cells were incubated for 5.5 - 6 h to allow infection, prior to analysis of infection. Data presented are the mean infection percentage across three independent experiments, each consisting of triplicate wells in a 96 well plate format. Error bars are the standard deviation between the experiments.

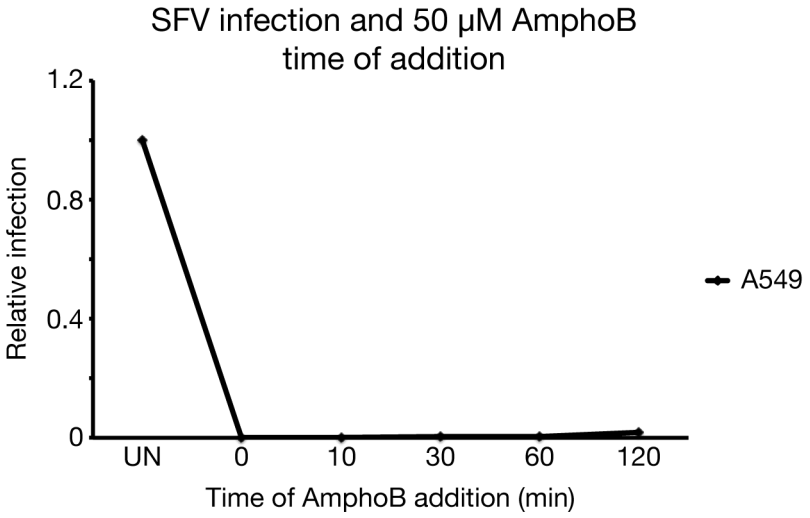

Figure 4.19: **High concentration AmphoB inhibits SFV infection.** SFV (5 pfu/cell) was added to A549 or IFITM3 expressing cells and incubated for 1 h at 4℃. Cells were washed to remove unbound virus. Media containing 50 μM AmphoB, or media alone, at 37℃, were added to cells. Cells were incubated at 37℃ for between 10 and 120 min. At each indicated time, control media were replace with fresh media containing 50 μM AmphoB. Cells were incubated for a total of 5.5 - 6 h to allow infection prior to analysis of infection by immunofluorescence staining and microscopy. Data presented are infection percentage normalised to untreated cells (A549 ~54% infection). Data is from one experiment performed in 96 well plate format using triplicate wells.

4.20). To investigate the possibility that AmphoB treatment impacted SFV particles directly, virus was incubated with 1 μM for 10 min at 37℃ at an MOI 1000 fold higher than was to be used for infection. Following the incubation period, the virus was diluted 1000 fold in media lacking AmphoB, thus diluting AmphoB to 1 nM and then added to cells and allowed to infect for 5.5 - 6 h (Fig. 4.20 A). If 1 μM AmphoB directly impacted SFV particles, this incubation process would be expected to enhance SFV infectivity in the presence of IFITM3. However, this 1 μM to 1 nM infection was not seen to be any different to untreated samples, suggesting no impact from treating virus with 1 μM AmphoB (Fig. 4.20 B).

While the 1 μM AmphoB diluted to 1 nM treated virus did not show any enhanced infection in the presence of IFITM3, it may be the case that this dilution of AmphoB negated the enhancing affect. To test this possibility, IFITM3 expressing cells were incubated with 1 μM for 10 min at 37℃. Media were removed from the cells, and virus was added to the cells in 1 nM AmphoB media (with minimal exposure to the media prior to addition to cells; Fig. 4.20 A). These samples were again allowed to infect for 5.5 - 6 h and analysed for the percentage of infected cells. As can be seen in the '1 μM to 1 nM cells' sample, this process enhanced infection in the presence of IFITM3 (Fig. 4.20 B). The enhancement was not as large as that seen when virus and cells were both incubated with 1 μM AmphoB through the infection (though only statistically different at MOI = 5, and not at MOI = 1), but there was a statistically significant increase over the control level of infection (Fig. 4.20 B). This indicates that incubating cells for 10 min with 1 μM AmphoB could impact SFV infection of IFITM3 expressing cells. Since 1 nM AmphoB did not increase SFV infection in the presence of IFITM3, it is unlikely that mixing virus with 1 nM AmphoB was responsible for the increase see in the '1 μM to 1 nM cells' sample. It is speculated that the difference between cells and virus being treated with 1 μM AmphoB and the '1 μM to 1 nM cells' sample is as a result of AmphoB being diluted to the lower concentration, allowing greater inhibition from IFITM3.

The data suggest that AmphoB does not directly alter the infectivity of SFV particles in the presence of IFITM3. Additionally, as seen in previous (Fig. 4.15 and 4.16), AmphoB treatment did not alter SFV infectivity of A549 cells. It therefore appears that AmphoB treatment is altering IFITM3 expressing cells to allow a higher level of SFV infection.

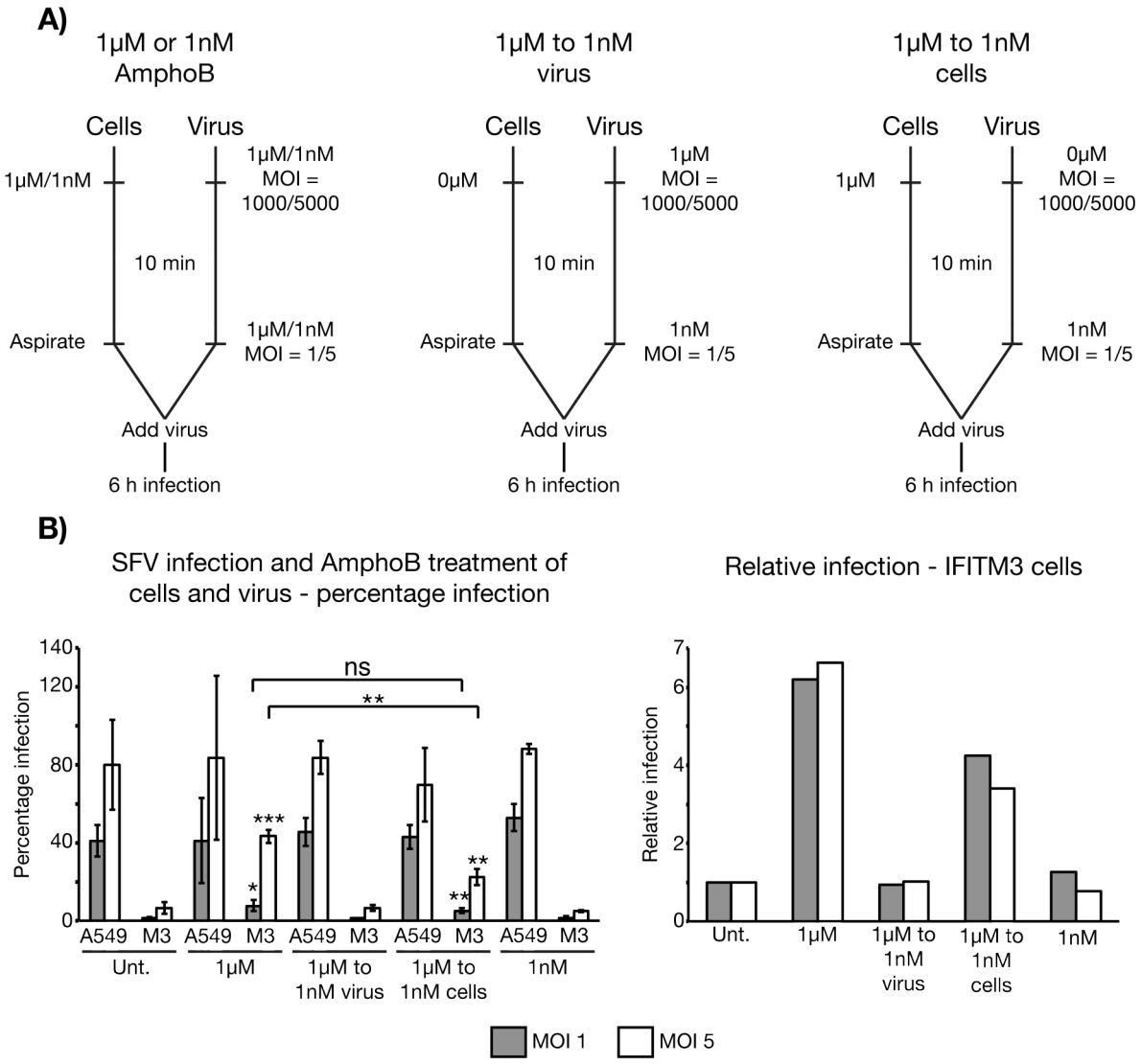

Figure 4.20: **AmphoB treatment does not appear to alter properties of SFV virions.** A) A diagram to display the experimental set up. In all cases there was a 10 min incubation at 37 ℃ of virus and cells separately. The first diagram represents the control conditions of treating cells and virus with 1 μM or 1 nM AmphoB. The middle diagram represents the set up for treating virus with 1 μM AmphoB and then diluting this to 1 nM to investigate whether 1 μM AmphoB impacts virus instead of the cells. The final diagram represents a control to test the impact of treating cells with 1 μM AmphoB and then diluting this to 1 nM, as it was unknown whether this dilution would cause a loss of the AmphoB enhancing affect. B) Percentage of SFV infected cells in the various conditions displayed in (A), with the addition of the untreated controls (Unt.). The data are from a representative experiment (n = 2) performed in a 96 well plate with triplicate wells of infection. The error bars represent the standard deviation between wells. The right hand graph displays the relative infection of IFITM3 expressing cells for each condition (normalised to untreated controls at each MOI). Significance tests relate to the difference in mean infection percentages as assess by unpaired student's t-tests. Stars directly above bars represent comparison of untreated and treated samples at each MOI (where no stars are displayed there was no statistically significant difference). Stars above the bars, connected by lines represent a comparison on the 1 μM and '1 μM to 1 nM cells' samples. * $p < 0.05$, ** $p < 0.01$, *** $p < 0.001$.

4.2.10 IFITM1 and IFITM3 can inhibit SFV infection by fusion at the plasma membrane

The data presented Fig. 4.1 and 4.2 indicated that IFITM3 could inhibit SFV infection when virus enters through the endocytic route, while IFITM1 and IFITM3-Y20A could not. The difference in restriction between these IFITM proteins could be related to their localisation within a cell, with IFITM3 being localised to early endosomes, from where SFV normally penetrates to the cytosol, while IFITM1 and IFITM3-Y20A are mostly at the plasma membrane. It was therefore investigated whether IFITM3-mediated restriction could be bypassed by fusion of SFV at the cell surface, and whether this route of entry into the cell would be sensitive to the plasma membrane localised IFITM proteins.

SFV can enter cells by fusion directly at the plasma membrane following a transient low pH treatment (pH 5.5; [46]). To ensure that any infection of cells was as a result of fusion at the plasma membrane, and not low pH-dependent entry through endosomes, cells were pre-treated for 15 min at 37°C with Baf A as described in Section 4.2.6 (page 151) and Chapter 2 (Section 2.6.7 [page 83]). Virus was bound to the cell surface at 4°C for 1 h, as previously described. Cells were subsequently treated with media (containing Baf A) at pH 5.5 for 3 min at 37°C, to activate the E1/E2 fusion machinery at the cell surface (as seen in Fig. 4.12) and induce fusion of the plasma membrane and viral lipid envelope. Following the transient low pH treatment, cells were returned to pH 6.8 media, containing Baf A, and incubated for 5.5 - 6 h to allow production of *de novo* E1/E2 as a read-out for infection. As controls, cells were treated with pH 6.8 media for 3 min or treated with DMSO instead of Baf A.

When virus was bound at the cell surface (5 pfu/cell input), then allowed to internalise and fuse with early endosomes (pH 6.8 DMSO), ∼65-80% of A549 cells (OS, P1 and P2) were infected with SFV (Fig. 4.21 A). When cells were treated with Baf A, and no low pH pulse was given at the cell surface (pH 6.8 Baf A), infection was inhibited by >90% (Fig. 4.21 A). When A549 cells were pre-treated with Baf A, and given a 3 min low pH pulse (pH 5.5 Baf A), ∼20-50% of cells were infected (Fig. 4.21 A). Treating cells with Baf A prior to the low pH pulse did no affect the result since pre-treatment with DMSO, followed by Baf A in the infection media (pH 5.5 DMSO/Baf A [D/B]) gave similar levels of infection. This bypass of Baf A inhibition seen with low pH treatment is the level of

infection by direct plasma membrane fusion. This route is not as efficient as infection through the endocytic route, but has some variability based on the cell line used [97].

In order to make direct comparisons, the level of infection through plasma membrane fusion and the endocytic route were compared. Within each independent experiment, infection percentages from low pH treatment were set relative to the pH 6.8 DMSO control (endocytic infection) for each individual cell line. The relative infection for both pH 5.5 treatments (pH 5.5 Baf A and pH 5.5 D/B) showed very little difference, and were therefore considered equivalent by averaging the two. These relative infection levels were then averaged across three independent experiments to give a value that can be used to assess the efficiency of infection by plasma membrane fusion in each cell line. In OS-A549 cells the relative infection level from plasma membrane fusion was 0.34. In P1- and P2-A549 cells, these values were 0.62 and 0.44, respectively. It therefore appeared that there was some variability in the efficiency of plasma membrane fusion even in different A549 cell lines, which may be due to the different derivation of these cells (OS-A549 are parental, P1-A549 have an empty puromycin resistant vector stably transfected, P2-A549 stably express GFP).

As seen previously, IFITM1 did not inhibit the endosomal route of SFV infection in either OS- or P1-IFITM1 cells, with both showing similar infection levels to their respective A549 controls (Fig. 4.21 A). Baf A potently inhibited SFV infection of IFITM1 expressing cells. When virus bound to the surface of IFITM1 expressing cells was given a low pH pulse to promote entry at this membrane site, the infection percentage was consistently lower than that observed in the comparable A549 cells (Fig. 4.21 A). In the OS cell set, the fact that the efficiency of infection by plasma membrane fusion in the A549 control cells was low meant that the inhibition by IFITM1 was modest, and not statistically significant. However, in the P1 set, the difference between infection percentage of A549 and IFITM1 cells was much greater, and statistically significant. The relative infection levels of plasma membrane fusion, compared to endocytic entry were 0.19 and 0.15 for OS- and P1-IFITM1, respectively, compared to 0.34 (OS) and 0.62 (P1) in the A549 cells. Overall, from these data it is concluded that IFITM1 can inhibit infection by SFV through fusion at the plasma membrane, but that effect is modest.

Plasma membrane localised P2-IFITM3-Y20A did not inhibit SFV infection through

the endocytic route (Fig. 4.21 A and 4.2 B). However, when virus was fused at the plasma membrane, P2-IFITM3-Y20A inhibited infection by ∼95% (Fig. 4.21 A). This relative infection level is lower than that seen for either OS- or P1-IFITM1 (0.05 compared to 0.19 and 0.15, respectively). It has previously been noted that IFITM expression levels are important for the anti-SFV function (Section 4.2.2, Fig. 4.2). P2-IFITM3-Y20A expression levels are similar to, or lower than those seen for either OS- or P1-IFITM1(Fig. 4.2), suggesting that P2-IFITM3-Y20A has greater potency for inhibiting SFV plasma membrane fusion than IFITM1.

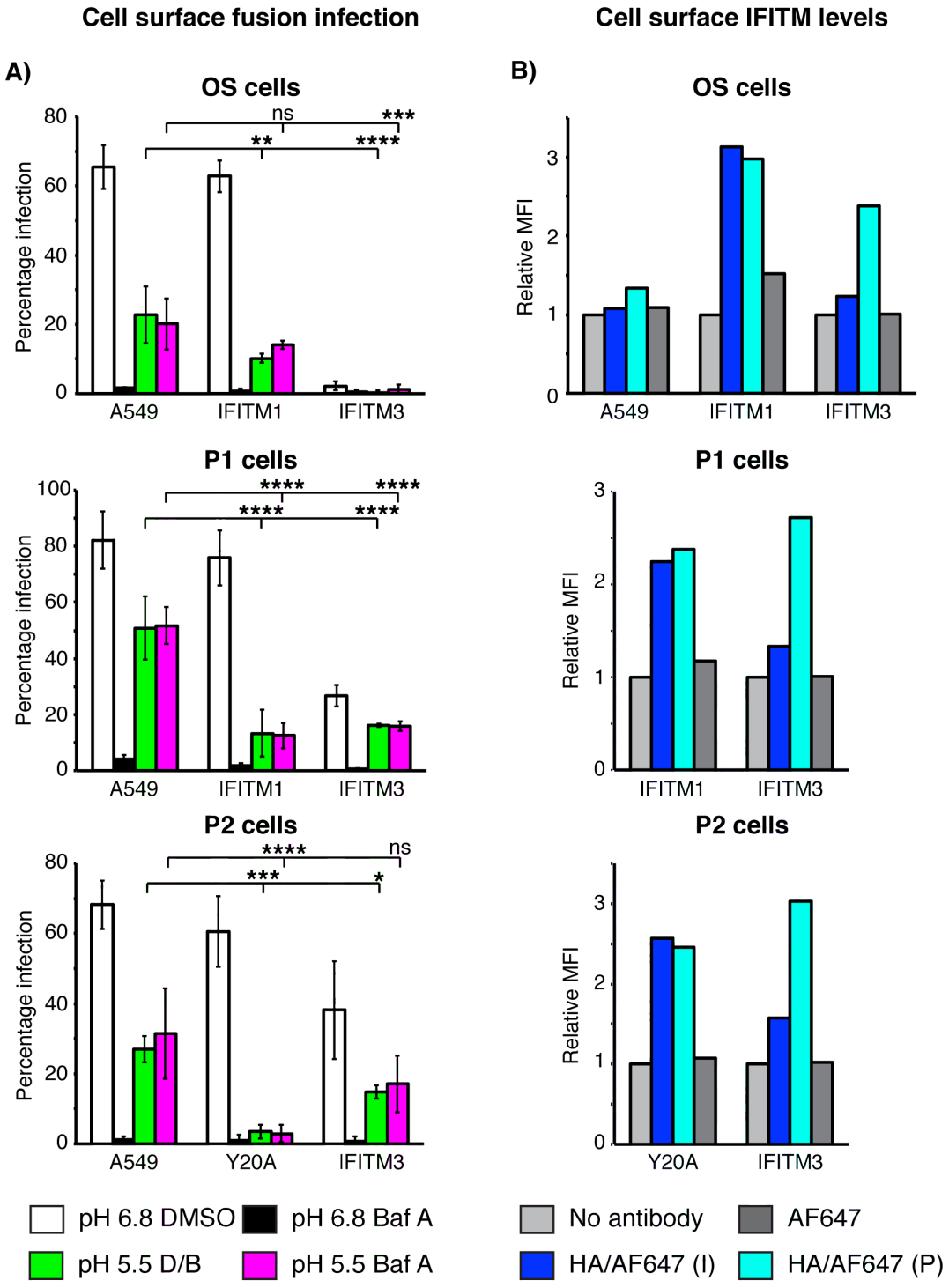
Cell surface fusion infection
Cell surface IFITM levels
A)
B)
OS cells
OS cells
Percentage infection
Relative MFI
ns
***
**
****
A549
IFITM1
IFITM3
P1 cells
P1 cells
****
****
****
****
P2 cells
P2 cells
****
ns
***
*
Y20A
pH 6.8 DMSO
pH 6.8 Baf A
pH 5.5 D/B
pH 5.5 Baf A
No antibody
AF647
HA/AF647 (I)
HA/AF647 (P)

Figure 4.21: **IFITM1 and IFITM3 can inhibit SFV infection by fusion at the cell surface.** A) Infection by plasma membrane fusion: OS, P1 and P2 cells were pre-treated with media containing 100 nM bafilomycin A1 (Baf A; pH 5.5 Baf A and pH 6.8 Baf A samples) for 15 min at 37°C (or DMSO as a control; pH 6.8 DMSO and pH 5.5 D/B samples [see further detail below]). Cells were then cooled by addition of media at 4°C (with or without Baf A) and placed on ice. SFV (5 pfu/cell) was added and allowed to bind to the cell surface for 1 h at 4°C. Unbound virus was removed by washing. Cells were treated with media (with or without Baf A) pre-warmed to 37°C for 3 min to promote fusion at the cell surface (pH 5.5 Baf A and pH 5.5 D/B [see further detail below]). As a control, cells were incubated with pH 6.8 media for 3 min, which would not activate the fusion machinery. Following the 3 min incubation periods, all media were replaced with pH 6.8 media with or without Baf A. Cells were then incubated for 5.5 - 6 h to allow infection, prior to fixation and immunofluorescence staining for the E1/E2 proteins as a marker of infection. As a control for the Baf A pre-treatment steps, cells were incubated with control media up to the pH 5.5 treatment, and then incubated with pH 6.8 media containing Baf A through the 5.5 - 6 h incubation period (pH 5.5 D/B). The bars represent mean infection percentage from three independent experiments (each containing triplicate wells for each sample). Error bars represent the standard deviation between experiments. Statistical significance was determined using normalised infection values, comparing pH 5.5 D/B (green) or pH 5.5 Baf A (magenta) of A549 samples, with IFITM samples (described in Materials and Methods). * $p < 0.05$, ** $p < 0.01$, *** $p < 0.001$, **** $p < 0.0001$. B) Analysis of IFITM expression by flow cytometry: OS-, P1- or P2-IFITM cells were labelled with anti-HA antibodies either intact (I) or following saponin permeabilisation (P). Anti-HA antibody was detected with AF647 and analysed by flow cytometry to determine the relative levels of cell surface IFITM protein. To control for the specificity of labelling, cells were either incubated with no antibody, or without anti-HA antibody (i.e. AF647 secondary antibody only). The mean fluorescence intensity (MFI), relative to the no antibody control displayed for each cell line. Plots are representative of 3-4 independent experiments.

SFV infection by the endocytic route of entry was low in all three IFITM3 cell groups, with OS-IFITM3 being the most restrictive (Fig. 4.21, as seen in Fig. 4.1 and 4.2). Treatment of IFITM3 expressing cells with Baf A reduced the infection level to <1%. It was hypothesised that fusion of virus at the plasma membrane would not only bypass the inhibition imposed by Baf A, but also that of IFITM3. It was therefore surprising to see no increase in the level of infection following low pH treatment, and that these infection levels were consistently lower than those seen in all A549 cells (Fig. 4.21 A). As above, to make comparisons, the relative infection levels of plasma membrane fusion against the endocytic route were analysed. If SFV could bypass inhibition from IFITM3, these values would be expected to be above 1 as a result of comparison to the endocytic route of entry (which is blocked by IFITM3). The OS-IFITM3 cells showed the greatest inhibition of infection by fusion at the plasma membrane, with a relative infection level of 0.01, compared to the

A549 control cells which had a relative infection level of 0.34. The P1-A549 cells had a relative infection level of 0.62, compared to 0.2 for the P1-IFITM3 expressing cells. While the P2-IFITM3 expressing cells had a relative infection level of 0.24, compared to 0.44 of the P2-A549 controls.

Overall, it appears that, even though predominantly localised to early endosomes (Fig. 3.17 [page 127]), IFITM3-mediated inhibition of SFV was not bypassed through fusion at the plasma membrane, and therefore the protein could still inhibit infection. The infection percentages seen by plasma membrane fusion in OS-IFITM3 cells were lower than observed for any other set of cells. The P1- and P2-IFITM3 cells show similar levels of infection as the OS- and P1-IFITM1 cells. Together, these data suggest that IFITM3 inhibits SFV infection by plasma membrane fusion to a similar, or greater extent than IFITM1.

It was interesting to see that IFITM3 could inhibit SFV infection through plasma membrane fusion, even though much of the protein appeared to be localised in the endosomal system (Fig. 3.17 [page 127] and Fig. 3.7 [page 105]). To further investigate the levels of IFITM protein at the plasma membrane, cells were labelled with anti-HA antibody either intact, or following saponin permeabilisation and were analysed by flow cytometry. The mean fluorescence intensity of labelled OS-IFITM1, P1-IFITM1 and P2-IFITM3-Y20A was similar on intact and permeabilised cells, suggesting the majority of the HA-tag is present at the cell surface (Fig. 4.21 B). For all three sets of IFITM3 expressing cells, significant fluorescent signal was only detected following permeabilisation, suggesting the majority of the protein is within intracellular pools (Fig. 4.21 B). Nevertheless, the MFI of intact IFITM3 expressing cells was slightly above background, suggesting some IFITM3 protein is present at the cell surface (as previous described in Chapter 3, e.g. Fig. 3.2 [page 97]). This may be sufficient to explain the efficient inhibition of infection through plasma membrane fusion by IFITM3.

In summary, despite low levels of protein at the plasma membrane, IFITM3 appeared to be able to inhibit SFV fusion at the cell surface to an equivalent, or greater extent than IFITM1; and that IFITM3-Y20A also appeared to inhibit to a greater extent than IFITM1. It therefore seems that IFITM3 may be a more potent inhibitor of SFV infection than IFITM1.

4.3 Conclusions and Discussion

While the IFITM proteins have been suggested to inhibit infection by a wide range of viruses (Tables 1.1 and 1.2), there had been little work to investigate whether they could inhibit alphaviruses, and there had been the suggestion that they do not [9, 11]. The work presented in this chapter indicates that IFITM3, and to a lesser extent IFITM2, can inhibit infection of A549 cells by the alphaviruses SFV and SINV. When virus entered through the endocytic route, neither IFITM1 nor IFITM3-Y20A, inhibited infection, initially suggesting the endosomal localisation of IFITM proteins may be required for their anti-SFV function. Focusing on SFV, it was demonstrated that IFITM proteins do not impact on virus binding. Moreover, IFITM3 was found to not inhibit endocytosis or delivery to acidic compartments of the cell where the envelope protein could undergo pH-induced conformational changes. However, while E1 could trimerise, the viral capsid was not released into the cytosol of IFITM3 expressing cells. These results suggest that IFITM3 inhibits fusion between viral and cellular membranes, and/or uncoating of the viral capsid. Shortly after the publication of this work [16], a study was published showing that IFITM3 could inhibit the alphaviruses CHIKV, O'nyong nyong, VEEV, SFV and SINV [184], further supporting our own findings. Additionally, this second study also suggesting that IFITM3 was important for control of the early stages of CHIKV infection and mortality from VEEV infection in mice, pointing towards *in vivo* relevance for this antiviral function.

IFITM3 was not found to block the formation of the E1 HT within the endosomal system (Fig. 4.12). This suggests that IFITM3 does not inhibit viral infection by altering endosomal acidification, and does not directly impact conformational changes of the viral envelope glycoprotein. A suggestion has been made that formation of the E1 HT, is dependent on interaction with membrane [194], perhaps suggesting that IFITM3 is also not inhibiting this process. It is noted that only a small fraction of the E1 protein becomes trimeric, either upon endocytic internalisation to cells, or when given a low pH treatment at the cell surface, regardless of IFITM expression (Fig. 4.12). This result could be explained either if the E1 HT is unstable and therefore mostly in a monomeric form, or if there is indeed a requirement for membrane interaction, which is suggested because only a low fraction of the envelope proteins on the surface of an SFV virion will be in contact

with a target membrane. The low proportion of trimeric E1 may therefore further suggest that membrane interaction is required, and therefore not inhibited by IFITM3.

Much of the work defining IFITM proteins as inhibitors of viral entry has been through the use of pseudotyped virus particles (Tables 1.1 and 1.2). IFITM3-mediated inhibition of IAV has been much more highly characterised with work suggesting that inhibition occurs either prior to membrane fusion [13], or at the point of hemifusion to block resolution to a full fusion pore [14]. Additionally, Lin *et al.* have suggested that IFITM3-mediated inhibition of IAV infection can be modulated by treatment with the antifungal drug AmphoB [156]. The precise mechanism(s) of this effect remains unclear, but the suggestion was made that by binding to cholesterol, AmphoB may modulate the fluidity of cellular membranes to disrupt IFITM-mediated inhibition. Similarly to the results with IAV, IFITM3-mediated inhibition of SFV is also sensitive to AmphoB treatment, suggesting a similar mechanism of restriction for both viruses. SFV is amenable to various assays to investigate whether fusion is occurring, for instance, labelling with lipophilic dyes such as DiD (as has been done for IAV [14]), and therefore can be used to better understand whether IFITM proteins inhibit before, or after hemifusion.

It was observed that the antiviral action of IFITM3 could be saturated by increasing the amount of virus, or by lowering the level of IFITM expression. This ability to saturate IFITM3-mediated inhibition of SFV infection could be explained if there is a need for direct interaction between IFITM3 and sites at which SFV fusion occurs. Since SFV fusion requires cholesterol in the target membrane, and IFITM3-mediated inhibition of SFV is diminished in the presence of AmphoB, it is possible that IFITM3 may cluster to cholesterol-rich regions of cellular membranes, where it can disrupt membrane fusion events.

It was interesting to see that IFITM1 did not effectively inhibit SFV infection. Even though the majority of viruses shown to be inhibited by the IFITM proteins fuse in endosomes, many of these show at least some sensitivity to IFITM1 (Tables 1.1 and 1.2). It was speculated that the endocytic uptake of SFV allows it to escape the plasma membrane localised IFITM1 in this A549 cell system; however why other endocytosed viruses would be sensitive to IFITM1 remains unclear. A potentially contributing factor to the lack of IFITM1-mediated inhibition of SFV may be as a result of intrinsic differences

in the potency of IFITM1 and IFITM3 for inhibiting SFV infection. Even though there are relatively low levels of IFITM3 at the plasma membrane, when SFV fusion was triggered at this site, IFITM3 could inhibit infection to a similar or greater extent than IFITM1. If, as suggested above, IFITM3 clusters to cholesterol-rich regions of cellular membranes, this may explain how a relatively low level of protein at the plasma membrane can still inhibit SFV fusion. However, a caveat should be noted when interpreting the results of plasma membrane fusion and surface levels of IFITM3; whether Baf A treatment can alter IFITM3 levels at the cell surface has not been tested. An alternative explanation for the observed inhibition of SFV infection by plasma membrane fusion may be that Baf A treatment could cause IFITM3 accumulation at the cell surface. However, it still appears that IFITM1 has limited anti-SFV activity compared to IFITM3. Future research could be aimed at investigating what regulates these apparent differences between IFITM1 and IFITM3. All IFITM proteins contain a highly conserved CD225 domain which spans the first membrane interacting domain and the CIL (Fig. 1.6 [page 44]). The second membrane domain is also highly conserved. The differences between IFITM1 and IFITM3 are therefore mostly in the NTD and CTD. SFV will act as a good model system to work with to investigate how the NTD and CTD of IFITM1 and IFITM3 may regulate their apparent differential antiviral potency, for instance, through the use of chimeric IFITM proteins. Investigating these differences may help to better understand the antiviral function of the human IFITM proteins.

Many of the ideas suggested here will be built on further in the subsequent chapter with an investigation of IFITM-mediated inhibition of flavivirus infection, and how this differs to that seen for inhibition of alphaviruses.

Chapter 5

Comparing IFITM-mediated alphavirus restriction with other viral families

5.1 Introduction

In the previous chapter, IFITM proteins were shown to inhibit alphavirus infection (focusing on SFV), with IFITM3 seemingly being the most potent inhibitor. This inhibition was sensitive to treatment with the antifungal drug amphotericin B (AmphoB) and a suggestion was made that there could be a link between IFITM3 and cholesterol for the anti-SFV activity. In this chapter, work is presented comparing the antiviral function of IFITM proteins against alphaviruses with other viruses, members of the *Flaviviridae* and vaccinia virus (VACV) of the *Poxviridae*. The flaviviruses used here and VACV are internalised to cells through endocytic mechanisms, and have low pH-induced membrane fusion with endosomes, similarly to alphaviruses. The flaviviruses are also structurally similar to alphaviruses and have a type II fusion protein machinery for penetration of cellular membranes. Work has previously been published to analyse IFITM-mediated inhibition of flaviviruses, with all three of the IFITM proteins shown to have at least some antiviral function [7, 144, 147, 154]. In contrast VACV has not been analysed in any great detail for IFITM-mediated inhibition, although the IFITM proteins were not detected as hits in

an RNAi screen for host factors that modify VACV infection in HeLa cells [195].

The experiments presented in this chapter are divided into two parts. Firstly, a comparison between the inhibition of alphaviruses and flaviviruses is made. In agreement with previous studies, all IFITM proteins were found to inhibit infection by different flaviviruses, in contrast to results with alphaviruses which were insensitive to the plasma membrane localised IFITM proteins. Additionally, IFITM-mediated inhibition of flavivirus infection was found to be insensitive to AmphoB treatment, perhaps suggesting different underlying mechanisms of antiviral function. In the second part of this chapter, VACV is suggested to be insensitive to IFITM-mediated inhibition, arguing that not all viruses that enter cells through the endocytic system are sensitive to IFITM proteins. However, the experiments with VACV led to the identification of a potentially interesting feature of high levels of IFITM expression, which appear to enhance cell motility.

5.2 Comparison of alphavirus and flavivirus inhibition by IFITM proteins

5.2.1 IFITM proteins inhibit flavivirus infection and this is not altered by AmphoB treatment

To test whether IFITM proteins can inhibit flavivirus infection, dengue (serotype 2; DENV), Zika (African strain; ZIKV) and yellow fever (17D strain; YFV) viruses were used (most work focused on DENV). Cells were infected with DENV at an input of 1 or 0.3 pfu/cell and incubated for 27 h prior to fixation and labelling to determine infection percentage by immunofluorescence microscopy. In OS-A549 controls ∼57% of cells were infected with 1 pfu/cell, and ∼21% of cells were infected with 0.3 pfu/cell (Fig. 5.1 A). As with SFV, OS-IFITM3 inhibited DENV infection of A549 cells; with 1 pfu/cell there was ∼8% infection ($p = 0.0001$). OS-IFITM2 could also inhibit infection, though not as potently as OS-IFITM3 (∼30% infection with 1 pfu/cell [$p = 0.0009$, compared to A549]), again similarly to the results seen with alphaviruses. In contrast to alphaviruses, OS-IFITM1 was also able to inhibit DENV infection, and in fact showed greater potency than OS-IFITM2, with ∼20% infection ($p = 0.0005$, compared to A549) at 1 pfu/cell (Fig. 5.1

A).

To further investigate similarities and differences in IFITM-mediated inhibition of alphaviruses and flaviviruses, the impact of AmphoB treatment was also tested. Treating cells with 1 μM AmphoB (using 1 h pre-treatment as previously in Chapter 4) did not boost DENV infection of the OS-IFITM cells. There were no significant differences in the infection percentage of treated and untreated IFITM1 ($p = 0.1886$) and IFITM3 ($p = 0.6372$) expressing cells (Fig. 5.1 A). While IFITM2 expressing cells treated with AmphoB appeared to show a small decrease in infection percentage following treatment with AmphoB ($p = 0.0005$ [Fig. 5.1 A]). This is in clear contrast to results with SFV where a ~6.5 fold increase in infection of IFITM3 expressing cells was observed following treatment with AmphoB (Fig. 4.15 [page 157]).

P1-IFITM cells showed largely similar results to OS-IFITM cells, with IFITM3 being the most potent inhibitor ($p = 0.0007$, compared to A549 at 1 pfu/cell) of DENV followed by IFITM1 ($p = 0.0019$, compared to A549 cells at 1 pfu/cell) then IFITM2 ($p = 0.0146$, compared to A549 at 1 pfu/cell [Fig. 5.1 B]). P2-IFITM3 also inhibited DENV infection ($p = 0.0001$ compared to A549 cells at 1 pfu/cell) to a similar extent as P1-IFITM3. P2-IFITM3-Y20A was capable of inhibiting DENV infection ($p < 0.0001$, compared to A549 cell at 1 pfu/cell) even though, like IFITM1, it did not inhibit SFV infection through the endocytic route (Fig. 5.1 C). P2-IFITM3-Y20A expressing cells did not inhibit infection as potently as any of the IFITM3 expressing cells, but had similar inhibition to OS- and P1-IFITM1 cells. P1- and P2-IFITM-mediated inhibition of DENV was also unaffected by treatment with AmphoB (Fig. 5.1 B and C). Therefore, in contrast to SFV, all IFITMs inhibited DENV infection, even those localised at the plasma membrane, and the mechanism of DENV inhibition was insensitive to treatment with AmphoB.

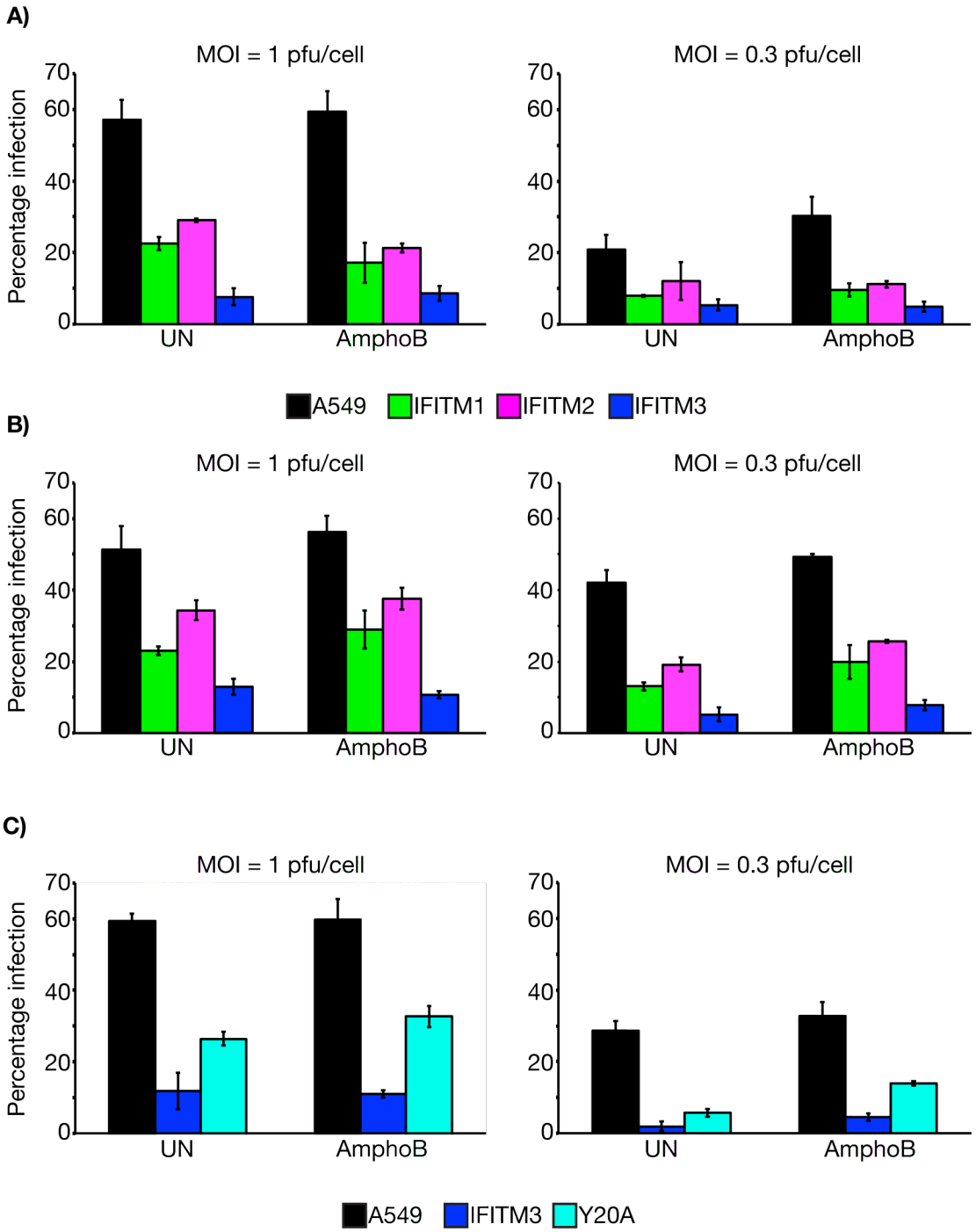
A)
MOI = 1 pfu/cell
MOI = 0.3 pfu/cell
Percentage infection
70
60
40
20
0
UN
AmphoB
A549
IFITM1
IFITM2
IFITM3
B)
MOI = 1 pfu/cell
MOI = 0.3 pfu/cell
Percentage infection
UN
AmphoB
C)
MOI = 1 pfu/cell
MOI = 0.3 pfu/cell
Percentage infection
UN
AmphoB
A549
IFITM3
Y20A

Figure 5.1: **All IFITM proteins inhibit DENV and this is insensitive to AmphoB treatment.** A549 control, or IFITM expressing cells were pre-incubated for 1 h at 37℃ with 1 μM AmphoB, or left untreated (UN), and then infected with DENV (serotype 2) using 1 or 0.3 pfu/cell (with AmpohoB as labelled). Cells were incubated for 6 h prior to AmphoB media being replaced with infection media lacking AmphoB, to mimic the incubation time of cells with AmphoB used for SFV experiments. Infection was allowed to proceed for a total of 27 h, prior to fixation and staining to determine infection percentage by immunofluorescence microscopy. A) OS-IFITM cells. B) P1-IFITM cells. C) P2-IFITM cells. AmphoB did not alter DENV infection of IFITM expressing cells. The same AmphoB stock was used as for SFV infections in Chapter 4, and SFV infections were run in parallel to confirm the AmphoB affect on SFV (data not shown). Data presented are from representative experiments (n = 3 for UN and n = 2 for AmphoB) performed in a 96 well plate format with triplicate wells of infection. Bars are the mean infection percentage with error bars representing the standard deviation. (All DENV infections performed by Dr. Michela Mazzon.)

ZIKV showed a similar pattern of restriction as DENV. Both OS-IFITM1 and IFITM3 expressing cells inhibited ZIKV ($p = 0.0005$ and 0.0003, respectively, as compared to A549 cells at 1 pfu/cell [Fig. 5.2 A]). OS-IFITM2 only had a minor impact on ZIKV infection, which did not show a statistically significant difference compared to infection of A549 cells (Fig. 5.2 A). All of P2-IFITM3, P2-IFITM3-Y20A and P1-IFITM1 inhibited ZIKV to a similar extent as each other (all three $p < 0.0001$, compared to A549 cells at 1 pfu/cell [Fig. 5.2 B]). Therefore, as for DENV, it seems that IFITM1 and IFITM3 can both inhibit ZIKV, and the endosomal localisation of IFITM3 is not essential for this function, in contrast to results seen with SFV (Fig. 4.1 and 4.2, pages 135 and 138). Like DENV, AmphoB treatment had limited impact on ZIKV infection of IFITM expressing cells.

YFV 17D showed similar restriction patterns as the two other flaviviruses, with one exception. IFITM3 and IFITM1 inhibited YFV 17D (Fig. 5.3), with statistically significant differences compared to A549 cells (OS-IFITM3 and OS-IFITM1 $p < 0.0001$, P2-IFITM3 $p = 0.0066$ and P1-IFITM1 $p = 0.0089$). Within the OS cell set, OS-IFITM2 expressing cells had the lowest level of inhibition, but still demonstrated a statistically significant decrease compared to A549 cells ($p = 0.0042$). In comparison, P2-IFITM3-Y20A expressing cells did no inhibit YFV 17D as potently as the other two flaviviruses tested, and did not show statistically significant differences compared to A549 cells (Fig. 5.3 B compared to Fig. 5.1 C and Fig. 5.2 B). The lack of IFITM3-Y20A-mediated inhibition was probably not as a result of expression levels since P1-IFITM1, which has similar population level expression (see Fig. 4.2 [page 138]) could potently inhibit YFV 17D (Fig. 5.3 B). Similarly

to results with DENV and ZIKV, AmphoB treatment had no impact on IFITM-mediated inhibition of YFV 17D (Fig. 5.3), suggesting similar properties for inhibition of three different flaviviruses.

5.2.2 Higher concentrations of AmphoB do not inhibit DENV infection

In the experiments described in Fig. 5.1, 5.2 and 5.3, AmphoB treatment was performed to mimic that of the SFV infections described in Chapter 4. To that end, cells were incubated with 1 μM AmphoB for 1 h at 37°C, prior to addition of virus in AmphoB containing media. Virus and AmphoB were incubated with cells for 6 h and media was then replaced for normal infection media. This replacement was made to match the time period that cells were incubated with AmphoB for SFV infections to avoid any potential toxic affects. However, there is a clear difference in that the SFV replication cycle is completed within 6 h, while the flavivirus replication cycle takes much longer (27 h infection period used here). This raised the question of whether removal of AmphoB was responsible for the lack of impact on IFITM-mediated inhibition of flavivirus infection. Time of addition experiments with SFV suggested that AmphoB only impacted IFITM3-mediated inhibition at early time points (Fig. 4.17 [page 160]), therefore it seemed unlikely that removing AmphoB would alter the flavivirus life cycle in the context of IFITM-mediated inhibition. However, to test this, cells were pre-treated with AmphoB, and incubated with virus for 6 h, prior to media changing, or left in AmphoB media for the full 27 h. A549 cells incubated with AmphoB containing media for 27 h showed no decrease in infection percentage, suggesting cells could effectively produce viral protein (as used to detect infected cells) and that there were presumably no cytotoxic affects from the longer incubation with drug. IFITM expressing cells incubated with AmphoB for 27 h inhibited infection to a similar extent as the cells incubated with AmphoB for 6 h (no statistically significant difference seen), further arguing that AmphoB treatment does not alter IFITM-mediated inhibition of DENV (Fig. 5.4 A). The lack of AmphoB impact on DENV infection does not appear to be as a result of not having the drug present through the full virus replication cycle.

For SFV infection, it was determined that 1 μM AmphoB gave the largest increase of infection in the presence of IFITM3. It may have been the case that higher concentrations

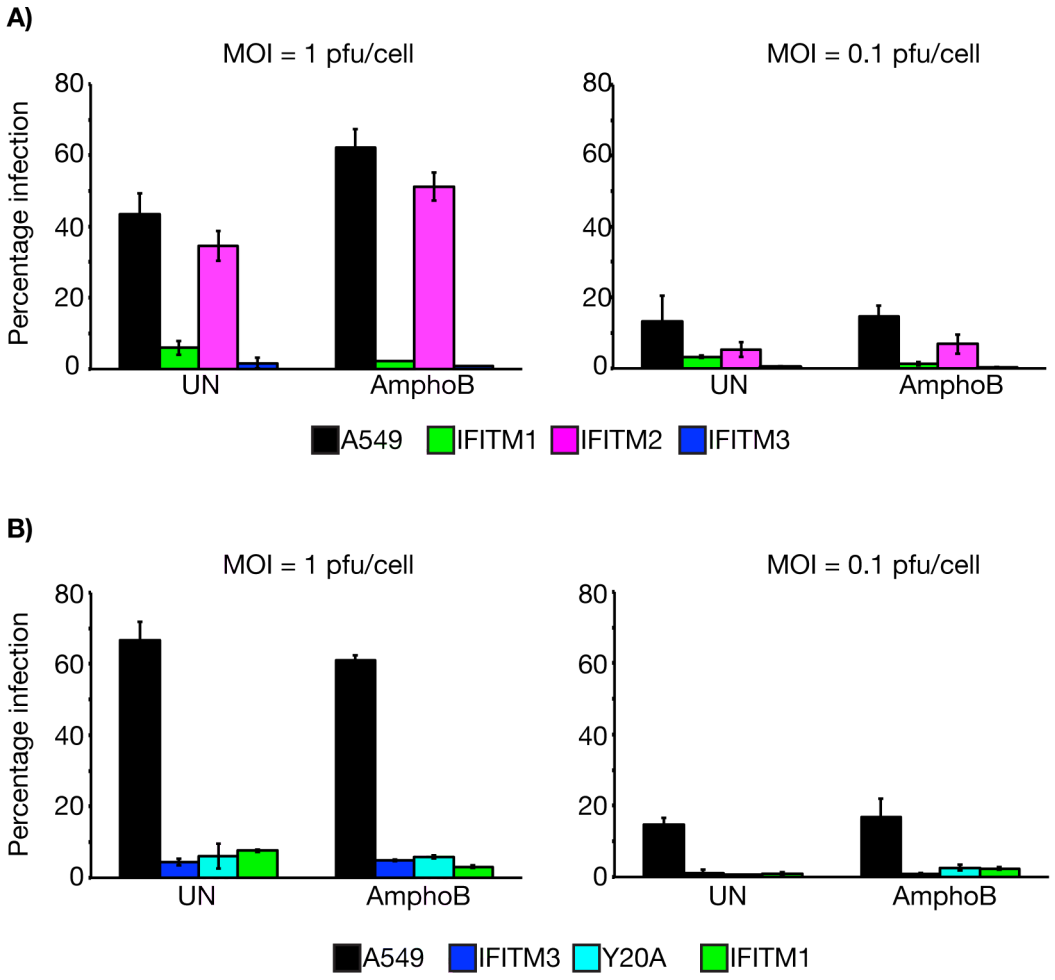

Figure 5.2: **IFITM proteins inhibit ZIKV and this is insensitive to AmphoB treatment.** A549 control, or IFITM expressing cells were pre-incubated for 1 h at 37℃ with 1 μM AmphoB, or left untreated (UN), and then infected with ZIKV (African strain) using 1 or 0.1 pfu/cell (with AmphoB as labelled). Cells were incubated for 6 h prior to AmphoB media being replaced with infection media lacking AmphoB, to mimic the incubation time of cells with AmphoB used for SFV experiments. Infection was allowed to proceed for a total of 27 h, prior to fixation and staining to determine infection percentage by immunofluorescence microscopy. A) OS-IFITM cells. B) P2-IFITM cells and P1-IFITM1 cells. Treating cells with AmphoB had minimal impact on ZIKV infection. The same AmphoB stock as used for other experiments was used here. Data presented are from representative experiments (n = 2 for UN and n = 1 for AmphoB) performed in a 96 well plate format with triplicate wells of infection. Bars are the mean infection with error bars representing the standard deviation.

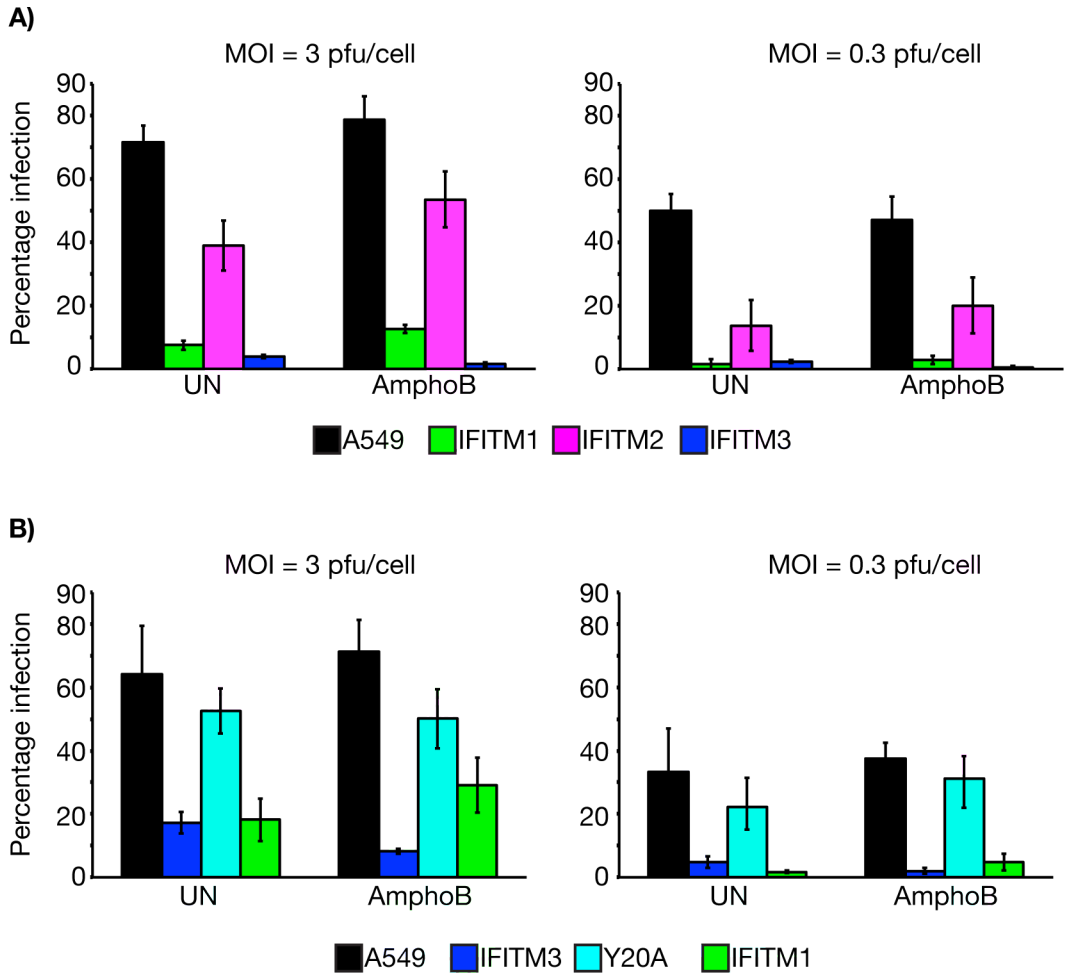

Figure 5.3: **IFITM proteins inhibit YFV 17D and this is insensitive to AmphoB treatment.** A549 control, or IFITM expressing cells were pre-incubated for 1 h at 37°C with 1 μM AmphoB, or left untreated (UN), and then infected with YFV (17D strain) using 3 or 0.3 pfu/cell (with AmphoB as labelled). Cells were incubated for 6 h prior to AmphoB media being replaced with infection media lacking AmphoB, to mimic the incubation time of cells with AmphoB used for SFV experiments. Infection was allowed to proceed for a total of 27 h, prior to fixation and staining to determine infection percentage by immunofluorescence microscopy. A) OS-IFITM cells. B) P2-IFITM cells and P1-IFITM1 cells. Treating cells with AmphoB had minimal impact on YFV 17D infection. The same AmphoB stock as used for other experiments was used here. Data presented are from representative experiments (n = 3 for UN and n = 2 for AmphoB) performed in a 96 well plate format with triplicate wells of infection. Bars are the mean infection with error bars representing the standard deviation.

were needed to impact flavivirus infection. To test this, cells were treated with a range of different AmphoB concentrations and infected with DENV (similarly to experiments with SFV; Fig. 4.18 [page 161]). These data showed that even at higher concentrations of AmphoB, IFITM3-mediated inhibition of DENV was not altered (Fig. 5.4 B). Interestingly, unlike with SFV, the higher concentrations of AmphoB did not inhibit DENV infection in either A549 controls, or IFITM3 expressing cells, except for maybe a small impact at the highest concentration of 50 μM (Fig. 5.4). Overall, it appears that treating cells with AmphoB does not impact IFITM-mediated inhibition of DENV, even with longer time of treatment, or at higher concentrations.

5.2.3 Discussion

IFITM1, 2 and 3 were all found to inhibit flavivirus infection. IFITM3 had the most potency, followed by IFITM1, and IFITM2 had the least potency. Like alphaviruses, flaviviruses are internalised to cells through endocytic mechanisms and enter the cytosol through pH-induced fusion with endosomes. IFITM1 did not inhibit SFV infection and this was initially speculated to be as a result of localisation at the plasma membrane, away from the site of SFV fusion. However, data from plasma membrane fusion experiments (Fig. 4.21 [page 168]) suggested that there may be intrinsic differences between IFITM1 and IFITM3 for their potency against SFV. The results with flaviviruses further argue that the basal localisation of IFITM proteins is not the main determining feature of restriction. IFITM1 is predominantly localised to the plasma membrane, and yet can still inhibit flavivirus infection. By electron microscopy minor pools of IFITM1 were detected within the endocytic pathway (see Chapter 3). These pools of protein may, to an extent, be responsible for IFITM1-mediated inhibition of flavivirus infection, but it may also be the case that protein is internalised with the virus from the cell surface.

Like IFITM1, IFITM3-Y20A localises to the plasma membrane and did not inhibit SFV infection. IFITM3-Y20A was able to inhibit DENV and ZIKV infection, but had little impact on YFV 17D. It can be speculated that there are some intracellular pools of IFITM3-Y20A, similarly to IFITM1, and that protein may be internalised with endocytosed virus, perhaps explaining inhibition of DENV and ZIKV. However, why IFITM3-Y20A has comparatively little impact on YFV 17D, while IFITM1 does is unclear. The

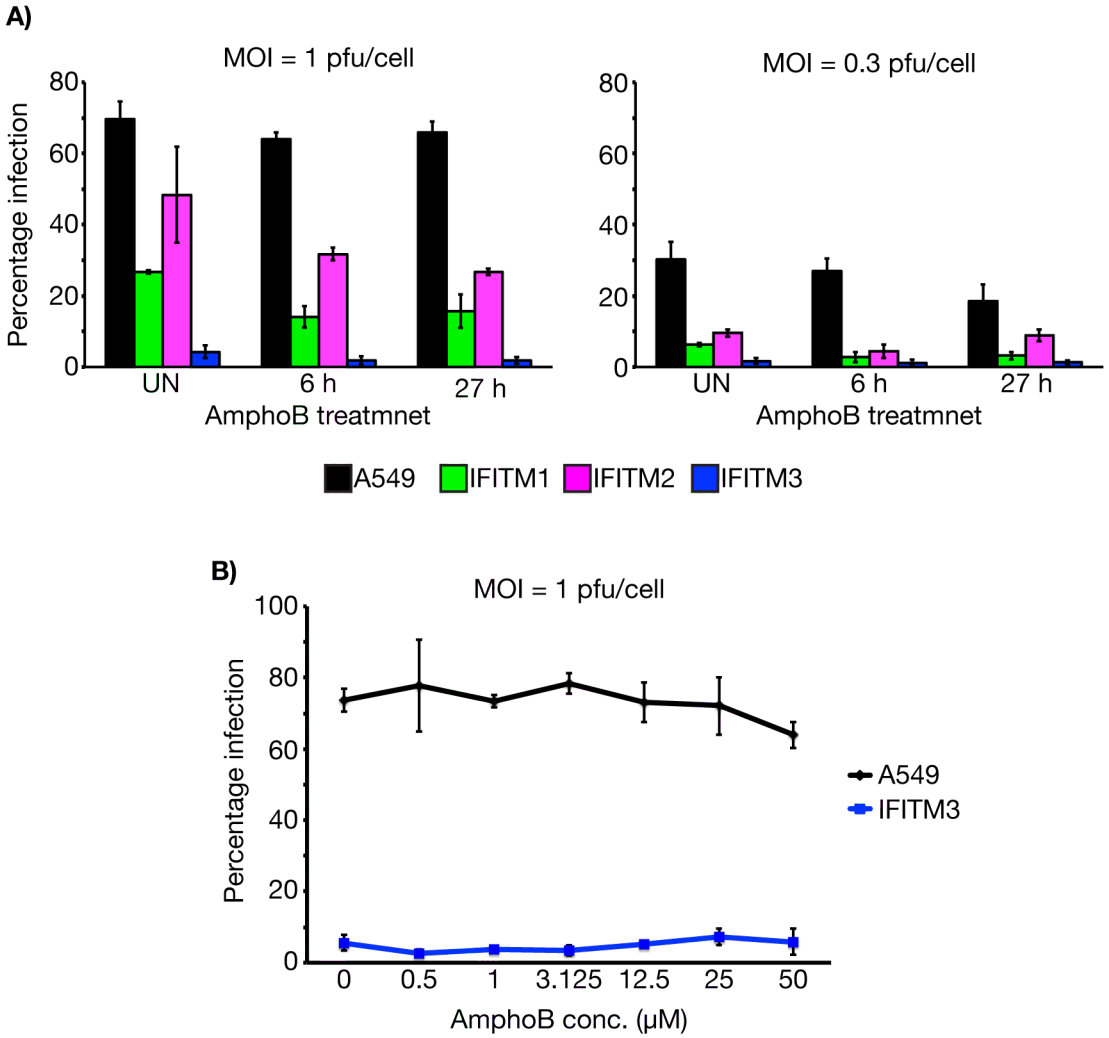

Figure 5.4: **High concentrations of AmphoB do not inhibit DENV infection.** A) For the experiments described in Fig. 5.1, 1 μM AmphoB containing media were removed after 6 h incubation of cells with virus (plus 1 h pre-treatment) and replaced with media lacking drug and virus. To control for any lack of AmphoB affect being as a result of removing the drug, a direct comparison was made between replacing AmphoB media after 6 h, or leaving it for the full infection time of 27 h (using OS-IFITM cells). All cells were pre-incubated with AmphoB for 1 h (or left untreated [UN]) prior to addition of DENV at the labelled MOI and incubated for a total of 27 h to allow infection. Data is from a representative experiment (n = 2) performed in a 96 well plate format with triplicate wells of infection. Bars represent the mean infection percentage and error bars represent the standard deviation. B) OS-IFITM cells were pre-treated with the indicated AmphoB concentrations for 1 h, prior to addition of 1 pfu/cell DENV in the presence of AmphoB. Virus was incubated with cells for 6 h prior to replacing AmphoB containing media with infection media lacking AmphoB. Cells were incubated for a total of 27 h, prior to fixation and analysis of infection by immunofluorescence microscopy. Data is from a representative experiment (n = 2) performed in a 96 well plate format with triplicate wells of infection. Data points represent the mean infection percentage and error bars represent the standard deviation. (All DENV infections performed by Dr. Michela Mazzon.)

17D strain of YFV is a live attenuated form of the virus used for vaccination. Many of the mutations responsible for the attenuation have been found to be in the viral envelope (E) protein [196]. The E protein regulates YFV entry, and it has been suggested that these attenuating mutations of E have altered the entry route of the virus [197]. Like DENV, wild-type YFV is internalised to cells through CME (DENV; [198–201], wild-type YFV; [197]), however, YFV 17D was found to enter HeLa cells through a clathrin-independent, dynamin-dependent, caveolae-independent pathway [197]. Whether this different route of internalisation is altering the sensitivity towards IFITM proteins (sensitive to IFITM1, but insensitive to IFITM3-Y20A) is an interesting possibility that remains to be investigated.

It was suggested that the difference in potency for inhibiting SFV between IFITM1 and IFITM3 may have a link to cholesterol in cellular membranes. SFV requires cholesterol at the site of membrane fusion [100], therefore if IFITM3 preferentially localises to cholesterol-rich regions of cellular membranes, this may explain its potency for inhibiting SFV, particularly at the plasma membrane were there are relatively low levels of IFITM3. The suggested importance of cholesterol is supported by the fact that AmphoB, which binds sterols, can disrupt IFITM3-mediated inhibition of SFV, and at high concentrations can even disrupt SFV infection. In contrast, DENV has been suggested to not require cholesterol for fusion [100]. Indeed, AmphoB treatment did not impact IFITM-mediated inhibition of DENV, and high concentrations of the drug had no inhibitory affect. The experiments of flaviviruses also suggest that 50 μM AmphoB did not cause cytotoxic affects (which were again not observed by microscopy [data not shown]). Furthermore, since A549 cells treated with 50 μM AmphoB could effectively produce viral protein (as used to determine infection), this suggests that 50 μM AmphoB was not killing cells, and therefore this was not the cause of lack of SFV infection (Fig. 4.19 [page 161]).

While AmphoB is suggested to alter SFV but not flavivirus infection of IFITM expressing cells through binding to cholesterol and disrupting IFITM function, an alternative explanation can be made. AmphoB treatment of cells may alter the entry pathways of viruses, which may allow certain viruses to enter at sites which do not have inhibitory IFITM proteins, similarly to the proposed explanation for YFV 17D insensitivity to IFITM3-Y20A. It may therefore be the case that SFV can enter cells through an alternative pathway, which is insensitive to IFITM-mediated inhibition, following Am-

phoB treatment. Comparatively, AmphoB treatment may not alter the route of flavivirus entry, therefore maintaining IFITM sensitivity. Analysing the impacts AmphoB treatment has on the entry pathways of these different viruses may aid in understanding how this antiviral drug can modular IFITM antiviral function.

In the same manner that comparatively low levels of IFITM3 at the plasma membrane inhibited SFV infection through fusion at this site, comparatively low levels of IFITM1 at endosomal membranes appear to inhibit flavivirus infection. It can therefore be suggested that IFITM1 may have enhanced potency towards inhibiting flaviviruses. While DENV does not require cholesterol for fusion, there is a dependency on anionic lipids [52], perhaps this has some impact on sensitivity towards IFITM1. As was discussed with regards to SFV, the determinants of these apparent differences remain to be explored, but the use of chimeric IFITM proteins with terminal domain swaps may be informative.

In summary, there are clear differences between the features of IFITM-mediated inhibition of alphaviruses and flaviviruses, which potentially suggests differences in the underlying mechanisms of antiviral activity. Developing a better understanding of these differences may help to further the understanding of IFITM-mediated antiviral activity (as will be discussed in further detail in Chapter 6).

5.3 Comparison of alphavirus and poxvirus inhibition by IFITM proteins

5.3.1 IFITM proteins do not inhibit vaccina virus infection

To further test IFITM-mediated inhibition of viral infection, VACV was tested for sensitivity to IFITM-mediated inhibition in the stable A549 cells. Infection with VACV was initially assessed by plaque assay across a range of MOI following 48 h infection with the Western Reserve strain (mature virions; MVs - see Fig. 5.5 for example images). When cells were infected with an input of 50 pfu/well (titred on BSC-40 cells), an average (n = 3) of 38 plaques were detected on A549 cells, with 34 on IFITM1 expressing cells (Fig. 5.6). This minimal difference suggested no IFITM1-mediated inhibition of VACV infection. IFITM2 expressing cells appeared to have an increased number of plaques, with

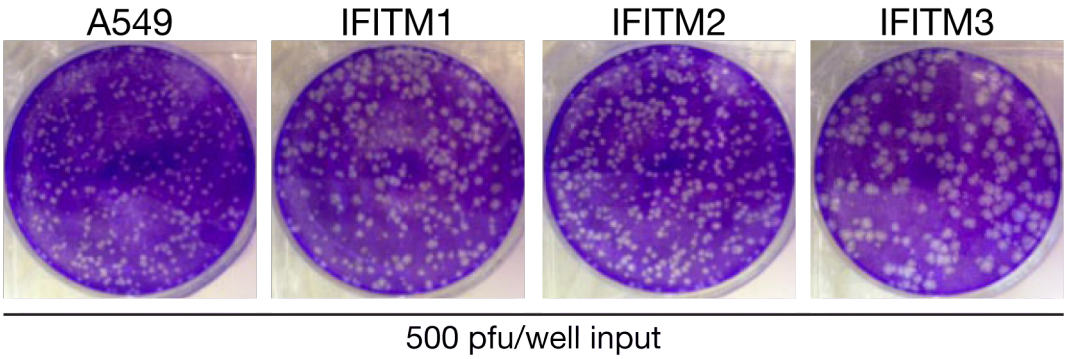

Figure 5.5: **Images of enlarged VACV plaques.** A549 cells or IFITM expressing cells were infected with Western Reserve strain of VACV (mature virions) for 48 h, in a 6 x 35 mm well plate format, prior to plaque assay using crystal violet staining. Images of representative wells infected with 500 pfu/well VACV. The data in in Fig. 5.6 is from infection with 50 pfu/well VACV, the images here are from the higher MOI to display a larger number of example plaques.

an average of 56 plaques detected, perhaps suggesting some enhancement of infection in IFITM2 expressing cells, although this difference was not statistically significant (Fig. 5.6). IFITM3 expressing cells had a decrease in the number of plaques, with an average of 19 per well (Fig. 5.6), which was a statistically significant difference to the A549 control cells, but not compared to the other IFITM expressing cells. While there were fewer plaques on the IFITM3 expressing cells, these were significantly larger than those seen on A549 cells, with a ∼3.5 fold increase in the mean plaque area (see Fig. 5.6 A for measures of plaque area and Fig. 5.5 for example plaques from 500 pfu/well input). It was therefore unclear whether IFITM3 was in fact inhibiting VACV infection. When plaque areas were measured a small, but significant, increase in plaque size was also detected in IFITM1 expressing cells (1.4 fold increase; Fig. 5.6 A and Fig. 5.5). Very little difference in plaque size was detected between A549 cells and IFITM2 expressing cells (1.1 fold increase; Fig. 5.6 A and Fig. 5.5).

To further test whether there was any inhibition of VACV infection by IFITM proteins, cells were infected with 1 pfu/cell, and virus production was analysed at 8, 16 and 24 h (Fig. 5.7). During the VACV life cycle, two infectious forms of virus are produced, an extracellular enveloped virion (EEV) and MVs. EEVs are produced in an infected cell and wrapped in three lipid bilayers prior to transport to, and fusion with the plasma membrane. A double membrane wrapped form of virus is then released into the extracellular space, or transported to neighbouring cells along virus-induced actin tails (see [202] for review

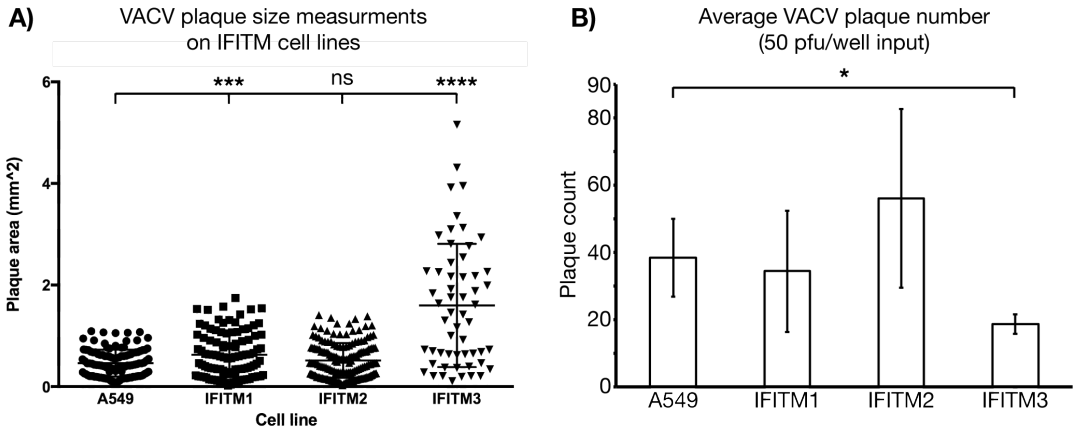

Figure 5.6: **VACV plaques are enlarged in IFITM expressing cells.** A549 cells or IFITM expressing cells were infected with Western Reserve strain of VACV (mature virions) for 48 h, in a 6 x 35 mm well plate format, prior to plaque assay using crystal violet staining. A) Measurements of VACV plaque area were made using ImageJ. Data presented are from three independent experiments. All plaques were measured from wells infected with 50 pfu/well VACV. Total data - A549; n = 115, μ = 0.46 mm^2, σ = 0.26 mm^2. IFITM1; n = 103, μ = 0.63 mm^2, σ = 0.44 mm^2. IFITM2; n = 168, μ = 0.52 mm^2, σ = 0.34 mm^2. IFITM3; n = 56, μ = 1.60 mm^2, σ = 1.21 mm^2. See Fig. 5.5 for images of plaques. Significance tests relate to the difference in plaque areas between A549 and IFITM expressing cells. *** $p < 0.001$, **** $p < 0.0001$. B) Graph displaying the average number of plaques for each cell line (infected with 50 pfu/well VACV) across the three independent experiments (error bars display standard deviation). This data are taken from A and the graph used to more clearly display the average number of plaques per well. Significance tests relate to difference in mean plaque counts between experiments as assessed by unpaired student's t-tests (* $p < 0.05$). For all other comparisons there were no statistically significant differences.

of VACV replication cycle). EEVs start to be released from cells around 6 - 8 h post infection. In contrast, MVs are retained in the cytosol of infected cells until these lyse, around 72 h post infection. Production of both forms of virus was analysed. To assess EEV production, media were collected from infected cells at each time point. For analysis of MV production, cells were collected from plates at each time point, by scraping, and lysed by three rounds of freeze-thawing (-80℃ to 37℃). Each form of collected virus was then titred on BSC-40 cells. These data suggested that IFITM1 may have a minor affect on VACV production, resulting in close to half a log drop in virus titre at each collection time. IFITM2 and IFITM3 showed only minor differences in virus titre compared to the A549 control cells (Fig. 5.7). Importantly, at 8 h there were only minor differences between A549 controls and IFITM3 expressing cells, suggesting there was no inhibition of a single round infection. Therefore, even though there were fewer plaques on IFITM3 expressing cells (Fig. 5.6), IFITM3 expression does not inhibit VACV production, suggesting there is no inhibition of infection. While IFITM2 expressing cells appeared to have more plaques than A549 cells (Fig. 5.6), there was no clear change to virus production, suggesting IFITM2 is not enhancing VACV infection. Finally, while IFITM1 expression appeared to result in a small drop in VACV production at each of the three time points, there was no clear difference in plaque number (Fig. 5.6), suggesting that IFITM1 has limited, if any, inhibitory activity against VACV.

5.3.2 IFITM3 enhances cell motility in the absence of VACV infection

It appeared that IFITM proteins did not inhibit VACV infection, based on production of infectious virus, however this left the question of why enlarged plaques were detected on IFITM expressing cells. To investigate the cause of the increased plaque size, a recombinant VACV expressing EGFP from an early/late fusion promoter was used because the spread of EGFP can be used to analyse spread of virus in the monolayer. Cells were infected for 24 or 48 h and EGFP was analysed by immunofluorescence microscopy (Fig. 5.8 A). IFITM3 and IFITM1 expressing cells showed a larger EGFP area than A549 cells, while IFITM2 showed no clear difference (and if any difference, there may have been a minor decrease; Fig. 5.8 B). It appeared that as the EGFP infection zone increased in size,

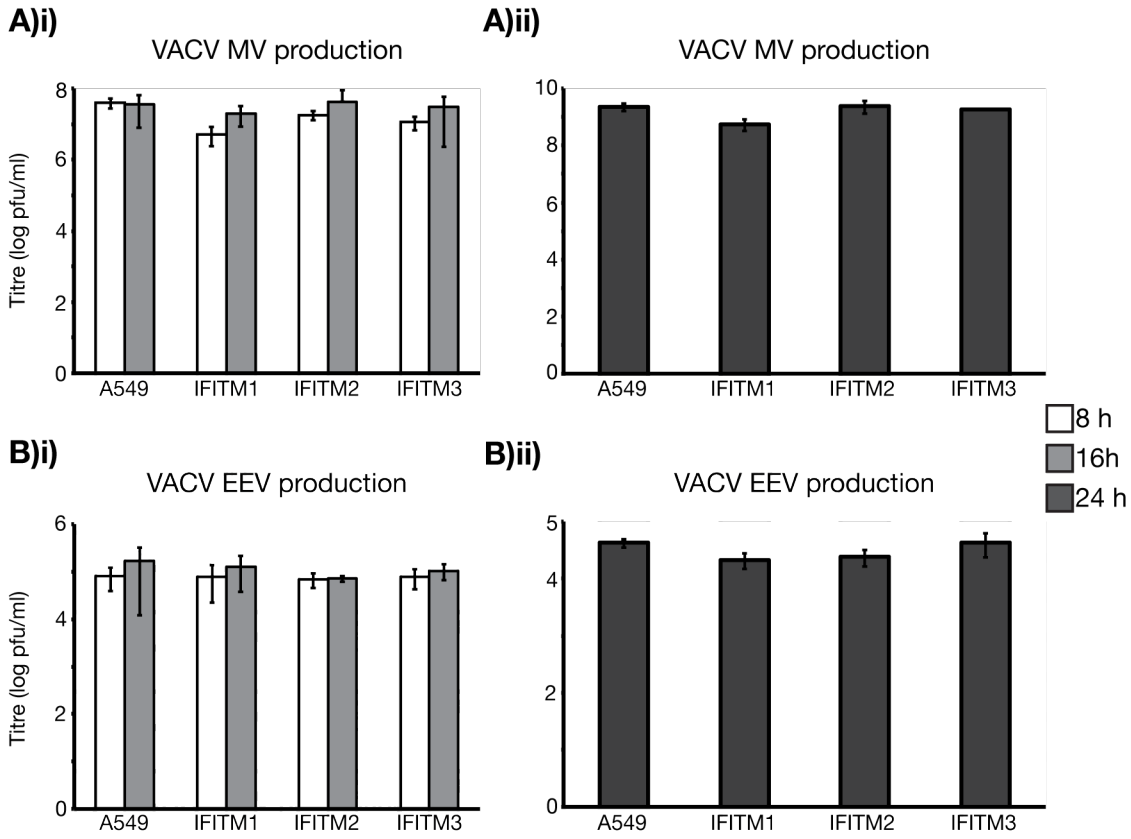

Figure 5.7: **IFITM expression does not alter VACV production.** A549 or IFITM expressing cells were infected with 1 pfu/cell VACV Western Reserve strain (mature virions [MVs]). Media were collected at 8, 16 or 24 h post infection to analyse extracellular envelope virion production (EEV). At the same time points, cells were collected from plates by scraping and lysed by three rounds of freeze-thawing (-80℃ to 37℃) to collect progeny MVs. The titre of the collected virus was determined on BSC-40 cells by plaque assay after 48 h infection. A) MV production from 8 and 16 h infections (i) and 24 h infections (ii). B) EEV production from 8 and 16 h infections (i) and 24 h infections (ii). All data presented is the mean average titre (log pfu/ml) from 3 independent infections with the standard deviation given as error bars.

so too did the clearance zone at the centre of the plaque (Fig. 5.8 A). Nuclei bunching at the edge of large plaques was also observed (most clear for IFITM3 expressing cells [Fig. 5.8 A]). Both of these features of the plaques suggested that there may be enhanced motility in IFITM3 and IFITM1 expressing cells.

To test whether IFITM expressing cells were indeed more motile, a scratch assay was performed in the absence of VACV infection. Cells were plated on glass coverslips to form a monolayer and a scratch was made through this with a P200 tip. Migration of cells into this wound was then monitored over a 36 h period (imaging at 24 and 36 h after the scratch). The results showed that IFITM3 expressing cells closed the wound more rapidly than A549 expressing cells (Fig. 5.9). IFITM1 expressing cells also appeared to have enhanced motility, though little difference between A549 and IFITM2 expressing cells was detected (Fig. 5.9). The migration of cells into the scratch matched with the cells that produced the largest plaques; IFITM3 expressing cells had the highest motility and largest plaques, followed by IFITM1 expressing cells, and IFITM2 expressing cells showed little difference to A549 controls (Fig. 5.9 and Fig. 5.6).

An important caveat to the apparent increase in cell motility should be noted. These results were generated using the OS-IFITM cell lines which were produced by clonal selection. It is therefore possible that the increased cell motility is as a result of the clonal nature of the stable cell line production, rather than as a consequence of IFITM3 (or IFITM1) expression. In an attempt to test this, similar scratch assays were performed in P1-IFITM3 cells. As seen in Fig. 5.10, the P1-IFITM3 cells did not show enhanced motility, as observed for OS-IFITM3 cells. The motility of OS-IFITM3 cells could therefore be a consequence of clonal selection. However, it should also be noted that the OS-IFITM3 expressing cells have higher expression of IFITM3 (Fig. 4.2 [page 138]), so it could be the case that high IFITM3 expression is necessary for increasing cell motility.

Overall, it appears that IFITM3, and to a lesser extent, IFITM1 highly expressing cells have enhanced motility, which is made evident by VACV infection. Although it cannot be ruled out that there could be affects from the clonal nature of the OS-IFITM cells. However, it does appear that IFITM proteins, do not inhibit VACV infection, unlike results with alphaviruses and flaviviruses which were IFITM-sensitive.

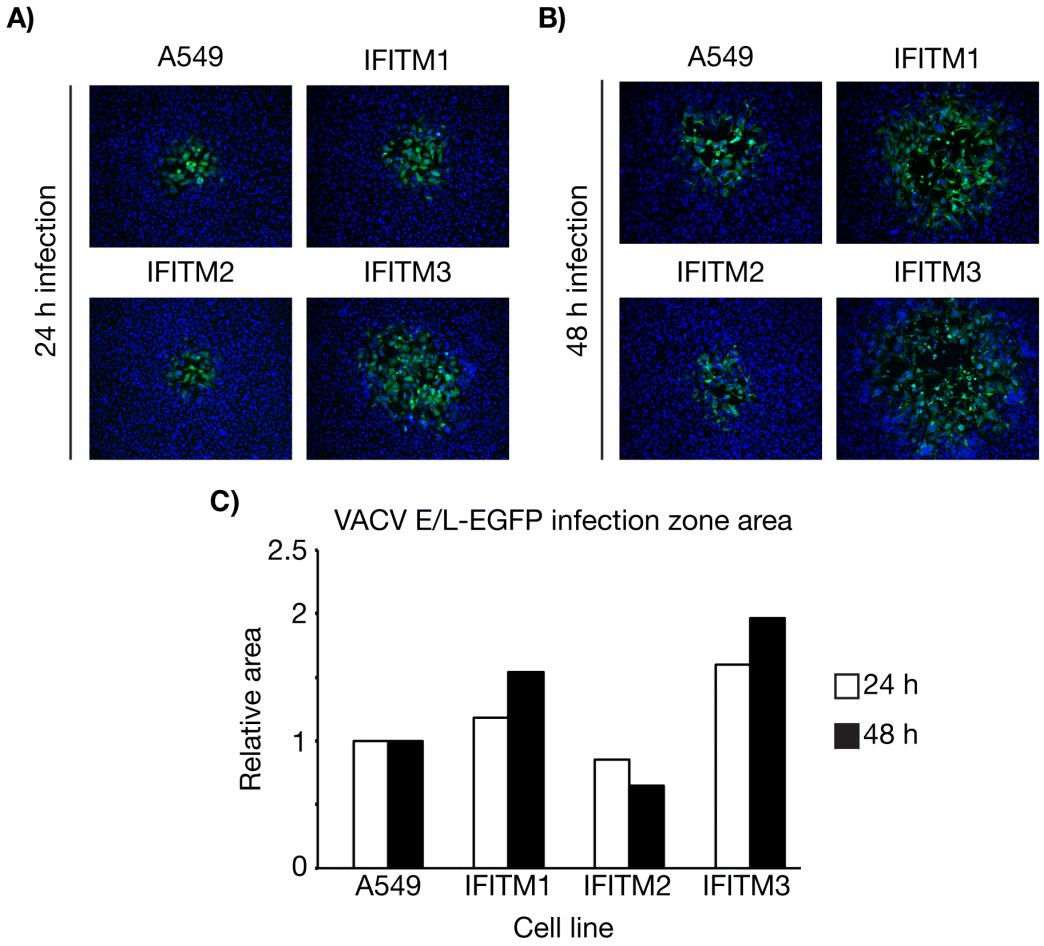

Figure 5.8: **Enlarged VACV plaques associated with enhanced cell motility.** A549 or IFITM expressing cells were infected with VACV Western Reserve strain (50 pfu/well), engineered to express EGFP from an early/late (E/L) fusion promoter. At 24 or 48 h post infection cells were fixed, permeabilised and immunofluorescence stained with anti-GFP antibody (detected with AF488) to boost signal, and Hoechst to detect nuclei. Plaques were then imaged using an epifluorescence microscope. Representative images from 24 (A) and 48 h (B) infection. C) GFP infection zone size was measured using ImageJ. The mean values were calculated and set relative to A549 control cells at each time point. Data are form a single experiment.

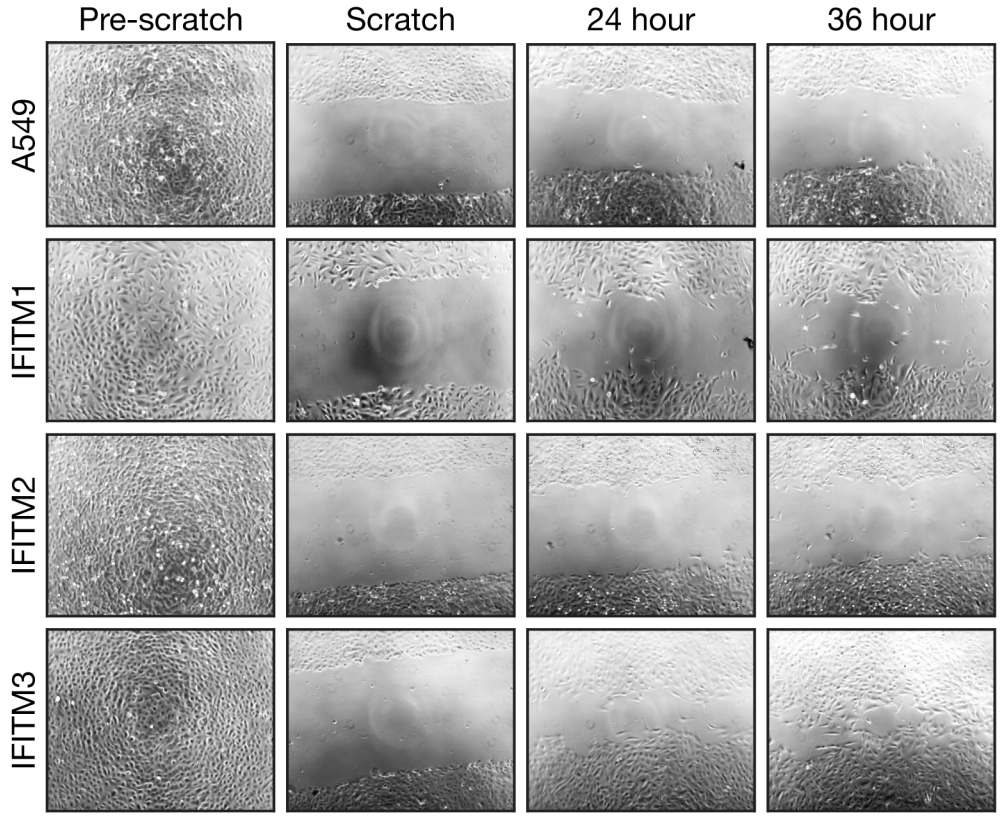

Figure 5.9: **Scratch assays show enhanced cell motility in IFITM3 and IFITM1 expressing cells.** A549 or IFITM expressing cells were plated to glass coverslips in LabTech chambers and grown to form a confluent monolayer. Cells were then imaged, scratched with a P200 tip and imaged again. Cells were incubated under normal culture conditions for 36 h, taking images at 24 h and 36 h to monitor closure of the wound. Representative images are displayed from n = 3 experiments, 5 wells each for A549 and IFITM3, and n = 2 experiments, 2 wells each for IFITM1 and IFITM2 (all images are from the same experiment).

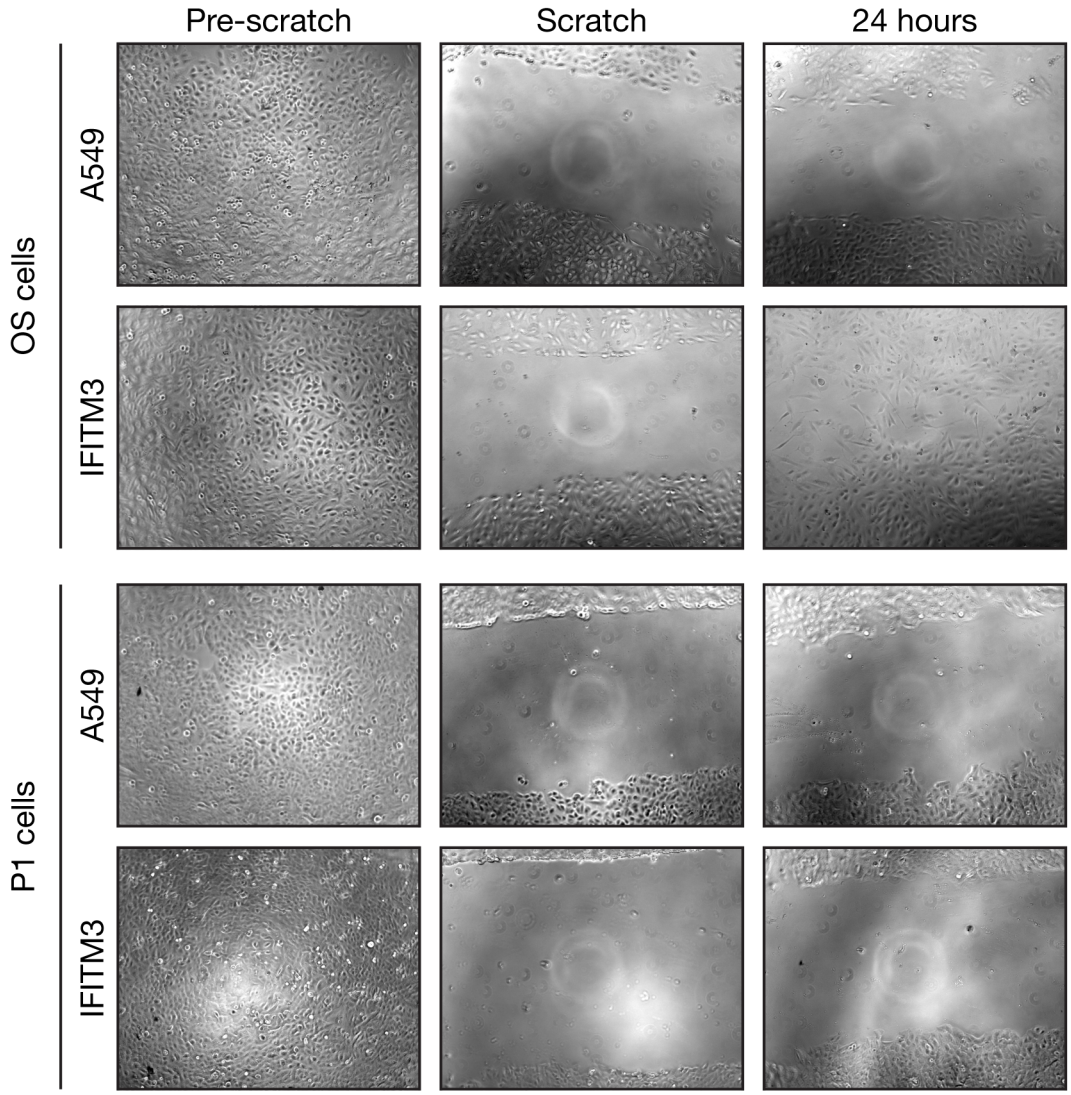

Figure 5.10: **Comparison of OS- and P1-IFITM3 cell motility.** A549 or IFITM3 expressing cells were plated to glass coverslips in LabTech chambers and grown to form a confluent monolayer. Cells were then imaged, scratched with a P200 tip and imaged again. Cells were incubated under normal culture conditions for 24 h and imaged again. Representative images are displayed from n = 2 wells for each cell line.

5.3.3 Discussion

Very few viruses have been shown to be insensitive to IFITM-mediated inhibition, compared to those that have. To date, only areanaviruses, a retrovirus (murine leukaemia virus), papillomaviruses, cytomegalovirus and adenoviruses have been shown to be insensitive (see Table 1.3 [page 48]). The papillomaviruses and adenoviruses are non-enveloped, and therefore do not use membrane fusion to enter cells, perhaps explaining their insensitivity to IFITM-mediated inhibition. Why other enveloped viruses are not inhibited remains to be fully explored. Here, data is presented suggesting that VACV, an enveloped virus, which enters cells by fusion with internal membranes following macropinocytic uptake from the cell surface, is not inhibit by IFITM expression. However, the studies of VACV demonstrated that OS-IFITM1 and IFITM3 expressing cells have enlarged VACV plaques. A potential explanation for enlarged plaques (that has not been investigated in this work) may be that IFITM proteins interfere with spread of VACV through a monolayer, to restrict infection to neighbouring cells. Alternatively, being that VACV activates cell motility upon infection, for instance through an interaction of the viral F11L protein with RhoA [203], the enlarged plaques may be explained by an increase to cell motility. Indeed, VACV-induced motility led to the observation that OS-IFITM1 and IFITM3 expressing were more motile compared A549 control cells even in the absence of VACV infection. It cannot be ruled out that this increased motility is a consequence of the clonal selection of these cells. However, IFITM proteins have been linked to an increase in invasiveness and metastatic potential of cancer cells (reviewed in [204], see also [205–207]). It could therefore be the case that at the higher levels of IFITM3 expression, there may be disruption of normal cellular function which has the knock-on affect of enhancing cellular motility, however the precise mechanism(s) underlying this effect have not been explored.

5.4 Conclusions and Discussion

In summary of the work presented in this chapter, it appears that not all viruses that enter cells by endocytosis and pH-dependent fusion with endosomal membranes are equally sensitive to IFITM-mediated inhibition. In contrast to the alphaviruses, which were inhibited by IFITM3 and IFITM2, DENV and ZIKV appeared to be sensitive to all IFITM pro-

teins. YFV 17D appeared to be sensitive to IFITM1, 2 and 3, but IFITM3-Y20A had little affect. These differences further suggest that protein localisation may not be a key determinant of IFITM restriction of viral infection. Additionally, IFITM-mediated inhibition of flaviviruses is insensitive to treatment with AmphoB, unlike the alphaviruses and IAV [156], but similarly to EBOV [142]. These differences perhaps point towards mechanistic differences within the IFITM proteins in the modes of antiviral function. Furthermore, it has been shown that VACV is not inhibited by IFITM proteins, further supporting previously published data that the IFITM proteins do not inhibit all viruses. While there was no inhibition of VACV, the data suggested a possible role of high IFITM expression in enhancing cell motility, perhaps point towards consequences of sustained high expression. The IFITM proteins have been linked to cancer invasiveness and metastatic potential, in agreement with a potential role in promoting cell motility, perhaps suggesting why the proteins need to be IFN-inducible.

Chapter 6

Discussion

The work presented in this thesis has helped to develop an understanding of IFITM protein membrane topology, better define the localisation of the IFITM proteins in A549 cells, and defined how IFITM3 can inhibit SFV infection. The data have also suggested that there are potential differences in the potency of IFITM isoforms towards different viruses, and that the mechanisms of antiviral activity may vary. Furthermore, a suggestion was made that high IFITM expression may enhance cell motility, so could have negative consequences outside of an *in vitro* scenario.

6.1 Topology and Localisation

The membrane topology of the IFITM proteins had been a contentious issue at the commencement of this work, with two models being debated. Before the IFITM proteins were studied for antiviral function, they were suggested to have roles in embryonic development, germ cell migration, and proliferation of immune cells [114–116]. These early studies pointed towards extracellular regions of IFITM proteins based on the ability of antibodies to bind, and proposed interactions between IFITMs on different cells, although no thorough analysis was undertaken. The IFITM proteins were initially suggested to have a dual-pass transmembrane topology with both the N- and C-terminal domains (NTD and CTD) exposed extracellularly/lumenally (see Fig. 3.1 [page 96], Model 1). When Brass *et al.* later identified the IFITM proteins as having antiviral function, their work suggested a similar structure based on the extracellular availability of a CTD HA-tag, and the NTD

to antibodies for FACS labelling [7]. However, this work was limited in the controls used and left questions about the topology.

Subsequent studies suggested there were post-translational modification to the IFITM3 NTD, leading to the suggestion of an intramembrane topology model (see Fig. 3.1 [page 96], Model 2). A tyrosine residue in the IFITM3 NTD (Y20) was shown to be phosphorylated by Fyn kinase, which resides on the cytosolic leaflet of cell membranes [163]. The Y20 residue was later shown to be part of a functional Yxxϕ sorting motif (where Y is tyrosine, x is any amino acid and ϕ is a hydrophobic residue), which could interact with AP-2 [143]. Similarly, IFITM3 can be ubiquitinated at any of four lysine resides [151]; one of which (K24) resides in the NTD, while the others reside in the conserved intracellular loop (CIL; K83, 88, 104). Since all known ubiquitinases are cytosolic, this further argued for an intracellular NTD. Indeed, it was later demonstrated that the cytoslic E3 ubiquitin ligase NEDD4 could interact with the IFITM3 NTD PPxY motif (17-PPNY-20) to regulate ubiquitination [160].

While published data strongly supported a cytosolic NTD, the data for the CTD was weaker, relying largely on engineered constructs. Murine Ifitm3 altered to have a CTD NxT motif (H136T mutation) was not detected as being glycosylated in the ER. Another Ifitm3 construct demonstrated prenylation of an engineered CTD CLVL motif [151]. The results from both of these mutant proteins were used to first suggest the cytosolic CTD. Additionally, murine Ifitm1 was later shown to have a non-conserved CTD cysteine that could be palmitoylated [155]. With debate over the two models, the initial investigations of the work presented here were designed to define the topology of human IFITM proteins in A549 cells.

Through the course of the work presented in Chapter 3, a third membrane topology model was produced. The work largely focused on IFITM1 as this protein is localised at the plasma membrane and is therefore amenable to many experimental approaches to investigate topology. The data presented suggested that IFITM1 has a membrane topology in which the NTD resides in the cytoplasm, while the CTD resides in the extracellular/lumenal space. IFITM2 and IFITM3 are found within internal membrane compartments, and are therefore less amenable to topological analysis than IFITM1. However, immunofluorescence staining and antibody feeding experiments (Fig. 3.2 [page 97], 3.4 [page

102], 3.3 [page 100] and 3.12 [page 117]) suggested that, at least in some cells, IFITM2 and IFITM3 have extracellularly available CTDs. This led to the hypothesis that the CTD HA-tags may be lost in the acidic/proteolytic environment of endosomal compartments, which was indeed found to be the case (Fig. 3.13 [page 120] and 3.14 [page 121]), further supporting the notion of a lumenal CTD. Finally, making use of the plasma membrane localised IFITM3-Y20A mutant, data was generated demonstrating that IFITM3 topology matches that of IFITM1 (Fig. 3.16 [page 124]). In sum, the data presented in Chapter 3 suggest that all three human IFN-inducible IFITM proteins have a type II transmembrane topology. This model has been supported by others who have shown murine Ifitm3 [153] and human IFITM3 [192] to have the same topological structure.

It appears that the cytosolic localisation of the NTD of IFITM proteins is functionally important. IFITM2 and IFITM3 have Yxxϕ sorting motifs that have been shown to interact with AP-2 and regulate the endosomal localisation of the proteins [143, 163, 169]. The disruption of this motif by Y20A mutation, or deletion of the first 21 amino acids of the IFITM3 NTD, causes accumulation of the protein at the plasma membrane and a reduced antiviral activity against IAV, HIV-1 and SFV ([16, 143, 158, 163, 174], and work presented in this thesis). Mutations of IFITM2-Y19F and IFITM3-Y20F have also been found to alter localisation and antiviral activity against different strains of HIV-1 [169]. The cytosolic NTD and ability to interact with AP-2 therefore appears essential for antiviral activity, at least in some cases. The Y20 residue of IFITM3 has additionally been proposed to be a site of phosphorylation by Fyn kinase, which seems to regulate IFITM3 membrane trafficking [158, 163].

In addition to phosphorylation of the NTD, K24 has been shown to be a ubiquitinated and play a role in turnover of IFITM3 [151]. K24 is also a site of K63-linked polyubiquitination, suggesting additional roles besides protein turnover [151]. The 17-PPxY-20 motif in the IFITM3 NTD determines the interaction between IFITM3 and the E3 ubiquitin ligase NEDD4 [160]. What interplay there may be between phosphorylation of Y20 and NEDD4 interaction with IFITM3 at the 17-PPxY-20 motif remains to be explored. Interestingly, loss of ubiquitination by mutation of IFITM3 lysine resides to alanine or loss of interaction with NEDD4 (through mutation to IFITM3 or knockdown/knockout of NEDD4) was seen to reduce IFITM3 turnover and enhance IFITM3 antiviral activity

against IAV [151, 160]. It will be interesting to investigate whether the phosphorylation status of Y20 can impact NEDD4 interaction with IFITM3, and whether this is modulated during an infection. Seeing that reduced turnover, and subsequent protein accumulation, enhances IFITM3 antiviral function is in agreement with data presented here suggesting that higher levels of IFITM3 have greater antiviral activity against SFV (Section 4.2.2 [page 136]). The enhanced antiviral function of IFITM3 in the context of NEDD4 knock-down led to the suggestion that pharmacological inhibition NEDD4 may have therapeutic value. However, high IFITM3 levels may cause an increase in cell motility, as implied by the data here (Fig. 5.9 [page 191]), meaning such intervention may have side affects. Overall, it appears that an intracellular NTD is important for regulating IFITM cellular distribution, protein turnover, and potentially other facets of their cell biology.

While the cytosolic NTD appears to regulate IFITM function, the consequences of other aspects of the proposed membrane topology are less clear. In the suggested model, the first membrane domain enters into, but does not cross lipid bilayers, perhaps resulting in alterations to membrane curvature which could influence membrane fusion events. Functionally important residues have been found within the highly conserved CD225 domain, which spans the first membrane domain and CIL [154]. For instance, two phenylalanine residues (F75 and F78 found in the first membrane domain of IFITM3) were suggested to be important for IFITM protein-protein interaction; mutation of both residues to alanine (F75A/F78A) resulted in a loss of IFITM3-mediated inhibition of IAV infection [154]. Perhaps this intramembrane structure is important interaction of IFITM proteins and antiviral function.

The work of John *et al.* [154] also had the interesting result that a chimeric protein with the IFITM3 NTD and all other parts of IFITM1 did not confer anti-IAV function, even though the localisation of the chimeric protein was on internal membranes, rather than the plasma membrane (i.e. localisation to endosomal membranes was not sufficient to inhibit IAV; [154]). The CD225 domain is very highly conserved, suggesting the determinants of the lack of anti-IAV function for the chimeric protein are in the second membrane domain and/or the CTD. These results suggest functional importance for these regions of IFITM proteins. Additionally, it has been proposed that IFITMs can interact with vesicle-associated membrane protein-associated protein A (VAPA) through the second membrane

spanning domain [152], the transmembrane structure of this domain could be important for that interaction.

The CTD has been suggested to be important for control of coronavirus (CoV) infection. IFITM2 and IFITM3 were found to enhance CoV-OC43 infection, while IFITM1 did not. Chimeras with altered CTDs changed these phenotypes, and it was suggested that the shorter length of the IFITM2 and IFITM3 CTDs, compared to IFITM1, were responsible [140]. However, the precise functional role of the CTDs for modulating CoV infection remains unclear. It is also unclear why CoV-OC43 is enhanced by IFITM2 and IFITM3, while SARS-CoV [139, 140] and many other viruses are restricted (Tables 1.1 [page 46] and 1.2 [page 47]). Finally, it has been suggested that there is a di-basic sorting motif (122-KRXX-125) in the IFITM1 CTD that can interact with AP-3 [159] and that the CTD can alter IFITM1 localisation and restriction of HIV-1 [185]. An AP-3 interaction seems at odds with an extracellular/lumenal orientation of the CTD, and even in that work evidence was found for such a topology [159]. It is therefore unclear what role such an interaction may play. Overall, how the extracellular/lumenal orientation of the CTD can modulate IFITM cell biology remains to be established.

While defining the type II transmembrane topology for the IFITM proteins, it became clear that analysing protein distribution within cells using a C-terminal HA-tag may be flawed. The HA-epitope can be lost from the C-terminus, particularly of IFITM2 and IFITM3, meaning functional pools of protein may potentially be missed when basing analysis on such a tag. Therefore a thorough investigation of the IFITM2 and IFITM3 cellular distribution was performed by co-staining cells for the NTD and makers of early, recycling and late endosomes as well as lysosomes (Fig. 3.17 [page 127]). These data suggested that IFITM3 is more closely associated with markers of early and recycling endosomes than IFITM2, while IFITM2 is more closely associated with markers of late endosomes and lysosomes.

When analysing IFITM3 protein distribution at an EM level (Fig. 3.7 [page 105]), it appeared that most of the HA labelling was on the intra-lumenal vesicles (ILVs) of multivesicular bodies (MVBs). This EM analysis used the HA-tag because the NTD antibodies only gave weak labelling (data not shown), therefore pools of protein were potentially missed, or tag no longer attached to the IFITM protein may have been observed. Nev-

ertheless, it remains intriguing that the majority of IFITM3 was found in MVBs with many ILVs, as these are typically considered to be late endosomal, staining positively for markers such as CD63, rather than EEA1 and TfR. Therefore, there appears to be some discrepancy between the immunofluorescence and EM localisation analysis. It could be hypothesised that IFITM3 expression may have an impact on the normal trafficking of proteins used as markers such as EEA1 and TfR. It has been suggested that IFITM3 expression results in enlarged and more acidic endosomal compartments [12, 137, 208], perhaps further supporting the notion that this protein can disrupt normal trafficking events. As discussed, IFITM3 is ubiquitinated by NEDD4, and ubiquitination of membrane proteins has been shown to direct their trafficking into ILVs [43]. Whether having a high concentration of ubiquitinated IFITM3 can influence the formation of MVBs and what affect this may have on inhibition of incoming viruses could be an interesting subject for future research. It is also tempting to speculate that if IFITM3 is disrupting the endosomal system, this may have negative consequences for the normal functioning of the cell, perhaps being linked to the apparent increased motility of cells expressing high levels of IFITM3.

6.2 Antiviral action

The data presented in Chapter 4 demonstrated for the first time that IFITM3 could inhibit alphavirus infection (SFV and SINV) by blocking release of the capsid into the cytosol. Shortly after we published this [16], additional research was published demonstrating that IFITM3 could inhibit infection from SFV, SINV, chikungunya (CHIKV), O'nyong nyong and Venezuelan equine encephalitis (VEEV) viruses [184]. This second study also demonstrated relevance of this antiviral function *in vivo*, with IFITM3 appearing to be important for control of CHIKV and VEEV infections in mice [184]. The two studies complement one another and suggest that IFITM proteins, in particular IFITM3, can inhibit alphavirus infection of cells and are important to control pathogenesis of infections in mice. It has been suggested that a single nucleotide polymorphism (SNP) in IFITM3 (rs12252-C) is associated with severe IAV infection [174, 177, 179, 180]. It will be interesting to investigate whether there is any genetic link between the severity of alphavirus infection in humans

and IFITM3 SNPs.

The antiviral function of IFITM proteins has been most highly characterised using IAV. Studies have shown that IFITM3 expression blocks nuclear translocation of the viral ribonuclear proteins, causing them to accumulate in endosomes [12]. It therefore appears that IFITM3 is capable of blocking fusion of IAV with cellular membranes, however, there is debate over whether this occurs before hemifusion [13] or after establishment of hemifusion but before resolution to a fusion pore [14]. Much of the other published data on IFITM restriction of virus infection has used pseudotyped viruses (see Tables 1.1 and 1.2) to argue that IFITM proteins are inhibiting the glycoprotein-mediated fusion reaction, though these studies rarely investigate earlier events in the virus entry pathway. From the data presented here, it appears that IFITM3 inhibits alphavirus infection by blocking fusion between viral and cellular membranes, as proposed for other viruses. While SFV could be internalised to acidic cellular compartments in IFITM3 expressing cells, and the E1 glycoprotein could undergo conformational changes, the capsid was not released into the cytosol. It has been suggested that the formation of the E1 homotrimer (HT) is dependent on the presence of membrane [194], and a relatively small proportion of E1 was found in the HT form in our experiments (Fig. 4.12 [page 152), perhaps supporting the notion of membrane interaction being necessary for the stabilisation of the HT. The E1 HT could form in IFITM3 expressing cells, leading to the suggestion that IFITM3 may not be blocking interaction of E1 with endosomal membranes. However, even though the E1 HT could form, and potentially interact with membrane, the capsid was not released into the cytosol, suggesting an inhibition of membrane fusion imposed by IFITM3; similarly to the IFITM3 function characterised for anti-IAV activity. There are further similarities between the inhibition of IAV and SFV in that treating cells with AmphoB diminishes the antiviral activity of IFITM3 against both viruses ([156], Fig. 4.15 [page 157], Fig. 4.16 [page 158] and Fig. 4.20 [page 163]). These similarities may suggest similar underlying mechanisms of orthomyxovirus and alphavirus inhibition. SFV may therefore provide a powerful tool to better establish whether IFITM3 inhibits hemifusion formation, or resolution of hemifusion intermediates.

It was noted that increasing the amount of input virus reduced the level of IFITM-mediated inhibition of both SFV and SINV (Fig. 4.1 [page 135]), suggesting that high

levels of virus can saturate the antiviral action of IFITM proteins. The converse was also the case, such that cells with lower IFITM expression were less restrictive of SFV infection (Fig. 4.2 [page 138]). If there is a need for direct interaction between IFITM protein and the sites of SFV fusion, this may explain the saturability. With a higher level of input virus there will be more fusion events and therefore a greater chance of successful fusion. Conversely, with lower IFITM protein expression there is potentially a reduced likelihood of IFITM protein being at sites of fusion. Developing an understanding of whether, and how, IFITM proteins localise to sites of virus binding and fusion may help to develop a better understanding of the mechanism(s) of antiviral activity.

While IFITM3 could inhibit SFV infection through the endocytic route, IFITM1 could not, in contrast to many other viruses tested (Tables 1.1 and 1.2). The hypothesis was that because IFITM1 is localised at the plasma membrane, internalisation and fusion of SFV in early endosomes means low levels of IFITM1 at sites of fusion. In agreement, plasma membrane localised IFITM3-Y20A similarly failed to inhibit SFV infection through the endocytic route. Comparatively, IFITM3 is localised to early endosomal compartments, and therefore presumably present at high concentration where viral fusion occurs (virus and IFITM3 were indeed found to co-localise; Fig. 4.5 [page 143]). This initial hypothesis was challenged by the results of plasma membrane fusion experiments (Fig. 4.21 [page 168]) that suggested there may be additional complexity. IFITM3 has relatively low abundance in the plasma membrane, yet it was able to inhibit SFV infection by fusion at the cell surface to a similar or greater extent than IFITM1. These results argue that IFITM3 may have intrinsically higher potency for inhibiting SFV infection than IFITM1. IFITM3-Y20A also appeared to have greater anti-SFV action than IFITM1 when virus was fused at the cell surface.

It is speculated that the increased potency of IFITM3 for inhibiting SFV may be as a consequence of its interaction with cholesterol. SFV requires cholesterol at the site of membrane fusion [100], therefore if IFITM3 preferentially clusters to cholesterol-rich regions of cell membranes this may explain how relatively low levels of protein can inhibit viral fusion at the plasma membrane. The converse argument would be that while IFITM1 is at high abundance at the plasma membrane, if it does not associate with cholesterol-rich regions of membrane there may be lower likelihood of being at the site of SFV fusion. It

could be speculated that IFITM1 preferentially localises to other regions of cell membranes, which could influence its antiviral function (as discussed below with regards to flaviviruses). That cholesterol may play a role is supported by the fact that AmphoB treatment can disrupt IFITM3-mediated inhibition of SFV. Perhaps AmphoB binding to cholesterol is capable of disrupting IFITM3 association with the lipid, without interfering with the SFV E1-mediated fusion reaction (at least at lower concentrations; Fig. 4.18 [page 161]). However, as discussed in Chapter 4, an alternative explanation for the inhibition of SFV infection through plasma membrane fusion may be that Baf A treatment could be causing accumulation of IFITM3 at the plasma membrane, which remains to be examined.

It seems likely that there would be some uptake of IFITM3-Y20A from the plasma membrane to endosomal compartments, even without the functional Yxxϕ motif. This raises the question of why low levels of IFITM3-Y20A didn't inhibit SFV through the endocytic route, in the same way IFITM3 could inhibit plasma membrane fusion. It is possible that the concentration of IFITM3-Y20A at internal sites is too low to see any anti-SFV activity. Alternatively, since IFITM3-Y20A lacks interaction with AP-2, perhaps the internal pools are within different endosomal sub-populations, and therefore not present at the sites of SFV fusion (as may also be true for IFITM1).

While IFITM1 was unable to inhibit the SFV endocytic route of infection, it was capable of inhibiting infection by the flaviviruses DENV, ZIKV and YFV 17D. Flaviviruses are very similar to alphaviruses in that both rely on clathrin-mediated endocytosis (CME) and pH-dependent activation of type II fusion machinery for entry into cells [198, 199, 201]. There have been suggestions of DENV using alternate routes of entry, but in A549 cells it appears the virus uses CME and pH-dependent fusion [200]. However, while the entry pathways are very similar, there are clear differences in sensitivity to IFITM proteins. How IFITM1, a protein predominantly localised at the plasma membrane, is able to block the entry of viruses which fuse in the endosomal system remains unclear. As detected by EM, there are pools of IFITM1 within endosomal compartments (Fig. 3.5 [page 103]). However, since the expression level of IFITM proteins appears to influence their antiviral activity (Section 4.2.2), it seems unlikely that this low level of protein would be responsible for the observed inhibition. Unlike SFV, IFITM-mediated inhibition of flaviviruses was not altered by treatment with AmphoB (Fig. 5.1 [page 177], 5.2 [page 179] and 5.3 [page 180]),

and high concentrations of AmphoB had no impact on DENV infection (Fig. 5.4 [page 182). In agreement, previous studies have suggested that nystatin, a similar cholesterol binding compound, does not inhibit DENV infection of A549 cells [200] and that DENV does not require cholesterol for fusion [100]. It is therefore tempting to speculate that while IFITM3 appears to have enhanced potency towards SFV, potentially through the viral dependency on cholesterol, IFITM1 may have similarly lipid-based enhanced potency against flaviviruses. DENV has been shown to require anionic lipids for fusion [52], perhaps this plays a role in determining sensitivity to IFITM1.

Understanding whether there are indeed differences in the way IFITM proteins interact with membrane lipids, and what the determining features of these differences are will be an interesting source of future study. The CD225 domain of IFITM proteins is very highly conserved between all isoforms, and it is therefore speculated that that any IFITM protein determinants of these differences would reside in the NTD, CTD or second membrane interacting domain. Having developed the alphavirus and flavivirus systems in this work, there is now a platform to investigate these aspects of IFITM function, for instance, through the use of chimeric IFITM proteins.

As discussed in Chapter 1, relatively few viruses have been assessed for sensitivity towards IFITM proteins *in vivo*, compared to the work performed *in vitro*. However, a flavivirus, West Nile virus (WNV), has been examined. The work of Gorman *et al.* demonstrated that mice lacking Ifitm3 expression (*Ifitm3 -/-*) were more vulnerable to lethal WNV infection; implicating Ifitm3 in regulation of WNV pathogenesis [183]. This would be in keeping with results presented here showing that IFITM3 can inhibit the three flaviviruses in this work. It would be interesting to see if *Ifitm1 -/-* mice similarity suffer a more severe WNV infection, or whether *Ifitm -/-* have exacerbated severity to *Ifitim3 -/-* mice, to determine whether Ifitm1 plays roles for control of flavivirus infection *in vivo*, as suggested by the *in vitro* data here.

While the results with AmphoB potentially provide interesting insight into different underlying mechanism(s) of IFITM-mediated antiviral function, a caveat needed to be examined. It could have been the case that AmphoB treatment directly impacted the virus particle, either instead of, or potentially in addition to influencing IFITM activity. SFV has been shown to require cholesterol at sites of budding, and has cholesterol in the

host-derived lipid envelope [110]. It could therefore be the case that AmphoB is binding to SFV and altering the properties of the viral envelope, to make the virus more infectious in the presence of IFITM3 (although not of control A549 cells). This possibility was examined in Fig. 4.20 (page 163). In those experiments, treatment of IFITM3 expressing cells with 1 μM AmphoB for 10 min, prior to dilution to 1 nM for infection with SFV showed enhanced infection. Treating cells with 1 nM AmphoB alone had no impact on SFV infection of IFITM3 expressing cells, suggesting that the 10 min incubation with 1 μM AmphoB was enough to reduce IFITM3 anti-SFV activity. Conversely, treating SFV particles with 1 μM AmphoB for 10 min, then diluting to 1 nM for infecting cells did not boost SFV infection of IFITM3 expressing cells, arguing that AmphoB is not directly impacting the infectivity of SFV particles.

It is currently unclear why IFITM3-Y20A can inhibit DENV and ZIKV, but not YFV 17D infection. All three viruses fuse within endosomes, and are sensitive to IFITM3. There are high levels of IFITM3 in endosomes, perhaps explaining why this protein can inhibit all three viruses. As suggested above, the inhibition of flaviviruses by IFITM1 could be as a consequence of enhanced potency of IFITM1, so that even low levels of protein in endosomes can inhibit infection. However, the variable sensitivity of DENV/ZIKV and YFV 17D towards IFITM3-Y20A is puzzling. The 17D strain of YFV, as used here, has been shown to enter HeLa cells through a clathrin-independent, dynamin-dependent, caveolae-independent pathway [197], unlike DENV and wild-type YFV, which are internalised by CME [197–201]. It is therefore possible that these different routes of internalisation into a cell may alter sensitivity towards IFITM proteins; it would be an interesting experiment to determine whether wild-type YFV is sensitive to IFITM3-Y20A-mediated inhibition. Why the different IFITM isoforms may have impacts on different endocytic pathways remains to be explored.

While IFITM proteins could inhibit alphaviruses and flaviviruses, to varying extents, the results in Chapter 5 further extended published data that not all viruses which enter cells through endocytosis and pH-dependent fusion in endosomal compartments are inhibited by IFITM proteins (Table 1.3). The prototypical poxvirus VACV (Western Reserve strain mature virions) was not inhibited by any of the IFITMs tested in this study. Similar results have also been found in an RNAi screen for host factor influencing VACV replication

[195]. VACV has been suggested to enter cells by fusion directly at the plasma membrane [209], as well as through a pH-dependent mechanism [210] following macropinocytic uptake from the cell surface [211]. The ability of VACV to enter cells through two routes may influence the lack of IFITM-mediated inhibition. Alternatively, the membrane fusion mechanism used by VACV may be insensitive to the affects of IFITM proteins.

Relatively few viruses have been shown to be insensitive to IFITM-mediated inhibition, but one family consistently shown to have such a property are the arenaviruses. It has been suggested that arenaviruses enter cells through macropinocytic mechanisms [58, 212], similarly to VACV. It could therefore be speculated that viruses entering cells through this route may be refractory to IFITM-mediated inhibition, perhaps as a consequence of trafficking to different endosomal sub-populations. However, EBOV, which has also been shown to use macropinocytosis to internalise to cells [213, 214], is inhibited by IFITM proteins [139]. Therefore, why VACV and arenaviruses are refractory to IFITM-mediated inhibition remains unclear.

While VACV was insensitive to IFITM-mediated inhibition, an interesting phenotype was noticed in that VACV infection of IFITM expressing cells resulted in an enlarged plaque phenotype (Fig. 5.6 [page 186]). Upon infection of cells, VACV activates signalling pathways leading to cell motility (for instance [203]). However, the work presented in Fig. 5.9 (page 191) suggested that IFITM expressing cells are already intrinsically more motile than the non-expressing A549 controls. This increased motility likely accounts for the enlarged plaque phenotype, rather than IFITM proteins having a direct affect on the VACV-induced signalling. An enhancement of cell motility as a result of IFITM expression is interesting as IFITM proteins have been linked to cancer in numerous studies, although there is no clear consensus on the role they play; much of this work is reviewed in [204]. Additionally to the work cited in [204], IFITM proteins have been implicated in enhanced migration of gliomal cells [205, 206] and the progression and invasiveness of breast cancer [207]. It is currently unclear how IFITM protein expression enhances cell motility and, as discussed in Chapter 5, further work is required to confirm the phenotype. However, there could be interesting links between high levels of IFITM protein expression and a disruption to normal cell physiology which may be worth exploring.

6.3 Concluding Remarks

Through the work presented here a more detailed understanding of IFITM cell biology and antiviral activity has been generated. Clarity has been drawn over the membrane topology of the human IFN-inducible IFITM proteins and with this knowledge, a more detailed understanding of the cellular distribution of IFITM proteins, in A549 cells, has emerged. IFITM3 has been shown to inhibit alphavirus infection. A detailed analysis of the inhibition mechanism demonstrated that SFV is internalised by cells and delivered to acidic compartments, to activate the E1 fusion protein, but capsid release into the cytosol is prevented. The interpretation is that IFITM3 blocks fusion between SFV and cellular membranes. This mechanism of inhibition is the same as is proposed for inhibition of IAV and has the similar property of being modulated by AmphoB treatment. Studies with SFV, and flaviviruses, have provided interesting clues as to potential differences in the mode of action between different IFITMs. IFITM1 only modestly inhibited SFV infection when the virus fused at the plasma membrane, and had no impact on the endocytic route of entry. Comparatively, even though IFITM3 has a low abundance at the plasma membrane it still inhibited SFV infection by fusion at this site, suggesting a greater potency for inhibition compared to IFITM1. Conversely, flaviviruses entering cells through the normal endocytic route were sensitive to IFITM1, even though the majority of the protein is at the plasma membrane, suggesting IFITM1 may preferentially inhibit flavivirus infection. AmphoB treatment of cells had no impact on IFITM-mediated inhibition of flaviviruses, perhaps pointing towards differences in the fusion reactions between alphaviruses and flaviviruses, and/or differences in the mechanisms of IFITM antiviral function. Moreover, interesting results were found even within the flaviviruses tested since IFITM3-Y20A could inhibit DENV and ZIKV but not YFV 17D, perhaps suggesting differences in the fusion reactions between these viruses, or that different endocytic routes into the cell can alter IFITM sensitivity. Finally, even though SFV, DENV, ZIKV and YFV 17D, all of which enter cells through endocytic mechanisms and pH-dependent fusion, had some sensitivity to IFITM proteins, the poxvirus VACV did not. Understanding why certain viruses are sensitive to IFITMs while others are not, and understanding the sensitivity of different viruses towards different IFITMs will hopefully generate a far more detailed understanding of the precise molecular mechanisms underlying IFITM-mediated inhibition of viral infection.

Bibliography

1. Isaacs, A & Lindenmann, J. Virus interference. I. The interferon. *Proc. Roy. Soc. Lond. B. Biol. Sci.* **147,** 258–267 (1957).

2. Sen, G. Viruses and Interferons. *Annual Reviews Microbiology* **55,** 255–281 (2001).

3. Schoggins, J. W. *et al.* A diverse range of gene products are effectors of the type I interferon antiviral response. *Nature* **472,** 481–485 (2011).

4. Liu, S.-Y., Sanchez, D. J., Aliyari, R., Lu, S. & Cheng, G. Systematic identification of type I and type II interferon-induced antiviral factors. *Proceedings of the National Academy of Sciences* **109,** 4239–4244 (2012).

5. Schoggins, J. W. *et al.* Pan-viral specificity of IFN-induced genes reveals new roles for cGAS in innate immunity. *Nature* **505,** 691–695 (2014).

6. Li, J., Ding, S. C. & Cho, H. A Short Hairpin RNA Screen of Interferon-Stimulated Genes Identifies. *American Society for Microbiology* **4,** e00385–13 (2013).

7. Brass, A. L. *et al.* The IFITM proteins mediate cellular resistance to influenza A H1N1 virus, West Nile virus, and dengue virus. *Cell* **139,** 1243–54 (2009).

8. Perreira, J. M., Chin, C. R., Feeley, E. M. & Brass, A. L. IFITMs Restrict the Replication of Multiple Pathogenic Viruses. *Journal of Molecular Biology* **425,** 4937–4955 (2013).

9. Diamond, M. S. & Farzan, M. The broad-spectrum antiviral functions of IFIT and IFITM proteins. *Nature Reviews Immunology* **13,** 46–57 (2013).

10. Smith, S., Weston, S., Kellam, P. & Marsh, M. IFITM proteins - cellular inhibitors of viral entry. *Current Opinion in Virology* **4,** 71–77 (2014).

11. Bailey, C. C., Zhong, G., Huang, I.-C. & Farzan, M. IFITM-Family Proteins: The Cell's First Line of Antiviral Defense. *Annual Review of Virology* **1,** 261–283 (2014).

12. Feeley, E. M. *et al.* IFITM3 inhibits influenza A virus infection by preventing cytosolic entry. *PLoS Pathogens* **7,** e1002337 (2011).

13. Li, K. *et al.* IFITM Proteins Restrict Viral Membrane Hemifusion. *PLoS Pathogens* **9** (ed Emerman, M.) e1003124 (2013).

14. Desai, T. M. *et al.* IFITM3 Restricts Influenza A Virus Entry by Blocking the Formation of Fusion Pores following Virus-Endosome Hemifusion. *PLoS Pathogens* **10,** e1004048 (2014).

15. Weston, S. *et al.* A membrane topology model for human interferon inducible transmembrane protein 1. *PloS One* **9,** e104341 (2014).

16. Weston, S. *et al.* Alphavirus restriction by IFITM proteins. *Traffic* **17,** 997–1013 (2016).

17. WuDunn, D & Spear, P. G. Initial interaction of herpes simplex virus with cells is binding to heparan sulfate. *Journal of Virology* **63,** 52–58 (1989).

18. Chen, Y. *et al.* Dengue virus infectivity depends on envelope protein binding to target cell heparan sulfate. *Nature Medicine* **3,** 866–71 (1997).

19. Byrnes, A. P. & Griffin, D. E. Binding of Sindbis virus to cell surface heparan sulfate. *Journal of Virology* **72,** 7349–7356 (1998).

20. Schols, D *et al.* Sulphated polymers are potent and selective inhibitors of various enveloped viruses, including herpes simplex virus, vesicular stomatitis virus, respiratory syncytial virus, and toga-, arena-, and retroviruses. *Antiviral Chemistry & Chemotherapy* **1,** 233–240 (1990).

21. Marsh, M. & Helenius, A. Virus entry: open sesame. *Cell* **124,** 729–740 (2006).

22. Mercer, J., Schelhaas, M. & Helenius, A. Virus entry by endocytosis. *Annual Review of Biochemistry* **79,** 803–833 (2010).

23. Grove, J. & Marsh, M. The cell biology of receptor-mediated virus entry. *The Journal of Cell Biology* **195,** 1071–1082 (2011).

24. White, J. M., Delos, S. E., Brecher, M. & Schornberg, K. Structure and Mechanisms of Viral Membrane Fusion Proteins: Multiple variations on a common theme. *Critical Reviews in Biochemistry and Molecular Biology* **43,** 189–219 (2009).

25. Pearse, B. M. F. Clathrin: A unique protein associated with intracellualar transfer of membrane by coated vesicles. *Proceedings of the National Academy of Sciences* **73,** 1255–1259 (1976).

26. Ohno, H. *et al.* Interaction of Tyrosine-Based Sorting Signals with Clathrin-Associated Proteins. *Science* **269,** 21–24 (1995).

27. Honing, S. *et al.* Phosphatidylinositol-(4,5)-bisphosphate regulates sorting signal recognition by the clathrin-associated adaptor complex AP2. *Molecular Cell* **18,** 519–531 (2005).

28. Henne, W. M. *et al.* FCHo Proteins Are Nucleators of Clathrin-Mediated Endocytosis. *Science* **328,** 1281–1284 (2010).

29. Heuser, J. Three-dimensional visualization of coated vesicle formation in fibroblasts. *Journal of Cell Biology* **84,** 560–583 (1980).

30. Sweitzer, S. M. & Hinshaw, J. E. Dynamin undergoes a GTP-dependent conformational change causing vesiculation. *Cell* **93,** 1021–1029 (1998).

31. Schlossman, D. M., Schmid, S. L., Braell, W. A. & Rothman, J. E. An enzyme that removes clathrin coats: Purification of an uncoating ATPase. *Journal of Cell Biology* **99,** 723–733 (1984).

32. Doherty, G. J. & McMahon, H. T. Mechanisms of endocytosis. *Annual Review of Biochemistry* **78,** 857–902 (2009).

33. Mayor, S. & Pagano, R. E. Pathways of clathrin-independent endocytosis. *Nature Reviews. Molecular Cell Biology* **8,** 603–612 (2007).

34. Huotari, J. & Helenius, A. Endosome maturation. *The EMBO journal* **30,** 3481–3500 (2011).

35. Chavrier, P., Parton, R. G., Hauri, H. P., Simons, K. & Zerial, M. Localization of low molecular weight GTP binding proteins to exocytic and endocytic compartments. *Cell* **62,** 317–329 (1990).

36. Horiuchi, H. *et al.* A novel Rab5 GDP/GTP exchange factor complexed to Rabaptin-5 links nucleotide exchange to effector recruitment and function. *Cell* **90,** 1149–1159 (1997).

37. Zerial, M & McBride, H. Rab proteins as membrane organizers. *Nature Reviews Molecular Cell Biology* **2,** 107–117 (2001).

38. Wandinger-Ness, A. & Zerial, M. Rab Proteins and the Compatmentalization of the Endosomal System. *Cold Spring Harbor Perspectives in Biology* **6,** a022616 (2014).

39. Christoforidis, S *et al.* Phosphatidylinositol-3-OH kinases are Rab5 effectors. *Nature Cell Biology* **1,** 249–252 (1999).

40. Stenmark, H., Aasland, R., Toh, B. H. & D'Arrigo, A. Endosomal localization of the autoantigen EEA1 is mediated by a zinc- binding FYVE finger. *Journal of Biological Chemistry* **271,** 24048–24054 (1996).

41. Rink, J., Ghigo, E., Kalaidzidis, Y. & Zerial, M. Rab conversion as a mechanism of progression from early to late endosomes. *Cell* **122,** 735–749 (2005).

42. Vonderheit, A. & Helenius, A. Rab7 Associates with Early Endosomes to Mediate Sorting and Transport of Semliki Forest Virus to Late Endosomes. *PLoS Biology* **3,** e233 (2005).

43. Piper, R. C. & Katzmann, D. J. Biogenesis and Function of Multivesicular Bodies. *Annual Reviews Cell and Developmental Biology* **23,** 519–547 (2007).

44. Behnia, R. & Munro, S. Organelle identity and the signposts for membrane traffic. *Nature* **438,** 597–604 (2005).

45. Helenius, A, Kartenbeck, J, Simons, K & Fries, E. On the entry of Semliki forest virus into BHK-21 cells. *The Journal of Cell Biology* **84,** 404–420 (1980).

46. White, J, Kartenbeck, J & Helenius, A. Fusion of Semliki forest virus with the plasma membrane can be induced by low pH. *The Journal of Cell Biology* **87,** 264–272 (1980).

47. White, J & Helenius, A. pH-dependent fusion between the Semliki Forest virus membrane and liposomes. *Proceedings of the National Academy of Sciences* **77,** 3273–3277 (1980).

48. Kielian, M., Marsh, M & Helenius, A. Kinetics of endosome acidification detected by mutant and wild-type Semliki Forest virus. *The EMBO Journal* **5,** 3103–3109 (1986).

49. Maeda, T & Ohnishi, S.-I. Activation of influenza virus by acidic media causes hemolysis and fusion of erythrocytes. *FEBS Letters* **122,** 283–287 (1980).

50. White, J., Matlin, K. & HelenIus, A. Cell Fusion by Semliki Forest, Influenza, and Vesicular Stomatitis Viruses. *The Journal of Cell Biology* **89,** 674–679 (1981).

51. Skehel, J. J. *et al.* Changes in the conformation of influenza virus hemagglutinin at the pH optimum of virus-mediated membrane fusion. *Proceedings of the National Academy of Sciences* **79,** 968–972 (1982).

52. Zaitseva, E., Yang, S. T., Melikov, K., Pourmal, S. & Chernomordik, L. V. Dengue virus ensures its fusion in late endosomes using compartment-specific lipids. *PLoS Pathogens* **6** (2010).

53. Simmons, G. *et al.* Inhibitors of cathepsin L prevent severe acute respiratory syndrome coronavirus entry. *Proceedings of the National Academy of Sciences* **102,** 11876–11881 (2005).

54. Markosyan, R. M. *et al.* Induction of Cell-Cell Fusion by Ebola Virus Glycoprotein: Low pH Is Not a Trigger. *PLOS Pathogens* **12,** e1005373 (2016).

55. Carette, J. E. *et al.* Ebola virus entry requires the cholesterol transporter Niemann-Pick C1. *Nature* **477,** 340–3 (2011).

56. Sakurai, Y. *et al.* Two-pore channels control Ebola virus host cell entry and are drug targets for disease treatment. *Science* **347,** 995–998 (2015).

57. Cao, W *et al.* Identification of alpha-dystroglycan as a receptor for lymphocytic choriomeningitis virus and Lassa fever virus. *Science* **282,** 2079–2081 (1998).

58. Oppliger, J., Torriani, G., Herrador, A. & Kunz, S. Lassa virus cell entry via dystroglycan involves an unusual pathway of macropinocytosis. *Journal of Virology* **90,** 6412–6429 (2016).

59. Jae, L. T. *et al.* Lassa virus entry requires a trigger-induced receptor switch. *Science* **344,** 1506–1510 (2014).

60. Chang, A. & Dutch, R. E. Paramyxovirus fusion and entry: multiple paths to a common end. *Viruses* **4,** 613–36 (2012).

61. Akhtar, J. & Shukla, D. Viral entry mechanisms: Cellular and viral mediators of herpes simplex virus entry. *FEBS Journal* **276,** 7228–7236 (2009).

62. Moss, B. Membrane fusion during poxvirus entry. *Seminars in Cell & Developmental Biology* (2016).

63. Epand, R. M. Fusion peptides and the mechanism of viral fusion. *Biochimica et Biophysica Acta* **1614,** 116–121 (2003).

64. Kielian, M. Mechanisms of Virus Membrane Fusion Proteins. *Annual Review of Virology* **1,** 171–189 (2014).

65. Stieneke-Gröber, A *et al.* Influenza virus hemagglutinin with multibasic cleavage site is activated by furin, a subtilisin-like endoprotease. *The EMBO Journal* **11,** 2407–14 (1992).

66. Wilson, I. A., Skehel, J. J. & Wiley, D. C. Structure of the haemagglutinin membrane glycoprotein of influenza virus at 3 A resolution. *Nature* **289,** 366–373 (1981).

67. Wiley, D. C. & Skehel, J. J. The structure and function of the hemagglutinin membrane glycoprotein of influenza virus. *Annual Reviews Biochemistry* **56,** 365–394 (1987).

68. Lobigs, M & Garoff, H. Fusion function of the Semliki Forest virus spike is activated by proteolytic cleavage of the envelope glycoprotein precursor p62. *Journal of Virology* **64,** 1233–1240 (1990).

69. De Curtis, I & Simons, K. Dissection of Semliki Forest virus glycoprotein delivery from the trans-Golgi network to the cell surface in permeabilized BHK cells. *Proceedings of the National Academy of Sciences* **85,** 8052–8056 (1988).

70. Kielian, M., Chanel-Vos, C. & Liao, M. Alphavirus entry and membrane fusion. *Viruses* **2,** 796–825 (2010).

71. Wahlberg, J. M., Boere, W. A. & Garoff, H. The heterodimeric association between the membrane proteins of Semliki Forest virus changes its sensitivity to low pH during virus maturation. *Journal of Virology* **63,** 4991–4997 (1989).

72. Wahlberg, J. M. & Garoff, H. Membrane fusion process of Semliki Forest virus 1: low pH induced rearrangement in spike protein quarternary structure precedes virus penetration into cells. *Journal of Cell Biology* **116,** 339–348 (1992).

73. Wahlberg, J. M., Bron, R, Wilschut, J & Garoff, H. Membrane fusion of Semliki Forest virus involves homotrimers of the fusion protein. *Journal of Virology* **66,** 7309–7318 (1992).

74. Bron, R, Wahlberg, J. M., Garoff, H & Wilschut, J. Membrane fusion of Semliki Forest virus in a model system: correlation between fusion kinetics

and structural changes in the envelope glycoprotein. *The EMBO Journal* **12,** 693–701 (1993).

75. Roche, S., Bresanelli, S., Rey, F. A. & Gaudin, Y. Crystal Structure of the Low-pH Form of the Vesicular Stomatitis Virus Glycoprotein G. *Science* **313,** 187–191 (2006).

76. Heldwein, E. E. *et al.* Crystal structure of glycoprotein B from herpes simplex virus 1. *Science* **313,** 217–220 (2006).

77. Melikyan, G. B., Barnard, R. J. O., Abrahamyan, L. G., Mothes, W. & Young, J. A. T. Imaging individual retroviral fusion events: from hemifusion to pore formation and growth. *Proceedings of the National Academy of Sciences* **102,** 8728–8733 (2005).

78. Kielian, M. & Rey, F. A. Virus membrane-fusion proteins: more than one way to make a hairpin. *Nature Reviews Microbiology* **4,** 67–76 (2006).

79. Weissenhorn, W., Hinz, A. & Gaudin, Y. Virus membrane fusion. *FEBS Letters* **581,** 2150–2155 (2007).

80. Baquero, E. *et al.* Intermediate conformations during viral fusion glycoprotein structural transition. *Current Opinion in Virology* **3,** 143–150 (2013).

81. Smithburn, K. C. & Haddow, A. J. Semliki Forest Virus: I. Isolation and Pathogenic Properties. *The Journal of Immunology* **49,** 141–157 (1944).

82. Strauss, J. & Strauss, E. The alphaviruses: gene expression, replication, and evolution. *Microbiological Reviews* **58,** 491–562 (1994).

83. Kuhn, R. in *Fields' Virology* (eds Knipe, D. & Howley, P.) 1001–1022 (Philadelphia: Lippincott, Williams, & Wilkins, 2007).

84. Vogel, R. H., Provencher, S. W., von Bonsdorff, C. H., Adrian, M & Dubochet, J. Envelope structure of Semliki Forest virus reconstructed from cryo-electron micrographs. *Nature* **320,** 533–5 (1986).

85. Marsh, M. & Helenius, A. Adsorptive endocytosis of Semliki Forest virus. *Journal of Molecular Biology* **142,** 439–454 (1980).

86. Fries, E & Helenius, A. Binding of Semliki Forest virus and its spike glycoproteins to cells. *European Journal of Biochemistry* **97,** 213–220 (1979).

87. Cutler, D. F., Melancon, P & Garoff, H. Mutants of the membrane-binding region of Semliki Forest virus E2- protein: II. Topology and membrane-binding. *Journal Of Cell Biology* **102,** 902–910 (1986).

88. Doxsey, S. J., Brodsky, F. M., Blank, G. S. & Helenius, A. Inhibition of endocytosis by anti-clathrin antibodies. *Cell* **50,** 453–463 (1987).

89. DeTulleo, L. & Kirchhausen, T. The clathrin endocytic pathway in viral infection. *EMBO Journal* **17,** 4585–4593 (1998).

90. Sieczkarski, S. B. & Whittaker, G. R. Influenza Virus Can Enter and Infect Cells in the Absence of Clathrin-Mediated Endocytosis Influenza Virus Can Enter and Infect Cells in the Absence of Clathrin-Mediated Endocytosis. *Journal of Virology* **76,** 10455–10464 (2002).

91. Helenius, A *et al.* Human (HLA-A and HLA-B) and murine (H-2K and H-2D) histocompatibility antigens are cell surface receptors for Semliki Forest virus. *Proceedings of the National Academy of Sciences* **75,** 3846–3850 (1978).

92. Oldstone, M. B. *et al.* Does the major histocompatibility complex serve as a specific receptor for Semliki Forest virus? *Journal of Virology* **34,** 256–265 (1980).

93. Helenius, A, Marsh, M & White, J. Inhibition of Semliki forest virus penetration by lysosomotropic weak bases. *Journal of General Virology* **58,** 47–61 (1982).

94. Marsh, M., Wellsteed, J., Kern, H., Harms, E. & Helenius, A. Monensin inhibits Semliki Forest virus penetration into culture cells. *Proceedings of the National Academy of Sciences* **79,** 5297–5301 (1982).

95. Marsh, M., Bolzau, E. & Helenius, A. Penetration of Semliki Forest virus from acidic prelysosomal vacuoles. *Cell* **32,** 931–940 (1983).

96. Helenius, A, Kielian, M, Wellsteed, J, Mellman, I & Rudnick, G. Effects of monovalent cations on Semliki Forest virus entry into BHK-21 cells. *The Journal of Biological Chemistry* **260,** 5691–5697 (1985).

97. Marsh, M & Bron, R. SFV infection in CHO cells: cell-type specific restrictions to productive virus entry at the cell surface. *Journal of Cell Science* **110,** 95–103 (1997).

98. Gibbons, D. L. *et al.* Conformational change and protein-protein interactions of the fusion protein of Semliki Forest virus. *Nature* **427,** 320–325 (2004).

99. Ahn, A., Gibbons, D. L. & Kielian, M. The Fusion Peptide of Semliki Forest Virus Associates with Sterol-Rich Membrane Domains. *Journal of Virology* **76,** 3267–3275 (2002).

100. Umashankar, M *et al.* Differential cholesterol binding by class II fusion proteins determines membrane fusion properties. *Journal of Virology* **82,** 9245–9253 (2008).

101. Irurzun, A., Nieva, J. L. & Carrasco, L. Entry of Semliki forest virus into cells: effects of concanamycin A and nigericin on viral membrane fusion and infection. *Virology* **227,** 488–492 (1997).

102. Markosyan, R. M., Kielian, M. & Cohen, F. S. Fusion induced by a class II viral fusion protein, semliki forest virus E1, is dependent on the voltage of the target cell. *Journal of Virology* **81,** 11218–25 (2007).

103. Singh, I & Helenius, A. Role of ribosomes in Semliki Forest virus nucleocapsid uncoating. *Journal of Virology* **66,** 7049–7058 (1992).

104. Garoff, H, Simons, K & Dobberstein, B. Assembly of the Semliki Forest Virus Membrane Glycoproteins in the Membrane of the Endoplasmatic Reticulum in Vitro. *Journal of Molecular Biology* **124,** 587–600 (1978).

105. Melancon, P & Garoff, H. Reinitiation of translocation in the Semliki Forest virus structural polyprotein: identification of the signal for the E1 glycoprotein. *The EMBO journal* **5,** 1551–1560 (1986).

106. Lobigs, M, Zhao, H. X. & Garoff, H. Function of Semliki Forest virus E3 peptide in virus assembly: replacement of E3 with an artificial signal peptide abolishes spike heterodimerization and surface expression of E1. *Journal of Virology* **64,** 4346–4355 (1990).

107. Zhang, X., Fugère, M., Day, R. & Kielian, M. Furin processing and proteolytic activation of Semliki Forest virus. *Journal of virology* **77,** 2981–2989 (2003).

108. Uchime, O., Fields, W. & Kielian, M. The role of E3 in pH protection during alphavirus assembly and exit. *Journal of Virology* **87,** 10255–10262 (2013).

109. Suomalainen, M, Liljestrom, P & Garoff, H. Spike protein-nucleocapsid interactions drive the budding of alphaviruses. *Journal of Virology* **66,** 4737–4747 (1992).

110. Marquardt, M. T., Phalen, T. & Kielian, M. Cholesterol is required in the exit pathway of Semliki Forest virus. *Journal of Cell Biology* **123,** 57–65 (1993).

111. Martinez, M. G., Snapp, E.-L., Perumal, G. S., Macaluso, F. P. & Kielian, M. Imaging the Alphavirus Exit Pathway. *Journal of Virology* **88,** 6922–6933 (2014).

112. Jose, J., Snyder, J. & Kuhn, R. A structural and functional perspective of alphavirus replication and assembly. *Future Microbiology* **4,** 837–856 (2009).

113. Friedman, R. L., Manly, S. P., McMahon, M, Kerr, I. M. & Stark, G. R. Transcriptional and posttranscriptional regulation of interferon-induced gene expression in human cells. *Cell* **38,** 745–55 (1984).

114. Chen, Y. X., Welte, K, Gebhard, D. H. & Evans, R. L. Induction of T cell aggregation by antibody to a 16kd human leukocyte surface antigen. *Journal of Immunology* **133,** 2496–2501 (1984).

115. Evans, S. S., Lee, D. B., Han, T, Tomasi, T. B. & Evans, R. L. Monoclonal antibody to the interferon-inducible protein Leu-13 triggers aggregation and inhibits proliferation of leukemic B cells. *Blood* **76,** 2583–2593 (1990).

116. Takahashi, S, Doss, C, Levy, S & Levy, R. TAPA-1, the target of an antiproliferative antibody, is associated on the cell surface with the Leu-13 antigen. *Journal of Immunology* **145,** 2207–2213 (1990).

117. Bradbury, L. E., Goldmacher, V. S. & Tedder, T. F. The CD19 signal transduction complex of B lymphocytes. Deletion of the CD19 cytoplasmic domain alters signal transduction but not complex formation with TAPA-1 and Leu 13. *Journal of Immunology* **151,** 2915–27 (1993).

118. Frey, M., Appenheimer, M. M. & Evans, S. S. Tyrosine kinase-dependent regulation of L-selectin expression through the Leu-13 signal transduction molecule: evidence for a protein kinase C-independent mechanism of L-selectin shedding. *The Journal of Immunology* **158,** 5424–5434 (1997).

119. Sato, S, Miller, A. S., Howard, M. C. & Tedder, T. F. Regulation of B lymphocyte development and activation by the CD19/CD21/CD81/Leu 13 complex requires the cytoplasmic domain of CD19. *Journal of Immunology* **159,** 3278–87 (1997).

120. Tanaka, S. S. & Matsui, Y. Developmentally regulated expression of mil-1 and mil-2, mouse interferon-induced transmembrane protein like genes, during formation and differentiation of primordial germ cells. *Mechanisms of Development* **119S,** S261–7 (2002).

121. Saitou, M., Barton, S. C. & Surani, M. A. A molecular programme for the specification of germ cell fate in mice. *Nature* **418,** 293–300 (2002).

122. Tanaka, S. S. *et al.* Regulation of expression of mouse interferon-induced transmembrane protein like gene-3, Ifitm3 (mil-1, fragilis), in germ cells. *Developmental Dynamics* **230,** 651–659 (2004).

123. Tanaka, S. S., Yamaguchi, Y. L., Tsoi, B., Lickert, H. & Tam, P. P. L. IFITM/Mil/fragilis family proteins IFITM1 and IFITM3 play distinct roles in mouse primordial germ cell homing and repulsion. *Developmental Cell* **9,** 745–756 (2005).

124. Lange, U. C. *et al.* Normal germ line establishment in mice carrying a deletion of the Ifitm/Fragilis gene family cluster. *Molecular and Cellular Biology* **28,** 4688–4696 (2008).

125. Alber, D. & Staeheli, P. *Partial inhibition of vesicular stomatitis virus by the interferon-induced human 9-27 protein.* 1996.

126. Hickford, D., Frankenberg, S., Shaw, G. & Renfree, M. B. Evolution of vertebrate interferon inducible transmembrane proteins. *BMC Genomics* **13,** 155 (2012).

127. Sällman Almén, M., Bringeland, N., Fredriksson, R. & Schiöth, H. B. The dispanins: a novel gene family of ancient origin that contains 14 human members. *PloS one* **7,** e31961 (2012).

128. Zhang, Z., Liu, J., Li, M., Yang, H. & Zhang, C. Evolutionary dynamics of the interferon-induced transmembrane gene family in vertebrates. *PloS One* **7,** e49265 (2012).

129. Moffatt, P. & Gaumond, M. Bril : A Novel Bone-Specific Modulator of Mineralization. *Journal of Bone and Mineral Research* **23,** 1497–1508 (2008).

130. Xu, J. *et al.* Swine interferon-induced transmembrane protein, sIFITM3, inhibits foot-and-mouth disease virus infection in vitro and in vivo. *Antiviral Research* **109,** 22–29 (2014).

131. Lanz, C., Yángüez, E., Andenmatten, D. & Stertz, S. Swine Interferon-Inducible Transmembrane Proteins Potently Inhibit Influenza A Virus Replication. *Journal of Virology* **89,** 863–869 (2015).

132. Benfield, C., Benfield, C., Smith, S. E., Wash, R. S. & Temperton, N. J. Bat and pig Interferon-Induced Transmembrane Protein 3 restrict cell entry by influenza virus and lyssaviruses. *Journal of General Virology* **96,** 991–1005 (2015).

133. Compton, A. A. *et al.* Natural mutations in IFITM 3 modulate post-translational regulation and toggle antiviral specificity. *EMBO Reports* **Epub ahead,** e201642771 (2016).

134. Smith, S. E. *et al.* Chicken IFITM3 restricts Influenza viruses and Lyssaviruses in vitro. *Journal of Virology* **87,** 12957–12966 (2013).

135. Blyth, G. A. D., Chan, W.-F., Webster, R. G. & Magor, K. E. Duck IFITM3 mediates restriction of influenza viruses. *Journal of Virology* **90,** 103–116 (2015).

136. Melvin, W., McMichael, T., Chesarino, N., Hach, J. & Yount, J. IFITMs from Mycobacteria Confer Resistance to Influenza Virus When Expressed in Human Cells. *Viruses* **7,** 3035–3052 (2015).

137. Mudhasani, R. *et al.* Ifitm-2 and Ifitm-3 But Not Ifitm-1 Restrict Rift Valley Fever Virus. *Journal of Virology* **87,** 8451–8464 (2013).

138. Wrensch, F., Winkler, M. & Pöhlmann, S. IFITM Proteins Inhibit Entry Driven by the MERS-Coronavirus Spike Protein: Evidence for Cholesterol-Independent Mechanisms. *Viruses* **6,** 3683–3698 (2014).

139. Huang, I. *et al.* Distinct patterns of IFITM-mediated restriction of filoviruses, SARS coronavirus, and influenza A virus. *PLos Pathogens* **7,** e1001258 (2011).

140. Zhao, X. *et al.* Interferon induction of IFITM proteins promotes infection by human coronavirus OC43. *Proceedings of the National Academy of Sciences* **111,** 6756–6761 (2014).

141. Warren, C. J. *et al.* The Antiviral Restriction Factors IFITM1, 2 and 3 Do Not Inhibit Infection of Human Papillomavirus, Cytomegalovirus and Adenovirus. *PLoS One* **9,** e96579 (2014).

142. Wrensch, F. *et al.* Interferon-Induced Transmembrane Protein-Mediated Inhibition of Host Cell Entry of Ebolaviruses. *Journal of Infectious Diseases* **212,** S219–S218 (2015).

143. Jia, R. *et al.* Identification of an endocytic signal essential for the antiviral action of IFITM3. *Cellular Microbiology* **16,** 1080–1093 (2014).

144. Chan, Y. K., Huang, I.-C. & Farzan, M. IFITM proteins restrict antibody-dependent enhancement of dengue virus infection. *PloS One* **7,** e34508 (2012).

145. Wilkins, C. *et al.* IFITM1 is a tight junction protein that inhibits hepatitis C virus entry. *Hepatology* **57,** 461–469 (2013).

146. Narayana, S. K. *et al.* The interferon-induced transmembrane proteins - IFITM1, IFITM2 and IFITM3 inhibit hepatitis C virus entry. *Journal of Biological Chemistry* **23,** 25946–25959 (2015).

147. Jiang, D. *et al.* Identification of five interferon-induced cellular proteins that inhibit west nile virus and dengue virus infections. *Journal of Virology* **84,** 8332–8341 (2010).

148. Savidis, G. *et al.* The IFITMs Inhibit Zika Virus Replication. *Cell Reports* **15,** 2323–2330 (2016).

149. Zhang, W. *et al.* Human respiratory syncytial virus infection is inhibited by IFN-induced transmembrane proteins. *Journal of General Virology* **96,** 170–182 (2015).

150. Yount, J. S. *et al.* Palmitoylome profiling reveals S-palmitoylation-dependent antiviral activity of IFITM3. *Nature Chemical Biology* **6,** 610–614 (2010).

151. Yount, J. S., Karssemeijer, R. a. & Hang, H. C. S-palmitoylation and ubiquitination differentially regulate interferon-induced transmembrane protein 3 (IFITM3)-mediated resistance to influenza virus. *The Journal of Biological Chemistry* **287,** 19631–19641 (2012).

152. Amini-Bavil-Olyaee, S. *et al.* The Antiviral Effector IFITM3 Disrupts Intracellular Cholesterol Homeostasis to Block Viral Entry. *Cell Host & Microbe* **13,** 452–464 (2013).

153. Bailey, C. C., Kondur, H. R., Huang, I.-C. & Farzan, M. Interferon-Induced Transmembrane Protein 3 is a Type II Transmembrane Protein. *The Journal of Biological Chemistry* **288,** 32184–32193 (2013).

154. John, S. P. *et al.* The CD225 Domain of IFITM3 is Required for both IFITM Protein Association and Inhibition of Influenza A Virus and Dengue Virus Replication. *Journal of Virology* **87,** 7837–7852 (2013).

155. Hach, J. C., McMichael, T., Chesarino, N. M. & Yount, J. S. Palmitoylation on conserved and nonconserved cysteines of murine IFITM1 regulates its stability and anti-influenza A virus activity. *Journal of Virology* **87,** 9923–9927 (2013).

156. Lin, T.-Y. *et al.* Amphotericin B Increases Influenza A Virus Infection by Preventing IFITM3-Mediated Restriction. *Cell Reports* **5,** 895–908 (2013).

157. Shan, Z. *et al.* Negative Regulation of Interferon-Induced Transmembrane Protein 3 by SET7-mediated Lysine Monomethylation. *The Journal of Biological Chemistry* **288,** 35093–35103 (2013).

158. Chesarino, N. M., McMichael, T. M., Hach, J. C. & Yount, J. S. Phosphorylation of the Antiviral Protein IFITM3 Dually Regulates its Endocytosis and Ubiquitination. *The Journal of Biological Chemistry* **289,** 11986–11992 (2014).

159. Li, K. *et al.* A sorting signal suppresses ifitm1 restriction of viral entry. *The Journal of Biological Chemistry* **290,** 4248–4259 (2015).

160. Chesarino, N. M., McMichael, T. M. & Yount, J. S. E3 Ubiquitin Ligase NEDD4 Promotes Influenza Virus Infection by Decreasing Levels of the Antiviral Protein IFITM3. *PLoS Pathogens* **11,** e1005095 (2015).

161. Anafu, A. a., Bowen, C. H., Chin, C. R., Brass, A. L. & Holm, G. H. Interferon Inducible Transmembrane Protein 3 (IFITM3) Restricts Reovirus Cell Entry. *The Journal of Biological Chemistry* **288,** 17261–17271 (2013).

162. Lu, J. *et al.* The IFITM proteins inhibit HIV-1 infection. *Journal of Virology* **85,** 2126–37 (2011).

163. Jia, R. *et al.* The N-Terminal Region of IFITM3 Modulates Its Antiviral Activity by Regulating IFITM3 Cellular Localization. *Journal of Virology* **86,** 13697–13707 (2012).

164. Chutiwitoonchai, N. *et al.* Characteristics of IFITM, the newly identified IFN-inducible anti-HIV-1 family proteins. *Microbes & Infection* **15,** 280–290 (2013).

165. Ding, S., Pan, Q., Liu, S.-L. & Liang, C. HIV-1 mutates to evade IFITM1 restriction. *Virology* **454-455,** 11–24 (2014).

166. Compton, A. A. *et al.* IFITM Proteins Incorporated into HIV-1 Virions Impair Viral Fusion and Spread. *Cell Host & Microbe* **16,** 736–747 (2014).

167. Tartour, K. *et al.* IFITM proteins are incorporated onto HIV-1 virion particles and negatively imprint their infectivity. *Retrovirology* **11** (2014).

168. Qian, J. *et al.* Primate lentiviruses are differentially inhibited by interferon-induced transmembrane proteins. *Virology* **474,** 10–18 (2015).

169. Foster, T. L. *et al.* Resistance of Transmitted Founder HIV-1 to IFITM-Mediated Restriction. *Cell Host & Microbe* **20,** 429–442 (2016).

170. Weidner, J. M. *et al.* Interferon-induced cell membrane proteins, IFITM3 and tetherin, inhibit vesicular stomatitis virus infection via distinct mechanisms. *Journal of Virology* **84,** 12646–12657 (2010).

171. Xie, M. *et al.* Human Cytomegalovirus Exploits Interferon-Induced Transmembrane Proteins to Facilitate Morphogenesis of the Virion Assembly Compartment. *Journal of Virology* **89,** 3049–3061 (2015).

172. Van Meer, G., Voelker, D. R. & Feigenson, G. W. Membrane lipids: where they are and how they behave. *Nature Reviews Molecular Cell Biology* **9,** 112–124 (2008).

173. Yu, J. *et al.* IFITM Proteins Restrict HIV-1 Infection by Antagonizing the Envelope Glycoprotein. *Cell Reports* **13,** 145–156 (2015).

174. Everitt, A. R. *et al.* IFITM3 restricts the morbidity and mortality associated with influenza. *Nature* **484,** 519–23 (2012).

175. Bailey, C. C., Huang, I.-C., Kam, C. & Farzan, M. Ifitm3 limits the severity of acute influenza in mice. *PLoS pathogens* **8,** e1002909 (2012).

176. Wakim, L. M., Gupta, N., Mintern, J. D. & Villadangos, J. a. Enhanced survival of lung tissue-resident memory CD8 T cells during infection with influenza virus due to selective expression of IFITM3. *Nature Immunology* **14,** 238–245 (2013).

177. Zhang, Y.-H. *et al.* Interferon-induced transmembrane protein-3 genetic variant rs12252-C is associated with severe influenza in Chinese individuals. *Nature Communications* **4,** 1418 (2013).

178. Mills, T., Rautanen, A. & Elliott, K. IFITM3 and susceptibility to respiratory viral infections in the community. *Joural of Infectious Diseases* **209,** 1028–1031 (2014).

179. Wang, Z. *et al.* Early hypercytokinemia is associated with interferon-induced transmembrane protein-3 dysfunction and predictive of fatal H7N9 infection. *Proceedings of the National Academy of Sciences* **111,** 769–774 (2014).

180. Xuan, Y *et al.* IFITM3 rs12252 T>C polymorphism is associated with the risk of severe influenza: a meta-analysis. *Epidemiology and Infection* **143,** 2975–2984 (2015).

181. Zhang, Y. *et al.* Interferon-induced transmembrane protein-3 rs12252-C is associated with rapid progression of acute HIV-1 infection in Chinese MSM cohort. *AIDS* **29,** 889–94 (2015).

182. Everitt, A. R. *et al.* Defining the range of pathogens susceptible to ifitm3 restriction using a knockout mouse model. *PloS one* **8,** e80723 (2013).

183. Gorman, M. J., Poddar, S., Farzan, M. & Diamond, M. S. The interferon-stimulated gene IFITM3 restricts West Nile virus infection and pathogenesis. *Journal of Virology* **26,** 8212–8215 (2016).

184. Poddar, S., Hyde, J. L., Gorman, M. J., Farzan, M. & Diamond, M. S. The interferon-stimulated gene IFITM3 restricts infection and pathogenesis of arthritogenic and encephalitic alphaviruses. *Journal of Virology* **90,** 8780–8794 (2016).

185. Jia, R. *et al.* The C-Terminal Sequence of IFITM1 Regulates Its Anti-HIV-1 Activity. *PLoS One* **10,** e0118794 (2015).

186. Bonifacino, J. S. & Traub, L. M. Signals for sorting of transmembrane proteins to endosomes and lysosomes. *Annual Review of Biochemistry* **72,** 395–447 (2003).

187. Williams, D. E. J. *et al.* IFITM3 Polymorphism rs12252-C Restricts Influenza A Viruses. *PloS One* **9,** e110096 (2014).

188. Fraile-Ramos, A *et al.* The human cytomegalovirus US28 protein is located in endocytic vesicles and undergoes constitutive endocytosis and recycling. *Molecular Biology of the Cell* **12,** 1737–1749 (2001).

189. Bolte, S & Cordelières, F. P. A guided tour into subcellular colocalization analysis in light microscopy. *Journal of Microscopy* **224,** 213–232 (2006).

190. Reynolds, E. S. The use of lead citrate at high pH as an electron-opaque stain in electron microscopy. *The Journal of Cell Biology* **17,** 208–212 (1963).

191. Slot, J. W., Geuze, H. J., Gigengack, S, Lienhard, G. E. & James, D. E. Immuno-localization of the insulin regulatable glucose transporter in brown adipose tissue of the rat. *The Journal of Cell Biology* **113,** 123–135 (1991).

192. Ling, S. *et al.* Combined approaches of EPR and NMR illustrate only one transmembrane helix in the human IFITM3. *Scientific Reports* **6,** 24029 (2016).

193. Schmid, S, Fuchs, R, Kielian, M, Helenius, A & Mellman, I. Acidification of endosome subpopulations in wild-type Chinese hamster ovary cells and temperature-sensitive acidification-defective mutants. *The Journal of Cell Biology* **108,** 1291–1300 (1989).

194. Gibbons, D. L. *et al.* Multistep Regulation of Membrane Insertion of the Fusion Peptide of Semliki Forest Virus. *Journal of Virology* **78,** 3312–3318 (2004).

195. Beard, P. M. *et al.* A loss of function analysis of host factors influencing Vaccinia virus replication by RNA interference. *PloS one* **9,** e98431 (2014).

196. Hahn, C. S., Dalrymple, J. M., Strauss, J. H. & Rice, C. M. Comparison of the virulent Asibi strain of yellow fever virus with the 17D vaccine strain derived from it. *Proceedings of the National Academy of Sciences* **84,** 2019–2023 (1987).

197. Fernandez Garcia, Jouvenet, A. Vaccine and Wild-Type Strains of Yellow Fever Virus Engage Distinct Entry Mechanisms and Differentially Stimulate Antiviral Immune. *mBio* **7,** 1–15 (2016).

198. Krishnan, M. N. *et al.* Rab 5 is required for the cellular entry of dengue and West Nile viruses. *Journal of Virology* **81,** 4881–4885 (2007).

199. Van Der Schaar, H. M. *et al.* Dissecting the cell entry pathway of dengue virus by single-particle tracking in living cells. *PLoS Pathogens* **4,** e1000244 (2008).

200. Acosta, E. G., Castilla, V. & Damonte, E. B. Alternative infectious entry pathways for dengue virus serotypes into mammalian cells. *Cellular Microbiology* **11,** 1533–1549 (2009).

201. Ang, F., Wong, A. P. Y., Ng, M. M.-L. & Chu, J. J. H. Small interference RNA profiling reveals the essential role of human membrane trafficking genes in mediating the infectious entry of dengue virus. *Virology Journal* **7,** 24 (2010).

202. Bidgood, S. R. & Mercer, J. Cloak and dagger: Alternative immune evasion and modulation strategies of poxviruses. *Viruses* **7,** 4800–4825 (2015).

203. Valderrama, F., Cordeiro, J. V., Schleich, S., Frischknecht, F. & Way, M. Vaccinia virus-induced cell motility requires F11L-mediated inhibition of RhoA signaling. *Science* **311,** 377–381 (2006).

204. Siegrist, F., Ebeling, M. & Certa, U. The small interferon-induced transmembrane genes and proteins. *Journal of Interferon & Cytokine Research* **31,** 183–197 (2011).

205. Yu, F. *et al.* Knockdown of interferon-induced transmembrane protein 1 (IFITM1) inhibits proliferation, migration, and invasion of glioma cells. *Journal of Neuro-Oncology* **103,** 187–95 (2011).

206. Zhao, B., Wang, H., Zong, G. & Li, P. The role of IFITM3 in the growth and migration of human glioma cells. *BMC Neurology* **13,** 210 (2013).

207. Yang, M., Gao, H., Chen, P., Jia, J. & Wu, S. Knockdown of interferon-induced transmembrane protein 3 expression suppresses breast cancer cell growth and colony formation and affects the cell cycle. *Oncology Reports* **30,** 171–178 (2013).

208. Ranjbar, S., Haridas, V., Jasenosky, L. D., Falvo, J. V. & Goldfeld, A. E. A Role for IFITM Proteins in Restriction of Mycobacterium tuberculosis Infection. *Cell Reports* **13,** 874–883 (2015).

209. Carter, G. C., Law, M., Hollinshead, M. & Smith, G. L. Entry of the vaccinia virus intracellular mature virion and its interactions with glycosaminoglycans. *Journal of General Virology* **86,** 1279–1290 (2005).

210. Townsley, A. C., Weisberg, A. S., Wagenaar, T. R. & Moss, B. Vaccinia virus entry into cells via a low-pH-dependent endosomal pathway. *Journal of Virology* **80,** 8899–8908 (2006).

211. Mercer, J. & Helenius, A. Vaccinia virus uses macropinocytosis and apoptotic mimicry to enter host cells. *Science* **320,** 531–535 (2008).

212. Iwasaki, M., Ngo, N. & de la Torre, J. C. Sodium hydrogen exchangers contribute to arenavirus cell entry. *Journal of Virology* **88,** 643–654 (2014).

213. Nanbo, A. *et al.* Ebolavirus is internalized into host cells via macropinocytosis in a viral glycoprotein-dependent manner. *PLoS Pathogens* **6,** e1001121 (2010).

214. Saeed, M. F., Kolokoltsov, A. A., Albrecht, T. & Davey, R. A. Cellular entry of ebola virus involves uptake by a macropinocytosis-like mechanism and subsequent trafficking through early and late endosomes. *PLoS Pathogens* **6,** e1001110 (2010).

Appendix

Please find attached within this appendix, articles that have been published from data presented in this thesis. These have been referenced throughout the thesis [10, 15, 16]. The articles are presented in chronological order of publication.

Available online at www.sciencedirect.com

ScienceDirect

Current Opinion in Virology

IFITM proteins — cellular inhibitors of viral entry

SE Smith[1], S Weston[2], P Kellam[1,3] and M Marsh[2]

Interferon inducible transmembrane (IFITM) proteins are a recently discovered family of cellular anti-viral proteins that restrict the replication of a number of enveloped and non-enveloped viruses. IFITM proteins are located in the plasma membrane and endosomal membranes, the main portals of entry for many viruses. Biochemical and membrane fusion studies suggest IFITM proteins have the ability to inhibit viral entry, possibly by modulating the fluidity of cellular membranes. Here we discuss the IFITM proteins, recent work on their mode of action, and future directions for research.

Addresses
[1] Wellcome Trust Sanger Institute, Wellcome Trust Genome Campus, Hinxton CB10 1SA, UK
[2] MRC Laboratory for Molecular Cell Biology, University College London, Gower Street, London WC1E 6BT, UK
[3] MRC/UCL Centre for Medical Molecular Virology, Division of Infection and Immunity, University College London, Gower Street, London WC1E 6BT, UK

Corresponding authors: Kellam, P (pk5@sanger.ac.uk) and Marsh, M (m.marsh@ucl.ac.uk)

Current Opinion in Virology 2014, **4**:71–77

This review comes from a themed issue on **Virus entry**

Edited by **Mark Marsh** and **Jane A McKeating**

For a complete overview see the Issue and the Editorial

Available online 28th January 2014

1879-6257/$ – see front matter,

http://dx.doi.org/10.1016/j.coviro.2013.11.004

Introduction

In recent years, studies of innate defence mechanisms have identified a number of cellular proteins that interfere with the replication of human and animal viruses. Many of these so-called 'restriction factors' have been most intensively studied for human immunodeficiency virus (HIV-1). For example, tripartite motif-containing protein 5 (TRIM5) [1], APOBEC3G [2], 2′,3′-cyclic-nucleotide 3′-phosphodiesterase [3] and tetherin [4] have been found to affect uncoating, reverse transcription, virus assembly and virus release, respectively. A new addition to this antiviral repertoire is myxoma resistance protein B (MxB/Mx2) [5] that inhibits HIV-1 at a late post-entry step. However, restriction factors for other viruses have also been identified, including: RNA-activated protein kinase (PKR), that restricts Hepatitis C and other viruses [6]; MX1, that restricts influenza A virus (IAV) and measles virus [7]; and 2′-5′-oligoadenylate synthase/RNase L, that restricts Hepatitis C and other viruses [8]. Many of these factors are components of the broad antiviral response induced by interferons, collectively known as interferon stimulated genes (ISGs: for review see [9]).

Although recognised to act at different stages in viral replication cycles, most of the well-characterised restriction factors affect steps following virus entry. Recently, a new family of proteins has been identified that appears to act specifically on virus entry, the interferon inducible transmembrane (IFITM) proteins. Here we review the antiviral capacity of three of these proteins, IFITM1–3.

Identification of IFITMs

The IFITM gene family was initially identified more than 20 years ago [10], with particular interest in the interferon-stimulated response elements (ISREs) they contained. The IFITM transcripts were originally named 9-27, 1-8D and 1-8U, however, the antiviral properties of the encoded proteins were only identified in 2009 in an RNAi screen for host factors that influence IAV replication. Knock-down of IFITM3 led to enhanced viral replication. Conversely, overexpression of IFITM1, 2, or 3 inhibited early viral replication [11•].

Subsequent genome analyses have indicated that the IFITM genes are likely to have arisen by gene duplication very early in vertebrate evolution [12], since 'lower' vertebrates, such as lampreys, possess at least one *IFITM*-like gene [13]. To date, five *IFITM* genes have been identified in humans, of which *IFITM1*, *2*, *3* and *5* are clustered within a 26 kb region towards the telomere on the short arm of chromosome 11. *IFITM5* is not IFN inducible and is involved in bone mineralisation [14]. The fifth gene, *IFITM10*, is located 1.4 Mb towards the centromere, but little is known about its function. *IFITM4* is not present in humans, but is located close to *Ifitm1*, *2*, *3*, and *5* in the mouse genome [15], in which the locus has expanded to encode seven *Ifitm* genes. Analogous genes have also been found in other mammals [12], including marsupials [13], and avian species [16].

Although the molecular function of these proteins has been largely studied in cell culture systems, studies in mice and humans suggest IFITM proteins, and IFITM3 in particular, restrict IAV infection *in vivo*. *Ifitm3*$^{-/-}$ mice fail to control infection by mildly-pathogenic strains of IAV compared to their wild type littermates, developing fatal fulminant viral pneumonia [17•,18]. Everitt *et al.* also found that the minor C allele of human *IFITM3* (synonymous single nucleotide polymorphism (SNP) rs12252) was enriched in a cohort of Caucasian patients

hospitalised with either IAV H1N1/09 or influenza B in the 2009 pandemic [17•]. Although the C allele is rare in Caucasians, replication of this genetic association was shown in a cohort of Han Chinese patients (the SNP is more prevalent in this population) with severe symptoms following influenza infection. The minority CC genotype was found in 69% of patients with severe disease compared to only 25% with mild symptoms [19], further suggesting that deleterious changes in the *IFITM3* gene can influence the severity of influenza infection. It is currently unclear how this allele impacts IAV pathogenesis, but the alteration of a splice acceptor site may lead to the synthesis of a truncated IFITM3 protein that lacks the N-terminal 21 amino acids, and is expressed primarily on the cell surface rather than in endosomes (see below) [17•,20]. Aside from rs12252, little investigation has been carried out into other SNPs reported for IFITM3. One study carried out by John *et al.* [21] made alterations of non-synonymous SNPs H3Q/rs1136853, D56G/rs55794999, H57D/rs1553883, N69D/rs12778, and G95R/rs61744108, with only G95R showing a small reduction in IAV restriction compared to wild type.

Broad-spectrum antiviral function

Using cell culture systems, and often pseudotype viruses, several groups demonstrated that, in addition to IAV, entry and infection by representatives of multiple virus families (including filoviruses, rhabdoviruses and flaviviruses) [22•,23,24] were also inhibited by overexpression of IFITMs, particularly IFITM3 (see Table 1). Interestingly, these restricted viruses are all enveloped, with ssRNA genomes, and considered to enter cells by membrane fusion following endocytosis. However, some retroviruses (e.g. Moloney leukaemia virus (MLV)) and several arenaviruses were apparently not restricted. Although restriction of HIV-1 infection was not initially detected [11•], several more recent studies have reported some restriction of cell infection [20,25,26]. Most

Table 1

Summary of viruses IFITM proteins have been tested against

Family	Virus	pH dependent	Restricts infectivity	Prevents cell–cell fusion	Pseudotyped virions (P) or live virus (L)	Restriction status	Reference
Enveloped							
Orthomyxoviridae	Influenza A virus	✓✓	✓	✓	P L	M1–3	Brass *et al.* [11•], Smith *et al.* [16]
	Influenza B virus	✓✓	✓		L	M1–3	Everitt et al. [17•]
Flaviviridae	West Nile virus	✓	✓		P	M1–3	Brass *et al.* [11•]
	Dengue virus	✓✓	✓		P	M1–3	Brass *et al.* [11•]
	Hepatitis C virus	✓	✓/×		P L	M3 — no, M1 — yes	Brass *et al.* [11•], Wilkins *et al.* [24]
Rhabdoviridae	Vesicular stomatitis virus	✓	✓	✓	P L	M1–3	Weidner *et al.* [23]
	Rabies virus	✓✓	✓		P	M2–3	Smith *et al.* [16]
	Lagos Bat virus	✓✓	✓		P	M2–3	Smith *et al.* [16]
Filoviridae	Marburg virus	Δ	✓		P L	M1–3	Huang *et al.* [22•]
	Ebola virus	Δ	✓		P L	M1–3	Huang *et al.* [22•]
Coronaviridae	SARS coronavirus	Δ	✓		P L	M1–3	Huang *et al.* [22•]
Retroviridae	HIV-1	×	✓/×		P L	Mixed results	Brass *et al.* [11•], Lu *et al.* [26], Jia *et al.* [20]
	Moloney leukaemia virus	×	×		P L	No	Brass *et al.* [11•], Huang *et al.* [22•]
	Jaagsiekte sheep retrovirus	✓	✓	✓	P	M1 best	Li *et al.* [28•]
Arenaviridae	Lassa virus	✓	×		P	No	Brass *et al.* [11•]
	Machupo virus	✓	×		P	No	Brass et al. [11•]
	Lymphocytic choriomeningitis virus	✓	×		P	No	Brass *et al.* [11•]
Alphaviridae	Semliki Forest virus	✓	✓	✓	L	M2 and M3 best	Li *et al.* [28•]
Bunyaviridae	La Crosse virus	✓✓	✓		L	M1-3	Mudhasani *et al.* [30]
	Hantaan virus	✓✓	✓		L	M1-3	Mudhasani *et al.* [30]
	Andes virus	✓✓	✓		L	M1-3	Mudhasani *et al.* [30]
	Rift Valley fever virus	✓✓	✓		L-attenuated	M2 and M3	Mudhasani *et al.* [30]
	Crimean–Congo haemorrhagic fever virus	✓✓	×		L	No	Mudhasani *et al.* [30]
Non-enveloped							
Reoviridae	Reovirus	✓✓	✓		L	M3	Anafu *et al.* [27]

✓, fuses at pH >6; ✓✓, fuses at pH <6; ×, does not require fusion; Δ, requires cathespin L in lysosome.

recently, evidence that IFITM3 can also restrict a non-enveloped reovirus has been published [27], suggesting the range of viruses influenced by the IFITM proteins is not limited to those with an envelope.

Using a pseudotype virus carrying the Jaagsiekte sheep retrovirus (JSRV) envelope protein (Env), for which fusion requires initial Env priming by receptor binding and subsequent exposure to pH 6.3, IFITM1 seems to restrict replication more potently than IFITM2 and 3 [28•]. As IFITM1 appears to be located earlier in the endocytic pathway, where the pH is higher [29], these data suggest that the cellular location of different IFITM proteins determines the range of viruses that each restricts. Although not strictly pH-related, restriction correlates with the cellular compartment where fusion or penetration occurs. Differential restriction of viruses in the vector-borne *Bunyaviridae* family has also been found [30] (Table 1); only IFITM 2 and 3 were capable of restricting Rift Valley fever virus (RVFV) and none of the IFITM proteins prevented replication of Crimean–Congo haemorrhagic fever virus (CCHFV). The reason(s) underlying this difference in susceptibility are unclear as the bunyaviruses share similar morphologies and glycoproteins (G_N and G_C) on their envelopes.

IFITMs: protein structure and cellular distribution

IFITM3 is expressed constitutively in cells of the upper airway and visceral pleura [18], but otherwise its expression, and that of IFITM1 and 2, *in vivo* is poorly understood. In both cell lines and primary cells *ex vivo*, IFITM protein expression is upregulated by IFNs, though the relative levels of each protein in a given cell type or tissue has yet to be determined. All three IFN-inducible human IFITM proteins show high amino acid sequence similarity and all are membrane located, though their topologies remain to be clearly established [31]. Initially proposed as transmembrane proteins (Figure 1), with both the N-termini and C-termini located externally, subsequent studies suggested both the N-termini and C-termini, as well as the so-called conserved intracellular loop (CIL), are located cytoplasmically, with the hydrophobic domains interacting with the membrane but not spanning it [31]. More recently, a model for IFITM3 in which the N-terminal and CIL domains are located in the

Figure 1

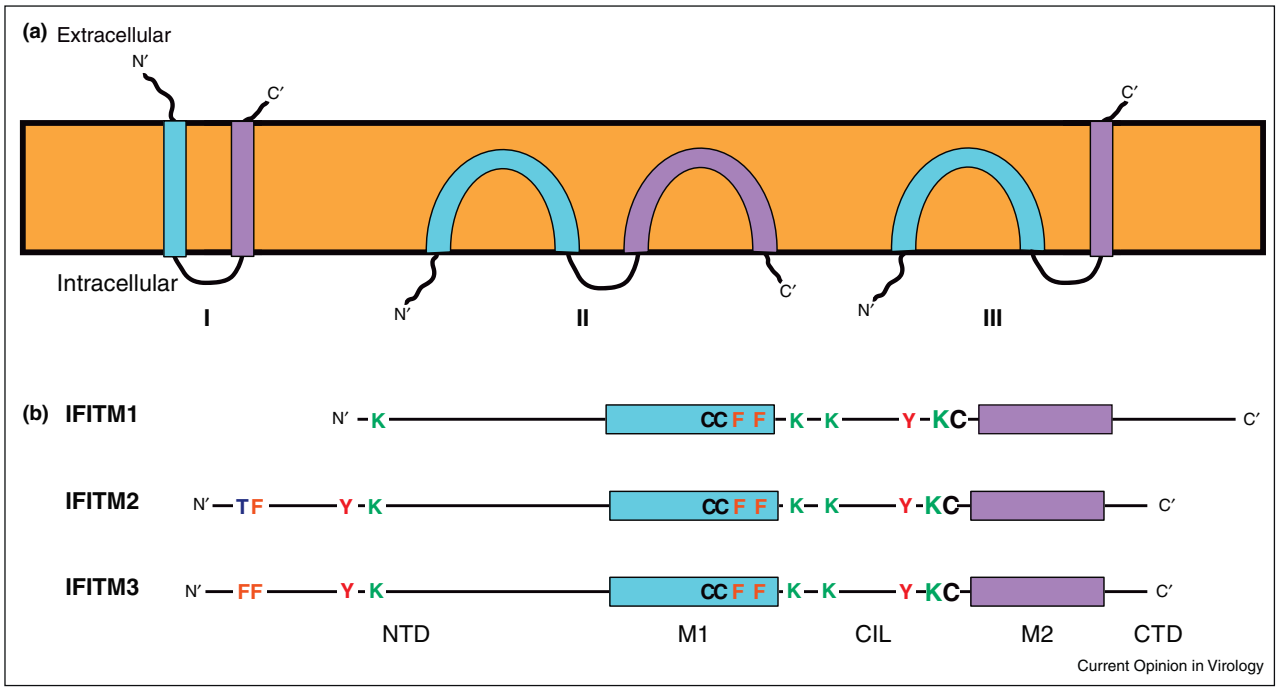

IFITM protein topology and domain organisation. Panel **(a)** Topological models for IFITM proteins. (I) Represents an initial model for the proteins as transmembrane molecules with both the N-terminal and C-terminal domains (NTD and CTD) extracellular and the conserved intracellular loop (CIL) facing the cytoplasm [33]. Subsequently, an alternative model (II) was proposed with the NTD, CTD and CIL all positioned intracellularly, and neither membrane domain (M1 and M2, blue and purple respectively) spanning the bilayer [31]. The most recent model (III) combines models I and II, positioning the NTD and CIL in the cytoplasm and the CTD extracellularly. Currently, the topology represented by III is only established for murine IFITM3 [32]. Panel **(b)** Linear representation of human IFITM1, 2 and 3 showing key amino acids. In all cases, modifications and functional activities have only been established with IFITM3, but conserved residues in IFITM1 and 2 are shown.

cytoplasm and the C-terminal domain is extracellular, suggested a type II transmembrane topology for the second hydrophobic domain [32]. Our own work suggests a similar topology for human IFITM1 (S Weston *et al.*, unpublished data). This topology is consistent with observations that all three IFN-inducible IFITM proteins contain conserved cysteine residues at the junctions of the CIL domain, and the putative membrane interacting domains. These cysteines (C71, 72 and 105 in human IFITM3) are palmitoylated, and this modification is required for full viral restriction [33]. Substitution of the cysteines for alanines in IFITM3 inhibits protein clustering in membranes and reduces its antiviral function [21]. IFITM3 can also be ubiquitinated on any of four lysines in the N-terminal and CIL domains. Ubiquitination enhances IFITM3 turnover [31], thus substitution of the lysines with alanines slows the protein's degradation and increases its antiviral activity [25].

The N-terminal domains of IFITM2 and 3 are 20 and 21 amino acids longer, than IFITM1, respectively (Figure 1). These N-terminal extensions include a key tyrosine (Y20 in IFITM3 that appears to control the cellular distributions of the two longer IFITMs) [17•,20,21]. Thus IFITM1 is predominantly at the plasma membrane, while IFITM2 and 3 are located mainly in intracellular compartments. IFITM3 is reported to reside primarily in endosomal organelles, identified by co-labelling with endosomal markers, including Lamp1, Rab7 and CD63 [21,34,35•], but the location of IFITM2 remains to be clearly established (Figure 2). Therefore, Y20 may be a component of a YxxØ-type sorting signal for clathrin-mediated trafficking [20]. Significantly, Y20 has also been identified as a target for Fyn-mediated phosphorylation, suggesting that perhaps the activity of this motif as a trafficking signal can be regulated [20,36].

It is important to note that studies of the subcellular location of the IFITMs to date have for the most part used epitope-tagged proteins, where tagging and/or overexpression (in transient systems) may have an impact on protein localisation and/or detection. Recently John *et al.* [21] showed that IFITM3 can interact with itself, as well as IFITM1 and 2, and that phenylalanine residues (F75 and F78) are required for this interaction. Although the significance of this association is unclear, the formation of homo-oligomers and/or hetero-oligomers might also influence the distribution and functional activities of these proteins.

Mode of action

Reovirus subvirus particles (ISVPs), in contrast to replication competent reovirus, do not require endosomal acidification for entry and are not inhibited by IFITM3 expression, suggesting that IFITM3 may perturb endosomal acidification [27]. However, studies with various enveloped viruses suggest a different mode of action. Morphological analysis of IFITM3-restricted IAV in cells showed the accumulation of viral particles in acidified endosomal compartments, suggesting there is no effect on receptor-binding, endocytosis or acidification [22•,34].

Studies using cell-cell fusion assays suggest that IFITM3 blocks enveloped virus entry by preventing fusion of the viral membrane with a limiting membrane of the host cell, either the plasma membrane and/or endosomal membranes [28•]. Fusion is an essential step in enveloped virus entry, and results in the transfer of viral capsids into the cytoplasm of a target cell. This process is extremely well characterised for a number of viruses, in particular IAV. Low pH in the endosomal lumen triggers conformational changes in one of the viral envelope proteins, haemagglutinin (HA). This change results in fusion of the outer leaflet of the viral membrane with the luminal leaflet of endosomal membranes forming a short-lived hemifusion intermediate. Resolution of the hemifusion intermediate allows fusion of the viral membrane inner leaflet with the cytoplasmic leaflet of endosomal membranes and the opening of a stable fusion pore [37]. Although often not a reflection of the pathway of infectious virus entry, a commonly used approach to studying viral fusion mechanisms is the formation of syncytia by cell-cell fusion. This requires the presence of viral fusion proteins in the plasma membrane of cells and appropriate signals, such as receptor-bearing cells and/or a transient change in the pH of the medium. Using the JSRV Env discussed previously, the IFITMs had no effect on either priming or pH-induced conformational changes [28•]. Moreover, syncytia formation induced by representatives of all three classes of viral fusion proteins [38] could be blocked by IFITM1. Using cold to arrest fusion at the hemifusion state, and chlorpromazine to resolve this, IFITM proteins were found to inhibit the early stages of viral envelope fusion with cellular membranes [28•].

The mechanism(s) through which the IFITMs inhibit the early stages of fusion is unclear. Two-photon laser scanning and fluorescence lifetime imaging (FLIM) of Laurdan-labelled cells, together with the effects of oleic acid treatment on cell-cell fusion, suggest that IFITM proteins may reduce membrane fluidity and increase spontaneous positive curvature in the outer leaflet of membranes [28•]. Such changes might be expected to impact on fusion, but how IFITMs affect membrane fluidity, and whether this has consequences for other membrane functions in the absence of infection, is unclear. One mechanism, however, has been suggested from experiments on IFITM3. Amini-Bavil-Olyaee *et al.* show IFITM3 interacts with vesicle membrane protein associated protein A (VAPA) and disrupts its association with an oxysterol binding protein that regulates the cholesterol content of endosomal membranes. Overexpression of IFITM3 increases endosomal cholesterol,

Figure 2

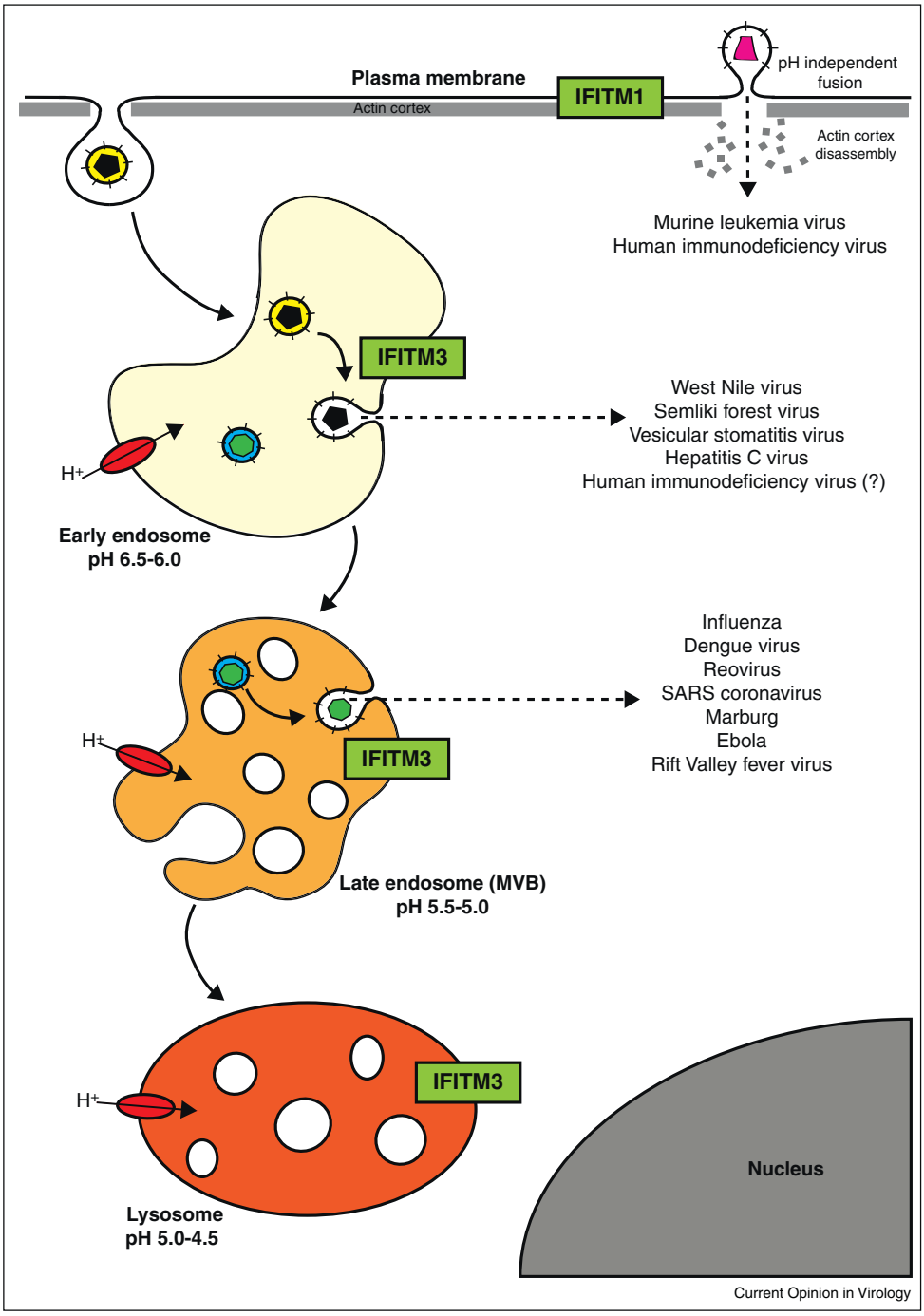

IFITM proteins inhibit virus entry at different stages of cell trafficking. Viruses enter cells by fusing with or penetrating a limiting cellular membrane. For most enveloped viruses fusion occurs either at the cell surface or, following uptake by endocytosis, from within endosomes. Acid-dependent viruses require acidification of the endosomal lumen by the membrane-associate vacuolar proton ATPase for fusion (shown in red). Trafficking through the endocytic system, from early to late endosomes, exposes virions to increasingly acidic environments. IFITM proteins (green) can inhibit entry and infection by a number of viruses that fuse/penetrate at the cell surface or from within endosomes. IFITM1 is expressed primarily at the cell surface, while IFITM2 and 3 are primarily intracellular. IFITM3 has been localised to endosomal compartments, but the distribution of IFITM2 still needs to be clearly established.

which may impact on viral fusion through a corresponding decrease in endosomal membrane fluidity [35•].

Although other mechanisms may contribute to IFITM inhibition of virus entry [39], analysis of changes in the physical properties of cellular membranes induced by IFITM expression is likely to shed light on the processes underlying the broad anti-viral effects of these proteins, as well as the mechanisms involved in the fusion/penetration and entry of a number of viruses.

Conclusions and outlook

Knock-down of IFITM proteins in cell culture can increase infection by a range of enveloped and non-enveloped viruses, and knock-out of *IFITM* genes *in vivo* can influence pathogenesis. By contrast, overexpression of the proteins in human cells can inhibit infection at an early stage of the replication cycle. Although the mechanism of IFITM antiviral activity remains unclear, possible IFITM induced decreases in membrane fluidity, or increased outward curvature, may inhibit the initial stages of enveloped virus fusion. Why each protein can exhibit variable restriction on viruses of the same family, for instance the *Bunyaviridae*, and how a virus that does not require fusion for entry (reovirus) is restricted under the proposed mechanisms remains unclear.

In many cases viruses have evolved mechanisms to antagonise the activity of a number of cellular restriction factors (e.g. see [2,4]). As yet no mechanisms to inhibit the activity of the IFITM proteins have been identified, though the indication that the IFITM proteins do not inhibit the entry of some viruses suggests that these agents are either refractory to the effects of the IFITM proteins, or have indeed evolved mechanisms to antagonise their function.

Although questions about the topology and intracellular distribution of the IFN-induced IFITMs remain, when taken together a model emerges suggesting that these proteins may have evolved to provide coverage of the main cellular membrane systems that have been implicated in virus entry, that is, the plasma membrane and compartments of the endocytic pathway. The implication is that perhaps IFITM1 primarily restricts viruses that fuse or penetrate at the cell surface, whereas IFITM2 and 3 primarily restrict viruses entering from endocytic organelles. That two IFITM proteins appear to function intracellularly may reflect the fact that endocytosis has been implicated in the entry of an increasing number of both pH-dependent and independent vertebrate viruses [40]. While there is some suggestion that this pattern may be true (see Table 1), there are exceptions. It is clear that there is much to be learned about the mechanisms through which these newly identified cellular proteins inhibit virus entry, and their full potential to restrict viral transmission *in vivo*.

Acknowledgements

This work was supported by the Wellcome Trust grant (098051), and funding from the Medical Research Council grant (G1000413) as well as core funding to the MRC Laboratory for Molecular Cell Biology. We thank Joe Grove for help with Figure 2 and Jason Mercer for critical comments on the manuscript.

References and recommended reading

Papers of particular interest, published within the period of review, have been highlighted as:

- • of special interest

1. Stremlau M, Owens CM, Perron MJ, Kiessling M, Autissier P, Sodroski J: **The cytoplasmic body component TRIM5alpha restricts HIV-1 infection in Old World monkeys**. *Nature* 2004, **427**:848-853.

2. Sheehy AM, Gaddis NC, Choi JD, Malim MH: **Isolation of a human gene that inhibits HIV-1 infection and is suppressed by the viral Vif protein**. *Nature* 2002, **418**:646-650.

3. Wilson SJ, Schoggins JW, Zang T, Kutluay SB, Jouvenet N, Alim MA, Bitzegeio J, Rice CM, Bieniasz PD: **Inhibition of HIV-1 particle assembly by 22,32-cyclic-nucleotide 32-phosphodiesterase**. *Cell Host Microbe* 2012, **12**:585-597.

4. Neil SJ, Zang T, Bieniasz PD: **Tetherin inhibits retrovirus release and is antagonized by HIV-1 Vpu**. *Nature* 2008, **451**:425-430.

5. Goujon C, Moncorge O, Bauby H, Doyle T, Ward CC, Schaller T, Hue S, Barclay WS, Schulz R, Malim MH: **Human MX2 is an interferon-induced post-entry inhibitor of HIV-1 infection**. *Nature* 2013, **502**:559-562.

6. García MA, Meurs EF, Esteban M: **The dsRNA protein kinase PKR: virus and cell control**. *Biochimie* 2007, **89**:799-811.

7. Haller O, Staeheli P, Kochs G: **Interferon-induced Mx proteins in antiviral host defense**. *Biochimie* 2007, **89**:812-818.

8. Silverman RH: **Viral encounters with 2′,5′-oligoadenylate synthetase and RNase L during the interferon antiviral response**. *J Virol* 2007, **81**:12720-12729.

9. Duggal NK, Emerman M: **Evolutionary conflicts between viruses and restriction factors shape immunity**. *Nat Rev Immunol* 2012, **12**:687-695.

10. Lewin AR, Reid LE, McMahon M, Stark GR, Kerr IM: **Molecular analysis of a human interferon-inducible gene family**. *Eur J Biochem* 1991, **199**:417-423.

11. • Brass AL, Huang IC, Benita Y, John SP, Krishnan MN, Feeley EM, Ryan BJ, Weyer JL, van der Weyden L, Fikrig E, Adams DJ *et al.*: **The IFITM proteins mediate cellular resistance to influenza A H1N1 virus, West Nile virus, and Dengue virus**. *Cell* 2009, **139**:1243-1254.
This study used a genome-wide siRNA knock-down screen and identified IFITM proteins as potent inhibitors of several viruses at the early stages of the virus life cycle.

12. Siegrist F, Ebeling M, Certa U: **Phylogenetic analysis of interferon inducible transmembrane gene family and functional aspects of IFITM3**. *Cytokine* 2009, **48**:87-89.

13. Hickford DE, Frankenberg SR, Shaw G, Renfree MB: **Evolution of vertebrate interferon inducible transmembrane proteins**. *BMC Genomics* 2012, **155**:1-7.

14. Moffatt P, Gaumond MH, Salois P, Sellin K, Bessette MC, Godin E, de Oliveira PT, Atkins GJ, Nanci A, Thomas G: **Bril: a novel bone-specific modulator of mineralization**. *J Bone Miner Res* 2008, **23**:1497-1508.

15. Sällman Almén M, Bringeland N, Fredriksson R, Schiöth HB: **The dispanins: a novel gene family of ancient origin that contains 14 human members**. *PLOS ONE* 2012, **7**:e31961.

16. Smith SE, Gibson MS, Wash RS, Ferrara F, Wright E, Temperton N, Kellam P, Fife M: **Chicken IFITM3 restricts Influenza viruses and Lyssaviruses in vitro**. *J Virol* 2013, **87**:12957-12966.

17. • Everitt AR, Clare S, Pertel T, John SP, Wash RS, Smith SE, Chin CR, Feeley EM, Sims JS, Adams DJ, Wise HM *et al.*: **IFITM3 restricts the morbidity and mortality associated with influenza**. *Nature* 2012, **484**:519-523.
This work was the first to report that IFITM3 was required for the *in vivo* control of IAV infection in a mouse model and that the IFITM3 SNP rs12252-C was strongly associated with worse clinical outcomes for patients infected with 2009 pandemic IAV.

18. Bailey CC, Huang IC, Kam C, Farzan M: **Ifitm3 limits the severity of acute influenza in mice**. *PLoS Pathog* 2012, **8**:e90991002.

19. Zhang YH, Zhao Y, Li N, Peng YC, Giannoulatou E, Jin RH, Yan HP, Wu H, Liu JH, Liu N, Wang DY *et al.*: **Interferon-induced transmembrane protein-3 genetic variant rs12252-C is associated with severe influenza in Chinese individuals**. *Nat Commun* 2013, **8**:1-5.

20. Jia R, Pan Q, Ding S, Rong L, Liu SL, Geng Y, Qiao W, Liang C: **The N-terminal region of IFITM3 modulates its antiviral activity by regulating IFITM3 cellular localization**. *J Virol* 2012, **86**:13697-13707.

21. John SP, Chin CR, Perreira JM, Feeley EM, Aker AM, Savidis G, Smith SE, Elia AE, Everitt AR, Vora M, Pertel T *et al.*: **The CD225 domain of IFITM3 is required for both IFITM protein association and inhibition of influenza A virus and dengue virus replication**. *J Virol* 2013, **87**:7837-7852.

22. • Huang IC, Bailey CC, Weyer JL, Radoshitzky SR, Becker MM, Chiang JJ, Brass AL, Ahmed AA, Chi X, Dong L, Longobardi LE *et al.*: **Distinct patterns of IFITM-mediated restriction of filoviruses, SARS coronavirus, and influenza A virus**. *PLoS Pathog* 2011, **7**:e1001258.
An extensive cell based study which showed that IFITM1-3 were able to restrict more viruses of the *Filoviridae* and *Coronaviridae* families.

23. Weidner JM, Jiang D, Pan X-B, Chang J, Block TM, Guo J-T: **Interferon-induced cell membrane proteins, IFITM3 and tetherin, inhibit vesicular stomatitis virus infection via distinct mechanisms**. *J Virol* 2010, **84**:12646-12657.

24. Wilkins C, Woodward J, Lau DT, Barnes A, Joyce M, McFarlane N, McKeating JA, Tyrrell DL, Gale M Jr: **IFITM1 is a tight junction protein that inhibits hepatitis C virus entry**. *Hepatology* 2013, **57**:461-469.

25. Chutiwitoonchai N, Hiyoshi M, Hiyoshi-Yoshidomi Y, Hashimoto M, Tokunaga K, Suzu S: **Characteristics of IFITM, the newly identified IFN-inducible anti-HIV-1 family proteins**. *Microbes Infect* 2013, **15**:280-290.

26. Lu J, Pan Q, Rong L, Liu S-L, Liang C: **The IFITM proteins inhibit HIV-1 infection**. *J Virol* 2011, **85**:2126-2137.

27. Anafu AA, Bowen CH, Chin CR, Brass AL, Holm GH: **Interferon inducible transmembrane protein 3 IFITM3 restricts reovirus cell entry**. *J Biol Chem* 2013, **24**:17261-17271.

28. • Li K, Markosyan RM, Zheng Y-M, Golfetto O, Bungart B, Li M, Ding S, He Y, Liang C, Lee JC, Gratton E *et al.*: **IFITM proteins restrict viral membrane hemifusion**. *PLoS Pathog* 2013, **9**:e1003124.
Use cell–cell fusion assays to show that IFITM proteins block the fusion lipid membrane bilayers and increase the rigidity of the membrane, further decreasing the fusion potential.

29. Mellman I, Fuchs R, Helenius A: **Acidification of the endocytic and exocytic pathways**. *Annu Rev Biochem* 1986, **55**:663-700.

30. Mudhasani R, Tran JP, Retterer C, Radoshitzky SR, Kota K, Altamura LA, Smith JM, Packard BZ, Kuhn JH, Costantino J, Garrison AR *et al.*: **Ifitm-2 and Ifitm-3 but not Ifitm-1 restrict Rift Valley fever virus**. *J Virol* 2013, **87**:8451-8464.

31. Yount JS, Karssemeijer RA, Hang HC: **S-palmitoylation and ubiquitination differentially regulate IFITM3-mediated resistance to influenza virus**. *J Biol Chem* 2012, **287**:19631-19641.

32. Bailey CC, Kondur HR, Huang I-C, Farzan M: **Interferon-induced transmembrane protein 3 is a type II transmembrane protein**. *J Biol Chem* 2013, **288**:32184-32193.

33. Yount JS, Moltedo B, Yang Y-Y, Charron G, Moran TM, Lopez CB, Hang HC: **Palmitoylome profiling reveals S-palmitoylation-dependent antiviral activity of IFITM3**. *Nat Chem Biol* 2010, **6**:610-614.

34. Feeley EM, Sims JS, John SP, Chin CR, Pertel T, Chen L-M, Gaiha GD, Ryan BJ, Donis RO, Elledge SJ, Brass AL: **IFITM3 inhibits influenza A virus infection by preventing cytosolic entry**. *PLoS Pathog* 2011, **7**:e1002337.

35. • Amini-Bavil-Olyaee S, Choi YJ, Lee JH, Shi M, Huang IC, Farzan M, Jung JU: **The antiviral effector IFITM3 disrupts intracellular cholesterol homeostasis to block viral entry**. *Cell Host Microbe* 2013, **13**:452-464.
IFITM3 associates with VAPA, increasing the levels of intracellular cholesterol and thereby blocking viral replication.

36. Shiratori T, Miyatake S, Ohno H, Nakaseko C, Isono K, Bonifacino JS, Saito T: **Tyrosine phosphorylation controls internalization of CTLA-4 by regulating its interaction with clathrin-associated adaptor complex AP-2**. *Immunity* 1997, **6**:583-589.

37. Sieczkarski SB, Whittaker GR: **Viral entry**. *Curr Top Microbiol Immunol* 2005, **285**:1-23.

38. Igonet S, Rey FA: **SnapShot: viral and eukaryotic protein fusogens**. *Cell* 2012, **151**:1634.

39. Wee YS, Roundy KM, Weis JJ, Weis JH: **Interferon-inducible transmembrane proteins of the innate immune response act as membrane organizers by influencing clathrin and v-ATPase localization and function**. *Innate Immun* 2012, **30**:30.

40. Mercer J, Helenius A: **Gulping rather than sipping: macropinocytosis as a way of virus entry**. *Curr Opin Microbiol* 2012, **15**:490-499.

OPEN ACCESS Freely available online

PLOS ONE

A Membrane Topology Model for Human Interferon Inducible Transmembrane Protein 1

Stuart Weston[1]*, Stephanie Czieso[1], Ian J. White[1], Sarah E. Smith[2], Paul Kellam[2,3], Mark Marsh[1,3]*

1 MRC Laboratory for Molecular Cell Biology, University College London, London, United Kingdom, **2** Wellcome Trust Sanger Institute, Wellcome Trust Genome Campus, Hinxton, United Kingdom, **3** MRC Centre for Medical Molecular Virology, Division of Infection and Immunity, University College London, London, United Kingdom

Abstract

InterFeron Inducible TransMembrane proteins 1–3 (IFITM1, IFITM2 and IFITM3) are a family of proteins capable of inhibiting the cellular entry of numerous human and animal viruses. IFITM1-3 are unique amongst the currently described viral restriction factors in their apparent ability to block viral entry. This restrictive property is dependant on the localisation of the proteins to plasma and endosomal membranes, which constitute the main portals of viral entry into cells. The topology of the IFITM proteins within cell membranes is an unresolved aspect of their biology. Here we present data from immunofluorescence microscopy, protease cleavage, biotin-labelling and immuno-electron microscopy assays, showing that human IFITM1 has a membrane topology in which the N-terminal domain resides in the cytoplasm, and the C-terminal domain is extracellular. Furthermore, we provide evidence that this topology is conserved for all of the human interferon-induced IFITM proteins. This model is consistent with that recently proposed for murine IFITM3, but differs from that proposed for murine IFITM1.

Citation: Weston S, Czieso S, White IJ, Smith SE, Kellam P, et al. (2014) A Membrane Topology Model for Human Interferon Inducible Transmembrane Protein 1. PLoS ONE 9(8): e104341. doi:10.1371/journal.pone.0104341

Editor: Ludger Johannes, Institut Curie, France

Received December 20, 2013; **Accepted** July 13, 2014; **Published** August 8, 2014

Funding: SW is supported by the MRC Laboratory for Molecular Cell Biology Graduate Programme. MM, SC, IW are supported by MRC core funding to the MRC LMCB, UCL University Unit. SS and PK are supported by the Wellcome Trust (098051) and the Medical Research Council (G1000413). The funders had no role in study design, data collection and analysis, decision to publish, or preparation of the manuscript.

Competing Interests: The authors have declared that no competing interests exist.

* Email: stuart.weston.09@ucl.ac.uk (SW); m.marsh@ucl.ac.uk (MM)

Introduction

The InterFeron Inducible TransMembrane (IFITM) protein family of viral restriction factors was defined in 2009 in a screen for host-modifying proteins of influenza A virus (IAV) infection [1]. Initially identified over 30 years ago [2], and named 9–27 (IFITM1), 1-8D (IFITM2) and 1-8U (IFITM3) [3], these proteins received little attention until human IFITM3 depletion was found to enhance IAV infection in cell culture assays. Conversely, over-expression of IFITM3, or the closely related IFITM1 and IFITM2, could inhibit IAV replication [1]. Studies in mice and humans have suggested that IFITM3, at least, also protects against IAV infection *in vivo* [4,5]. However, the IFITM proteins are not IAV-specific and, in cell culture at least, have broad-spectrum antiviral activity [6], though in some systems they may enhance cellular infection of human coronavirus OC43 [7] and human papillomavirus 16 [8].

Shortly after the identification of IFITM1-3 as antiviral factors, over-expression of IFITM3 was shown to cause an accumulation of intact IAV particles in endocytic organelles [9], suggesting that IFITM3 interfered with viral entry following endocytosis. Furthermore, this activity was dependent on localisation of IFITM3 to endosomes [10]. More recent studies suggested that IFITM over-expression may increase membrane rigidity and positive curvature, preventing the early events in membrane fusion [11]. Alternatively, IFITM protein interaction with vesicle membrane protein associated protein A (VAPA), disrupts cholesterol homeostasis and may increase membrane rigidity [12]. However, more recent work has questioned the role of cholesterol [13,14]. Thus, the precise molecular mechanism(s) for IFITM inhibition of viral entry remains to be established.

From their first descriptions, the IFITM proteins were thought to be membrane proteins [15]. Indeed, sequence analyses identified two hydrophobic, putative membrane interacting domains in each of the proteins. Additional studies demonstrated palmitoylation of cysteine residues adjacent to the hydrophobic domains, a post-translational modification indicative of membrane proteins [16]. However, the membrane topology of the IFITM proteins has remained ambiguous. Initially, they were suggested to be dual pass, transmembrane proteins with both N- and C-terminal domains (NTD and CTD) exposed extracellularly and a conserved intracellular loop (CIL) (Fig. 1, model 1). This model was based on the ability of antibodies against unknown IFITM1 external epitopes to aggregate leukaemia cells [15,17], immunoprecipitation of extracellular radiolabelled IFITM1 [18] and the accessibility of IFITM3 NTD and CTD epitope tags at the cell surface by FACS and immunofluorescence assays, respectively [1].

This topology was subsequently challenged by studies demonstrating that the NTD and CIL domain of IFITM3 are post-translationally modified by cytoplasmic enzymes [10,19]. Moreover, engineered myristoylation and prenylation sites at the NTD and CTD of murine IFITM3 can be detected as lipidated with selective chemical reporters alk-12 and alk-FOH, respectively [19]. These data suggested that both the NTD and CTD of IFITM3 are intracellular, and that the two hydrophobic sequences, enter, but do not span, the lipid bilayer [19] (Fig. 1, model 2). Murine IFITM1 was also proposed to have this topology [20].

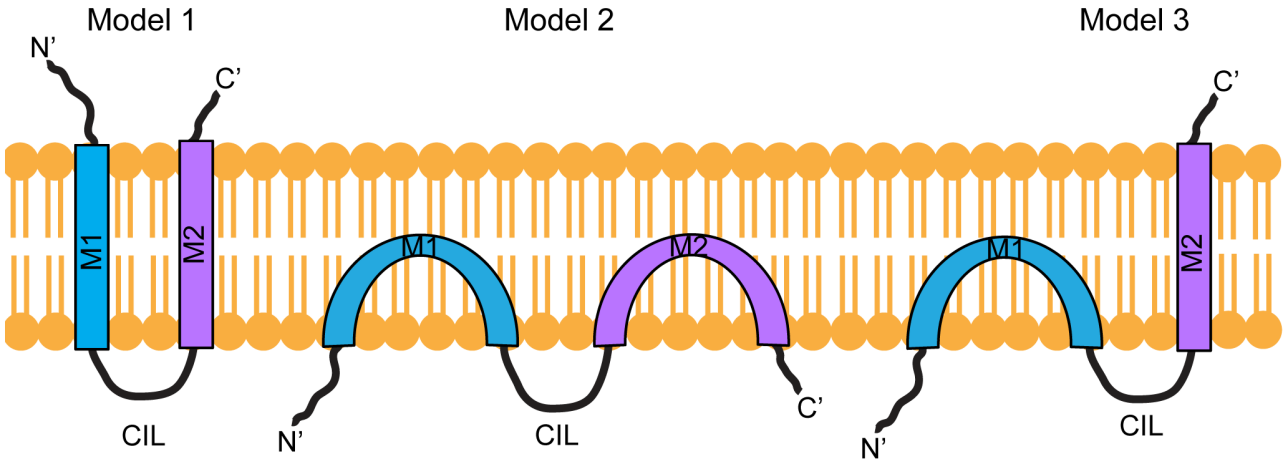

Figure 1. IFITM membrane topology models. In Model 1, the N- and C-terminal domains are extracellular and are connected by two transmembrane domains (M1 and M2) and the conserved intracellular loop (CIL). In Model 2 the two hydrophobic domains (M1, M2) do not span the membrane, resulting in NTD, CTD and CIL domain being located in the cytoplasm. In Model 3, the NTD and CIL domain are intracellular, suggesting M1 does not span the membrane, but the CTD is located on the extracellular side of the membrane and requires that M2 spans the membrane.
doi:10.1371/journal.pone.0104341.g001

Based on multiple approaches a third model has since been proposed for mu IFITM3, with the NTD and CIL facing the cytoplasm and the CTD located in the extracellular space, or within the lumen of vesicular organelles [21] (Fig. 1, model 3). While this manuscript was under revision, an additional study suggested a similar topology for human IFITM3 [22]. However, it remains unclear whether C-terminal epitope tags influence the topology, and whether the proposed topology applies to other human IFITM proteins.

Using immunofluorescence microscopy, protease cleavage assays, immuno-electron microscopy and biotin-labelling approaches, our data support the notion that the NTD of human IFITM1 is located in the cytoplasm, while the CTD is extracellular (Fig. 1, model 3). We provide evidence that the presence of a HA-tag at the IFITM1 C-terminus does not induce this topology. We also show that, although human IFITM2 and IFITM3 reside predominantly in intracellular membranes, they adopt the same topology. Together our data are consistent with the recently proposed model for mu IFITM3 [21], but not with that proposed for mu IFITM1 [20].

Materials and Methods

Cell lines and constructs

A549 (adenocarcinoma of human lung epithelia) cell lines stably expressing C-terminally HA-tagged human (hu) IFITM1, IFITM2 or IFITM3, as well as untransfected A549 cells [23], were cultured in Ham's F-12-GlutaMAX media (tissue culture reagents were from Life Technologies, unless indicated otherwise) supplemented with 10% (v/v) foetal calf serum (FCS) (PAA) and 1% (v/v) Penicillin/Streptomycin (Pen/Strep, 10,000 unit/ml/10,000 µg/ml). HEK293T cells were cultured in DMEM-GlutaMAX supplemented with 10% (v/v) FCS and 1% (v/v) Pen/Strep. All cell lines were maintained at 37°C and 5% CO_2. Untagged IFITM1 and IFITM1-Vstop (a construct with a stop codon after Val109) were purchased from GeneArt and cloned into BamH1/Not1 sites of pcDNA3.1. Constructs were confirmed by sequencing (Source BioScience).

Antibodies

Rat anti-HA (100 µg/ml, clone 3F10, Roche), mouse anti-HA (1 mg/ml, clone HA.11, 16B12 Covance), rabbit anti-IFITM1-NTD (100 µg/ml, Sigma), rabbit anti-IFITM3-NTD (250 µg/ml, Abgent), rabbit anti-VDAC (1 mg/ml, Abcam), rabbit anti-calreticulin (Thermo Scientific), mouse anti-tubulin (clone DM1A, ascites fluid, Sigma), goat anti-rat Alexa-488, goat anti-rabbit Alexa-488, goat anti-mouse Alexa-594 and goat anti-rabbit Alexa-647 (all 2 mg/ml, Life Technologies), goat anti-rabbit IRDye 680 and goat anti-mouse IRDye 800 (1 mg/ml, Li-COR), and wheat germ agglutinin (WGA) conjugated to Alexa-647 fluorophore (1 mg/ml, Invitrogen), were used at the dilutions given below.

Permeabilised immunofluorescence

Cells cultured on coverslips were fixed in 3% (w/v) formaldehyde (FA) (TAAB) in phosphate buffered saline (PBS) for 15 minutes (min), quenched with 50 mM NH_4Cl and 0.2% (w/v) bovine serum albumin (BSA, Sigma) in PBS (PBS/BSA) for 15 min and then permeabilised in PBS/BSA and 0.05% (w/v) saponin (Sigma) (permeabilisation buffer [PB]) for 30 min at room temperature (RT). Primary antibodies were diluted in PB and incubated with the coverslips for 1 hour (h). Unbound antibody was washed off with PB (3×5 min). Primary antibodies were detected with appropriate secondary antibodies conjugated to Alexa-488, Alexa-594 or Alexa-647, again, diluted in PB. Coverslips were mounted on Mowiol (Sigma) and imaged using a Leica TSC SPE confocal microscope.

Intact cell immunofluorescence

Cells cultured on coverslips were washed with ice cold PBS/BSA then incubated with primary antibodies on ice for 1 h in ice cold PBS/BSA. Cells were washed to remove unbound antibody and fixed in ice cold 3% FA for 1 h (30 min on ice and 30 min at RT). Primary antibodies were detected with appropriate secondary antibodies in PBS/BSA. Cells were processed and imaged as described above.

Wheat germ agglutinin staining

WGA-Alexa-647 was bound to cells on ice for 10 min. The cells were then washed four times with PBS/BSA and labelled using the intact cell staining procedure described above.

Antibody feeding

Cells cultured on coverslips were incubated in media containing rat anti-HA for 3 h at 37°C. Unbound antibody was removed, and the cells then rinsed in PBS, fixed and permeabilised (as above) before incubation with anti-rat Alexa-488 in PB. Cells were mounted and imaged as described above.

For all immunofluorescence, the antibodies were used as follows: rat anti-HA 1:100, rabbit anti-IFITM1-NTD 1:200, rabbit anti-IFITM3-NTD 1:200, mouse anti-tubulin 1:100, goat anti-rat Alexa-488, goat anti-rabbit Alexa-488, goat anti-mouse Alexa-594 and goat anti-rabbit Alexa-647 all 1:500 and WGA-Alexa-647 1:200. Nuclei were stained with Hoechst-33258 (Sigma).

Image analysis

To calculate the Pearson's R-value and Mander's correlation coefficients, M1 and M2, individual cells were segmented and analysed using the JACoP plugin on ImageJ software [24]. For M1 and M2 values, a Costes' automatic threshold was applied (as described [24]). To calculate the relative areas of yellow, red and green signals, images were initially split into the red and green component channels. These two images were then processed with the 'AND' function in ImageJ (producing an image of pixels that are only both red AND green). This image was subject to a manual threshold to observe only cellular structures and remove background noise. The pixel area was then calculated and these pixels defined as "yellow." The "yellow" pixels were then super-imposed on the red and green single channel images, and removed from each of these (such that a pixel defined as "yellow" cannot be considered "red or "green"). The same approach of applying a threshold was then taken on the red channel to calculate the pixel area, with these being defined as "red." Again, once calculated, these "red" pixels were super-imposed on the green channel image and removed. This allowed a threshold to be applied to the green channel and the area of the remaining pixels calculated. The relative area for each colour was calculated for each field of view and the mean average of all values calculated.

qRT-PCR

The endogenous levels of *IFITM1*, *2*, and *3* mRNA in A549 and HEK293T cells were measured by QuantiTect SYBR green qRT-PCR (Qiagen) using the primers described in Table 1 and the following thermocycling conditions: RT step - 50°C for 30 min. PCR steps - 95°C for 15 min, 94°C for 15 s; 35 cycles of (94°C, 15 s; 60°C, 30 s; 72°C, 30 s) in a reaction volume of 50 µl.

Total RNA was extracted from a known number of cells (between 2.4×10^5 and 5.9×10^5) and quantitated (RNeasy minikit): 100 ng was used as a template in each qRT-PCR reaction.

Five standards from 10^7–10^3 copies were made using plasmids encoding the transcripts of human *IFITM1*, *2*, and *3*, using the following formula:

$$x\ \text{g} / [\text{plasmid length} \times 660] \times 6.022 \times 10^{23} = y\ \text{molecules}$$

Using the standards for each transcript, the quantity of transcript was determined relative to the standard curve for 100 ng input RNA. The number of copies per cell was estimated by dividing the total number of cells by the total RNA extracted, multiplied by 100. This gave the equivalent number of cells that produced 100 ng of RNA and from this the RNA copy number per cell was inferred.

Table 1. qRT-PCR primers.

Primer name	Sequence (5′ to 3′)
F'Human_IFITM3	ACTGTCCAAACCTTCTTCTCTC
R'Human_IFITM3	AGCACAGCCACCTCGTGCTC
F'Human_IFITM2	ATTGTGCAAACCTTCTCTCCTG
R'Human_IFITM2	ACCCCCAGCATAGCCACTTCCT
F'Human_IFITM1	AGCACCATCCTTCCAAGGTCC
R'Human_IFITM1	TAACAGGATGAATCCAATGGTC

A list of the primers used for qRT-PCR. F′ and R′ stand for forward and reverse, respectively.
doi:10.1371/journal.pone.0104341.t001

Western blotting

Cells were lysed in Triton X-100 lysis buffer (1% [v/v] Triton X-100, 150 mM NaCl, 50 mM Tris-HCl pH 8.0 and 1× complete protease inhibitor cocktail [Roche]). Protein concentrations were determined using the BCA method (Thermo Scientific) following the manufacturer's instructions. Equal amounts of protein were mixed with reducing 3× Laemmli sample buffer (LSB), heated at 95°C for 5 min, separated by 15% SDS-PAGE and semi-dry transferred to a PVDF membrane (Immobilon-FL, Millipore). Membranes were blocked in TBST (Tris-buffered saline pH 7.4 [TBS] with 0.05% [v/v] Tween 20) containing 5% (w/v) dried skimmed milk (Marvel) for 1 h and incubated with primary antibodies at 4°C overnight. For trypsin cleavage assays, samples were collected (as described below) and lysed directly in 1× reducing LSB then heated at 95°C for 5 min. Equal volumes of cell lysates were loaded.

Antibodies used for protein detection were as follows: rabbit anti-IFITM3-NTD 1:500, rabbit anti-IFITM1-NTD 1:1000, mouse anti-HA 1:1000 and rabbit anti-VDAC 1:3000. The primary antibodies were detected using goat anti-rabbit IRDye 680 or goat anti-mouse IRDye 800 secondary antibodies, both at 1:10,000 (in 5% milk-TBST), then imaged and quantified using an Odyssey system (Li-COR).

Trypsin treatment

IFITM1-HA expressing A549 cells, grown in 6×35 mm well plates, were treated with 100 µg/ml trypsin (Sigma) for 5–30 min at 37°C. Subsequently, the cells were transferred to microcentrifuge tubes on ice, the wells were rinsed with 1 mg/ml soybean trypsin inhibitor (SBTI) (Sigma) in PBS, and the rinse added to the microcentrifuge tubes. Untreated control cells, as well as cells treated with inactivated trypsin (1:1 volume ratio of SBTI to trypsin), were also collected. All samples were pelleted (5 min, 3000 RCF, 4°C) and washed with SBTI before direct lysis in LSB and western blotting, as described above.

Flow cytometry

Cells in 35 mm dishes were treated with trypsin for 10 and 30 min or PBS for 30 min (as described above). The cells were then fixed, quenched (as previously) and washed with PBS/BSA prior to labelling with rat anti-HA antibody in PBS/BSA for 1 h at RT. The cells were then washed 3× with PBS/BSA and labelled

with goat anti-rat Alexa-647 in PBS/BSA for 45 min. Cells were washed 3× with PBS and subject to flow cytometry (LSR-II; BD Bioscience). Cells were gated on forward and side scatter and analysed for fluorescence labelling. The data were processed using FlowJo vX.0.7 software (Tree Star). Antibodies were diluted as for immunofluorescence staining.

Biotin labelling and pulldown

HEK293T cells, grown in 10 cm dishes, were transfected with untagged IFITM1 or IFITM1-Vstop expressing plasmids using FuGENE6. After 24 h, cells were detached with 5 mM EDTA and re-plated into 6×35 mm well plates. After a further 24 h, cells were labelled with 1 mg/ml EZ-link Sulfo-NHS-SS-Biotin (Thermo Scientific) for 45 min at 37°C. The biotin label was washed off with TBS and the cells lysed with 100 µl Triton X-100 lysis buffer (as previously). The whole cell lysate (70 µl) was added to a 25 µl NeutrAvidin agarose bead pellet (Thermo Scientific) and incubated for 3 h at 4°C on a rotor. Beads were then pelleted and the unbound material collected. The bead pellet was then washed with Triton X-100 lysis buffer, TBS and a TE buffer (10 mM Tris, 5 mM EDTA), prior to elution of proteins in 70 µl of 1× reducing LSB and heating at 95°C for 10 min. Eluate was collected and the elution procedure repeated. Equivalent volumes of whole cell lysate, unbound material and eluate from the NeutrAvidin beads were separated by 15% SDS-PAGE and western blotted as previously. Calreticulin was used as a loading control and detected with an anti-calreticulin antibody diluted 1:5000 in 1% BSA-TBST.

Electron microscopy

Cells were fixed with 4% (w/v) FA in 0.1 M phosphate buffer pH7.4, infused with 2.3 M sucrose, supported in 12% (w/v) gelatin and frozen in liquid nitrogen. Ultrathin (70 nm) cryosections were cut at −120°C and picked up in 1:1 2% sucrose:-methylcellulose. Sections were labelled with primary antibody (mouse anti-HA 1:400), followed by rabbit anti-mouse intermediate antibody (DAKO) and protein A gold, as described [25,26]. Images were obtained using a Tecnai T12 transmission electron microscope (FEI) and captured using a Morada CCD camera (Olympus-SIS).

Results

The human IFITM1 C-terminal domain resides extracellularly

To investigate the cellular distributions of human (hu) IFITM1, 2 and 3 we used C-terminally HA-tagged proteins, stably expressed in A549 cells, and immunofluorescence microscopy. When cells were permeabilised and labelled with anti-HA antibodies, all three IFITM proteins were detected, and each had a different cellular distribution. IFITM1-HA was seen primarily at the plasma membrane (Fig. 2B). By contrast, IFITM2-HA and IFITM3-HA were seen mostly in intracellular compartments with distinct distributions. IFITM2-HA localised in a tight cluster of punctae close to the nucleus, while IFITM3-HA had a more dispersed, punctate distribution (Fig. 2C and D).

Cells were also stained in the absence of detergent, thus maintaining the integrity of the plasma membrane. For IFITM1, anti-HA labelling was very similar on intact and detergent-permeabilised cells (compare Fig. 2F and Fig. 2B). As a control for the integrity of the plasma membrane, cells were co-stained with an anti-tubulin antibody (Fig. S1). Detection of IFITM1-HA on non-permeabilised cells further demonstrated that the protein is located primarily at the cell surface in stable transfected A549 cells. Furthermore, the C-terminal HA-tag is accessible on intact cells and therefore located on the extracellular surface of the plasma membrane. Co-staining cells with fluorescent wheat germ agglutinin further confirmed this plasma membrane localisation (Fig. S2).

No anti-HA labelling was seen on intact IFITM2-HA expressing cells, in keeping with the notion that this protein is located on intracellular membranes (Fig. 2G). A similar result was seen for IFITM3-HA, although a low number of cells (<1%) did show some surface labelling with anti-HA antibodies (Fig. 2H and Fig. S3). This suggested that although the majority of IFITM3-HA is located on intracellular membranes (Fig. 2D), in some cells IFITM3-HA is either mis-sorted and/or is expressed at the cell surface where the C-terminal HA epitope is accessible.

IFITM N-terminal domains reside intracellularly

The observation that the HA-tag of IFITM1 is accessible at the surface of intact cells prompted us to investigate the topology of the protein. We used two commercially available antibodies against the hu IFITM1 and IFITM3 NTDs. The IFITM1 NTD antibody (anti-IFITM1-NTD) was raised against a peptide encoding the first 35 amino acids of hu IFITM1. This domain has 69% and 75% amino acid identity with hu IFITM2 and IFITM3, respectively. The IFITM3 NTD antibody (anti-IFITM3-NTD) was raised against a peptide with a sequence corresponding to the first 30 amino acids of hu IFITM3. Hu IFITM1 has an N-terminal 21 amino acid truncation compared to IFITM3, so contains only 9 amino acids overlapping with this domain. However, there is 90% amino acid identity between the first 30 amino acids of hu IFITM3 and IFITM2.

To determine the specificity of the NTD antibodies, both were tested on samples from the HA-tagged IFITM1-3 expressing A549 cells by western blot analysis. Anti-IFITM1-NTD detected IFITM1-HA and IFITM3-HA, but not IFITM2-HA (Fig. 3A). Anti-IFITM3-NTD detected both IFITM3-HA and IFITM2-HA, but not IFITM1-HA (Fig. 3B). No IFITM protein was detected in control A549 cells with either antibody by western blot. Multiple bands in the range of 12–17 kDa were seen with the NTD antibodies, but not the anti-HA, indicating possible post-translational modification of the proteins (see below).

When intact IFITM1, 2 or 3 cells were labelled with anti-IFITM1-NTD antibody, no staining was seen, suggesting intracellular NTDs (Fig. 4J, K and L). Following detergent treatment, all three IFITM expressing lines were labelled (Fig. 4B, C and D), though a weaker signal was seen for IFITM2, as expected from the western blot (Fig. 3A). By immunofluorescence, the anti-IFITM3-NTD antibody gave a low signal in the untransfected A549 control and IFITM1-HA cells (Fig. 4E and D), consistent with the low level of endogenous IFITM2 expression detected by qRT-PCR (Fig. S4). However, the antibody clearly detected IFITM2-HA and IFITM3-HA (Fig. 4G and H). The observed cellular distributions, using the anti-NTD antibodies, agree with those seen using anti-HA antibodies (Fig. 2), and the inaccessibility of the IFITM1-NTD to labelling on intact cells indicates the domain is on the cytoplasmic side of the plasma membrane.

The IFITM1 C-terminal domain is accessible to extracellular proteases

Immunofluorescence microscopy (Fig. 2 and 4) suggested that the IFITM1 C-terminal HA-tag resides on the extracellular face of the plasma membrane, while the NTD is cytoplasmic. To further investigate this topology, we used protease cleavage assays. Since IFITM1-HA is primarily localised to the plasma membrane we hypothesised that the CTD, and HA-tag, might be accessible to

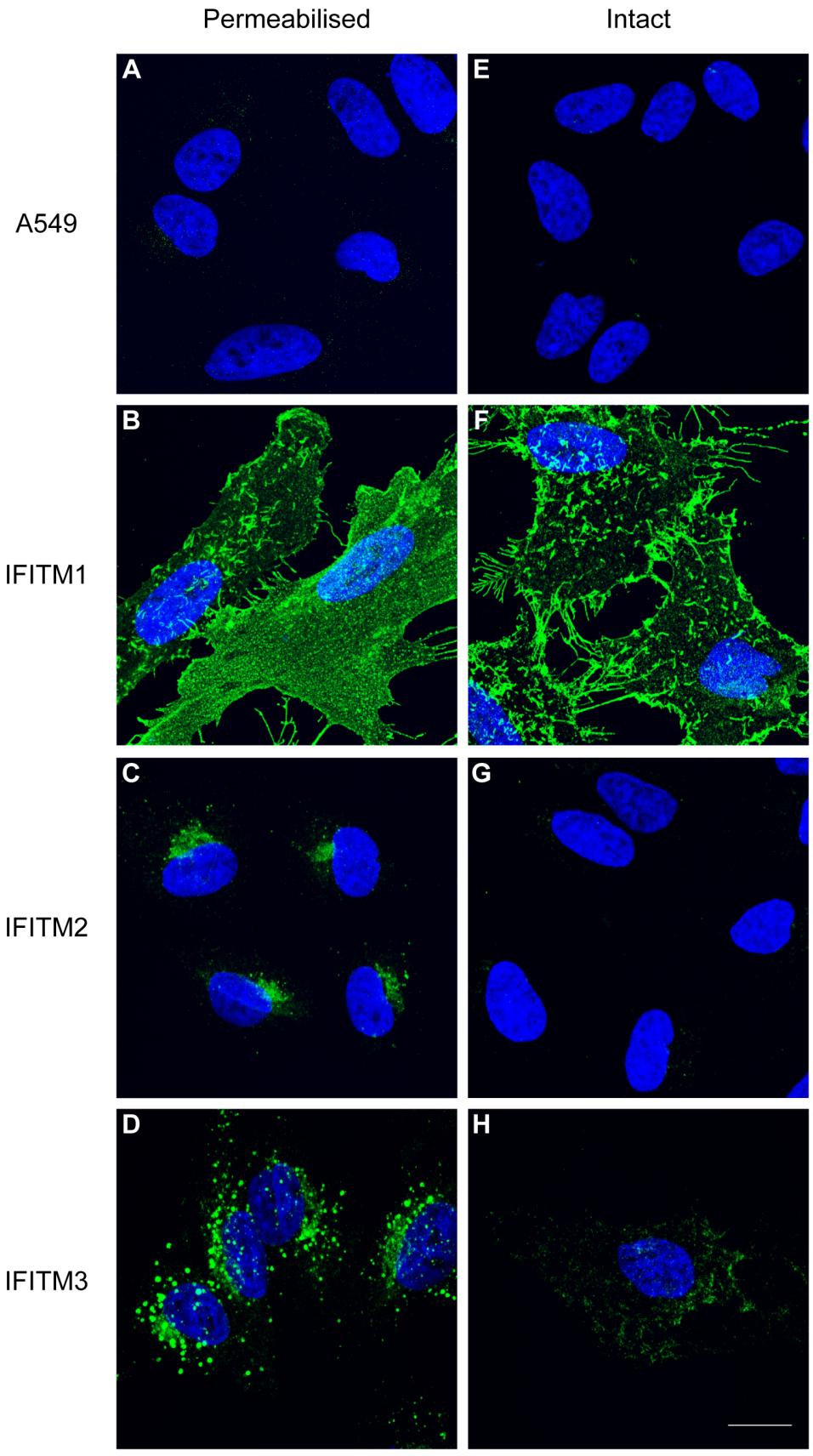
Permeabilised
Intact
A549
IFITM1
IFITM2
IFITM3
A
E
B
F
C
G
D
H

Figure 2. Cellular distribution of the human IFITM proteins. C-terminal domain HA-tagged IFITM1, IFITM2, IFITM3 and control A549 cell lines were stained intact, or following permeabilisation, with an anti-HA antibody and a secondary anti-rat Alexa-488 antibody. A) Permeabilised A549 cells show no specific staining. B-D) IFITM1-HA, IFITM2-HA and IFITM3-HA have distinct cellular distributions in permeabilised cells. E) Intact A549 cells (no detergent treatment) show no specific staining. F) Intact IFITM1-HA cells show positive cell surface HA staining. G) Intact IFITM2-HA cells show no detectable HA staining. H) Although the majority of intact IFITM3-HA cells show no anti-HA labelling, a minority (<1%) show low-level positive staining. Nuclei were labelled with Hoechst. All images are maximum projections of 0.25 μm optical sections taken through the depth of the cells using a confocal microscope. All images were taken using the same microscope settings and the levels adjusted uniformly. Scale bar represents 15 μm.
doi:10.1371/journal.pone.0104341.g002

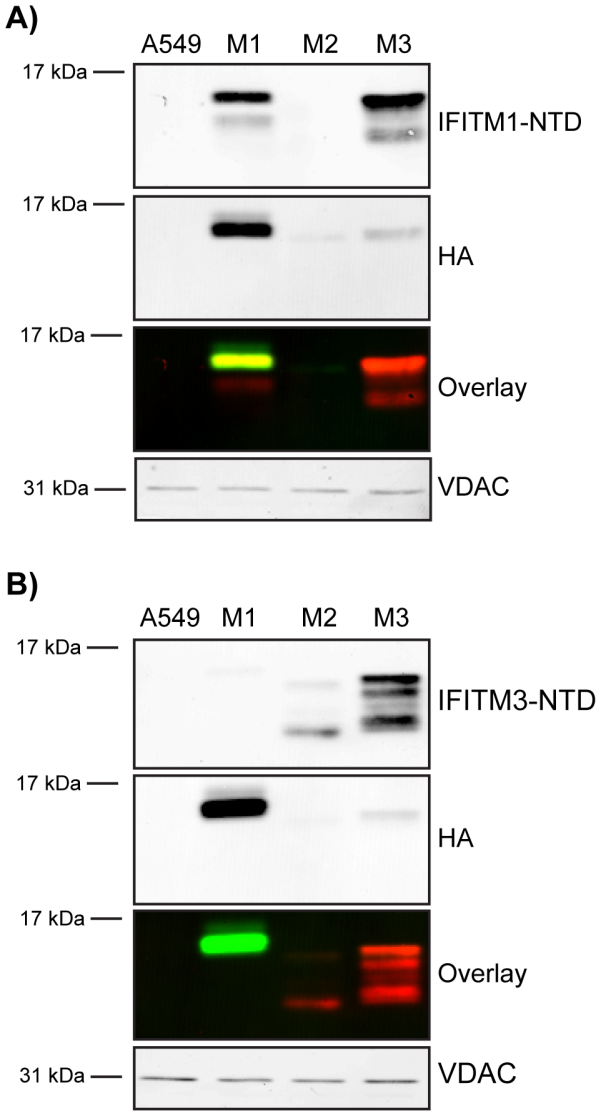

Figure 3. Analysis of IFITM NTD antibodies. Two commercially available antibodies targeting either the IFITM1-NTD or the IFITM3-NTD were screened by western blot to assess specificity using HA-tagged IFITM1-3 (M1, M2 and M3) cell lines along with control A549 cells. Proteins were also identified using the HA epitope. Blots were imaged on a Li-COR Odyssey system that uses far-red fluorophore conjugated secondary antibodies. In the overlay image, red represents anti-IFITM-NTD labelling and green represents anti-HA labelling. A) Anti-IFITM1-NTD detects IFITM1 and shows cross-reactivity with IFITM3. B) Anti-IFITM3-NTD detects IFITM3 and has cross-reactivity with IFITM2. VDAC was used as a loading control.
doi:10.1371/journal.pone.0104341.g003

digestion by extracellular proteases. Following analysis of the human IFITM1 CTD sequence with the ExPASy 'PeptideCutter' tool (http://web.expasy.org/peptide_cutter/) we chose to use trypsin, which was predicted to cleave at two positions close to the C-terminus of hu IFITM1 and thus expected to release the HA-tag (Fig. 5A).

IFITM1-HA cells were incubated with trypsin for up to 30 min at 37°C. The trypsin was then inactivated by addition of excess soybean trypsin inhibitor (SBTI) and the cells analysed by western blot using antibodies against both the C-terminal HA-tag and the NTD. Analysis of samples from untreated cells with anti-IFITM1-NTD indicated two IFITM1 bands (Fig. 5Bi), as previously seen (Fig. 3A). In samples from trypsin-treated cells the higher molecular weight band was rapidly lost, with a concomitant increase in the intensity of the lower band (Fig. 5Bi). This suggested that the higher molecular weight band is IFITM1-HA (confirmed in an anti-HA and anti-IFITM1-NTD overlay analysis [Fig. 5Biii]), and that the lower band is a cleavage product that has lost the HA-tag. We noted that about 8% (relative to untreated samples) of the HA-tagged protein was not digested by trypsin, even after long periods, suggesting that a small pool of IFITM1-HA protein was inaccessible to the protease (see below).

We also analysed trypsin cleavage of the HA epitope by flow cytometry. Cells were treated with trypsin for 10 or 30 min and the trypsin inactivated with SBTI. Cells were then fixed and labelled with an anti-HA antibody and detected with an Alexa-647 conjugated secondary antibody. Untreated IFITM1-HA cells showed a high level of staining that was lost upon treatment with trypsin, as determined by a shift in the peak fluorescence intensity and decrease in mean fluorescence intensity (Fig. S5).

Topology of untagged IFITM1

To exclude the possibility that C-terminal tagging influences the topology of IFITM1, we made use of a lysine residue (K122) present in the CTD that, if the observed topology is correct, will be accessible to labelling with NHS-biotin (Fig. 6A). To investigate this hypothesis, HEK293T cells were transfected with an untagged IFITM1 expression plasmid and incubated with cell impermeable Sulfo-NHS-SS-Biotin for 45 min at 37°C. While HEK293T cells appear to have a low level of IFITM1 mRNA (Fig. S4), no protein was detected by western blot of mock transfected cells (Fig. 6Biii).

Following biotin labelling of untagged IFITM1, cell lysates were precipitated using NeutrAvidin beads and analysed by western blot. IFITM1 labelled by biotin, and precipitated, is readily detected compared to unlabelled samples (Fig. 6B). The detection of IFITM1 in the biotin labelled, but unbound, fraction suggested that either the precipitation is not efficient, or only a proportion of IFITM1 has a CTD that is accessible to cell surface labelling.

To control for the specificity of labelling, a plasmid encoding an IFITM1 protein with a stop codon after the V109 codon (referred to as IFITM1-Vstop) that removes K122 (Fig. 6A), was transfected into HEK293T cells (Fig. 6C). After cells expressing this protein were incubated with Sulfo-NHS-SS-Biotin, none of the IFITM1-Vstop was absorbed to the beads (Fig. 6D).

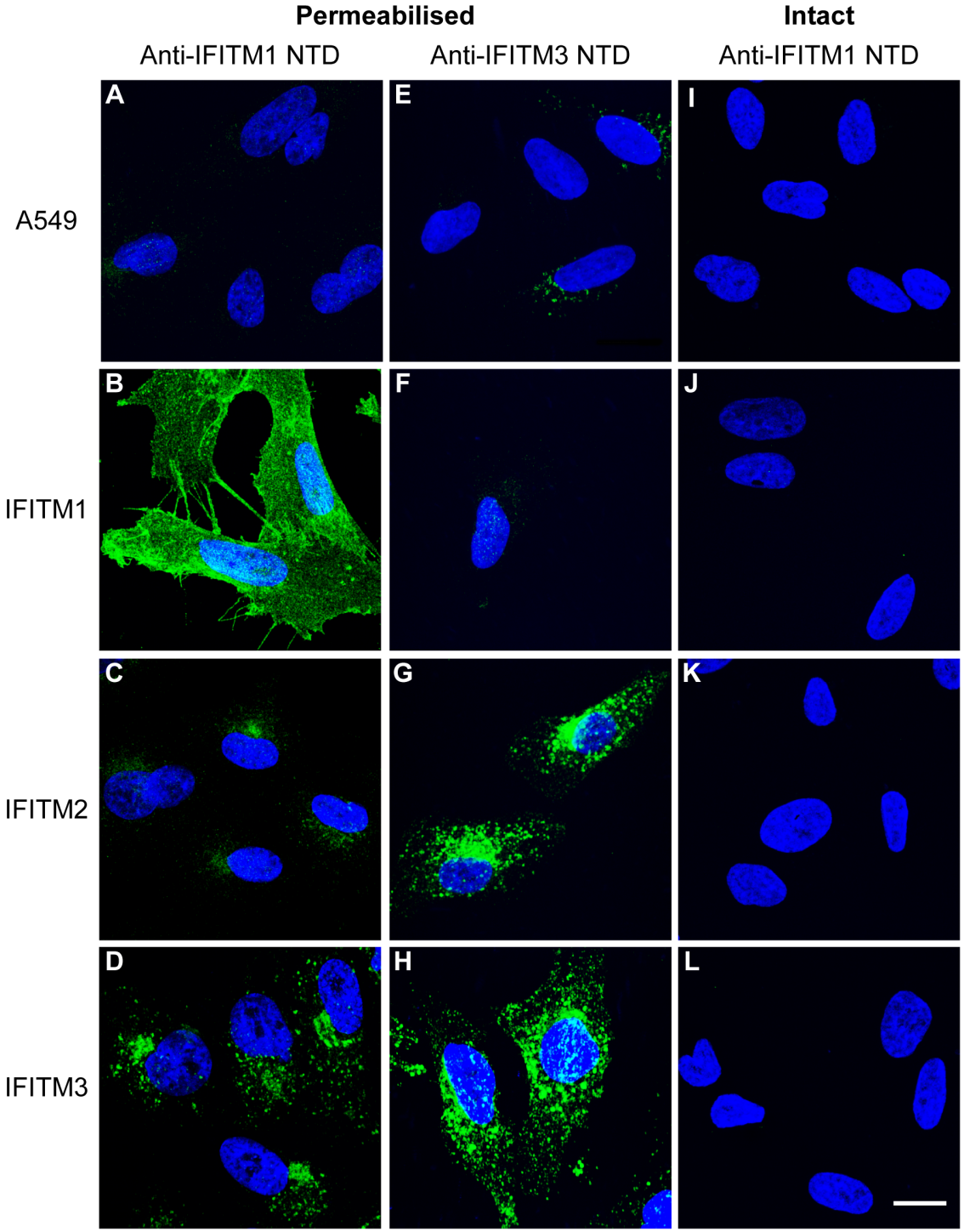

Figure 4. Analysis of the cellular distribution of the human IFITM proteins using anti-N-terminal domain antibodies. Immunofluorescence of A549 cells expressing HA-tagged IFITM1, IFITM2 and IFITM3 (or control A549 cells) using anti-IFITM1-NTD and anti-IFITM3 NTD antibodies. A) Permeabilised A549 cells show no specific staining. B-D) IFITM1-HA, IFITM2-HA and IFITM3-HA show distinct distributions in permeabilised cells. E and F) Anti-IFITM3-NTD detects low levels of endogenous protein in control A549 and IFITM1-HA cell lines. G and H) Anti-IFITM3-NTD detects IFITM2-HA and IFITM3-HA in permeabilised cells. I-L) No specific staining was seen on intact cells labelled with anti-IFITM1-NTD antibody. Nuclei were labelled with Hoechst. All images are maximum projections of 0.25 μm optical sections taken through the depth of the cells on a confocal microscope. All images were taken using the same microscope settings and the levels adjusted uniformly. Scale bar represents 15 μm.
doi:10.1371/journal.pone.0104341.g004

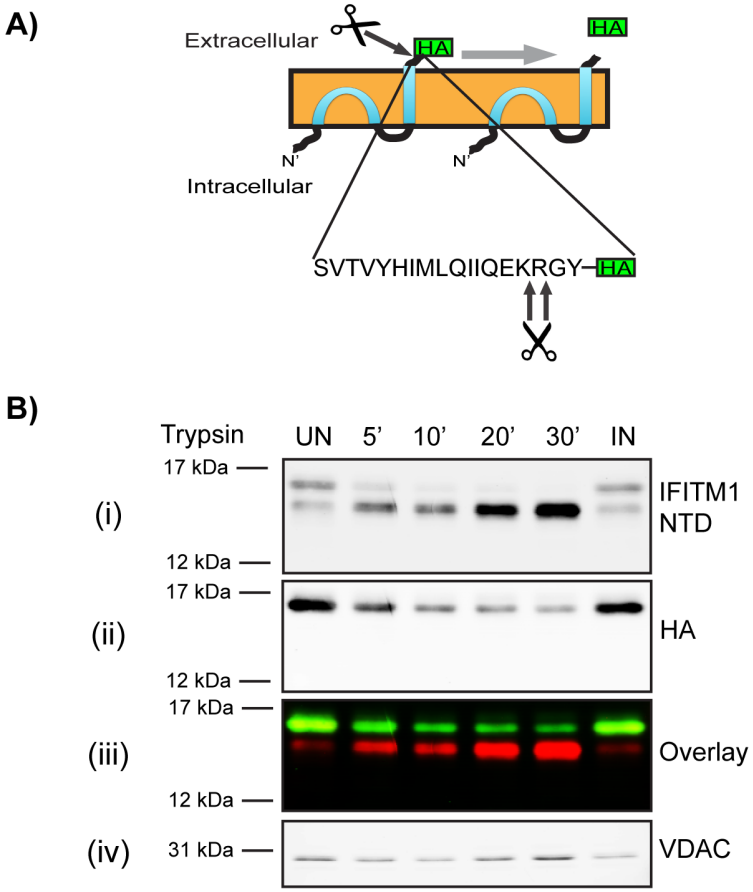

Figure 5. Trypsin cleavage of HA-tagged IFITM1. A) Predicted trypsin cleavage sites in hu IFITM1 CTD (Model 3, Fig. 1). B) IFITM1-HA cells were treated with exogenous trypsin for 5 to 30 mins at 37°C. The trypsin was inactivated with soybean trypsin inhibitor, the cells were lysed and the cellular proteins separated by SDS-PAGE. After transfer, proteins were identified with anti-IFITM1-NTD (i) and anti-HA (ii) antibodies. VDAC was used as a loading control (iii). Control samples were untreated (UN), or treated with SBTI-inactivated trypsin (IN). In the overlay image, red represents anti-IFITM1-NTD labelling and green represents anti-HA labelling (iv).
doi:10.1371/journal.pone.0104341.g005

The IFITM1 CTD HA-tag resides on the outer leaflet of the plasma membrane

To analyse hu IFITM1 in more detail, cryo-sections of IFITM1-HA cells were immuno-gold labelled for the HA-tag and examined by electron microscopy. As expected, labelling was seen predominantly at the plasma membrane (Fig. 7A and B). Close examination indicated that the majority of gold particles resided on the extracellular face of the plasma membrane, consistent with the notion that the hu IFITM1 CTD is located extracellularly. Labelling was also seen in the Golgi apparatus and in multi-vesicular bodies (Fig. 7C and D). These intracellular pools presumably indicate IFITM1 trafficking in the biosynthetic and endocytic pathways. This material would be inaccessible to extracellular proteases and labelling reagents, explaining the failure to completely digest IFITM1-HA with trypsin (Fig. 5B) and to fully label IFITM1 with biotin (Fig. 6B).

Conservation of the observed hu IFITM1 topology in hu IFITM2 and IFITM3

Our results indicate that hu IFITM1 is located predominantly in the plasma membrane, making it highly amenable to the topological analysis described above. Conversely, we show that hu IFITM2-HA and IFITM3-HA are primarily intracellular and less accessible to these investigative methods. Alternative approaches were therefore adopted to determine the location of the HA-tagged CTD of hu IFITM2 or IFITM3.

An antibody-feeding approach was used in which live cells were cultured in medium containing anti-HA antibody for 3 h, prior to washing, fixation and visualisation by immunofluorescence microscopy. As expected, control untransfected A549 cells, incubated with anti-HA antibodies, and IFITM3-HA cells that were not incubated with anti-HA antibodies, showed no labelling (Fig. 8A and C). IFITM1-HA expressing cells acted as a positive control and showed strong cell surface labelling (Fig. 8B). By contrast, most IFITM2-HA and IFITM3-HA cells showed little, if any, labelling. However, approximately 25% of IFITM3-HA cells and 10% of IFITM2-HA cells (calculated from 30 random fields of view at 40X magnification) showed intracellular, punctate labelling (Fig. 8D and E). Since the cells were labelled prior to fixation, this intracellular labelling suggested that, in some cells, the IFITM2-HA and IFITM3-HA proteins are trafficked to the cell surface where an externally exposed HA epitope could bind antibody, prior to internalisation into intracellular organelles. The lack of labelling in the majority of cells, which express the IFITM proteins, indicates the labelling is not due to non-specific fluid phase uptake of antibody. Together, we conclude that, in a

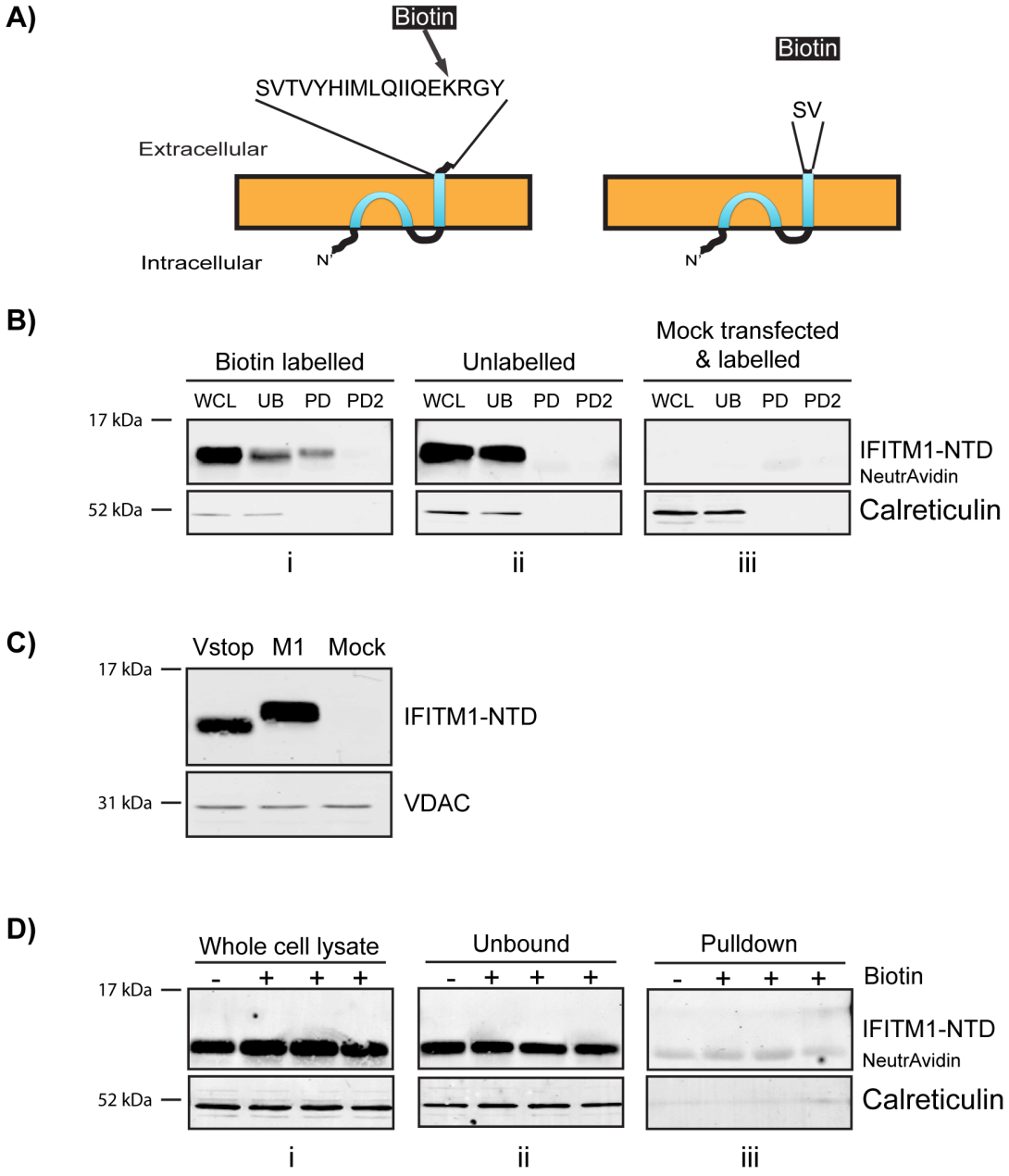

Figure 6. Biotin labelling and pulldown of untagged IFITM1. Untagged, wild type IFITM1 or IFITM1-Vstop expression plasmids were transfected into HEK293T cells. After two days the cells were labelled with cell impermeable Sulfo-NHS-SS-Biotin prior to incubation with NeutrAvidin agarose beads. A) Diagram to show the exposed CTD of IFITM1, with the targeted K122, or IFITM1-Vstop. B) Western blots probed with anti-IFITM1-NTD; WCL – whole cell lysates, UB – material that remained unbound by NeutrAvidin, PD1 and PD2 – two rounds of elution of protein from the NeutrAvidin beads. Gel i shows samples from cells labelled with biotin, gel ii shows unlabelled samples and gel iii shows samples from mock transfected HEK293T cells that were treated with Sulfo-NHS-SS-Biotin. NB. The elution step detached some NeutrAvidin monomers from the beads. These run at approximately 14 KDa and are seen as background bands in the western blots (labelled 'NeutrAvidin'). Calreticulin was used as a loading control and negative control for pulldown specificity. C) Western blot comparing the wild type IFITM1 (M1) with IFITM1-Vstop (Vstop), along with mock transfected HEK293T cells. D) Western blots probed with anti-IFITM1-NTD for whole cell lysates (i) material that remained unbound to NeutrAvidin (ii) and protein eluted from the NeutrAvidin beads (iii). As previously, NeutrAvidin monomers were eluted, and have the same molecular weight at IFITM1-Vstop. This can be clearly seen in the pulldown blot due to the presence of a band in the unlabelled lane.
doi:10.1371/journal.pone.0104341.g006

fraction of A549 cells, the CTDs of both IFITM2-HA and IFITM3-HA proteins are, at least transiently, exposed on the cell surface.

Previous results have suggested that IFITM2 and 3 are localised to endosomes (Fig. 2, 4 and [6]). The exposure of CTD HA-tags in the lumen of these organelles may result in their cleavage by endosomal/lysosomal proteases. This hypothesis is supported by western blots that showed low levels of HA-labelling for IFITM2 and 3 (Fig. 3). Moreover, when detected with anti-IFITM3-NTD, IFITM2-HA appears to have 3 bands in the range of 12–17 kDa,

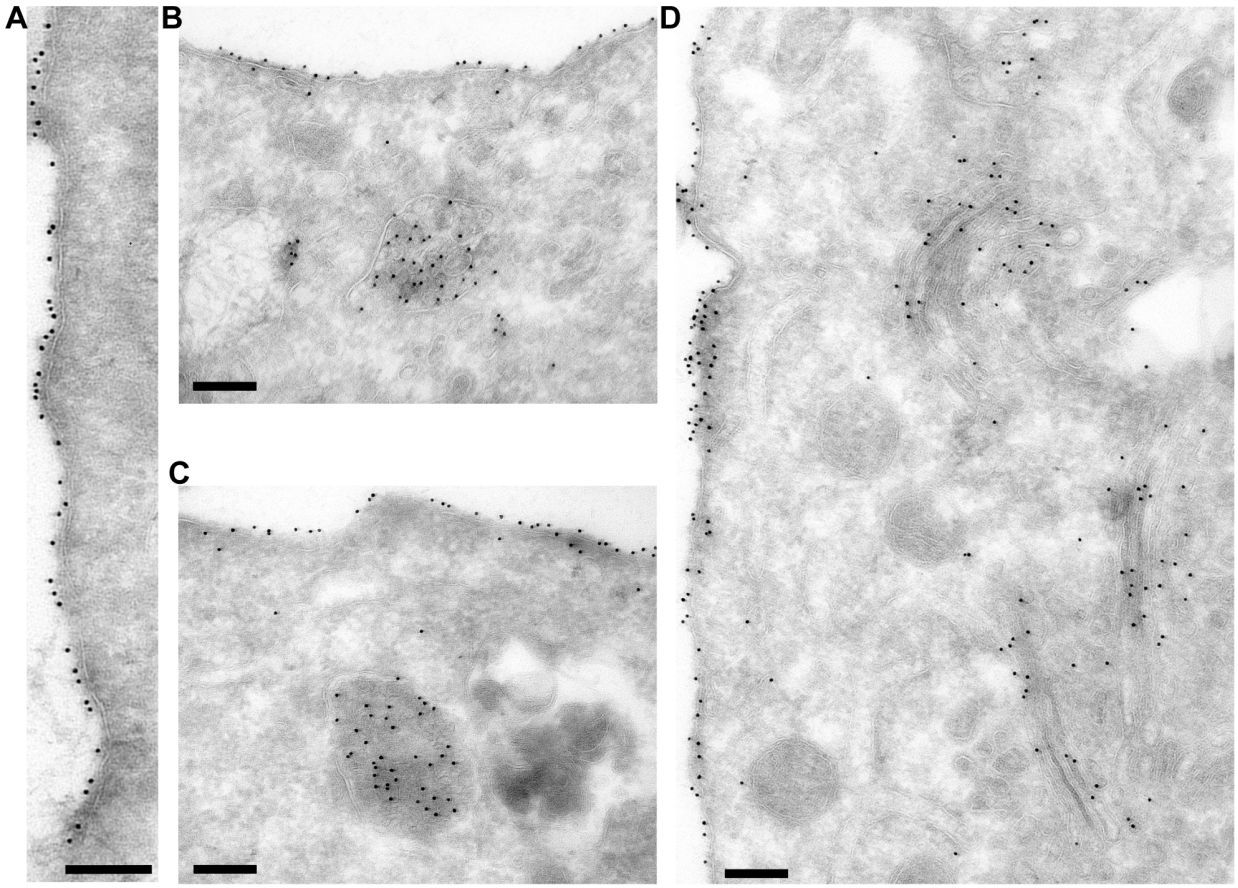

Figure 7. Immuno-gold labelling of A549 IFITM1-HA cell cryo-sections. Cryo-sections of the IFITM1-HA cells were labelled with anti-HA antibodies and Protein A gold. A) Plasma membrane labelling. B and C) Plasma membrane and multi-vesicular body labelling. D) Plasma membrane and Golgi apparatus labelling. Scale bars represent 200 nm.
doi:10.1371/journal.pone.0104341.g007

with the majority of the protein being of the lowest molecular weight, consistent with this protein having lost its HA-tag. A similar low molecular weight form was also seen for IFITM3-HA (Fig. 3).

IFITM expressing A549 cells were co-stained with antibodies against the NTD and the HA-tag. As IFITM proteins are relatively short (less than 133 amino acids) co-staining for the NTD and CTD should give apparent co-localisation. IFITM1-HA expressing cells showed a high degree of overlap between the anti-IFITM1-NTD and anti-HA antibodies (Fig. S6A). The overlap was seen across multiple images as demonstrated by Mander's correlation coefficients M1 and M2. Furthermore, analysis of the areas of different pixel colours demonstrated that around 70% ($\pm$1.8%) of pixels were detectable as yellow (Table S1).

By contrast, on IFITM3-HA expressing cells, a lower level of co-localisation was seen with both NTD antibodies (Fig. 9B and Fig. S6C). Importantly, clear red punctae were visible, suggesting that in some organelles IFITM3 contains intact NTDs but lacks the CTD HA-tag. This conclusion is supported by the quantification of multiple images that demonstrate a lower Mander's M1 and M2, compared to IFITM1-HA, and show an excess of red pixels (55% [$\pm$1.4%]) for IFITM3-HA expressing cells (Table 2, 3 and Table S1).

The anti-IFITM1-NTD antibody does not detect IFITM2-HA as well as IFITM1-HA and IFITM3-HA (Fig. 3); we therefore used the anti-IFITM3-NTD antibody for a similar investigation of IFITM2-HA (Fig. 9A). When multiple images were quantified, the results for IFITM2-HA and IFITM3-HA expressing cells were largely equivalent, with 49% ($\pm$1.1%) of pixels being red for IFITM2-HA cells, compared to 46% ($\pm$0.9%) for IFITM3-HA cells (Table 2 and 3). The observed excess of red pixels for both IFITM2-HA and IFITM3-HA indicates loss of the HA-tag, consistent with the western blots (Fig. 3). Overall, the data suggest a topology in which the HA-tagged CTDs of IFITM2 and IFITM3 are exposed to the endosomal/lysosomal system.

Discussion

The membrane topology of the interferon-induced IFITM proteins has been controversial. Initially it was suggested that both the NTD and CTD are located on the extracellular face of membranes and are connected by two transmembrane domains and the CIL domain (Fig. 1, model 1) [1,15,17,18]. However subsequent studies, demonstrating post-translational modification of both the hu IFITM3 NTD and CIL domain by cytosolic enzymes, led to the proposal of a model that placed the NTD, CIL and CTD all within the cytoplasm (Fig. 1 model 2) [10,19]. The same topology was also suggested for mu IFITM1 [20].

Here we present evidence that hu IFITM1, which localises primarily to the plasma membrane, has a topology with the NTD located in the cytoplasm and the CTD in the extracellular space

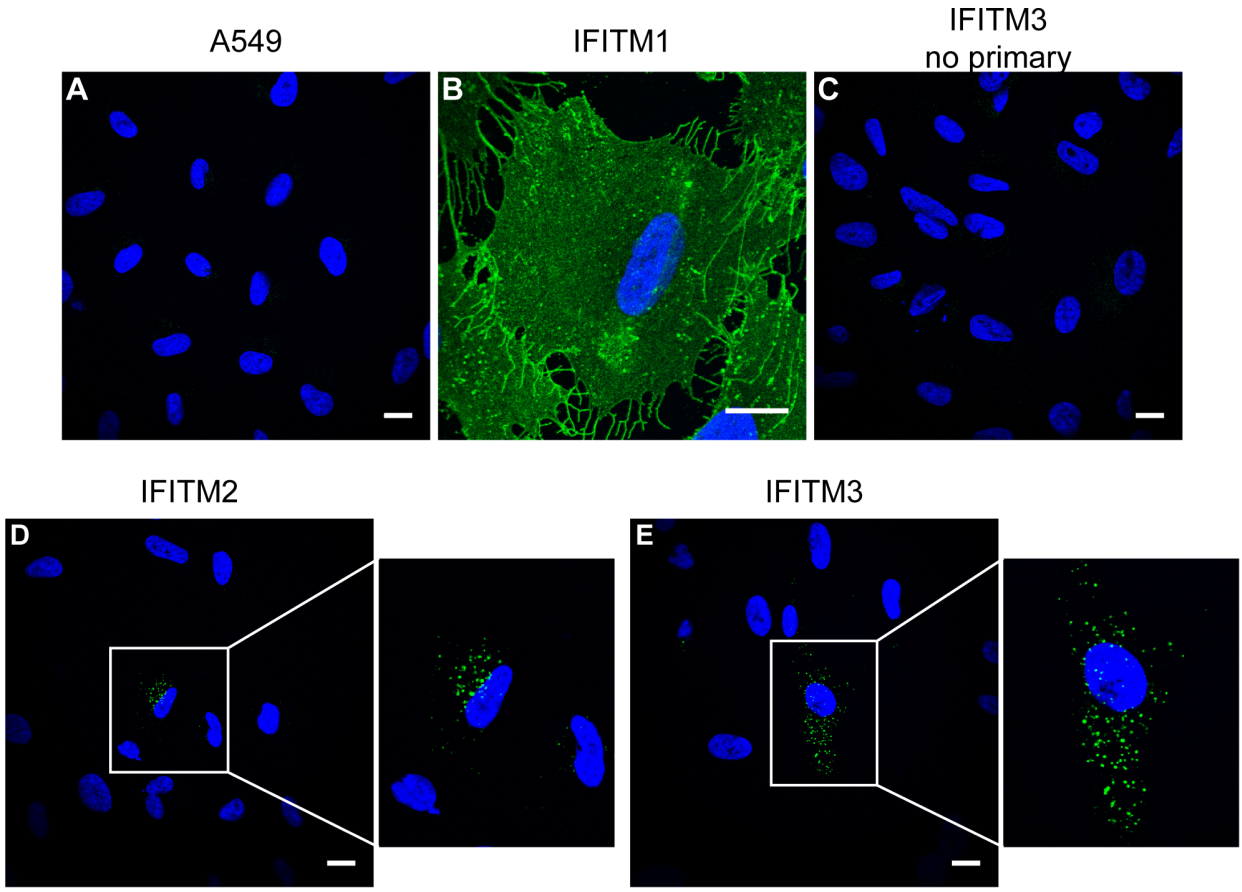

Figure 8. Antibody feeding of IFITM expressing cells. Live A549-IFITM-HA cells were incubated with 5 μg/ml anti-HA at 37°C to allow endocytosis of bound antibody molecules. Subsequently, the cells were washed, fixed, permeabilised and incubated with an anti-rat Alexa-488 conjugate. A) Control A549 cells show no specific staining. B) In IFITM1-HA cells the majority of labelling is at the plasma membrane. C) IFITM3-HA cells that were not incubated with anti-HA antibody show no labelling. For IFITM2-HA and IFITM3-HA expressing cells (D and E) the majority of cells are not labelled, however in both cases a minority of cells do show punctate labelling indicative of IFITM-mediated internalisation of anti-HA antibodies. In D and E, the boxed region has been enlarged. All images were taken using the same microscope settings and adjusted uniformly. Scale bars represent 15 μm.
doi:10.1371/journal.pone.0104341.g008

(Fig. 1, model 3). Immunofluorescence microscopy showed that on non-permeabilised cells the NTD is not accessible to antibody labelling, whereas the CTD (through an HA-tag) is accessible. In agreement, the majority of tagged IFITM1 was accessible to cleavage by exogenous trypsin.

Our results also suggested that the HA-tag itself did not induce the extracellular CTD topology since untagged IFITM1 could be biotinylated at K122 using a cell impermeable biotin-labelling reagent. However, while a large proportion of untagged IFITM1 could be biotin labelled and absorbed to NeutrAvidin beads, some protein remained in the supernatant. We propose that the unlabelled protein is that which resides in intracellular compartments such as the Golgi and multi-vesicular bodies, as seen by EM (Fig. 7), and that there could also be accessibility issues at the plasma membrane due to the short length of the CTD.

Although not accessible on intact cells, the NTD of IFITM1 was accessible to labelling with antibodies following detergent treatment of cells and showed a very similar cellular distribution to that seen with CTD anti-HA labelling. The NTD contains two potential trypsin cleavage sites, but we saw no evidence of these sites being accessible to exogenous trypsin. Thus our results are consistent with a model recently proposed for murine and human IFITM3 indicating a cytoplasmic NTD and CIL domain, connected by an intramembrane hydrophobic domain (M1) that does not fully span the membrane, and a second transmembrane domain (M2) linking the CIL domain to an extracellular CTD [21,22]. Our results with antibody labelling experiments indicate that hu IFITM2 and 3 are likely to have the same topology, suggesting this may be a common feature of human interferon-induced IFITM proteins, and mu IFITM3. However, this model is not consistent with published data on mu IFITM1 [20], in which palmitoylation of a CTD cysteine (mu IFITM1 C103) suggested a cytoplasmic location. This cysteine is not conserved in hu IFITM1, perhaps indicating why there is an apparent difference between hu and mu IFITM1 [20]. Whether palmitoylation of mu IFITM1 or other non-human IFITM proteins influence protein topology and/or its cellular distribution, as well as any possible effects on functional activities, remains to be examined.

The model for mu IFITM3 [21] and proposed here for hu IFITMs has important implications. Many studies of the IFITM proteins have used tagged constructs. If these tags are at the C-terminus they will reside in extracellular and lumenal spaces where they may be exposed to proteolytic conditions. Indeed, our results suggest that, even under normal culture conditions, IFITM-HA

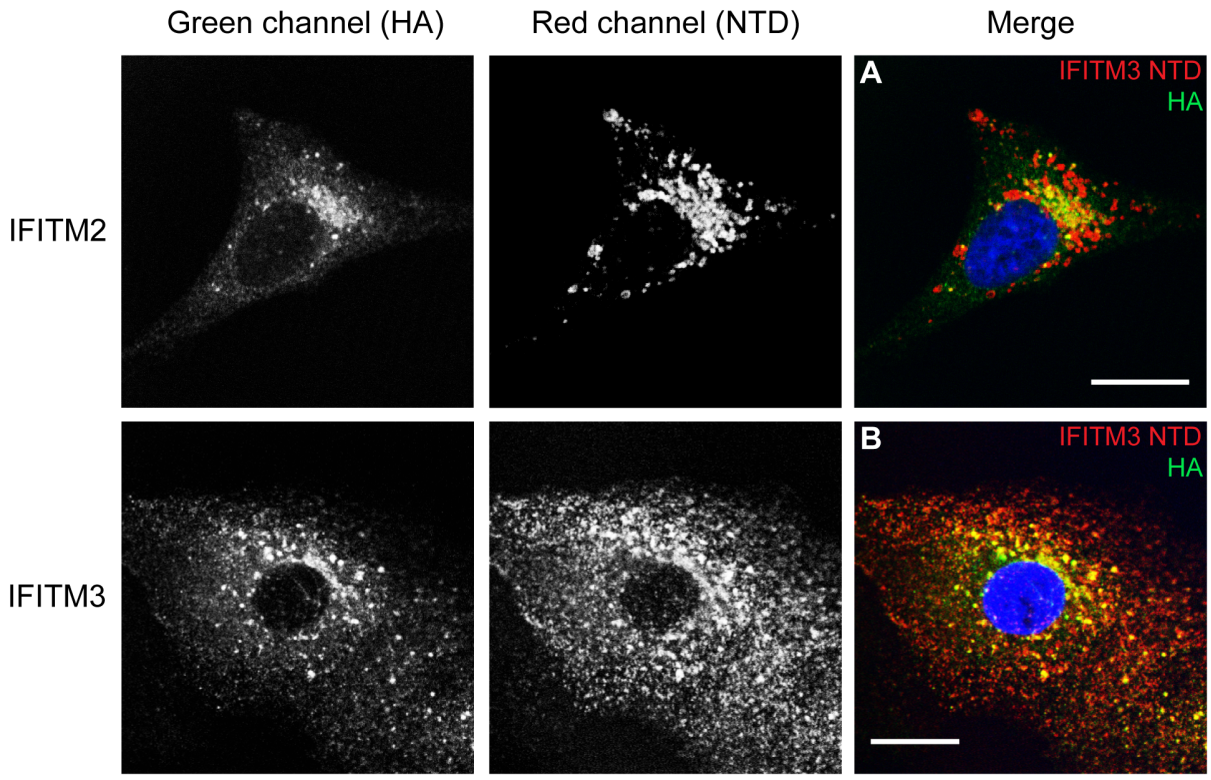

Figure 9. Co-staining with N- and C-terminal antibodies. Permeabilised IFITM2-HA (A) and IFITM3-HA (B) expressing cells were stained with antibodies against the C-terminal HA-tag (green [Alexa-488]) and the NTD, using the anti-IFITM3-NTD antibody (red [Alexa-647]). Images are single optical sections (0.25 μm thick) through the cells. Scale bars represent 15 μm. See also Table 2 and 3 for image analysis.
doi:10.1371/journal.pone.0104341.g009

expressing cells have cleavage products resulting from the loss of the HA-tag or residues from the CTD itself. Western blots of A549 cells stably expressing IFITM1 show two bands when using the anti-IFITM1-NTD antibody. The higher molecular weight band is the HA-tagged form of the protein, while the lower weight band is a cleaved form of the protein that has lost the HA-tag, and possibly other residues from the CTD. Since this band is seen in cells that were not treated with trypsin, we suggest that this C-terminal cleavage may occur in the endosomal system. This conclusion is supported by the observation that in A549 cells expressing HA-tagged IFITM2 or 3, intracellular organelles can be seen that contain IFITM2 or 3 with intact NTD epitopes but lacking the CTD HA-tag (Fig. 9).

The potential for loss of the CTD or C-terminal tags will affect the interpretation of cell localisation studies that rely on CTD epitopes. IFITM3 has been localised to endosomal compartments that co-label with markers for early and late endosomes (transferrin, CD63, Rab proteins, LAMP1, LAMP2 and Lyso-Tracker Red (as a marker for acidic compartments) [4,9,12,27,28]), but IFITM2 has proved harder to localise. Reliance on CTD epitope tags to determine the cellular distribution of the protein may not reveal the full cellular content of protein, and functionally important pools may be overlooked.

The relevance of the proposed topology to IFITM protein function is unclear at this stage. To date, published work has found that functionally important residues are located within the NTD [27] and the conserved CD225 domain [19,29], comprising the membrane interacting domains and the CIL loop, as well as the second membrane domain that is proposed to interact with VAPA [12]. Our data suggest the first membrane domain enters into, but does not span, the lipid bilayers, perhaps allowing the protein to induce membrane curvature. It could be further speculated that an

Table 2. Image analysis of anti-IFITM3-NTD antibody and anti-HA antibody co-labelling.

Cell line	Number of cells imaged	Pearson's R value	Mander's M1	Mander's M2
IFITM2	57	0.73 (±0.13)	0.85 (±0.16)	0.86 (±0.14)
IFITM3	49	0.72 (±0.04)	0.75 (±0.21)	0.77 (±0.17)

Co-localisation analysis of multiple images, for each cell line, from two independent experiments. Pearson's R-value represents the correlation in intensity between the red (anti-IFITM3-NTD) and green (HA) channels. Mander's correlation coefficients, M1 and M2, represent the overlap of red, in pixels that are green, and the overlap of green, in pixels that are red, respectively. Error given is of the standard deviation.
doi:10.1371/journal.pone.0104341.t002

Table 3. Image analysis of anti-IFITM3-NTD antibody and anti-HA antibody co-labelling.

Cell line	Fields of view	Yellow relative area	Red relative area	Green relative area
IFITM2	13	0.26 (±0.07)	0.49 (±0.11)	0.25 (±0.09)
IFITM3	14	0.27 (±0.04)	0.46 (±0.09)	0.27 (±0.09)

Relative areas of each colour were calculated as described in *materials and methods*. Red represents anti-IFITM3-NTD labelling, green represents anti-HA labelling and yellow represents overlap of the two stains. Error given is of the standard deviation.
doi:10.1371/journal.pone.0104341.t003

extracellular CTD may allow IFITM proteins to interact with key membrane components that are inaccessible on the cytoplasmic face of the membrane.

In conclusion, our data, together with those recently published for mu and hu IFITM3, provide a compelling case for hu IFITM proteins having an intracellular NTD and CIL domain, and an extracellular CTD. Whether all vertebrate IFITM proteins conform to the same organisation and, if not, the functional implications of other topologies, remain to be established.

Supporting Information

Figure S1 Tubulin co-staining on intact and permeabilised IFITM cell lines. C-terminal domain HA-tagged IFITM1-3 and A549 cell lines were co-stained intact, or following permeabilisation, with an anti-HA antibody and an anti-tubulin antibody. These antibodies were detected with Alexa-488 (green) and Alexa-594 (red), respectively. A) Permeabilised IFITM-HA cells show positive labelling for all IFITM proteins and tubulin. B) Intact IFITM-HA cells show no labelling for tubulin, indicating that the plasma membrane has remained intact and the antibody does not have access to the cytoplasm. As previously, IFITM1-HA can be labelled on intact cells, IFITM2-HA has no labelling and only a minority of IFITM3-HA expressing cells shows plasma membrane labelling. Nuclei were labelled with Hoechst. All images are maximum projections of 0.25 μm optical sections taken through the depth of the cells on a confocal microscope. All images were taken using the same microscope settings and the levels adjusted uniformly. Scale bars represent 15 μm.
(TIF)

Figure S2 Wheat germ agglutinin co-staining on intact IFITM cell lines. IFITM-HA cell lines co-labelled with anti-HA antibody, detected with Alexa-488 (green channel) and WGA-Alexa-647 (red channel). Images are of a single optical section (0.25 μm thick) through the middle surface of the cells. Scale bars represent 15 μm.
(TIF)

Figure S3 Immunofluorescence of intact IFITM3 cells. Intact IFITM3-HA cells stained with anti-HA antibody. A minority (<1%) of the cells show some plasma membrane labelling, although the vast majority do not. Labelling of permeabilised cells showed that all cells express IFITM3-HA (Fig. 2D) Scale bar represents 15 μm. The boxed region is enlarged in the right hand panel.
(TIF)

Figure S4 qRT-PCR of A549 and HEK293T cells. qRT-PCR of A549 and HEK293T cells to determine the expression levels of any endogenous IFITM proteins. Each bar is labelled with the mean number of RNA copies per cell with error bars representing the standard deviation from n = 3 amplifications.
(TIF)

Figure S5 Trypsin cleavage and flow cytometry analysis of IFITM1-HA. IFITM1-HA cells were treated with exogenous trypsin for 10 and 30 mins at 37°C. The trypsin was inactivated with soybean trypsin inhibitor, and cells fixed then labelled with anti-HA antibody. The HA labelling was detected with anti-rat Alexa-647 and the cells analysed by flow cytometry. A) Histograms representing the fluorescence intensity of HA labelling. The black line represents control A549 cells expressing no HA constructs. The green line represents untreated IFITM1-HA cells. The blue and red lines represent 10 and 30 mins of trypsin treatment, respectively. B) Mean fluorescence intensity of HA labelling. Data represent mean averages from n = 2 cleavages and error bars equal standard deviation.
(TIF)

Figure S6 Co-staining with anti-IFITM1-NTD and anti-HA antibodies. Permeabilised IFITM1-HA (A), IFITM2-HA (B) and IFITM3-HA (C) expressing cells were stained with antibodies against the C-terminal HA-tag (green [Alexa-448]) and the NTD, using the anti-IFITM1-NTD antibody (red [Alexa-647]). Images are of single optical sections (0.25 μm thick) through the middle the cell. Scale bars represent 15 μm.
(TIF)

Table S1 Image analysis of anti-IFITM1-NTD antibody and anti-HA antibody co-labelling. Co-localisation analysis of multiple images, for each cell line, from three independent experiments. Pearson's R-value represents the correlation in intensity between the red (anti-IFITM1-NTD) and green (HA) channels. Mander's correlation coefficients, M1 and M2, represent the overlap of red, in pixels that are green, and the overlap of green, in pixels that are red, respectively. Relative areas of each colour were calculated as described in *materials and methods*. Error given is of the standard deviation.
(DOCX)

Acknowledgments

We thank members of the Marsh and Kellam labs for input into the experiments described here and for critically reading the manuscript, Janos Kriston-Vizi for advice on the co-localisation analysis and Alexander Agrotis and Francisca Almeida for preliminary work on the trypsin cleavage assay.

Author Contributions

Conceived and designed the experiments: SW MM. Performed the experiments: SW SC IJW SES. Analyzed the data: SW SC IJW SES. Contributed reagents/materials/analysis tools: SW SES PK. Wrote the paper: SW MM.

References

1. Brass AL, Huang I-C, Benita Y, John SP, Krishnan MN, et al. (2009) The IFITM proteins mediate cellular resistance to influenza A H1N1 virus, West Nile virus, and dengue virus. Cell 139: 1243–1254. doi:10.1016/j.cell.2009.12.017.
2. Friedman RL, Manly SP, McMahon M, Kerr IM, Stark GR (1984) Transcriptional and posttranscriptional regulation of interferon-induced gene expression in human cells. Cell 38: 745–755.
3. Lewin AR, Reid LE, McMahon M, Stark GR, Kerr IM (1991) Molecular analysis of a human interferon-inducible gene family. Eur J Biochem 199: 417–423.
4. Bailey CC, Huang I-C, Kam C, Farzan M (2012) Ifitm3 limits the severity of acute influenza in mice. PLoS Pathog 8: e1002909. doi:10.1371/journal.-ppat.1002909.
5. Everitt AR, Clare S, Pertel T, John SP, Wash RS, et al. (2012) IFITM3 restricts the morbidity and mortality associated with influenza. Nature 484: 519–523. doi:10.1038/nature10921.
6. Smith SE, Weston S, Kellam P, Marsh M (2014) IFITM proteins - cellular inhibitors of viral entry. Curr Opin Virol 4: 71–77.
7. Zhao X, Guo F, Liu F, Cuconati A, Chang J, et al. (2014) Interferon induction of IFITM proteins promotes infection by human coronavirus OC43. Proc Natl Acad Sci U S A: 1–6. doi:10.1073/pnas.1320856111.
8. Warren CJ, Griffin LM, Little AS, Huang I-C, Farzan M, et al. (2014) The Antiviral Restriction Factors IFITM1, 2 and 3 Do Not Inhibit Infection of Human Papillomavirus, Cytomegalovirus and Adenovirus. PLoS One 9: e96579. doi:10.1371/journal.pone.0096579.
9. Feeley EM, Sims JS, John SP, Chin CR, Pertel T, et al. (2011) IFITM3 inhibits influenza A virus infection by preventing cytosolic entry. PLoS Pathog 7: e1002337. doi:10.1371/journal.ppat.1002337.
10. Jia R, Pan Q, Ding S, Rong L, Liu S (2012) The N-Terminal Region of IFITM3 Modulates Its Antiviral Activity by Regulating IFITM3 Cellular Localization. J Virol 86: 13697–13707. doi:10.1128/JVI.01828-12.
11. Li K, Markosyan RM, Zheng Y-M, Golfetto O, Bungart B, et al. (2013) IFITM Proteins Restrict Viral Membrane Hemifusion. PLoS Pathog 9: e1003124. doi:10.1371/journal.ppat.1003124.
12. Amini-Bavil-Olyaee S, Choi YJ, Lee JH, Shi M, Huang I, et al. (2013) The Antiviral Effector IFITM3 Disrupts Intracellular Cholesterol Homeostasis to Block Viral Entry. Cell Host Microbe: 452–464.
13. Lin T-Y, Chin CR, Everitt AR, Clare S, Perreira JM, et al. (2013) Amphotericin B Increases Influenza A Virus Infection by Preventing IFITM3-Mediated Restriction. Cell Rep 5: 895–908. doi:10.1016/j.celrep.2013.10.033.
14. Desai TM, Marin M, Chin CR, Savidis G, Brass AL, et al. (2014) IFITM3 Restricts Influenza A Virus Entry by Blocking the Formation of Fusion Pores following Virus-Endosome Hemifusion. PLoS Pathog 10: e1004048. doi:10.1371/journal.ppat.1004048.
15. Chen YX, Welte K, Gebhard DH, Evans RL (1984) Induction of T cell aggregation by antibody to a 16kd human leukocyte surface antigen. J Immunol 133: 2496–2501.
16. Yount JS, Moltedo B, Yang Y-Y, Charron G, Moran TM, et al. (2010) Palmitoylome profiling reveals S-palmitoylation-dependent antiviral activity of IFITM3. Nat Chem Biol 6: 610–614. doi:10.1038/nchembio.405.
17. Evans SS, Lee DB, Han T, Tomasi TB, Evans RL (1990) Monoclonal antibody to the interferon-inducible protein Leu-13 triggers aggregation and inhibits proliferation of leukemic B cells. Blood 76: 2583–2593.
18. Takahashi S, Doss C, Levy S, Levy R (1990) TAPA-1, the target of an antiproliferative antibody, is associated on the cell surface with the Leu-13 antigen. J Immunol 145: 2207–2213.
19. Yount JS, Karssemeijer RA, Hang HC (2012) S-palmitoylation and ubiquitination differentially regulate interferon-induced transmembrane protein 3 (IFITM3)-mediated resistance to influenza virus. J Biol Chem 287: 19631–19641. doi:10.1074/jbc.M112.362095.
20. Hach JC, McMichael T, Chesarino NM, Yount JS (2013) Palmitoylation on conserved and nonconserved cysteines of murine IFITM1 regulates its stability and anti-influenza A virus activity. J Virol 87: 9923–9927. doi:10.1128/JVI.00621-13.
21. Bailey CC, Kondur HR, Huang I-C, Farzan M (2013) Interferon-Induced Transmembrane Protein 3 is a Type II Transmembrane Protein. J Biol Chem. doi:10.1074/jbc.M113.514356.
22. Jia R, Xu F, Qian J, Yao Y, Miao C, et al. (2014) Identification of an endocytic signal essential for the antiviral action of IFITM3. Cell Microbiol: n/a–n/a. doi:10.1111/cmi.12262.
23. Smith SE, Gibson MS, Wash RS, Ferrara F, Wright E, et al. (2013) Chicken IFITM3 restricts Influenza viruses and Lyssaviruses in vitro. J Virol. doi:10.1128/JVI.01443-13.
24. Bolte S, Cordelières FP (2006) A guided tour into subcellular colocalization analysis in light microscopy. J Microsc 224: 213–232. doi:10.1111/j.1365-2818.2006.01706.x.
25. Slot JW, Geuze HJ, Gigengack S, Lienhard GE, James DE (1991) Immuno-localization of the insulin regulatable glucose transporter in brown adipose tissue of the rat. J Cell Biol 113: 123–135.
26. Deneka M, Pelchen-Matthews A, Byland R, Ruiz-Mateos E, Marsh M (2007) In macrophages, HIV-1 assembles into an intracellular plasma membrane domain containing the tetraspanins CD81, CD9, and CD53. J Cell Biol 177: 329–341. doi:10.1083/jcb.200609050.
27. Jia R, Pan Q, Ding S, Rong L, Liu S-L, et al. (2012) The N-Terminal Region of IFITM3 Modulates Its Antiviral Activity by Regulating IFITM3 Cellular Localization. J Virol 86: 13697–13707. doi:10.1128/JVI.01828-12.
28. Huang I, Bailey C, Weyer J, Radoshitzky S, Becker M, et al. (2011) Distinct patterns of IFITM-mediated restriction of filoviruses, SARS coronavirus, and influenza A virus. PLos Pathog 7: e1001258.
29. John SP, Chin CR, Perreira J, Feeley EM, Aker A, et al. (2013) The CD225 Domain of IFITM3 is Required for both IFITM Protein Association and Inhibition of Influenza A Virus and Dengue Virus Replication. J Virol. doi:10.1128/JVI.00481-13.

Traffic

doi:10.1111/tra.12416

Alphavirus Restriction by IFITM Proteins

Stuart Weston[1], Stephanie Czieso[1], Ian J. White[1], Sarah E. Smith[2], Rachael S. Wash[2], Carmen Diaz-Soria[2], Paul Kellam[2,3] and Mark Marsh[1,*]

[1]MRC Laboratory for Molecular Cell Biology, University College London, Gower Street, London, WC1E 6BT, UK
[2]Wellcome Trust Sanger Institute, Wellcome Trust Genome Campus, Hinxton, CB10 1SA, UK
[3]Division of Infection and Immunity, University College London, Gower Street, London, WC1E 6BT, UK
*Corresponding author: Mark Marsh, m.marsh@ucl.ac.uk

Abstract

Interferon inducible transmembrane proteins (IFITMs) are broad-spectrum antiviral factors. In cell culture the entry of many enveloped viruses, including orthomyxo-, flavi-, and filoviruses, is inhibited by IFITMs, though the mechanism(s) involved remain unclear and may vary between viruses. We demonstrate that Sindbis and Semliki Forest virus (SFV), which both use endocytosis and acid-induced membrane fusion in early endosomes to infect cells, are restricted by the early endosomal IFITM3. The late endosomal IFITM2 is less restrictive and the plasma membrane IFITM1 does not inhibit normal infection by either virus. IFITM3 inhibits release of the SFV capsid into the cytosol, without inhibiting binding, internalization, trafficking to endosomes or low pH-induced conformational changes in the envelope glycoprotein. Infection by SFV fusion at the cell surface was inhibited by IFITM1, but was equally inhibited by IFITM3. Furthermore, an IFITM3 mutant (Y20A) that is localized to the plasma membrane inhibited infection by cell surface fusion more potently than IFITM1. Together, these results indicate that IFITMs, in particular IFITM3, can restrict alphavirus infection by inhibiting viral fusion with cellular membranes. That IFITM3 can restrict SFV infection by fusion at the cell surface equivalently to IFITM1 suggests that IFITM3 has greater antiviral potency against SFV.

Keywords alphavirus, IFITM, interferon inducible transmembrane protein, restriction factor, Semliki Forest virus, SFV, virus entry, virus–host interaction

Received 16 February 2016, revised and accepted for publication 9 May 2016, uncorrected manuscript published online 24 May 2016, published online 24 June 2016

Human interferon inducible transmembrane proteins (IFITMs) are a family of five, 15–17 kDa membrane-associated proteins, of which three (IFITM1, 2 and 3) appear to function as broad-spectrum inhibitors of viral replication. Although detailed studies are lacking for most viruses, work on influenza A virus (IAV) has suggested that IFITM3, in particular, inhibits viral entry by interfering with endosomal, low pH-induced fusion (1–4). However, the precise molecular mechanism(s) for this inhibition remains unclear, and for some viruses alternative modes of action have been proposed (5–7).

Alphaviruses, especially Semliki Forest virus (SFV) and Sindbis virus (SINV), have been used extensively to study viral entry into cells (8–11). These small (~75 nm diameter), positive sense, single-stranded RNA viruses were amongst the first to be shown to use clathrin-mediated endocytosis and endosomal low pH-dependent fusion to enter cells (8,10). Despite the wealth of knowledge about their entry, IFITM-mediated inhibition of alphavirus infection has not been analyzed in any great detail, although an overexpression screen has suggested IFITMs inhibit Chikungunya virus infection but had less affect on Venezuelan equine encephalitis virus (12). It has also been suggested that low pH-induced fusion of SFV envelope glycoprotein expressing cells (fusion from within) can be inhibited by IFITM1 and IFITM3 (3). Nevertheless, there is a view that alphavirus infection is not restricted by IFITMs (13,14). Given the similarities, in terms of structure and mode of entry, between alphaviruses and flaviviruses, which are restricted by IFITMs (15–18), we investigated whether SFV and SINV can also be restricted.

We show that normal infection by both SFV and SINV is restricted by IFITM3 and, to a lesser extent, by IFITM2, but not by IFITM1. The expression of IFITM3 does not

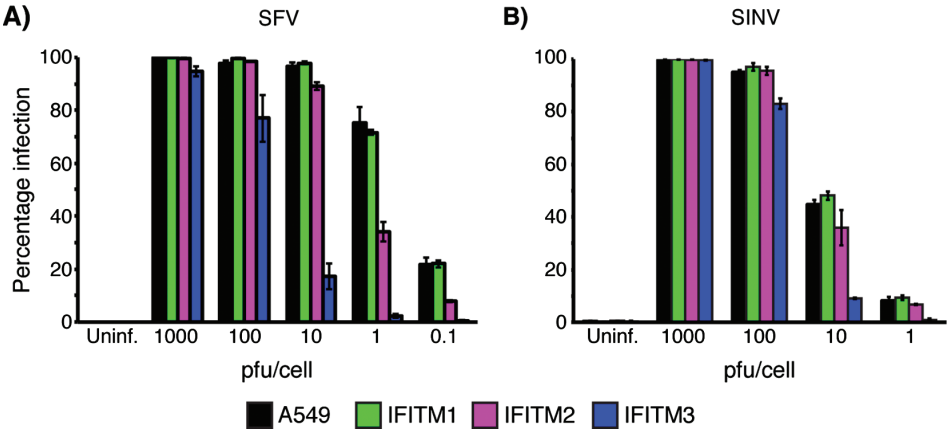

Figure 1: Alphavirus infection is inhibited by IFITM proteins. A549 cells stably expressing HA-tagged IFITM1, 2 or 3 were infected with SFV (A) or SINV (B) at the indicated MOI (pfu/cell) for 5.5–6 h prior to fixation. Cells were then stained for the respective viral envelope proteins and the proportion of infected cells counted using an Opera microscope system. Although SINV infection of A549 cells was not as efficient as SFV, IFITM3-HA expression inhibited infection by both viruses. IFITM2-HA expression had some effect on SFV infection at lower MOI, but minimal effect on SINV infection. IFITM1-HA had no effect on either virus. These data are from a representative experiment ($n = 2–3$) performed with triplicate wells in a 96 well plate. Each bar shows the mean infection percentage for the three wells and the standard deviation.

affect SFV binding, internalization or entry into early endosomes, which also contain IFITM3. Moreover, the SFV E1 glycoprotein undergoes a characteristic low pH-induced conformational change with similar kinetics in both IFITM3-expressing and non-expressing cells. However, release of the viral capsid protein into the cytosol is inhibited in IFITM3-expressing cells.

SFV infection induced by low-pH fusion with the cell surface was inhibited by the plasma membrane localized IFITM1, but was equally restricted by IFITM3, even though this protein is predominantly localized to intracellular compartment and is present at only low levels on the cell surface. Furthermore, a mutant of IFITM3, which is localized to the plasma membrane (Y20A), inhibited infection by plasma membrane fusion more potently than IFITM1, but did not inhibit the endosomal route of infection.

Together our results show that (i) alphaviruses are restricted by IFITMs, (ii) for SFV at least, IFITM3-mediated restriction appears to affect viral fusion and cytosolic delivery of the viral capsid, and (iii) that IFITM1 and IFITM3 have different potencies for inhibition of SFV infection.

Results

IFITMs can restrict alphavirus infection

To investigate whether IFITMs can restrict infection by alphaviruses, we used A549 cells stably expressing human C-terminally HA-tagged IFITM1, 2 or 3 (19,20). Cells were infected with SFV or SINV at MOIs ranging from 0.1 to 1000 pfu/cell for 5.5–6 h, prior to immunolabelling for newly synthesized viral envelope glycoproteins (E1/E2) as a marker of infection. IFITM3-HA inhibited infection by both viruses (Figure 1). At 1 pfu/cell, IFITM3-HA expression inhibited SFV infection by ~95%. Though requiring a higher MOI to see equivalent levels of infection, replication of SINV was also inhibited by IFITM3-HA. For both viruses, IFITM3-HA restriction was less efficient at higher MOIs (~20% inhibition at 100 pfu/cell and <10% at 1000 pfu/cell for SFV, and ~10% inhibition at 100 pfu/cell for SINV). IFITM2-HA also inhibited SFV infection (~50% at 1 pfu/cell) but had little activity against SINV. IFITM1-HA had no activity against either virus.

These data indicate that IFITM3-HA, and to a lesser extent IFITM2-HA, can restrict infection of A549 cells by two different alphaviruses, and that the restriction can be saturated with higher levels of input virus.

IFITM3 endosomal localization and expression levels impact antiviral activity

The A549 IFITM-HA cells used in Figure 1 were produced through single cell cloning of lentivirally transduced cells. To further test IFITM3-mediated inhibition, we used two additional sets of A549 stable cells produced using puromycin selection. One set (P1) was produced to stably express C-terminally HA-tagged IFITM1, 2 or 3, or an empty vector control. The other set (P2) included cells expressing IFITM3-HA, IFITM3-HA with a Y20A mutation and a GFP control. The Y20A mutation disrupts a Yxxϕ type endocytosis signal in the IFITM3 N-terminal domain (NTD), causing accumulation of the protein at the plasma membrane ((21), Figures S1 and 8B). IFITM3-Y20A-HA allowed us to investigate the importance of endosomal localization for antiviral activity (see Figures S1 and 3 for wild type IFITM3-HA localization). These three sets of cells are denoted as: OS – the original set produced by single cell cloning (Figure 1), and P1 and P2 for the puromycin selected cells.

IFITM expression levels in all cells were analyzed by western blot (Figure 2A). Antibodies against the NTDs of IFITM1 or IFITM3 were used, as previously described (20). The OS cells had the highest IFITM expression. P1 and P2 cells had expression levels similar to each other. OS- and P1-IFITM2-HA had low expression, or poor detection (detected by cross-reaction from the anti-IFITM3-NTD antibodies), possibly as a consequence of localization in more hydrolytic, late endosomal compartments (see Figure 3).

P1- and P2-IFITM3-HA expressing cells inhibited SFV in the range of 0.1 to 10 pfu/cell (Figure 2B), but restriction was reduced compared to that seen in OS-IFITM3-HA cells (compare Figures 2B with 1A). At 1 pfu/cell, OS-IFITM3-HA showed ∼95% inhibition while P1- and P2-IFITM3-HA cells showed ∼70% inhibition. The reduced levels of restriction correlate with the lower IFITM3-HA expression. P1-IFITM2-HA cells showed some inhibition of SFV infection, though this was lower than OS-IFITM2-HA and all IFITM3-HA cells. As with OS-IFITM1-HA, P1-IFITM1-HA did not restrict SFV infection. IFITM3-Y20A-HA, which localizes to the plasma membrane similarly to IFITM1-HA (Figure S1 and (20)), also did not inhibit SFV infection, suggesting that the endosomal localization of IFITM3 is essential for its anti-SFV activity.

Previously, we noted that OS-IFITM3-HA restriction was less efficient at high viral input (Figure 1). This effect was also observed for the P1- and P2-IFITM3-HA cells. Thus, IFITM3-mediated restriction can be saturated either by increasing the amount of virus or lowering the level of IFITM3-HA expression.

Unless otherwise indicated, all subsequent work was performed with OS-IFITM-HA cells.

IFITM3 preferentially localizes to early endosomes and IFITM2 to late endosomes

The majority of viruses restricted by IFITM3 are believed to fuse with late endosomes where some studies have suggested IFITM3 is localized (22,23). SFV by contrast, has been shown to fuse in early endosomes at pH ≤ 6.2 (8,11). Since IFITM3-HA more potently restricted SFV and SINV than IFITM2-HA, and the endosomal localization of the protein is necessary for its antiviral activity, we investigated IFITM2-HA and IFITM3-HA localization. Cells were co-immuno-labeled for the IFITM proteins and markers of early and recycling endosomes [Early Endosomal Antigen 1 (EEA1) and transferrin receptor (TfR), respectively] or late endosomes and lysosomes [CD63 and lysosomal associated protein 1 (LAMP1)]. IFITM3-HA showed more colocalization with TfR and EEA1 than IFITM2-HA, while IFITM2-HA showed more overlap with CD63 and LAMP1 than IFITM3-HA (Figure 3). Image analysis showed that a significant amount of both IFITM2-HA and IFITM3-HA did not colocalize with each of the single endosome/lysosome markers (Figure 3C, D). Given that early endosomes are heterogeneous and neither EEA1 nor TfR mark the entire early endosome population, and IFITM2-HA and IFITM3-HA have somewhat overlapping distributions, we conclude that in fixed A549 cells IFITM3-HA is associated more with early endocytic organelles and IFITM2-HA more with later endocytic compartments. The higher levels of early endosomal localization of IFITM3-HA may explain why this protein more effectively inhibited SFV and SINV infection than IFITM2-HA, and the plasma membrane-associated IFITM1-HA and IFITM3-Y20A-HA proteins.

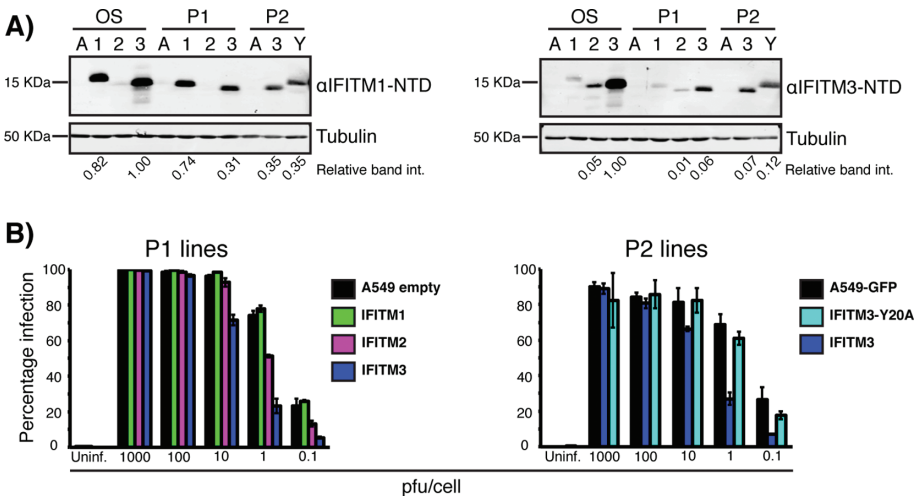

Figure 2: IFITM3 expression levels affect SFV restriction. Two sets of A549 cells stably expressing IFITM-HAs (P1 and P2: See *Materials and Methods*) were analyzed for IFITM expression levels and SFV restriction. A) Western blotting was used to analyze the IFITM expression of all three sets of cells (OS = the original single cell clones used in Figure 1). A, 1, 2 and 3 denote A549, IFITM1, IFITM2 and IFITM3, respectively. Antibodies against the IFITM1-NTD (which cross-react with IFITM3) or IFITM3-NTD (which cross-react with IFITM2) were used to analyze IFITM expression. Tubulin was used as a loading control. Fluorescence intensity (int.) of the IFITM and tubulin bands was quantified using LiCOR Odyssey software. IFITM band intensities were normalized to tubulin loading and arbitrarily set relative to the highest band intensity on each blot (OS-IFITM3-HA in both cases). B) The P1 and P2 sets were infected with SFV across a range of MOIs and analyzed for infection by immunofluorescence, as in Figure 1. In line with lower IFITM expression, P1- and P2-IFITM3-HA show reduced levels of SFV restriction compared to OS-IFITM3-HA (Figure 1). These data are from a representative experiment ($n = 2$) performed with triplicate wells in a 96 well plate. Each bar shows the mean infection percentage for the three wells and the standard deviation.

IFITM3 expression does not block SFV binding or endocytosis

Having determined that IFITM3-HA can inhibit alphavirus infection, and localizes to early endosomes, we hypothesized that the inhibition of viral protein production (the read out for Figures 1 and 2B) was due to inhibition of viral entry into cells. In order to infect a cell and replicate, alphaviruses need to deliver their RNA-containing capsid into the cytosol. Initially the virus must bind to the cell surface, prior to internalization by clathrin-mediated endocytosis (CME). Once in the endosomal system, the low pH environment triggers conformational changes in the envelope glycoproteins (E1/E2) to drive fusion of the viral and endosomal membranes and capsid release to the cytosol (24). We tested each of these aspects of the SFV entry pathway to determine the stage at which IFITM3 restricts infection.

Initially, we investigated whether IFITM-HA expression affected virus binding to the cell surface. Equal amounts of virus were added to IFITM-HA expressing A549 cells for 1 h at 4 °C, and the amount of bound virus determined by western blotting whole cell lysates for E1/E2. Similar amounts of bound virus were detected in IFITM negative A549 cells and cells expressing each of the three IFITM-HA proteins (Figure 4A).

Next, to investigate whether IFITM3-HA affected SFV endocytosis, we measured virus uptake using a protease resistance assay (9). SFV was bound to the surface of cells as previously, and the cells then warmed to 37 °C for 5, 15 or 30 min to promote endocytosis. After each time point, the cells were placed on ice and treated with subtilisin (25). Samples were lysed and analyzed for E1/E2 by western blot. To quantify uptake, the band intensities of E1 (bottom) and E2 (top) were measured across multiple experiments. Although subtilisin failed to remove ~22% of the surface virus, there was a clear increase in subtilisin resistant virus on warming the A549 cells to 37 °C (Figure 4B). This peaked at 15 min

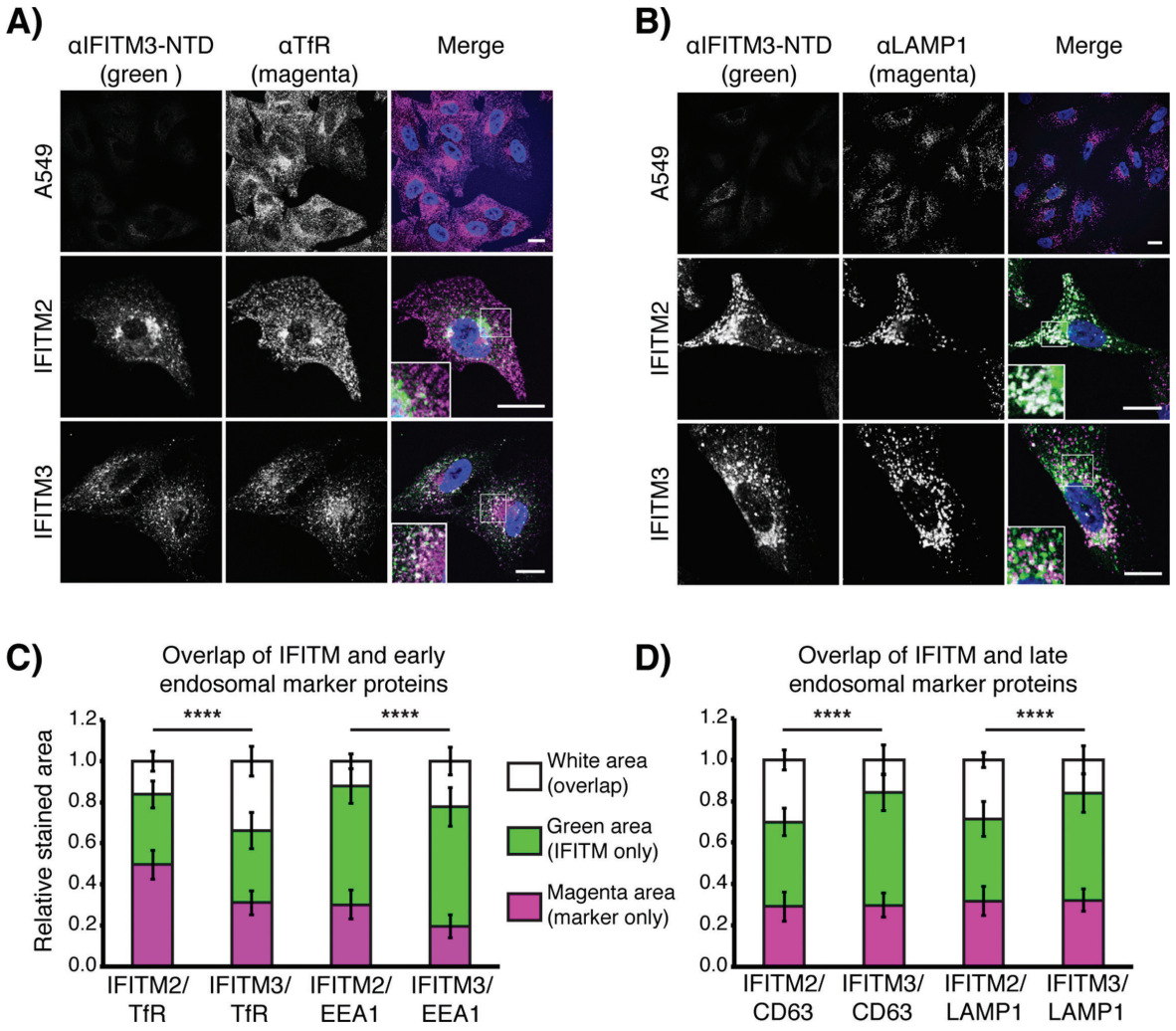

Figure 3: IFITM2 and IFITM3 are found in endosomal compartments. OS-IFITM2-HA and IFITM3-HA cells were fixed, permeabilized and stained using an anti-IFITM3-NTD antibody, and markers of early and late endosomes and lysosomes. A) Example images of cells co-stained for IFITM and transferrin receptor (TfR) and visualized with AF488 (IFITM – green) and AF647 (TfR – magenta) by confocal microscopy. Confocal sections are displayed. B) Example images of cells co-stained for IFITM (AF488) and LAMP1 (AF647) and imaged as in (A). Nuclei were detected with Hoechst staining. Scale bars represent 15 μm. C and D) Colocalizations of IFITMs with early endosome markers, TfR and EEA1, or late endosome/lysosome markers, CD63 and LAMP1, were quantified. Data are from three independent experiments using between 18 and 21 fields of view collected using a 63× objective lens. Quantification of overlapping pixels and significance testing is described in *Materials and Methods*. IFITM3-HA shows more overlap with TfR and EEA1 than IFITM2-HA. Conversely, IFITM2-HA shows greater overlap with CD63 and LAMP1 than IFITM3-HA. There are pixels that contain just IFITM protein or just cellular marker, suggesting the IFITMs are not limited to single compartments. Bars show the mean pixel area and error bars are the standard deviation. ****$p < 0.0001$.

when > 75% of the virus was internalized (Figure 4C). Very similar uptake was seen on IFITM3-HA cells. We conclude that IFITM3-HA expression does not affect either binding, or internalization of SFV into A549 cells.

Internalized SFV colocalizes with IFITM3

Since we observed that IFITM3-HA is associated with early endosomes (Figure 3), we investigated whether internalized SFV entered IFITM3-HA positive endosomes. As above, virus was bound and internalized into cells,

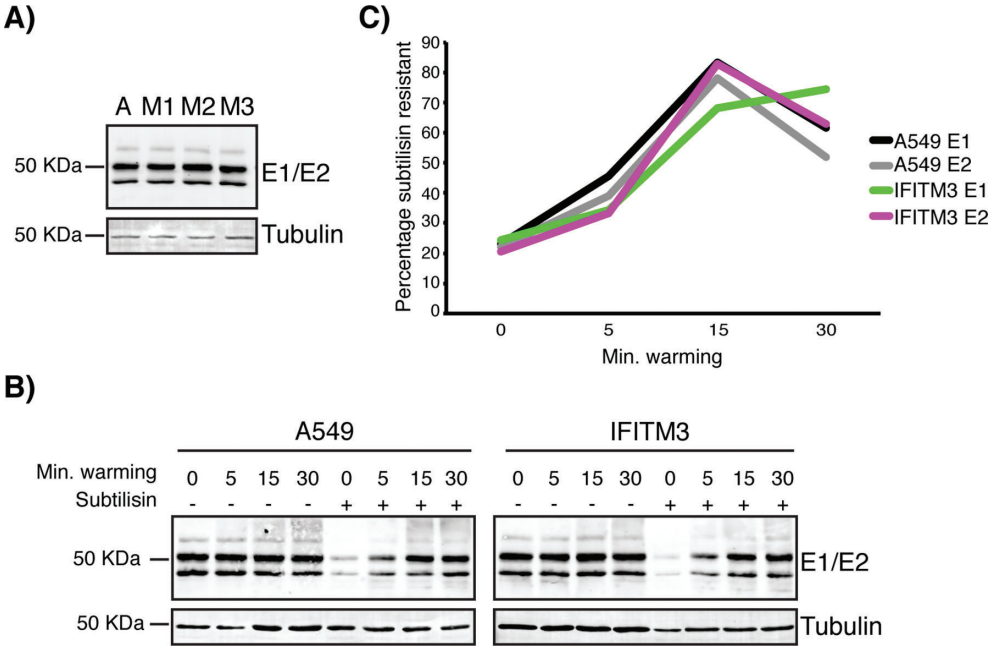

Figure 4: SFV binding to and internalization into IFITM expressing cells A) SFV (200 pfu/cell) was added to A549 cells or OS-IFITM expressing cells (A, M1, M2, M3) at 4°C. After 1 h, the cells were washed and analyzed by western blotting for the viral envelope proteins. Tubulin was used as a loading control. The results indicate similar levels of binding to all four cell lines. B) SFV (200 pfu/cell) was allowed to bind to cells at 4°C for 1 h. Endocytic uptake of virus was promoted by warming to 37°C for 0, 5, 15 or 30 min. Cells were then treated with subtilisin at 4°C to remove surface-bound virus, leaving only internalized virus associated with the cells. In each blot, controls of samples not treated with subtilisin were loaded to indicate the total cell-associated virus. C) Quantification of E1 and E2 subtilisin resistant band intensity. 3–4 independent experiments were performed. Band intensities of E1 (bottom) and E2 (top) were determined and adjusted based on tubulin band intensity for each sample. A measure of total cell-associated virus was determined by averaging band intensity for all untreated time points. The intensity of E1 or E2 at each treated time point was then set as a proportion of this total. Band intensities were averaged across experiments and plotted to display the percentage of subtilisin resistant E1 or E2 at each time point.

which were then fixed and immuno-labeled for E1/E2 and IFITM3-HA and analyzed by confocal microscopy (Figure 5). As a control, these experiments were repeated in A549 cells that were stained for EEA1 instead of IFITM3-HA (Figure S2). When kept at 4 °C ($t = 0$) or warmed for 5 min, virus particles were seen as faint puncta primarily around the cell edges, and there was little overlap with IFITM3-HA or EEA1. After 10 min at 37 °C, and at later time points, SFV staining appeared as larger, increasingly bright, punctae. The increase in EEA1 puncta intensity seen in Figure S2 was also seen in mock-infected cells (data not shown), suggesting this may be due to cooling and warming cells. A time-dependent increase in the overlap between E1/E2 and IFITM3-HA (Figure 5B) or EEA1 (Figure S3B) was detected over multiple experiments. These data suggest that endocytosed SFV was delivered to IFITM3-HA positive endosomes.

These observations were further confirmed by electron microscopy (EM), which revealed that SFV particles were internalized by CME (Figure S3). Subsequently, SFV particles were detected in multivesicular bodies that could be co-labeled for SFV and IFITM3-HA (Figure S4), further demonstrating that virus particles were delivered into IFITM3-HA containing endosomes.

To confirm that we were investigating time points relevant to infection, the kinetics of SFV capsid release in A549 cells were determined. SFV penetration of endosomes is low pH-dependent. Thus, ionophores such as monensin, that rapidly dissipate cellular low pH gradients, can be

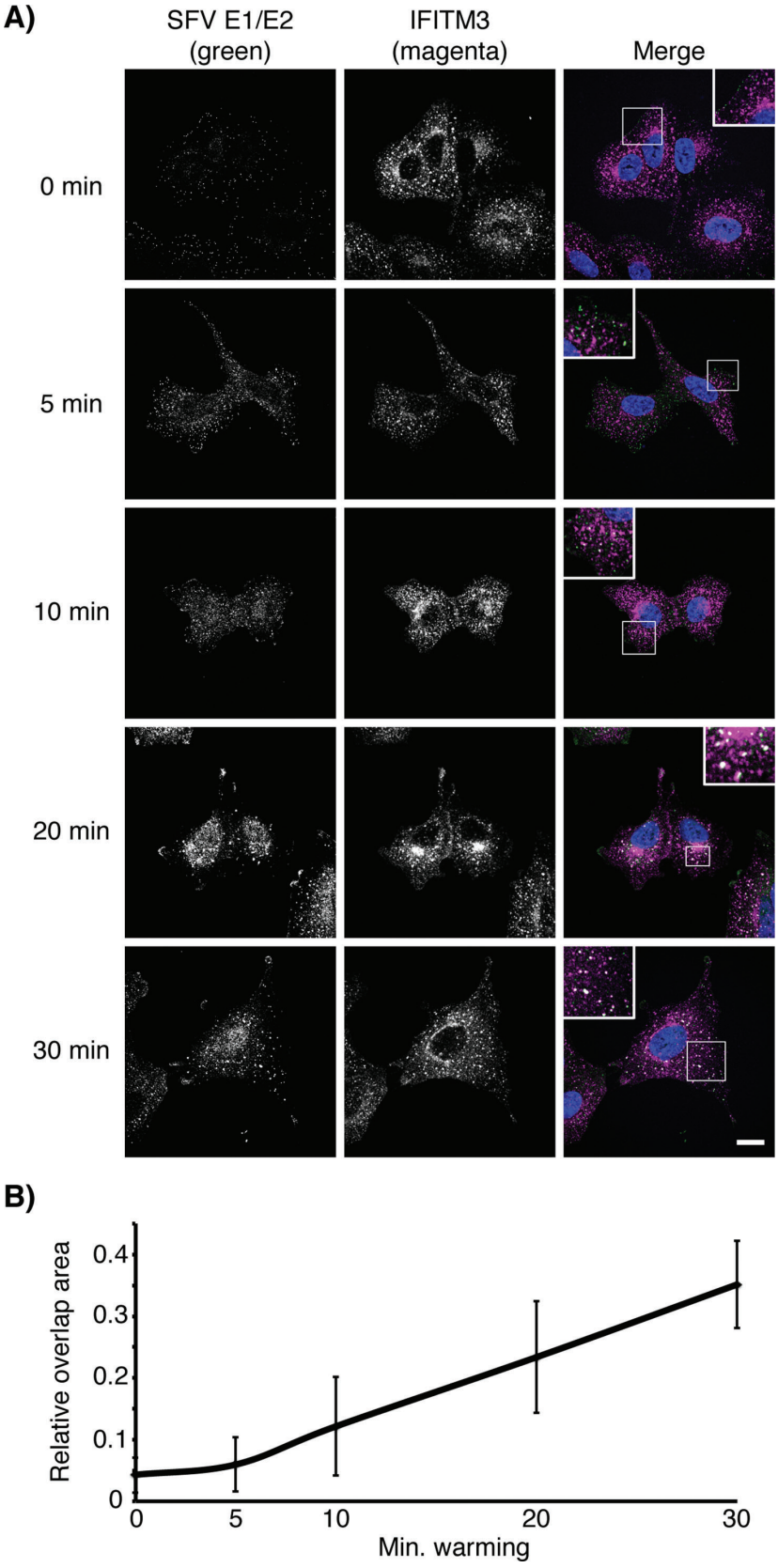

Figure 5: Internalized SFV colocalizes with IFITM3. A) SFV (50 pfu/cell) was bound to cells at 4°C for 1 h. After washing, the cells were warmed to 37°C for the indicated times, then fixed and labeled for SFV E1/E2 and OS-IFITM3-HA (via the HA-tag) and visualized with AF488 (green, E1/E2) and AF647 (magenta, HA). Confocal sections are displayed. E1/E2 labelling can be seen as small puncta mainly around the cell periphery at 0 and 5 min, with little overlap of SFV E1/E2 and IFITM3-HA. At later time points (10 min and onwards) larger and brighter puncta become visible closer to the nucleus, and overlap of SFV E1/E2 and IFITM3-HA is seen, which increases with time. Many IFITM3-HA positive, SFV negative puncta, can be seen suggesting that not all IFITM3-HA containing endosomes receive virus. By contrast, many SFV positive puncta co-label for IFITM3-HA at 20 and 30 min. Nuclei were detected with Hoechst staining. Scale bar represents 15 μm. B) The overlap between green (SFV E1/E2) and magenta (HA) pixels was quantified (see *Materials and Methods*). A total of three independent experiments were performed, and six images taken at 63× magnification for each. The average ratio of the relative area of overlapping pixels (green and magenta) to green pixels from each experiment is plotted, with the standard deviation used for the error bars.

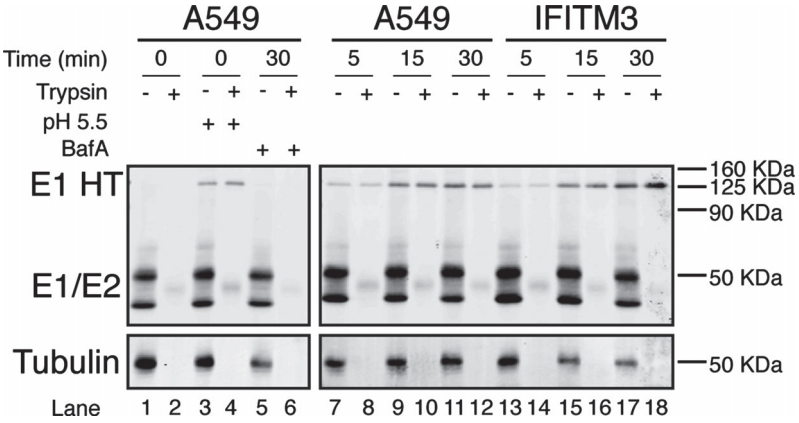

Figure 6: SFV is exposed to acidic pH in IFITM3 expressing cells. SFV (200 pfu/cell) was bound to A549 (lanes 1–12) or OS-IFITM3-HA expressing cells (lanes 13–18) at 4°C for 1 h. The cells were then washed and either kept at 4°C (lanes 1–4) or warmed to 37°C to allow virus uptake (lanes 5–18), as indicated. In lanes 3–4, cells with bound virus were briefly (3 min) treated with pH 5.5 medium at 37°C, or in lanes 5–6, were warmed to 37°C for 30 min in medium containing bafilomycin A1 (Baf A). Subsequently, all cells were placed on ice, lysed with 1% Triton X-100 and half of the lysate treated with trypsin at 37°C as indicated. All samples were then analyzed by non-reducing SDS-PAGE and western blotting for SFV E1/E2 and tubulin as a loading control. Following a pH 5.5 pulse (lanes 3–4), or incubation at 37°C (lanes 7–18), a high MW band corresponding to the acid-induced, trypsin-resistant, E1 homotrimer (HT) was seen. This band was absent at 0 min (lanes 1–2) and in Baf A-treated samples (lanes 5–6), indicating it is the low pH-induced form of E1.

used in time of addition experiments to determine when incoming virus has passed through the pH sensitive stage of entry (26). Virus particles were bound to A549 cells prior to warming to promote uptake, as previously. Monensin was added at times between 0 and 30 min. When added at 0 min, monensin nearly completely abolished infection (Figure S5). However, when added at later times, an increasing percentage of cells became infected. By 30 min, monensin addition had almost no inhibitory effect (Figure S5), suggesting the majority of infectious virus had penetrated the cells. Therefore, analysing SFV internalization within the first 30 min of warming is relevant to infection.

SFV is exposed to acidic pH in IFITM3 expressing cells

We next investigated whether the viral glycoproteins received the appropriate low pH trigger to become fusogenic in IFITM3-HA expressing cells. The acid-induced conformational changes in the E1/E2 complex generate a homotrimeric (HT) form of E1 that is resistant to trypsin digestion (27). Again, SFV was bound to cells and allowed to internalize for 0, 5, 15 or 30 min at 37 °C. As a positive control, virus particles bound to cells at 4 °C were treated with pH 5.5 medium for 3 min at 37 °C to activate the fusion protein directly at the cell surface. As a negative control, cells were pre-treated with bafilomycin A1 (Baf A; a vacuolar ATPase inhibitor) for 15 min at 37 °C, prior to binding and internalization of virus particles in the presence of Baf A. After appropriate treatments, cells were lysed and the lysates treated with trypsin, or not, and the viral E1/E2 proteins analyzed by western blot. Samples were not heated prior to SDS-PAGE as this can dissociate the E1 HT. With 0 min of internalization, the monomeric forms of E1 and E2 were seen with the expected molecular weights (MW) of ~50 kDa (Figure 6, lane 1). After trypsin treatment of samples kept at 4°C, the E1/E2 bands were undetectable (lane 2). Transient low pH treatment of surface-bound virus induced the formation of a high MW band that was resistant to digestion with trypsin (lanes 3 and 4), corresponding to the E1 HT. This trypsin-resistant, high MW band was seen, with increasing intensity, when virus was allowed to internalize into A549 cells for 5, 15 or 30 min (lanes 7–12), but not when virus was internalized into Baf A treated cells (lanes 5 and 6). When SFV was internalized into IFITM3-HA expressing cells the trypsin-resistant, high MW band appeared with kinetics similar to those seen in IFITM-negative A549 cells (lanes 13–18). We therefore conclude that IFITM3-HA does not interfere with acidification of endosomes, virus trafficking

to these compartments, or the conformational changes necessary for the viral glycoprotein to become fusogenic.

IFITM3 expression inhibits release of SFV capsid to the cytosol

The final step in the SFV entry pathway is release of the capsid into the cytosol. To determine whether IFITM3 affects this step, SFV particles were bound and internalized into cells, which were then analyzed by immunofluorescence staining for the SFV capsid protein. Between 0 and 20 min, in both A549 and IFITM3-HA cells, punctae of virus were seen at the cell surface and subsequently within endosomes (Figure 7A), as observed by E1/E2 labelling (Figures 5 and S3). In general the labelling was weak, even after treatment with Triton, presumably because the capsid protein is poorly accessible when packed within virions. At 40 min in A549 cells, diffuse cytosolic fluorescence was seen, which was further increased at 60 min. This cytosolic fluorescence was not seen following SFV uptake into monensin-treated A549 cells, or in IFITM3-HA cells, suggesting the diffuse fluorescence is from viral capsid protein released into the cytosol. To develop a more quantitative analysis of this capsid release, images were analyzed over multiple experiments to determine the mean cytosolic fluorescence intensity in each cell. This quantification indicated that over time there is an increase in the cytosolic capsid protein-associated fluorescence in A549 cells, that is not seen in monensin-treated A549 or IFITM3-HA cells (Figure 7B). In addition, in these latter cells the punctae of SFV staining appeared brighter at later times, suggesting that non-fused virus particles accumulated within endosomes (Figure 7A). Together these observations indicate that IFITM3-HA expression inhibits release of SFV capsid into the cytosol.

IFITM1 and IFITM3 can inhibit SFV infection by fusion at the plasma membrane

Our data indicate that IFITM3 is primarily localized to early endosomes and can block SFV capsid release into the cytosol. We therefore investigated whether IFITM3-mediated restriction could be bypassed by fusion of SFV at the cell surface, and whether plasma membrane localized IFITM1 (20) or IFITM3-Y20A (Figure S1) could restrict entry at this site. Cells were pre-treated with Baf A for 15 min at 37°C to inhibit SFV entry via the endocytic route, prior to binding virus to the surface at 4°C for 1 h. The cells were then treated with pH 5.5 medium for 3 min at 37°C to induce fusion at the plasma membrane, prior to returning to pH 6.8 medium containing Baf A for 5.5–6 h at 37°C to allow production of E1/E2 proteins as a read out for infection. As controls, cells with bound virus were given a 3 min pH 6.8 pulse and treated with DMSO or Baf A.

Through the normal endocytic route (pH 6.8 DMSO), between ~65% and ~80% of A549 cells (OS, P1 and P2), were infected with SFV (5 pfu/cell), and infection was inhibited by >90% with Baf A treatment (pH 6.8 Baf A; Figure 8A). When cells were pre-incubated with Baf A and transiently treated with low pH medium, ~20–50% of cells were infected (pH 5.5 Baf A; Figure 8A). The Baf A pre-treatment step did not affect the result, since pre-treatment with DMSO media, followed by Baf A media for the infection period (pH 5.5 DMSO/Baf A) showed similar results. This bypass of Baf A inhibition with pH 5.5 treatment is the level of infection by direct fusion at the plasma membrane. It appeared that the three A549 cells had different permissiveness to infection by plasma membrane fusion. The parental OS-A549 cells were the least permissive to plasma membrane fusion; the P1-A549 cells (stably transfected with an empty puromycin resistance vector) were the most permissive, while the P2-A549 cells (stably transfected with a GFP construct) were in the middle. We speculate that the different manipulations of these cells may be responsible for the variability.

Virus entering through the endocytic route infected OS- and P1-IFITM1-HA cells, similarly to A549 controls, and Baf A inhibited this. When virus bound to the surface of both OS- and P1-IFITM1-HA cells was transiently treated with pH 5.5 medium, the infection percentage was consistently lower than that seen in similarly treated A549 cells (Figure 8A). In the OS set, the fact that A549 control cells were not easily infected by plasma membrane fusion meant that inhibition by IFITM1-HA was modest. However, in the P1 set, the difference between infection by plasma membrane fusion of A549 and IFITM1-HA cells was much greater, arguing that IFITM1-HA can inhibit plasma membrane fusion to some extent.

Plasma membrane localized P2-IFITM3-Y20A-HA did not restrict SFV infection through the endocytic route (Figures 8A and 2B). However, when surface-bound virus was low pH treated, P2-IFITM3-Y20A-HA inhibited

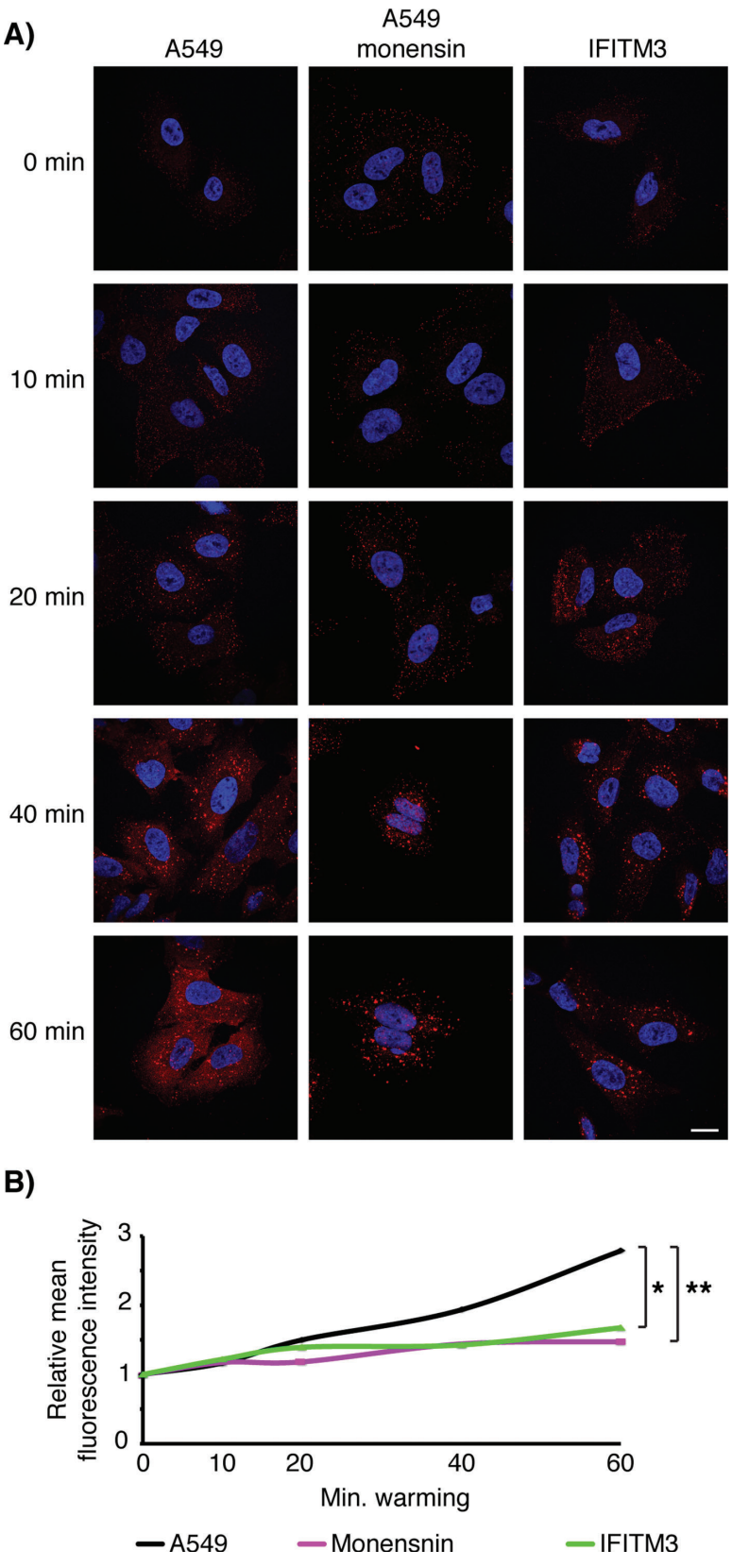

Figure 7: IFITM3 expression inhibits SFV capsid release. A) SFV (200 pfu/cell) was bound to cells for 1 h at 4°C prior to incubation at 37°C for the indicated times. At each time point the cells were fixed and permeabilized with 0.1% Triton-X100 and labeled with serum against the SFV capsid, which was detected with AF594. Confocal sections are displayed. Following internalization, virus particles were detected in cells, indicated by the typical punctate association of virus with endosomes. By 40 min after warm-up diffuse cytosolic fluorescence was seen in A549 cells, indicating release of the viral capsid protein to the cytosol. In A549 cells treated with 10 μM monensin, and in OS-IFITM3-HA expressing cells, the staining remains associated with puncta and the cytosolic staining was not observed even at 60 min after warm-up. Nuclei were detected with Hoechst staining. Scale bar represents 15 μm. B) Quantification of cytosolic fluorescence and significance testing is described in *Materials and Methods*. The data are from three independent infections with 3–7 images taken at each condition, with a total of at least 60 cells analyzed per cell line, per condition. Data presented is the average fluorescence intensity, normalized to the background intensity at 0 min of warming. *$p < 0.05$, **$p < 0.01$.

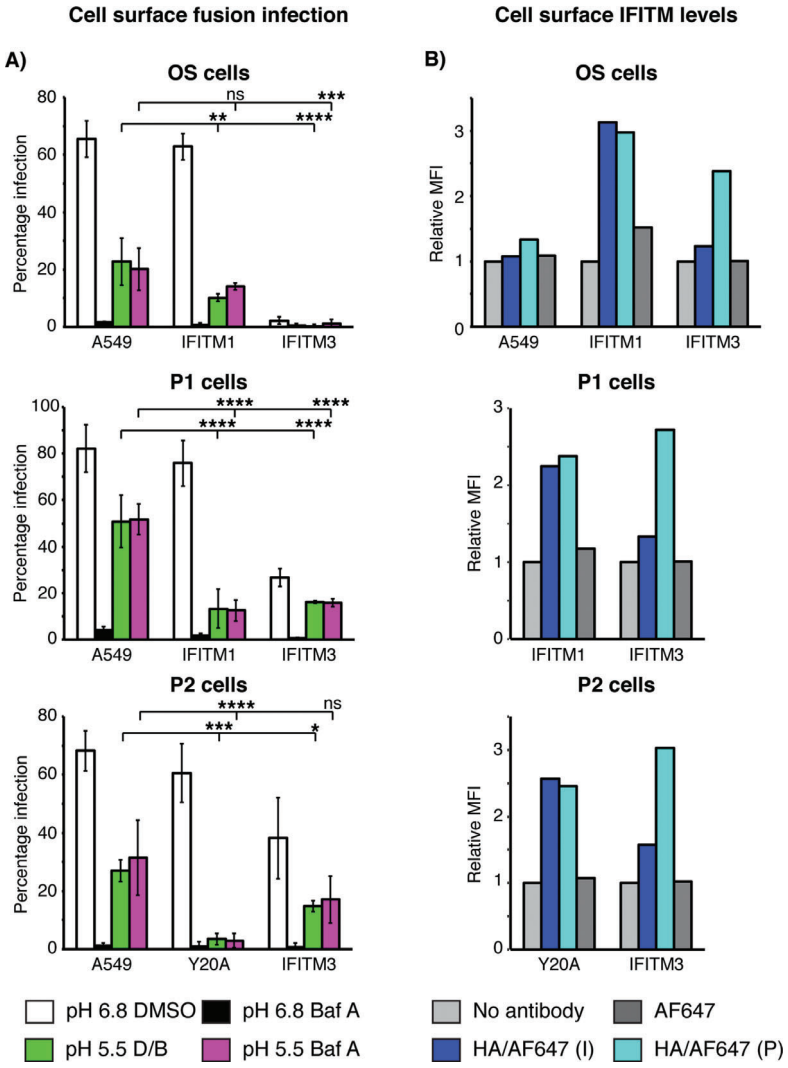

Figure 8: IFITM1 and IFITM3 can inhibit SFV infection by fusion at the cell surface. A) OS-, P1- and P2-IFITM-HA cells were infected by SFV through plasma membrane fusion. Cells were pre-treated with either DMSO or bafilomycin A1 (Baf A) prior to addition of SFV (5 pfu/cell) for surface binding at 4°C for 1 h (in the presence of DMSO or Baf A). Surface-bound virions were then allowed to enter cells by endocytosis (pH 6.8) or fused directly at the cell surface (pH 5.5). pH 6.8 media containing DMSO or Baf A (matched to the pre-treatment) was then added to the cells, which were incubated for 5.5–6 h at 37°C to allow infection. As a control for the Baf A pre-treatment, cells were instead pre-treated with DMSO, then incubated with Baf A containing media for the infection period (pH 5.5 D/B). Cells were fixed and infection determined by immunofluorescence microscopy. Baf A inhibited infection through the endocytic route (black bars compared to white bars). Low pH treatment resulted in bypass of Baf A inhibition, indicative of cell surface fusion (green and magenta bars). The bars indicate the mean infection percentages from three independent experiments (each containing triplicates for each sample) with standard deviation shown as the error bars. Statistical significance was determined using normalized infection values, comparing pH 5.5 DMSO/Baf A (green) or pH 5.5 Baf A (magenta) of A549 samples with IFITM samples, as detailed in the *Materials and Methods* section. *$p < 0.05$, **$p < 0.01$, ***$p < 0.001$, ****$p < 0.0001$. B) OS-, P1- and P2-IFITM-HA cells were labeled with anti-HA antibodies either intact (I) or following permeabilization (P), detected with AF647, and analyzed by flow cytometry to determine the relative levels of cell surface IFITM protein. As controls, cells were either incubated with no antibody or secondary antibody only. The mean fluorescence intensity (MFI), relative to the no antibody control for each cell line is displayed. Plots are representative of 3–4 independent experiments.

infection by ~95% (Figure 8A). This inhibition is greater than that seen for either OS- or P1-IFITM1-HA (Figure 8A), even though P2-IFITM3-Y20A-HA expression levels were lower than those of IFITM1-HA (Figure 2A).

Endocytic infection was low in all IFITM3-HA cells, with OS-IFITM3-HA being the most restrictive (Figure 8A as in Figures 1 and 2B). Baf A reduced this low level infection to < 1%. Surprisingly, there was no increase in infection of these cells following pH 5.5 treatment of cell surface-bound virus, and the infection was consistently lower than that seen in all A549 cells (Figure 8A). Indeed, OS-IFITM3-HA had the lowest infection percentages, even lower than either OS- or P1-IFITM1-HA. IFITM3-HA also inhibited SFV infection via plasma membrane fusion in the P1- and P2- cells to a similar extent to that seen with IFITM1-HA.

It was interesting to see such potent inhibition of cell surface fusion by IFITM3-HA since immunofluorescence microscopy indicated that the majority of IFITM3-HA is located in endosomal compartments (Figure 3) rather than at the cell surface. To confirm these observations, cells were stained either intact, or following permeabilization, and analyzed by flow cytometry to determine levels of each IFITM protein at the cell surface. Antibodies against the C-terminal HA-tag were used as we, and others, have shown the IFITM proteins to have a type-II transmembrane topology with the C-terminal domain facing the extracellular space (20,28,29). The mean fluorescence intensity (MFI) of labeled OS-IFITM1-HA, P1-IFITM1-HA and P2-IFITM3-Y20A-HA was essentially equivalent between intact and permeabilized cells, suggesting the HA-tag is accessible at the cell surface (Figure 8B). Conversely, for all three IFITM3-HA cases, significant labelling was only detected when cells were permeabilized, suggesting the majority of IFITM3-HA is in intracellular pools (Figure 8B). The MFI of intact IFITM3-HA cells was slightly above background levels, suggesting some surface IFITM3-HA (as we have previously observed (20)),

Overall, despite low levels of cell surface expression (Figure 8B), IFITM3-HA inhibited SFV infection by fusion at the plasma membrane to a similar or greater extent than IFITM1-HA (Figure 8A). Presumably IFITM3-HA that transiently transits the cell surface *en route* to endosomes is responsible for this inhibition (20,21,30). From this, we conclude that IFITM3-HA is a more potent inhibitor of SFV fusion than IFITM1-HA.

Discussion

IFITM proteins restrict the replication of a wide range of enveloped viruses, and at least one non-enveloped virus (22,23). However, to date there is little evidence that IFITMs restrict alphavirus infection. Here we show that IFITM3, and to a lesser extent IFITM2, can inhibit the replication of two alphaviruses in A549 cells. Using SFV, we show that virus binding, endocytosis, delivery to endosomes and exposure to acidic pH are unaffected by IFITM3 expression. The viral envelope proteins undergo an acid-dependent conformational change with similar kinetics in IFITM3 expressing and non-expressing cells. However, the viral capsid protein does not appear in the cytosol of IFITM3 expressing cells. These results indicate that IFITM3 restricts SFV infection by inhibiting endosomal fusion and/or uncoating of the viral capsid.

To date the broad antiviral activity of IFITMs has been largely seen through the use of retrovirus-based pseudotype reporter systems (22). However, for influenza A virus (IAV) the inhibitory activity of IFITM3 has been better characterized and appears to occur following virus endocytosis and delivery to endosomes, but prior to detection of the viral RNA in the nucleus (1). Nevertheless, the precise mechanism(s) of IFITM3-mediated restriction remains unclear. Based on lipid mixing assays, Desai *et al.* suggest that IFITM3 inhibits IAV genome release from endosomes after the formation of hemifusion intermediates (4). While Li et al. suggest that IFITM proteins inhibit the initial lipid mixing events leading to hemifusion, based on cell–cell fusion experiments with IAV and the retrovirus JSRV (3). Our experiments with SFV indicate that virus delivery to acidic endosomes and the initial steps in the fusion reaction, including low pH-induced conformational changes in the viral envelope protein are unaffected by IFITM3. Nevertheless, delivery of the capsid to the cytosol is blocked, suggesting that IFITM3 inhibits membrane fusion or, possibly, uncoating after fusion has occurred.

It is interesting to note that IFITM1 did not inhibit endocytic entry of either alphavirus since many other viruses

show at least some sensitivity to this protein (22). Furthermore, dengue virus, a type II fusion protein expressing virus, similar to alphaviruses, is restricted by IFITM1, 2 and 3 (17). We speculate endocytic uptake and fusion with early endosomes allows SFV to escape inhibition from the plasma membrane localized IFITM1, in this system. However, why the endocytic route of alphavirus entry is not inhibited by IFITM1, while other endocytosed, low pH-dependent viruses (such as dengue) are inhibited, remains unclear.

Previously the effect of IFITM protein expression on SFV E1/E2-mediated fusion from within (cell–cell fusion facilitated by E1/E2 expressed on the cell surface and exposure of cells to low pH medium) was reported (3). In that study IFITM1 and IFITM3 were found to inhibit syncytium formation. In agreement, we also see that both IFITM1 and IFITM3 can inhibit infection by SFV, when virus is fused at the cell surface. Immunofluorescence (Figure 3 and (20)), EM (data not shown) and flow cytometry (Figure 8B) show lower levels of IFITM3 at the cell surface than IFITM1. It is therefore interesting that IFITM3 seems to be able to inhibit infection by cell surface fusion to an equivalent or greater extent than IFITM1 (Figure 8A). Furthermore, when IFITM3 is relocated to the plasma membrane (IFITM3-Y20A) greater inhibition of infection was seen compared to IFITM1 (Figure 8A). We conclude that IFITM3 has greater potency for inhibiting SFV fusion than IFITM1. Understanding this difference may provide insights to the mechanism(s) underlying the ability of IFITMs to restrict viral replication.

Finally, we observed that the antiviral action of IFITM3 can be saturated by increasing the amount of virus, and is also influenced by the level of IFITM protein expression (Figures 1 and 2). Type I interferon treatment of A549 cells results in similar levels of IFITM expression as seen in the P1 and P2 cell sets (data not shown). This ability to saturate IFITM3 restriction could be explained if there is a level of direct interaction between IFITM3 and SFV fusion sites. Whether IFITM3 is recruited to sites of membrane fusion, or is localized to specific membrane domains conducive for fusion, remains to be established.

With the wealth of experimental data on SFV membrane fusion, using alphaviruses as a model may aid our understanding of the molecular mechanism(s) underlying IFITM-mediated inhibition of viral infection. Elucidating these mechanisms may help to generate novel therapeutic strategies that could be applied against a broad range of both human and animal pathogens, and to further our understanding of membrane fusion, a phenomenon that underpins many more biological functions than viral entry.

Materials and Methods

Cell lines and viruses

The previously described (19,20) original set (designated OS) of A549 cells stably expressing C-terminal HA-tagged human IFITM1, 2 or 3, were cultured in Ham's F-12 GlutaMAX media (all cell culture reagents were from Life Technologies, unless otherwise stated), supplemented with 10% (v/v) foetal calf serum [FCS (PAA)] and 1% (v/v) Penicillin/Streptomycin (Pen/Strep, 10 000 units/mL, 10 000 μg/mL), as previously described (20). The puromycin 1 (P1) set of cells, which consists of A549 cells stably expressing an empty puromycin resistance vector or C-terminal HA-tagged IFITM1, 2 or 3, and the puromycin 2 (P2) set of cells, which consists of A549 cells stably expressing GFP or C-terminal HA-tagged IFITM3 or IFITM3-Y20A, were cultured in the same conditions. BHK-21 cells were cultured in Glasgow-MEM supplemented with 5% FCS, 1% Pen/Strep and 10% (v/v) tryptose phosphate broth (Sigma).

SFV stocks were prepared as described (8). Briefly, BHK-21 cells were infected with SFV at an MOI of 0.05 pfu/cell and cultured for 22 h (h). Supernatants were collected and cleared of cellular debris by low speed centrifugation and the virus concentrated by ultracentrifugation (100,000 × g for 2.5 h at 4 °C). Virus pellets were resuspended in TN buffer (100 mM NaCl, 50 mM Tris pH 7.6) and stored at −80°C. Virus infectivity was determined on BHK-21 cells by serial dilution plaque assay.

Sindbis virus (SINV) AR339 (a kind gift from Dr. Penny Powell, University of East Anglia, Norwich, UK) stocks were prepared as for SFV.

Antibodies

Rabbit sera against the SFV envelope glycoprotein (E1/E2) and the capsid protein were previously described (31). Rabbit anti-SINV sera was provided by Dr. Penny Powell (University of East Anglia, Norwich, UK). Rat anti-HA (clone 3 F10, Roche), mouse anti-HA (clone HA.11 16B12, Covance), rabbit anti-IFITM1-N-terminal-domain (NTD), rabbit anti-IFITM3-NTD, mouse anti-tubulin, goat anti-rabbit AlexaFluor (AF)488, goat anti-rat AF647, goat anti-rabbit IRDye 680 and goat anti-mouse IRDye 800 were all previously described (20). Mouse anti-transferrin receptor (TfR, 1 mg/mL, clone MEM-189, Abcam), mouse anti-EEA1 (250 μg/mL, BD Biosciences), mouse anti-CD63 (32), goat anti-rabbit AF594 and goat anti-mouse AF647 (both 2 mg/mL, Life Technologies). All antibodies were diluted as described below.

Viral infections

To infect A549 cells, virus was diluted to the required MOI in F-12 infection media [F-12 media supplemented with 0.2% (w/v) bovine serum

albumin (BSA) and 10 mM HEPES (both Sigma), pH 6.8], and incubated with cells for 5.5–6 h at 37 °C. Infected cells were detected by immunofluorescence staining, as described below, using antibodies against the viral envelope glycoproteins. An Opera confocal microscope (Perkin-Elmer) was used to image cells and the number of infected cells counted using the Columbus software (Perkin-Elmer).

Virus binding to the cell surface

SFV particles were bound to the cell surface to promote synchronous internalization in the indicated experiments. Virus was diluted in 4 °C binding media [BM: RPMI medium without bicarbonate (Sigma), supplemented with 0.2% BSA, 10 mM HEPES and 10 mM MES (Sigma) at pH 6.8] and added to cells at the indicated MOIs for 1 h with gentle shaking. The cells were then rinsed twice with cold BM to remove unbound virus, prior to any further treatment, as detailed below.

SFV internalization

SFV internalization into cells was analyzed by immunofluorescence and EM (described below) or biochemically. For light microscopy analysis, SFV was bound to cells at an MOI of 50 or 200 pfu/cell prior to treatment with pre-warmed pH 6.8 BM and incubation at 37°C for the indicated times. Cells were then fixed, permeabilized and stained for E1/E2 or the capsid protein.

For the biochemical investigation of internalization, SFV (200 pfu/cell) was bound to cells at 4°C. The cells were then washed and warmed for the indicated times, or left on ice. Surface-bound virus was removed by treatment with subtilisin [2 mg/mL in PBS (Sigma)] for 1 h at 4°C with gentle shaking. Subtilisin was inactivated by addition of 1 mM PMSF in PBS with 30 mg/mL BSA. Cells were collected and washed with PBS containing 0.2% (w/v) BSA to remove detached virus. Internalized virus was then measured by western blot analysis of SFV E1/E2 in whole cell lysates. Subsequently, the band intensities were quantified: A measure of total cell-associated virus was determined by averaging the E1 or E2 band intensities at each time point, without subtilisin treatment. The E1 or E2 intensity at each subtilisin treated time point was then set as a proportion of this averaged total, thus giving a percentage of subtilisin resistant (internal) E1 or E2. All intensity values were adjusted based on the tubulin loading control. These values were calculated and averaged over 3–4 experiments.

SFV endosomal penetration

To determine the kinetics of endosomal penetration in A549 cells, 5 pfu/cell SFV was added and allowed to bind. Subsequently, F-12 infection media, pre-warmed to 37°C, containing DMSO or 10 μM monensin, was added to cells ($t = 0$). At indicated time points between 3 and 30 min, DMSO media was replaced with F-12 infection media containing 10 μM monensin. Cells were then incubated at 37°C for 5.5–6 h, after which they were fixed and analyzed for infection by immunofluorescence microscopy for the E1/E2 proteins.

Immunofluorescence staining and microscopy and flow cytometry

Immunofluorescence staining and microscopy was performed as previously described (20) with the exception that 0.1% Triton-X100 (Tx100, Sigma) was used for permeabilization in experiments to detect the SFV capsid protein.

For flow cytometry, cells were detached from plates using 5 mM EDTA and fixed in suspension with 3% formaldehyde for 15 min at room temperature. Formaldehyde was quenched with 50 mM NH_4Cl in 0.2% BSA diluted in PBS (PBS/BSA) for 15 min at room temperature. Samples were then permeabilized with 0.05% saponin in PBS/BSA [permeabilization buffer (PB)] or incubated with PBS/BSA alone for 30 min at room temperature, prior to labelling with rat anti-HA antibody for 1 h at room temperature (either in PB or PBS/BSA as appropriate). Cells were washed 3× with the appropriate solution and labeled with goat anti-rat AF647 for 45 min at room temperature. As controls, samples were incubated with no antibodies, or incubated with only AF647. Cells were washed 3× with PBS and subject to flow cytometry (LSR-II; BD Bioscience). Cells were gated on forward and side scatter and analyzed for fluorescence intensity. Data were processed using FlowJo (v10.1r5) software (Tree Star).

Antibodies were used at the following pre-determined dilutions form stocks (listed above): anti-HA 1:100, anti-IFITM1-NTD 1:200, anti-IFITM3-NTD 1:200, anti-SFV E1/E2 1:500, anti-SFV capsid 1:500, anti-SINV E1/E2 1:500, anti-TfR 1:200, anti-EEA1 1:200, anti-CD63 1:10 000 and anti-LAMP1 1:500. All secondary antibodies were used at 1:500.

Image analysis

Image analysis of colocalization between IFITM-HA and cellular markers was performed using ImageJ software as previously described (20). For the analysis of SFV E1/E2 colocalization with EEA1 or IFITM3-HA this procedure was slightly altered. Confocal sections were acquired and the multi-channel images of E1/E2 (green) co-stained with HA or EEA1 (magenta) were split into the component channels. These images were processed with an 'AND' function to generate a new image containing only pixels that are both green AND magenta ('overlapping pixels'). A threshold was set to remove background fluorescence, and the area of the remaining pixels was quantified. These 'overlapping pixels' were removed from the E1/E2 image, a threshold set, and the area of the remaining 'green pixels' was quantified. Relative pixel areas were then used to calculate the ratio between 'overlapping pixels' and 'green pixels' to determine the level of overlap between E1/E2 and the cellular proteins.

To quantify the SFV capsid cytosolic fluorescence, confocal sections were collected as displayed in Figure 7A and analyzed using ImageJ software as follows: The channels containing the nuclei and capsid staining were separated. Nuclei were segmented and any signal in the capsid channel that fell within the nuclei area was assumed to be non-specific and removed from the image. A threshold was then applied to these capsid images to only detect virus puncta, which were similarly removed, and the remaining signal was deemed to be cytosolic. Individual cells were then segmented and the mean fluorescence in each cell calculated.

Significance testing was performed using unpaired student's *T*-tests and GRAPHPAD PRISM software to compare the mean values of overlapping pixels for colocalization or the difference between mean capsid cytosolic fluorescence.

Electron microscopy

Epon section EM: 1000 pfu/cell SFV was added to cells grown on coverslips and allowed to bind as above. Cells were subsequently washed and warmed to allow internalization for the indicated times. The coverslips were fixed in EM-grade 2% paraformaldehyde/2% glutaraldehyde (TAAB Laboratories Equipment, Ltd.) in 0.1 M sodium cacodylate, secondarily fixed for 1 h in 1% osmium tetraoxide/1.5% potassium ferricyanide at 4°C and then treated with 1% tannic acid in 0.1 M sodium cacodylate for 45 min at room temperature. Samples were then dehydrated in sequentially increasing concentration of ethanol solutions, and embedded in Epon resin. Coverslips were inverted onto prepolymerized Epon stubs and polymerized by baking at 60°C overnight. The 70 nm thin sections were cut with a Diatome 45° diamond knife using an ultramicrotome (UC7; Leica). Sections were collected on 1 × 2 mm formvar-coated slot grids and stained with Reynolds lead citrate.

Immunolabelling EM: 5000 pfu/cell SFV was added to cells and allowed to bind and internalize as above. As previously described (20), cells were fixed with EM-grade 4% (w/v) paraformaldehyde in 0.1 M phosphate buffer pH 7.4, infused with 2.3 M sucrose, supported in 12% (w/v) gelatin and frozen in liquid nitrogen. Ultrathin (70 nm) cryosections were cut at −120°C and picked up in 1:1 2.3 M sucrose: 2% methylcellulose. Sections were labeled with primary antibody (mouse anti-HA 1:400), followed by rabbit anti-mouse intermediate antibody (1:180, DAKO) and protein A-gold. For double labelling experiments, sections were treated with 1% glutaraldehyde in PBS after the first protein A-gold incubation and quenched in 15 mM glycine before repeating the single labelling procedure with the second primary antibody (anti-E1/E2) and a different sized protein A-gold, as described (33). Finally, sections were contrast stained in 1:9 solution of 4% uranyl acetate: 2% methylcellulose solution pH 4.0. All samples were imaged using a transmission electron microscope (Tecnai T12; FEI) equipped with a charge-coupled device camera (SIS Morada; Olympus).

Antibodies were used at the following pre-determined dilutions from stocks (listed above): SFV E1/E2 1:50, mouse anti-HA 1:400.

SFV plasma membrane fusion

Cells, in a 96 well plate format, were pre-incubated with either DMSO or 100 nM bafilomycin A1 (Baf A) in BM for 15 min at 37°C. Cells were then placed on ice and washed with cold BM containing DMSO or Baf A prior to addition of 5 pfu/cell SFV to bind to the cell surface (in the presence of Baf A or DMSO). The cells were washed to remove unbound virus and treated with 37°C BM (containing DMSO or Baf A) adjusted to pH 5.5 for 3 min (or pH 6.8 as control), to trigger viral fusion at the cell surface. Cells were subsequently incubated for 5.5–6 h in F-12 infection media containing DMSO or Baf A. Control samples, pH 6.8 DMSO, were treated with F12 infection media containing DMSO, allowing viral entry through the normal endosomal route. Cells pre-treated with Baf A and pH 6.8 media were incubated with infection media containing Baf A, allowing endocytosis but inhibiting low pH-induced viral fusion in endosomes. Cells pre-treated with Baf A and given a pH 5.5 pulse were incubated with infection media containing Baf A to trigger fusion at the plasma membrane, while inhibiting acidification of endosomes, such that the low pH trigger was only received at the plasma membrane. Cells pre-treated with DMSO and given a pH 5.5 pulse were incubated with infection media containing Baf A, to again block endosomal acidification and as a control for Baf A pre-treatment. Infected cells were detected by immunofluorescence, as described above, using antibodies against E1/E2. Three random epifluorescence images, at 20× magnification, were taken for each well and analyzed for infection percentage using IMAGEJ software. Briefly, nuclei were segmented to detect the total number of cells per field. The segmented nuclei were super-imposed on the fluorescence channel marking infected cells (E1/E2 stained cells) and a ring of 10 pixels was expanded around each super-imposed nuclei. The E1/E2 fluorescence intensity within this ring was used to score cells as infected or uninfected. The percentage of infected cells was determined for each image and used to determine the percentage of infected cells per well. All infections were carried out in triplicate wells, and the mean infection percentage calculated. In order to test statistical significance of inhibition all infection percentages were set relative to the A549 pH 6.8 DMSO condition within each cell line set (such that OS-IFITMs were only compared to OS-A549, for example), thus giving a measure of the relative infection percentage induced by the pH 5.5 treatments. The difference in relative infection percentages was then analyzed across experiments using unpaired student's *T*-tests in GRAPHPAD PRISM software to compare the difference in relative infection percentage from pH 5.5 treatments in A549 controls against IFITM expressing cells.

SFV E1 trypsin insensitivity

Cells were initially pre-incubated with either DMSO or 100 nM Baf A in BM as described for SFV plasma membrane fusion. Virus was added at an MOI of 200 pfu/cell. Where indicated, cells with bound virus were warmed to 37°C to allow virus uptake (with Baf A as labeled), briefly (3 min) treated with pH 5.5 BM, or left on ice. Cells were lysed in 60 µL 1% Tx100 in PBS for 15 min on ice, and the nuclei removed by centrifugation. 40 µL of cell lysate were divided in two. One sample was mixed with 20 µL trypsin [800 µg/mL in 1% Tx100 (Sigma)] and incubated for 10 min at 37 °C, the other with 20 µL 1% Tx100. Both samples were then mixed with 20 µL of soybean trypsin inhibitor [2 mg/mL (Sigma)]. Finally, 6× non-reducing Laemmli sample buffer (LSB) was added and an equal volume of each sample was separated by SDS-PAGE and western blotted for SFV E1/E2, as described below. Samples were not heated prior to SDS-PAGE to maintain the E1 homotrimer.

Western blotting

Unless otherwise indicated, cell lysates were produced by incubating cells with Tx100 lysis buffer [1% (v/v) Tx100, 150 mM NaCl, 50 mM Tris–HCl at pH 8.0] containing 1× complete protease inhibitor cocktail (Roche) for 15 min on ice. Nuclei were removed by centrifugation and the protein concentrations determined using the bicinochoninic acid method

(Thermo Scientific). Equal amounts of protein for each sample were mixed with 3× LSB containing 100 mM dithiothreitol (unless otherwise indicated). Samples were separated on 10% or 15% SDS-PAGE gels, transferred to PVDF membranes (Immobilon-FL, Millipore), and blocked with 5% (w/v) milk powder (Marvel) in Tris-buffered saline (pH 7.4) with 0.05% Tween-20 (TBST) for 1 h at room temperature. The membranes were incubated with primary antibodies overnight at 4 °C, washed with TBST and probed with appropriate secondary antibodies conjugated to Li-COR IRDye fluorophores at room temperature before imaging on a Li-COR Odyssey system. Quantification of band fluorescence intensity was performed using the Odyssey software.

Antibodies were used at the following pre-determined dilutions from stocks (listed above): anti-SFV E1/E2 1:1000, anti-IFITM1-NTD 1:1000, anti-IFITM3-NTD 1:500, anti-VDAC 1:300, anti-tubulin 1:1000. Both Li-COR secondary antibodies were used at 1:10 000.

Acknowledgments

We thank Dr. Penny Powell, University of East Anglia, Norwich, UK, for providing SINV and anti-SINV antibodies. Christin Luft for Opera imaging and analysis. Michela Mazzon and Scott Lawrence for discussions and critical comments on the manuscript. S. W., S. C., I. J. W. and M. M. are supported by UK Medical Research Council core funding to the MRC-UCL LMCB University Unit (Grant MC_U122665002). S. S., R. W., C. D. and P. K. are supported by a Wellcome Trust grant (098051) and funding from the Medical Research Council (G1000413).

The Editorial Process File is available in the online version of this article.

Supporting Information

Additional Supporting Information may be found in the online version of this article:

Figure S1: IFITM3 Y20A localizes to the plasma membrane. P2-IFITM3-HA (wild type; WT) and P2-IFITM3-Y20A-HA cells were fixed, permeabilized and labeled with anti-IFITM1-NTD antibodies (which cross-react with IFITM3) followed by AF488 (green). The images were captured using an epifluorescence microscope. WT IFITM3 was seen in intracellular compartments (also see Figure 3), where as IFITM3-Y20A-HA was seen at the plasma membrane. Nuclei were detected with Hoechst staining. Scale bar represents 15 µm. Figure S1 – Associated with Figures 2 and 8. The figure displays the localization of the IFITM3-Y20A mutant, compared to wild type. This localization has been published by others, and is included here as a demonstration of the plasma membrane localization of the mutant in this system.

Figure S2: Internalized SFV colocalizes with EEA1. A) SFV (50 pfu/cell) was bound to A549 cells for 1 h at 4°C prior to warming for the indicated periods to promote endocytic uptake. Cells were then fixed and labeled for SFV E1/E2 and EEA1, and visualized with AF488 (green, E1/E2) and AF647 (magenta, EEA1). Single confocal sections are displayed. As seen in Figure 5, E1/E2 labelling at 0 and 5 min was seen as small puncta. At later time points following endocytosis, larger and brighter puncta were seen. EEA1 and E1/E2 were seen to overlap from 10 min, indicating trafficking of SFV to early endosomes. The apparent increase in EEA1 intensity with time was also seen in mock-infected samples (data not shown), and may be due to cooling and warming the cells. Nuclei were detected with Hoechst staining. Scale bar represents 15 µm. B) The overlap between green (SFV E1/E2) and magenta (EEA1) pixels was quantified over multiple experiments (see *Materials and Methods*). A total of three independent experiments were performed, and six images taken at 63× magnification. The average ratio of the relative area of overlapping pixels (green and magenta) to green pixels from each experiment is plotted, with the standard deviation used for the error bars. Figure S2 – Associated with Figure 5. This figure is equivalent to the data in Figure 5, but is performed in the control A549 cells, stained for EEA1 and SFV, rather than staining for IFITM3-HA as in Figure 5.

Figure S3: EM imaging of SFV uptake. SFV (1000 pfu/cell) was bound to A549, or OS-IFITM3-HA expressing cells for 1 h at 4°C prior to warming for the indicated periods to promote endocytic uptake. Samples were fixed and processed for Epon section EM, as detailed in *Materials and Methods*. Virus particles were seen at the plasma membrane at 0 min, then in coated vesicles after 5 min at 37°C. By 20 and 30 min, virus particles appear in endosomal structures, but it was hard to distinguish viral particles from other intraluminal vesicles. Figure S3 – Associated with Figure 5. This figure displays Epon EM micrographs for SFV internalization to complement the IF data of Figure 5.

Figure S4: Immuno-gold labelling of cryosections and EM imaging of SFV uptake. SFV (5000 pfu/cell) was bound to cells and allowed to internalize, prior to processing for cryosectioning and immunogold labelling. A) Sections were labeled with antibodies against SFV E1/E2. Viral particles were detected at the cell surface at 0 min. By 30 min viral particles were found within multivesicular bodies in both A549 and OS-IFITM3-HA expressing cells. B) Sections were labeled for SFV E1/E2 and the HA-tag. The primary antibodies were detected with 10 nm colloidal gold (SFV) or 15 nm colloidal gold (HA) conjugated secondary antibodies. There was minimal HA background detected in the A549 cells, whereas most HA labelling in the IFITM3-HA cells was associated with multivesicular bodies, where SFV particles were detected following 30 min at 37°C. Scale bars represent 200 nm. Figure S4 – Associated with Figure 5. This figure displays immuno-gold labeled cryosections and EM micrographs for SFV internalization to complement the IF data of Figure 5

Figure S5: Kinetics of SFV penetration into A549 cells. SFV (5 pfu/cell) was bound to A549 cells for 1 h at 4°C prior to warming to 37°C with media containing DMSO or 10 µM monensin to allow endocytic uptake. At time points between 3 and 30 min, DMSO containing media was replaced with media containing monensin. After 5.5–6 h infection, the cells were fixed and analyzed for infection by immunofluorescence microscopy. The data show the percentage of infected cells compared to DMSO controls. Although monensin added at early time points effectively inhibited infection, addition at 30 min had almost no effect. The data displayed are mean infection percentage from three independent infections (each containing duplicates of each sample) with standard deviation between experiments as error bars. Figure S5 – Associated with Figures 4 and 5, 6 and 7. This figure details the results for the monensin time of addition experiment to determine the time course for SFV passing the pH-dependent step of entry.

References

1. Feeley EM, Sims JS, John SP, Chin CR, Pertel T, Chen L-M, Gaiha GD, Ryan BJ, Donis RO, Elledge SJ, Brass AL. IFITM3 inhibits influenza A virus infection by preventing cytosolic entry. PLoS Pathog 2011;7:e1002337.
2. Amini-Bavil-Olyaee S, Choi YJ, Lee JH, Shi M, Huang I, Farzan M. The antiviral effector IFITM3 disrupts intracellular cholesterol homeostasis to block viral entry. Cell Host Microbe 2013;13:452–464.
3. Li K, Markosyan RM, Zheng Y-M, Golfetto O, Bungart B, Li M, Ding S, He Y, Liang C, Lee JC, Gratton E, Cohen FS, Liu S-L. IFITM proteins restrict viral membrane hemifusion. PLoS Pathog 2013;9:e1003124.
4. Desai TM, Marin M, Chin CR, Savidis G, Brass AL, Melikyan GB. IFITM3 restricts influenza A virus entry by blocking the formation of fusion pores following virus-endosome hemifusion. PLoS Pathog 2014;10:e1004048.
5. Compton AA, Bruel T, Porrot F, Mallet A, Sachse M, Euvrard M, Liang C, Casartelli N, Schwartz O. IFITM proteins incorporated into HIV-1 virions impair viral fusion and spread. Cell Host Microbe 2014;16:736–747.
6. Tartour K, Appourchaux R, Gaillard J, Nguyen X-N, Durand S, Turpin J, Beaumont E, Roch E, Berger G, Mahieux R, Brand D, Roingeard P, Cimarelli A. IFITM proteins are incorporated onto HIV-1 virion particles and negatively imprint their infectivity. Retrovirology 2014;11:103.
7. Yu J, Li M, Wilkins J, Liang C, Chen BK, Liu S, Yu J, Li M, Wilkins J, Ding S, Swartz TH, Esposito AM, Zheng Y. IFITM proteins restrict HIV-1 infection by antagonizing the envelope glycoprotein. Cell Rep 2015;13:145–156.
8. Helenius A, Kartenbeck J, Simons K, Fries E. On the entry of Semliki forest virus into BHK-21 cells. J Cell Biol 1980;84:404–420.
9. Marsh M, Helenius A. Adsorptive endocytosis of Semliki Forest virus. J Mol Biol 1980;142:439–454.
10. White J, Helenius A. pH-dependent fusion between the Semliki Forest virus membrane and liposomes. Proc Natl Acad Sci USA 1980;77:3273–3277.
11. Marsh M, Bolzau E, Helenius A. Penetration of Semliki Forest virus from acidic prelysosomal vacuoles. Cell 1983;32:931–940.
12. Schoggins JW, Wilson SJ, Panis M, Murphy MY, Jones CT, Bieniasz P, Rice CM. A diverse range of gene products are effectors of the type I interferon antiviral response. Nature 2011;472:481–485.
13. Bailey CC, Zhong G, Huang I-C, Farzan M. IFITM-family proteins: the cell's first line of antiviral defense. Annu Rev Virol 2014;1:261–283.
14. Diamond MS, Farzan M. The broad-spectrum antiviral functions of IFIT and IFITM proteins. Nat Rev Immunol 2013;13:46–57.
15. Brass AL, Huang I-C, Benita Y, John SP, Krishnan MN, Feeley EM, Ryan BJ, Weyer JL, van der Weyden L, Fikrig E, Adams DJ, Xavier RJ, Farzan M, Elledge SJ. The IFITM proteins mediate cellular resistance to influenza A H1N1 virus, West Nile virus, and dengue virus. Cell 2009;139:1243–1254.
16. Jiang D, Weidner JM, Qing M, Pan X-B, Guo H, Xu C, Zhang X, Birk A, Chang J, Shi P-Y, Block TM, Guo J-T. Identification of five interferon-induced cellular proteins that inhibit west Nile virus and dengue virus infections. J Virol 2010;84:8332–8341.
17. Chan YK, Huang I-C, Farzan M. IFITM proteins restrict antibody-dependent enhancement of dengue virus infection. PLoS One 2012;7:e34508.
18. John SP, Chin CR, Perreira J, Feeley EM, Aker A, Savidis G, Smith SE, Elia AEH, Everitt AR, Vora M, Pertel T, Elledge SJ, Kellam P, Brass AL. The CD225 domain of IFITM3 is required for both IFITM Protein association and inhibition of influenza A virus and dengue virus replication. J Virol 2013;87:7837–7852.
19. Smith SE, Gibson MS, Wash RS, Ferrara F, Wright E, Temperton N, Kellam P, Fife M. Chicken IFITM3 restricts Influenza viruses and Lyssaviruses in vitro. J Virol 2013;87:12957–12966.
20. Weston S, Czieso S, White IJ, Smith SE, Kellam P, Marsh M. A membrane topology model for human interferon inducible transmembrane protein 1. PLoS One 2014;9:e104341.
21. Jia R, Xu F, Qian J, Yao Y, Miao C, Zheng Y-M, Liu S-L, Guo F, Geng Y, Qiao W, Liang C. Identification of an endocytic signal essential for the antiviral action of IFITM3. Cell Microbiol 2014;16:1080–1093.
22. Smith SE, Weston S, Kellam P, Marsh M. IFITM proteins - cellular inhibitors of viral entry. Curr Opin Virol 2014;4:71–77.
23. Perreira JM, Chin CR, Feeley EM, Brass AL. IFITMs restrict the replication of multiple pathogenic viruses. J Mol Biol 2013;425:4937–4955.
24. Kielian M, Chanel-Vos C, Liao M. Alphavirus entry and membrane fusion. Viruses 2010;2:796–825.
25. Schmid S, Fuchs R, Kielian M, Helenius A, Mellman I. Acidification of endosome subpopulations in wild-type Chinese hamster ovary cells and temperature-sensitive acidification-defective mutants. J Cell Biol 1989;108:1291–1300.
26. Marsh M, Wellsteed J, Kern H, Harms E, Helenius A. Monensin inhibits Semliki Forest virus penetration into culture cells. Proc Natl Acad Sci USA 1982;79:5297–5301.
27. Helenius A, Kielian M, Wellsteed J, Mellman I, Rudnick G. Effects of monovalent cations on Semliki Forest virus entry into BHK-21 cells. J Biol Chem 1985;260:5691–5697.
28. Bailey CC, Kondur HR, Huang I-C, Farzan M. Interferon-induced transmembrane protein 3 is a Type II transmembrane protein. J Biol Chem 2013;288:32184–32193.
29. Ling S, Zhang C, Wang W, Cai X, Yu L, Wu F, Zhang L, Tian C. Combined approaches of EPR and NMR illustrate only one transmembrane helix in the human IFITM3. Sci Rep 2016;6:24029.
30. Jia R, Pan Q, Ding S, Rong L, Liu S-L, Geng Y, Qiao W, Liang C. The N-terminal region of IFITM3 modulates its antiviral activity by regulating IFITM3 cellular localization. J Virol 2012;86:13697–13707.
31. Marsh M, Bron R. SFV infection in CHO cells: cell-type specific restrictions to productive virus entry at the cell surface. J Cell Sci 1997;110:95–103.
32. Fraile-Ramos A, Kledal TN, Pelchen-Matthews A, Bowers K, Schwartz TW, Marsh M. The human cytomegalovirus US28 protein is located in endocytic vesicles and undergoes constitutive endocytosis and recycling. Mol Biol Cell 2001;12:1737–1749.
33. Slot JW, Geuze HJ, Gigengack S, Lienhard GE, James DE. Immuno-localization of the insulin regulatable glucose transporter in brown adipose tissue of the rat. J Cell Biol 1991;113:123–135.